POLITECNICO DI MILANO
Dipartimento di Bioingegneria
Scuola di Dottorato in Bioingegneria

Development of methods for the employment of Near Infrared Spectroscopy (NIRS) devices in clinics and research

Tutors: Prof. Sergio Cerutti

Prof.ssa Anna Maria Bianchi

Course coordinator: Prof.ssa Maria Gabriella Signorini

PhD Candidate : Erika Molteni

Number: 738494

XXIV cycle, Year 2012

Abstract

This three-years work aimed at evaluating the feasibility of the employment of Near Infrared Spectroscopy (NIRS) devices in the neurophysiopathological field. Indeed, this technology, by allowing the estimation of the values of oxygenated and deoxygenated hemoglobin in the blood, and the changing of the tissue blood flux in specific regions of the brain, candidates as a useful tool for the investigation of the hemodynamics in the brain, especially in the cognitive field. Moreover, it looms as a valuable alternative with respect to the more expensive and complex Magnetic Resonance instrumentation for functional studies (fMRI).

The present study have pursued three main aims. First of all, it was intended to verify the knowledge improvement provided by NIRS method, and by its potential applications, as alternative tool to more invasive instrumentation for functional investigation of the brain (fMRI, PET, etc…). Secondly, the advantages deriving from the employment of time-of-flight NIRS technique were exploited, in a comparison with the older and more common "continuous wave" devices. Last, efforts were deployed in the identification of a set of methods for signal processing, aiming at integrating the information provided by spectroscopy (in both "time-of-flight" and "continuous wave" mode) with those measurements provided by other and different investigation techniques.

During the past three years, particular attention has been devoted to the integration of cerebral hemodynamics data provided by NIRS with recordings of cerebral electrical phenomena (electroencephalography), of heart electrical activity (electrocardiography) and of perfusion (LaserDopplerMetry) obtained during the administration of controlled cognitive protocols (tests of attention and memory) to healthy adult volunteers. The final scope of the work has been the transfer of protocols and knowledge, together with the technological and methodological advancement to the neurological and rehabilitative clinical field.

Estratto

Questo lavoro triennale ha avuto l'obiettivo di valutare le potenzialità applicative dei dispositivi di spettroscopia nel vicino infrarosso (NIRS) nell'ambito neurofisiopatologico. Questa tecnologia infatti, offrendo la possibilità di stimare i valori dell'emoglobina ossigenata e deossigenata nel sangue e la variazione del flusso ematico tissutale cerebrale a livello regionale, si candida come utile strumento di indagine dell'emodinamica cerebrale -specialmente in ambito cognitivo-, e come valida alternativa alla più costosa e più complessa strumentazione di risonanza magnetica per lo studio funzionale (fMRI).

Lo studio in oggetto si è posto un triplice scopo. Innanzitutto la verifica del contributo conoscitivo fornito dalla metodica NIRS e delle sue eventuali potenzialità come alternativa a mezzi di indagine funzionale più invasivi (es. fMRI o PET). Secondariamente l'esplorazione dei vantaggi derivanti dall'impiego della recente tecnologia NIRS "tempo-di-volo" (time of flight) rispetto alle possibilità offerte dai più datati ma più diffusi dispositivi NIRS "tempo-continuo" (time-continuous); infine la identificazione di un set di metodi di elaborazione del segnale efficaci per l'integrazione dell'informazione fornita dalla spettroscopia (sia essa "tempo-di-volo" o "tempo-continuo") con quella ottenuta mediante altre e diverse tecniche di indagine.

Durante il triennio, particolare enfasi è stata posta sull'integrazione dei dati di emodinamica cerebrale forniti dalla NIRS con registrazioni dei fenomeni elettrici cerebrali (elettroencefalografia), cardiaci (elettrocardiografia) e di perfusione (LaserDopplermetria) ottenuti durante la somministrazione di protocolli cognitivi controllati (test di attenzione e di memoria) a soggetti volontari sani. Scopo ultimo del lavoro è stato il trasferimento del guadagno tecnologico, metodologico, protocollare e conoscitivo alla clinica neurologica e all'ambito riabilitativo.

Extended Abstract

1. Introduction

In this PhD work, we will discuss the clinical and research impact of the employment of multichannel time domain functional Near-Infrared-Spectroscopy (fNIRS). This emerging optical technique widens the applicability of the more traditional "continuous wave" NIRS, as it is able to separate photons probing different tissue layers. Neurological field seems to be the most promising, as time domain NIRS can successfully overcome the limitations due to the presence of multiple tissue layers in the head (skin, skull, meninges, and so on). A number of "open questions" in neurology could then take advantage from the use of fNIRS for probing the brain hemodynamics.

1.1 Neurovascular Coupling

Neurovascular coupling refers to the relationship between local neural activity and subsequent changes in cerebral blood flow (CBF) in the brain. Indeed, it has been shown that brain activity is associated with focal cortical hyperemia, that is, the changes of neural electrical activity are coupled with a functionally induced focal cortical hyper-oxygenation. Despite hemodynamic and electrical activities have been widely investigated individually, interesting physiological concerns could only be clarified by considering them conjointly. Unfortunately, the considerable differences existing between hemodynamic and electrical signals, their different physiological nature and time dynamics make it difficult to investigate neurovascular coupling as a whole. Despite functional Magnetic Resonance Imaging (fMRI) is the gold standard for studying the hemodynamic transients in the brain, it shows many drawbacks: it is only sensitive to the blood vascular response, it has a low temporal resolution, and it gives indirect measures of oxygenation in the blood. In the present PhD work, we used the Near-Infrared Spectroscopy (NIRS), detecting the changes in concentration of the two blood cromophores oxy and deoxygenated-haemoglobin (HbO and HHb), for the study of neurovascular coupling phenomena.

1.2 Cognitive load and activation patterns

Another open issue in neuroscience is the investigation of the modulatory effect risen in the cerebral hemodynamic pattern by means of a stimulation with differential cognitive load, i.e. with graded levels of cognitive difficulty. One aim of this work was to determine whether multichannel time domain fNIRS is capable to discern differences in frontal patterns of activation due to pure attentional, working memory and high cognitive tasks, and to assess time domain fNIRS sensitivity in detecting modulation effects induced by the mnemonic demand of a cognitive task with graded levels of difficulty. This was done by focusing on frontal cortical activation during a n-back task with different stages of memory requirement.

1.3 Data integration

The last challenge discussed in the PhD thesis is the choice and employment of mathematical and statistical methods for the integration of biological information, and – specifically- for the fusion of NIRS data with other biological information. Data integration should not be interpreted as a strategy for graphical representation of a number of different data. Rather, it can be approached by applying mathematical and statistical methods for

the concurrent processing of different sources of information. In this work, the use of proper methods, such as General Linear Models, and the manipulation of parameters for enhancement of data fusion will be discussed.

2. Protocols

During the first year of the PhD course, part of the efforts were addressed to the creation of a small database of computerized audio-visual tests for neuropsychological assessment. This battery was initially created by using a specific licensed software environment (Presentation®, NeourobehaviouralSystems Inc, Albany, CA), while afterwards some of the algorithms were translated into MATLAB code for a larger diffusion to clinics, and for a better sharing with other research groups. The availability of computerized routines offers some advantages, which have been irremissible in our research activity:

- The possibility to synchronize the behavioral task (i.e. subjects' cognitive activity) to the NIRS hardware;
- The possibility to synchronize the task to more than one recording device, thus allowing multimodal data recording for a direct comparison of NIRS tracks with signals acquired by other techniques;
- The possibility of event-related data processing (i.e., the processing of tracks with reference to the protocol design, to rest and activity time intervals, to the timing of the endogenous or exogenous stimuli, etc.)

Last, the majority of computerized tests were built as a precise replica of some published versions of the same tests. Though, in the case of The Divided Attention Test, a modified version was created, due to some limitations declared by the same authors. In this last case, a validation trial was set up, before using the modified test for data acquisition.

3. Methods

3.1 Hardware

The time-of-flight NIRS system, designed and built by the Dipartimento di Fisica of Politecnico di Milano, is based on pulsed semiconductor lasers at two wavelength 690nm and 820 nm, on an injection optics which multiplies the source channels and on four independent detection chains based on time correlated single photon counting scheme for a total of up to 16 detection channels. This system is part of a more complex apparatus in which the NIRS instrument synchronizes and controls all the experimental setup: a personal computer for stimuli presentation and another PC for on-line analysis and the acquisition of bio-signals.

3.2 General Linear Model

Generalized Linear Model (GLM) is a well-known statistical method, suitable for analyzing time series data. The GLM approach has been extensively applied in fMRI data analysis; only more recently GLM has been introduced also for analysis of fNIRS data.

According to GLM, a time series for a given channel is modeled as a linear combination of L regressors (known functions) plus an error term:

$$\underset{(T\times 1)}{Y} = \underset{(T\times L)}{X}\underset{(L\times 1)}{\beta} + \underset{(T\times 1)}{\varepsilon} \qquad (1)$$

X (TxL matrix) is called the design matrix (DM), in which each column is a regressor and T is the number of time points. Each column L of matrix X contains the predicted

hemodynamic response for one experimental block over time T. β is the vector of the unknown parameters, one for each regressor, weighting (i.e. quantifying) the contribution of each predictor (i.e. regressor) for modeling the functional time series (i.e. columns of matrix Y), and it serves as the parameter set for subsequent hypothesis testing. Errors ε are assumed to have normal distribution with zero mean and covariance $\sigma^2 V$.

Origin for correlation on error terms can be found in cardiac, respiratory and vasomotor effects. The ordinary least squares estimation of the parameters is:

$$\hat{\beta} = \left(X^T X\right)^{-1} X^T Y \qquad (2)$$

inference is then performed by testing the predictor variables through the t-statistic:

$$T = \frac{\hat{X}(r)}{\sqrt{C_{\hat{X}}(r)}} \qquad (3)$$

Where $\hat{X}(r)$ is the product of the transposed contrast vector with the response signal strength, and $C_{\hat{X}}(r)$ is the error variance.
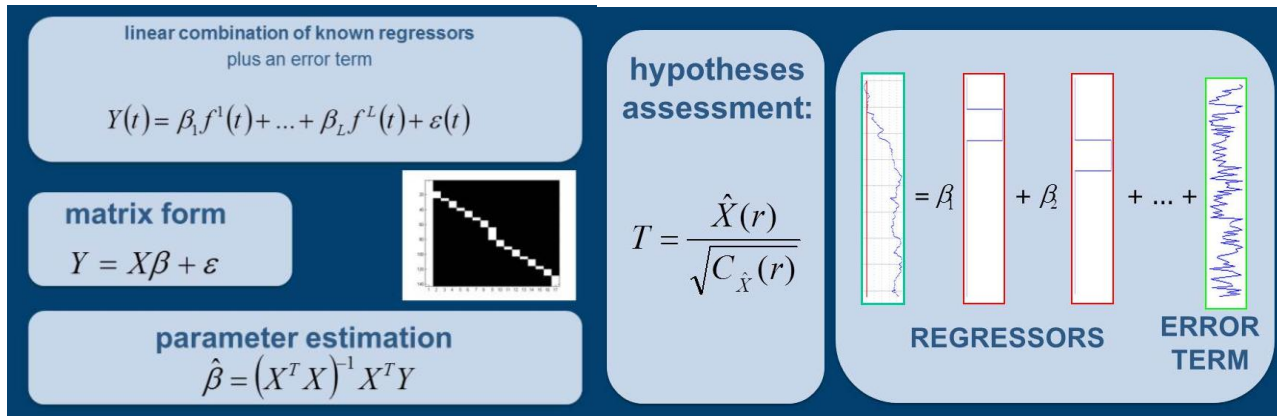

Fig.A. GLM workflow: the time series is modeled as a linear combination of regressors, and an error term which collects the unmodeled part of the series. After the estimation of model parameters, a T statistics is verified for couples of regressors.

The interest of our work has been the analysis of the mean level of brain activation, deducible from levels of HbO and HHb, and of their time course. The computerized tasks were modeled as a series of consecutive boxcar regressors, each one marking with a unit value a single condition (e.g. two activation periods with the same cognitive load) and with a zero value all the remaining part of the task. The timing of the regressors was chosen accordingly to the different activities performed during the experiments. The GLM was applied separately for HbO, HHb and HbT data.

Inferential procedures at a second level (e.g. about activated channels over all subjects) were then performed, and the DM was accordingly modified.

Contrast matrixes were designed for a direct comparison of: (1) activation during the task periods and rest condition with respect to the reference (whole test), and (2) activation during each cognitive load and rest condition with respect to the load/rest immediately harder/easier or with respect to the reference.

Cerebral activation was indicated by positive t-values in the HbO and HT time-series, and by negative t-values for HHb. The results from second level analyses were plotted as statistical parametric maps in NIRS_SPM, which illustrate the brain regions where increased or decreased HbO, HHb and HbT correlate with the stimulation protocol over time.

A second group of contrast matrixes, including both the task design and some preprocessed biological signals was also constructed. Biological data included inside the design matrix could be either:

(1) Electrocardiographic dynamics
(2) Electroencephalographic power in specific frequency bands (alpha, beta, gamma, etc.)
(3) Electromyographic power

4. Validation

An open issue in the assessment of the relationship between the NIRS signal and the functional response of the prefrontal cortex is the need for an accurate and reliable disentanglement of systemic hemodynamic changes from functional changes, being the latter related to cortical activations in response to proper stimuli or tasks and the former to cardiovascular (CV) autonomic and local regulation. Models based on time-resolved measures have been recently proposed, in order to separate skin flow confounding effects from cortical activity, which can be traced back to early and late photons, respectively. However, a few assumptions underlying these models still need more investigation, since their validation has been mainly carried out by comparing the information extracted from fNIRS and fMRI measurements. An alternative option may be the assessment of the optical response of different layers of the head, from the pre-frontal cortex up to the more superficial layers of the forehead and temples skin. To fulfill this purpose, simultaneous measurements of skin flowmotion by laser Doppler flowmetry (LDF) and of pre-frontal cortex hemodynamics by fNIRS are necessary. The experimental recordings which were analyzed in this work included a time resolved, frontopolar (Fp2), fNIRS and two LDF measurements. A preliminary protocol was necessary in order to determine if either device could be a source of noise and disturbance. Then, an experimental protocol of autonomic stimulation was set up, for the disentanglement of the hemodynamic effects due to cortex functional response and surface skin flowmotion.

The results of the preliminary experiment suggested that the strong hemodynamic perturbation induced by Valsalva (VM) provocative test generated: a) first, a sharp synchronization of central and peripheral oscillations during a forced expiratory maneuver, indicated by the high value of correlation between the two LDF channels; b) a desynchronization of oscillatory rhythms following the VM, which characterized the recovery epoch. Good correlation was found between the information captured by the laser Doppler system and the time continuous NIRS device during the evaluation of the scalp influence in the measurement of the arterial oscillations in the brain. In addition, the normalized cross-correlation coefficients further emphasized the relationship between surface hemodynamics related to local flowmotion and the component of the NIRS data which are interpreted as unrelated to either the functional cortical activation and hemodynamics. This preliminary study demonstrated the feasibility of parallel fNIRS and LDF optical measures and confirmed the effectiveness of time resolved fNIRS in separating deep from surface signals during provocative maneuvers like Valsalva.

5. Results

5.1 Neurovascular Coupling

Mental processes bring about electrical, hemodynamic and autonomic changes in the brain cortex. Due to the different nature of these modifications, their onsets show no synchrony and time dynamics is often strongly dissimilar. After having acquired data from a group of sixteen subjects, we applied correlation in order to assess possible influence induced by an attentive task of divided attention on electroencephalographic,

electrocardiographic, oxygenation and deoxygenation NIRS signals. We also investigated correlations and time delays between couples of the same signals. This allowed the isolation of a subgroup of subjects showing similar tracks. Cardiac and oxygenation signals displayed a strong nexus with the task design: interbeat interval series (RR series) and oxygenation tracks showed the highest correlation values with the task design, with opposite trend. Electroencephalographic alpha rhythm, instead, showed more faint correlation with the task evolution, and a trend opposite to it. Correlation among couples of signals showed tightest relationship between interbeat interval series and oxygenation tracks, probably due to their shared cardiovascular origin.

Neural electrical response was nearly instantaneous with respect to the task progression (less than 1 s), autonomic response showed a mean delay of 12 s and a slower hemodynamic response (mean delay above 20 s) was finally induced. Globally, the task elicited a cascade of responses, in which delays could be quantified. Unfortunately, though, intersubject variability remained very high, causing high standard deviations. For this reason, surrogate analysis was conducted for any subject, in order to further validate the results.

5.2 Cognitive load and activation patterns

We then evaluated frontal brain activation during a mixed attentional/working memory task with graded levels of difficulty in a group of 19 healthy subjects, by means of time domain functional near infrared spectroscopy (fNIRS). Brain activation was assessed, and load-related HbO and HHb changes were studied. Generalized Linear Model (GLM) was applied to the data in order to explore the metabolic processes occurring during the mental effort and, possibly, their involvement in short term memorization. GLM was applied to the data twice: for modeling the task as a whole, as well as for specifically investigating brain activation at each cognitive load. This twofold employment of GLM has allowed: (1) the extraction and isolation of different information from the same signals, obtained through the modeling of different cognitive categories (sustained attention and working memory), (2) the evaluation of model fitness, by inspection and comparison of residuals (i.e. unmodeled part of the signal) obtained in the two different cases. Results attested the presence of a persistent attentional-related metabolic activity, superimposed to a task-related mnemonic contribution. Some hemispherical differences have also been highlighted frontally: deoxy-hemoglobin changes manifested a strong right lateralization, while modifications in oxy- and total-hemoglobin showed a medial localization. The present work successfully explored the capability of fNIRS to detect the two neurophysiological categories under investigation and to distinguish their activation patterns. Unfortunately, though, NIRS technique could not prove its efficacy in discerning the cognitive load.

5.3 Data integration

Data integration was performed, while applying General Linear Model, by entering preprocessed electroencephalographic, electrocardiographic and/or electromiographic data into the regressor matrix. This "data informed" GLM allowed the identification of areas in the brain in which hemodynamic activation is coupled with biological dynamics of different origin, such as those of data capturing the electrical activity of the brain, the heart and the muscles. It was thus possible to investigate the functional role of the brain regions involved in neurovascular coupling, also highlighting the **regional specificity**, due to the difference in data coupling. For example, regional hemodynamic patterns often displayed different coupling with alpha and beta EEG rhythm respectively. The "informed" GLM seems then to be a powerful method for a refined investigation of the functional implications of neurovascular coupling.

Moreover, "informed" GLM allowed the investigation of **regional growth** due to the increasing difficulty of the task. Right-handed subjects performed a right handgrip (with the dominant hand), a left handgrip (with the non-dominant hand), and the most complicated task, alternating right and left handgrip (using both dominant and non-dominant hands). In this application, GLM proved to be sensitive to the enlargement of the region(s) involved in neurovascular coupling in the beta EEG range. This result is in line with the theories of neuronal recruiting which explain the regional growth of activation with a gradual involvement of neurons supporting a "minimal" neural network during the performance of difficult tasks.

6. Clinical Applications

The final aim of this PhD work is the exploitation of clinical employment of NIRS devices. Specifically, in this section, some applications in the neurological field are described and discussed. As Functional Near InfraRed Spectroscopy (fNIRS) is a low-cost, portable and easy-to-use tool to non-invasively monitor changes of HbO and HHb concentration in the human tissues, some effort has been focused on the assessment of the feasibility of fNIRS cognitive investigations in Myotonic Dystrophy type 1 (DM1), Unverricht-Lundborg patients and photosensible patients.

Cognitive impairment is common in DM and is often the major disabling component of the disease. The timely assessment of cognitive deficits is thus of primary importance. Central nervous system tissue damage in DM1 patients may not be visible at conventional MR technique. On the other hand, functional neuroimaging techniques such as PET/SPECT imaging and fMRI can provide valuable information regarding brain compromission, at the cost of some uneasiness and patient's discomfort.

Results highlighted a much larger hemodynamic activation in DM1 patients with respect to healthy subject in two different attentive tests: Continuous Performance Test and Conners' Test. These findings confirmed previous results obtained by PET and fMRI, and thus support the belief that fNIRS could help in assessing the neurological outcome of DM1 subjects in clinics, also allowing a comfortable, uninvasive and relatively cheap assessment of some neurofunctional correlates of myotonic dystrophy. Further encouraging research on cohorts affected by Unverricht-Lundborg epilepsy supports broader extension of NIRS employment to a large part of the neurological field.

7. Conclusion

This PhD work explored the applicability of Near Infrared Spectroscopy in the neuropsychophysiologic field. This could be done by means of a set of methods, among which General Linear Model was shortly presented here, which aimed at integrating hemodynamic information captured by time-domain Near Infrared Spectroscopy devices with electroencephalographic, electrocardiographic and electromiographic data. Effort was done for highlighting the potential advantage deriving from the combined use of optical information from the brain with other biological signals. Some major "open issues" in physiology, which seem to be interested by the use of NIRS devices, have been highlighted: neurovascular coupling, the identification of cognitive pattern and the study of cognitive load. A broader extension of NIRS employment to a large part of the neurological field has also been discussed, providing an example for Myotonic Distrophy and Unverricht-Lundborg disease.

List of Contents

Introduction

>>KeyPoints

>NIRS quantifies changes in **oxyhemoglobin,** deoxyhemoglobin and total hemoglobin concentration in the blood.

> NIRS is an **optical** method: portable, noninvasive, safe.

> NIRS can find applications in physiology **research** and in clinical **neurology**

> This PhD work aims at defining the improvements brought about by **time resolved** NIRS, with respect to the previous generation of *continuous wave* NIRS devices.

> This PhD work also aims at the identification of methods for the **integration** of NIRS information with other biological signals obtained from other techniques.

Near-infrared spectroscopy (NIRS) and diffuse optical imaging (DOI) are finding widespread application in the study of human brain activation, motivating further application-specific development of the technology. NIRS and DOI offer the potential to quantify changes in oxyhemoglobin (HbO), deoxyhemoglobin (HHb) and total hemoglobin (HbT) concentration, thus enabling distinction of oxygen consumption and blood flow changes during brain activation. While the techniques implemented presently provide important results for cognition and the neurosciences through their relative measures of HbO, HHb and HbT concentrations, there is much to be done to improve sensitivity, accuracy, and resolution.

In this PhD work, we will discuss some of these technical issues emerging from NIRS use; moreover, we will focus on the clinical and research impact of the employment of multichannel time resolved functional Near-Infrared-Spectroscopy (tr-NIRS): the newest technology available in the field. This emerging optical technique widens the applicability of the more traditional "continuous wave" NIRS (cw-NIRS), as it is able to separate photons probing different tissue layers. Neurological field seems to be the most promising for time domain fNIRS employment, as the technique can successfully overcome the presence of multiple tissue layers, having different optical characteristics. In the head, indeed, the presence of skin, skull, meninges, and the cortex – all bearing different optical properties- makes the investigation with cw-NIRS particularly harsh. A number of "open questions" in neurology, which will be listed in this section, could then take advantage from the use of tr-fNIRS for probing the brain hemodynamics.

1.1 Near Infrared Spectroscopy (NIRS)

Near-infrared spectroscopy (NIRS) and diffuse optical imaging (DOI) are emerging techniques used to study neural activity in the human brain. DOI employs safe levels of optical radiation in the wavelength region 650–950 nm, where the relatively low attenuation of light accounts for an optical penetration through several centimeters of tissue. As a result, it is possible to noninvasively probe the human cerebral cortex using near-infrared light and to monitor the cerebral concentration of hemoglobin, which is the dominant near-infrared absorbing species in the brain. Furthermore, the difference in the near-infrared absorption spectra of oxyhemoglobin (HbO) and deoxyhemoglobin (HHb) allows the separate measurement of the concentrations of these two species.

To achieve this goal, it is sufficient to perform NIRS measurements at two wavelengths. The sum of the concentrations of oxy- and deoxyhemoglobin provides a measure of the cerebral blood volume (CBV), while the individual concentrations of the two forms of hemoglobin result from the interplay between physiological parameters such as regional blood volume, blood flow, and metabolic rate of oxygen consumption. fNIRS thus offers an advantage over BOLD signal in functional Magnetic Resonance (fMRI), which cannot disentangle blood flow and oxygen consumption changes, unless also acquiring blood flow images (Davis et al., 1998; Hoge et al., 1999). This capability is potentially important for a wide range of brain studies particularly of the developing and diseased brain. Extension of a spectroscopic measurement in a single location to include a large number of sources and detectors enables reconstruction of diffuse optical images of a large area of the brain.

1.1.1 Hemodynamic Response Function

Neuronal activation originates in the neurons as electrical signals are transmitted between cells. During this activation, the metabolic demand of neurons changes, provoking an increase in oxygen consumption, local cerebral blood flow (CBF) and oxygen delivery. A typical hemodynamic response (see Fig. 1.1) to cortical neuronal activation in adults shows an increase in blood flow, leading to an increase in oxy-hemoglobin (HbO) and a (relatively smaller) decrease in deoxy-hemoglobin (HHb) as it is displaced from the veins, leading to an increase in total-hemoglobin (HbT) (Villringer and Chance, 1997).
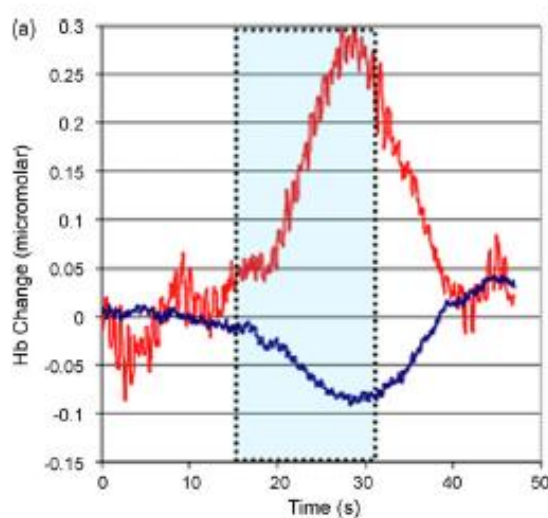

Fig.1.1. A typical hemodynamic response showing an increase in HbO (red) and a decrease in HHb (blue) resulting from cortical activation

Neuroimaging methods either detect the direct activation related to electrical activity of the brain (e.g. electroencephalography (EEG), magnetoelectroencephalography (MEG)) or the consequent hemodynamic response (e.g. positron emission tomography (PET), functional magnetic resonance imaging (fMRI), functional near infrared spectroscopy (fNIRS)).The relative attributes of the functional neuroimaging techniques that have been and are currently used with humans are outlined in Fig. 1.2. EEG and fMRI bear the closest relation to fNIRS: the former uses a similar experimental setting, whilst the latter similarly measures the hemodynamic response. The major advantage of fNIRS compared with EEG is the negligible susceptibility to data corruption by movement artifacts and the higher spatial resolution of activation allowing the localization of brain responses to specific cortical regions (yet lower than fMRI). In addition, compared with fMRI, fNIRS has high temporal resolution, is silent, allowing easy presentation of auditory stimuli, and can measure both oxy- and deoxy-hemoglobin chromophores, thus providing a more complete measure of the hemodynamic response. Though fMRI and fNIRS conceptually measure the same hemodynamic response, generally fMRI techniques have an intrinsically limited acquisition rate at a minimum of one hertz (Huettel et al., 2003; Weishaupt et al., 2008), whereas fNIRS can acquire data rapidly, upto tens of hertz, thus providing a more complete temporal picture (Huppert et al., 2006). On the other hand, as with any technique there are also limiting factors of NIRS:

- the temporal resolution is lower than that of EEG (the precision of which can reach up to thousands of hertz);
- the depth resolution is dependant on the age of the infants, on the thickness of adults' skull and on the optical properties of the tissues (see Fukui et al.,2003);
- the technique offers lower spatial resolution compared with MRI;
- and there is no way for measuring brain structure for anatomical reference (see Minagawa-Kawai et al., 2008 forfurther discussion of these limitations).
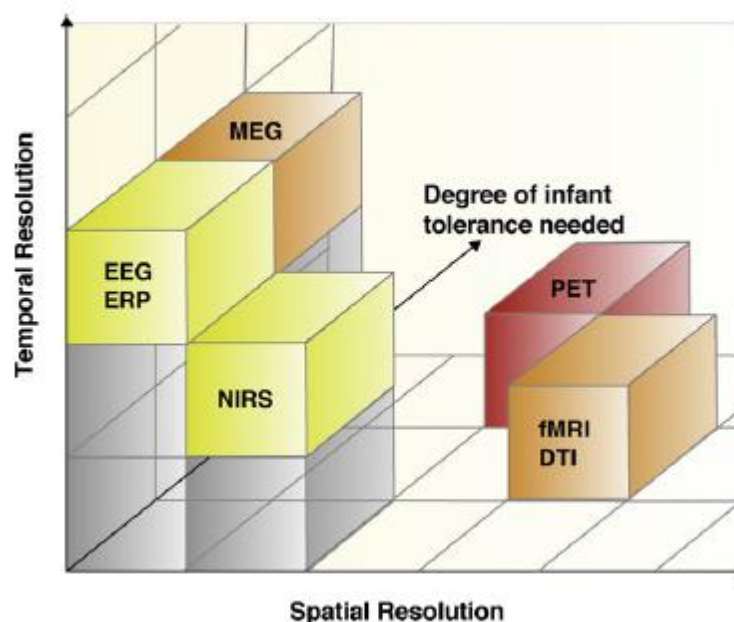
Fig 1.2. This figure shows the spatial and temporal resolution of NIRS compared with other functional neuroimaging methods. It also illustrates the relative degree of tolerance needed from the subject for each method, ranging from yellow (low) to red (high). EEG, electroencephalography; ERP, event-related potential; MEG, magnetoencephalography; NIRS, near infrared spectroscopy; fMRI, functional magnetic resonance imaging; DTI, diffusion tensor imaging; PET, positron emission tomography. (Walsh and Cowey, 2000.)

Despite these shortcomings, a niche exists for fNIRS in neuroimaging. Moreover, research is underway to provide optimized measurements of brain activation by combining the advantages of several neuroimaging methods. This practice has been successfully implemented in research with human participants, e.g. combined fNIRS and EEG(Moosmann et al., 2003), fNIRS and MRI (Steinbrink et al., 2006) and fNIRS and MEG (Sander et al., 2007).

1.2 NIRS in neurophysiology

Jobsis reported in 1977 that the relatively high degree of transparency of myocardial and brain tissue in the near-infrared (NIR) range enabled real-time non-invasive detection of tissue oxygen saturation using transillumination spectroscopy first (Jobsis, 1977). By 1985, Ferrari and colleagues (Ferrari et al., 1985) reported some of the first human cerebral oximetry studies using near-infrared spectroscopy (NIRS).

Since the mid-1990s, an increasing number of researchers have used near-infrared spectroscopy and diffuse optical imaging for human functional brain studies. They have employed the technique to study cerebral response to visual (Heekeren et al., 1997; Meek et al., 1995; Ruben et al., 1997), auditory (Sakatani et al., 1999), and somatosensory (Franceschini et al., 2003; Obrig et al., 1996) stimuli; other areas of investigation have included the motor system (Colier et al., 1999; Hirth et al., 1996; Kleinschmidt et al.,1996) and language (Sato et al., 1999). In all cognitive tasks, NIRS activation studies have demonstrated that generally HbO and HbT increase, while HHb conjointly decreases in the prefrontal cortex (Hoshi et al., 2001; Sakatani et al., 1999; Hock et al., 1997). In the last few years, some efforts have been made in order to extend fNIRS application to the investigation of the modulatory mechanisms in the human body, as well as to the assessment of the impact of dietary enrichments in the brain oxygenation and networking (Jackson et al., 2011).

1.3 NIRS in clinics

Thanks to the non-invasiveness, the handiness and the working costs, noticeably lower than those required by more sophisticated instrumentation, such as Magnetic Resonance, from the outset, clinics has foreseen the chance to employ Near-Infrared Spectroscopy for diagnostic purposes, in the neuropathological and neuropsychological fields, as well as in sport medicine.

Chronologically, though, the first scientific studies which testify the employment of this technique in clinics exploit the potentialities of Near-Infrared Spectroscopy in the monitoring of the hemodynamic parameters of the critically ill patient.

Specifically, in the middle eighties, studies carried out in the neonatology and neonatal intensive care introduced and discussed the employment of Near-Infrared Spectroscopy for the monitoring of the critically ill neonate, putting forward the technology as a "natural advancement" of the more widespread and well-established pulsioxymetry (Ferrari et al., 1985; Ferrari et al., 1986; Edwards et al., 1990). Although showing some limitations in the experimental design and data analysis, these trail-blazing works have the great merit of having promptly highlighted the valuable advantage introduced by Near-Infrared Spectroscopy: the possibility to evaluate at the brain level those variations of blood oxygenation which are correspondingly observed at the periphery. In the periphery,

though, the pulsioxymeter records variations of blood oxygenation characterized by smoothing effects, and by a delay component.

At the beginning of the nineties, beside a wide group of neurophysiological studies (Bacon et al., 1990 just as an example), some works began to report some important methodological advancements in the processing of the clinical Near-Infrared Spectroscopy data (Ferrari et al., 1993). During those years, researchers began to put forward the hypothesis to use the new technology not only as an instrument for monitoring the hemodynamic parameters (such as blood oxygenation, district blood volume, blood flux, etc.), but also as a device for the topographic localization of the changes of such parameters. In other words, the possibility to evolve from a single-channel device, suitable for the evaluation of the shifts of some specific hemodynamic parameters over time, to a more complex instrumentation, suitable for the detection of the districts of the body involved in such changes, is made feasible. It is the birth of Near-Infrared Spectroscopy imaging. If, on one hand, this new approach seems to make feasible a direct comparison with Magnetic Resonance and Positron Emission Tomography techniques (Villringer, 1997), it should be acknowledged that, since the beginning, clinic has needed to tackle the relevant limitations of the technique, which have been made even more overt by such comparison. The strength of Infrared spectroscopy certainly stands in the possibility of reaching time resolutions well exceeding those permitted by the other two technologies; in addition to that, as mentioned, the possibility of bringing the equipment at the bedside and the advantageous purchase and operating costs should be mentioned. However, the low spatial resolution and the limited ability of photons to penetrate deeper layers of tissue (especially bone and compact tissues) make the path towards a successful clinical imaging tortuous, especially in neurophysiology (Hoshi, 2005). Nevertheless, the nineties saw a progressive flowering of NIRS applications in neurophysiopathology. Precursors of the later literature produced in this area are the studies of epilepsy, who tried to take advantage of infrared spectroscopy to investigate the link between the presence of epileptogenic foci and the occurrence of perfusion abnormalities (Steinhoff et al., 1996). Among the particularly encouraging results (Sokol et al., 2000) and cautious attempts to link hemodynamic parameters such as cerebral blood volume to the onset of seizures (Watanabe et al., 2000), this line of clinical research has always been very prolific, up today (Roche-Labarbe et al., 2008). Despite this, it must be pointed out that nowadays infrared spectroscopy rather should be considered an adjunct tool in the investigation of epilepsy, as it is certainly far from having reached diagnostic value.

Even psychiatry accepts the challenge of assessing the potential of Infrared Spectroscopy, and in 1997 the first article debating on this new opportunity is published (Hoch et al., 1997). The authors, already known for previous neurophysiological work employing spectroscopy, identify in the behavioral problems and in the most common psychiatric disorders a possible recipient of the optical imaging research.

In 1994 one first work studying schizophrenia is published (Okada et al.,1994). After few years, another one appears, that combines the study of perfusion abnormalities in schizophrenia with the use of a cognitive controlled protocol (Fallgatter and Strik, 2000). This is also a first enlightened hint at what will then become the practice: the use of cognitive controlled, and often computerized, protocols for the functional investigation of the brain. The possibility to evaluate the pathological deviations from physiology during specific cognitive tasks clearly opens up new questions and new perspectives in neuroscience in general, and in the application of optical imaging instruments particularly. Studies about the employment of Infrared spectroscopy in schizophrenia specifically focus on the deepening of processing abnormalities of exogenous information, and of the already well-known attention deficits (Shinba et al., 2004). As a result, the study of the frontal lobes is the most pursued (Shinba et al., 2004, Nishimura et al., 2011 for example).

In 2005 the first survey work on fNIRS imaging in ADHD (Attention Deficit/Hyperactivity Disorder) appears (Weber et al., 2005). This first work is followed by a number of studies (Ehlis et al. 2008; Schecklmann et al., 2010) that extend the investigation to the memory abilities of subjects, and to the longitudinality of cerebral hemodynamic correlates of ADHD up to adulthood. Even the more infrequent studies about autism finally enter the debate (Kita et al., 2011). Isolated employment of fNIRS to the study of depression(Eschweiler et al., 2000; Matsuo et al., 2000; Okada et al., 1996b),anorexia and other psychiatric disorders complete the picture of the existing literature.

A separate chapter would be deserved by the application of infrared spectroscopy to physical medicine and sports field, but this falls beyond the purpose of our work. It will also become clear that the possibility offered by infrared spectroscopy to assess perfusion and oxygenation of tissues is an attractive prospect for those who, for various reasons, are interested in the study of muscle tissue during exercise, with either the aim of enhancing the performance or of containing/slowing down the degeneration. A rich literature, perhaps more recent, exist on this subject. Here we will only mention a few references (Taelman et al. 2011; Yu et al., 2011).

Given that InfraRed spectroscopy alone cannot be a decisive tool in the diagnosis of a disease, and being ascertained that, even more so, none of the functional brain imaging techniques can fully explain the etiopathology, the new challenge of the study of the brain is the search for genetic bases resulting in functional abnormalities. With these premises, for example in the case of schizophrenia, during the last three years pioneering studies have been published that in some cases search for genetic polymorphisms related to metabolic processes and neuronal signalling (Reif et al., 2011, Takizawa et al ., 2009), while in some other cases even look into polyglutamine expansions in the genes coding for the binding protein of the TATA box (TBP) (Ohi et al., 2009) for an association with hemodynamic evidence revealed by Infrared Spectroscopy. What now seems to be a treasure hunt in the genome will be the new book to be written in the next decades.

1.4 Open issues in NIRS employment

1.4.1 Data integration

There are numerous sources of systemic signal interference that reduce sensitivity to weaker brain activation signals. These systemic signals include cardiac pulsations, respiration, and blood pressure variations, including Mayer waves with an approximately 10-s period and other slower variations. In humans, the cardiac pulsation typically has a period of 0.7 to 1.5 s and gives rise to a systemic transient arterial blood volume increase. Respiration typically has a period of 3 to 8 s and varies thoracic pressure causing a modulation of systemic venous blood volume and a delayed heart rate increase with a corresponding raise in blood pressure. The arterial blood pressure varies on multiple time scales including the cardiac pulsation, respiration and approximately 10-s Mayer waves (Obrig et al., 2000). An additional concern is that these systemic signals have been observed to phase-lock with certain types of stimuli, thus confounding the interpretation of the spatialtemporal maps of brain activation.

To improve the optical sensitivity to brain activation, as well as the interpretability of the measured hemodynamic response function, it is necessary to develop signal processing methods that distinguish the different source signals in space and time. While such approaches have been discussed extensively in the fMRI literature where the same systemic signals interfere with the brain activation signal (Lin et al., 2003; Thirion and

Faugeras, 2003), there has been little application to diffuse optical imaging. Barbour et al. (2001) have long argued that diffuse optical imaging methods can provide rich physiological information through analysis of the systemic dynamic vascular signals. Prince et al. (2003) have applied state space estimation techniques to the time-varying reconstruction to distinguish cardiac, respiratory, and brain activation signals. Zhang et al. (2004) used a principal component analysis (PCA) to determine the principle spatial components of the spatial-temporal covariance of baseline optical data, and then used it to filter systemic signal variation from optical data of brain activation. The one step further is the interpretation of the "disturbing" fringe biological contributions to the fNIRS signal as a valuable source of information, giving hints about the interplays standing between distinct body compartments. The first challenge discussed in the PhD thesis is the choice and employment of mathematical and statistical methods for the integration of biological information, and – specifically- for the fusion of NIRS data with other biological information. Data integration should not be interpreted as a strategy for graphical representation of a number of different data. Rather, it can be approached by applying mathematical and statistical methods for the concurrent processing of different sources of information. In this work, the use of proper methods, such as General Linear Models, and the manipulation of parameters for enhancement of data fusion will be discussed.

1.4.2 Technical and methodological issues

Several techniques have been developed to measure the hemodynamic response using NIRS: continuous wave, time-resolved, spatially-resolved and frequency-resolved spectroscopy (for review see Wolf et al., 2007). The majority of fNIRS research has been undertaken using continuous wave (cw) systems, as they provide the simplest approach. In addition to cw-NIRS systems, time-resolved (tr-NIRS) and frequency-resolved (fr-NIRS) spectrometers can be used to derive absolute concentrations of oxy and deoxy-hemoglobin.

The ambition and drive to use fNIRS for increasingly complex studies continuously fuels the development of technologies and methods. Practical issues that have arisen include:

1. the development of the probe and head gear to reduce the effects of movement (especially for children) and of parasitic environmental light;
2. the design of the study, considering the effects of boredom, anticipation and the synchronization of systemic/biorhythmic responses;
3. an understanding of the hemodynamic response and the interpretation of significant results;
4. and coregistration between the hemodynamic response measured at the surface of the head and the underlying cortical anatomy.

Recent work in various research labs has led to major progress in these areas. For example, the development of multiple source-detector separation arrays to investigate depth discrimination of the hemodynamic response; an ever-increasing number of channels allowing for a wider coverage of the head; and advances in the design of the headgear providing improved quality of the optical signals. This work will consider these methodological and technological advances with particular focus on studies in awake adults. Importantly we will highlight the advantages of using trNIRS for the study of the hemodynamics of the human brain, with respect to other non-optical techniques and to cw-fNIRS technology.

1.4.3 Cognitive load and activation patterns

Another open issue in neuroscience is the investigation of the modulatory effect risen in the cerebral hemodynamic pattern by means of a stimulation with differential cognitive load, i.e. with graded levels of cognitive difficulty. One aim of this work was to determine whether multichannel time domain fNIRS is capable to discern differences in frontal patterns of activation due to pure attentional, working memory and high cognitive tasks, and to assess time domain fNIRS sensitivity in detecting modulation effects induced by the demand of a cognitive task with graded levels of difficulty. This was done by focusing on frontal cortical activation during a n-back task with different stages of memory requirement.

1.4.4 Neurovascular Coupling

Neurovascular coupling refers to the relationship between local neural activity and subsequent changes in cerebral blood flow (CBF) in the brain. Indeed, it has been shown that brain activity is associated with focal cortical hyperemia, that is, the changes of neural electrical activity are coupled with a functionally induced focal cortical hyper-oxygenation (Sheth et al., 2004). Despite hemodynamic and electrical activities have been widely investigated individually, interesting physiological concerns could only be clarified by considering them conjointly. Unfortunately, the considerable differences existing between hemodynamic and electrical signals, their different physiological nature and time dynamics make it difficult to investigate neurovascular coupling as a whole. Despite fMRI is the gold standard for studying the hemodynamic transients in the brain, it shows many drawbacks: it is only sensitive to the blood vascular response, it has a low temporal resolution, and it gives indirect measures of oxygenation in the blood. In the present PhD work, we used the NIRS, detecting the changes in concentration of the two blood chromophores oxy and deoxygenated-hemoglobin (HbO and HHb), for the study of neurovascular coupling phenomena.

Temporal correlation

The fMRI–BOLD signal arises from the paramagnetic properties of deoxyhemoglobin, and thus a correlation is expected between the BOLD signal and the optical deoxyhemoglobin signal. In recent years, a number of studies have been published comparing hemoglobin concentration changes measured with NIRS and BOLD–fMRI signals in humans (Ye et al., 2009; Steinbrinket al., 2006; Strangman et al., 2002; Toronov et al., 2001; Kleinschmidt et al., 1996). While all theoretical studies to date support the expectation of a strong correlation between deoxyhemoglobin and BOLD, experimental confirmation remains controversial. In some publications, better temporal correlation between oxyhemoglobin and BOLD has been reported (Hoshi et al., 2001; Strangman et al., 2002), while others (Huppert et al., 2006; Toronov et al., 2003; Kleinschmidt et al., 1996; MacIntosh et al., 2003; Siegel et al., 2003; Toronov et al., 2001) have shown better correlation between BOLD and deoxyhemoglobin. The literature suggests this discrepancy could reflect the higher signal to noise ratio for HbO compared with HHb. Indeed, it is nowadays clear that in adults both HbO and HHb changes are correlated with BOLD fMRI signal changes.

It is known that a typical hemodynamic response to brain activation is initiated by an increase in blood flow and total hemoglobin (HbT) concentration, possibly preceded by an increase in oxygen consumption (Buxton et al., 1998; Malonek et al., 1997),followed by a venous washout of deoxyhemoglobin delayed by 1 to 2 s relative to the total hemoglobin increase (Frostig et al., 1990;Jasdzewski et al., 2003; Kwong et al., 1992; Malonek and Grinvald, 1996; Obrig et al., 1996; Ogawa et al., 1992; Wolf et al., 2002). The initial total hemoglobin increase occurs within the arterial vascular compartment and is concomitant with an increase in oxyhemoglobin. Oxyhemoglobin then increases above total

hemoglobin as it displaces deoxyhemoglobin from the veins. Thus, an fMRI and optical comparison with good temporal resolution and signal-to-noise ratio should be able to clearly distinguish a BOLD correlation with deoxyhemoglobin or oxyhemoglobin based on the early temporal response to brain activation. This comparison has been made with an event-related 2-s finger-tapping task by Huppert et al. (2004). Fig. 1.3. shows the typical hemodynamic response risen. The hemodynamic response begins within 1–3 s following the start of subject finger tapping, with the expected increase in oxyhemoglobin preceding that in deoxyhemoglobin by approximately 1.5 s. A cross-correlation comparison between normalized BOLD and optical response profiles showed significant differences from zero for the period 0- to 15-s poststimulus onset. The BOLD response was also shifted by 1.5 s relative to the onset of the oxyhemoglobin response and aligned fully with the deoxyhemoglobin profile, as shown in the normalized comparison of the responses in Fig. 1.3.These data clearly indicate that the BOLD signal correlates more strongly with the optical measurements of HHb than withHbO and HbT, in agreement with theoretical expectations.
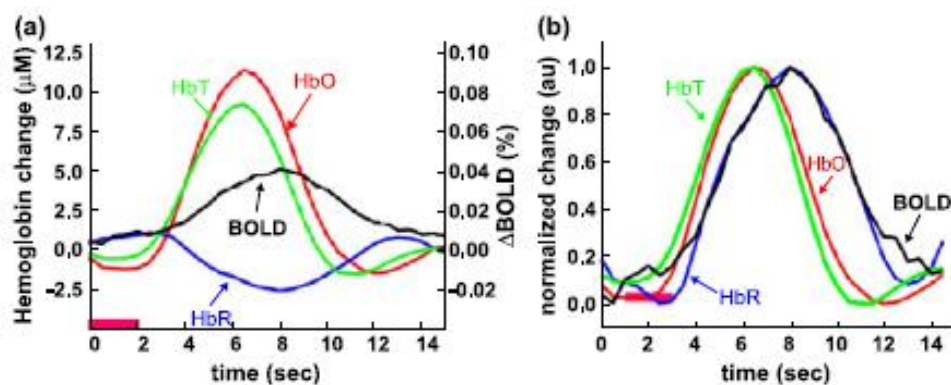

Fig.1.3. (a) Response functions of hemoglobin concentrations and BOLD for event-related finger tapping as measured through simultaneously acquired fMRI–BOLD and DOI optical recordings of the primary motor cortex. (b) Normalized and rescaled response functions for the event-related finger tapping to allow visualization of the four variables on the same linear scale. The deoxyhemoglobin data have also been inverted to emphasize the strong correlation between deoxyhemoglobin and BOLD. (Huppert et al., 2004)

Spatial correlation

Comparisons of the spatial correlation of fMRI and DOI are beginning to appear in the literature (Kleinschmidt et al., 1996;Strangman et al., 2002; Toronov et al., 2001).

While a qualitative spatial correlation is easy to observe, literature simultaneously applying fMRI and DOI often observes a displacement of 2 to 3 cm of the two activations. Theoretically, it is expected to find them spatially coregistered. This discrepancy could easily result from the spatial transformation between the MRI coordinate system and the DOI coordinate system. While the MRI coordinate system is in true 3D space, DOI images are usually produced assuming a flat planar surface underneath the array of sources and detectors. This distortion from the curved surface of the head to a flat surface could produce the spatial misregistration of fMRI and DOI that is often observed.

To overcome this problem, the optical images need to be reconstructed within the proper curved surface of the head and with the cortical constraint, since we know from simulation studies that otherwise the DOI depth will be incorrect.

Most importantly, in our work, we have been following the goal of isolating intra-cortical and extra-cortical NIRS information during physiologic cognitive effort by separating and studying, with a multi-channel trNIRS, "early photons" and "late photons" contributions to the impulse response emerging from the scalp. This procedure allowed the isolation of a "cleaned version" of the original NIRS signal, purged from non-cortical hemodynamic activation.

1.5 MOTIVATION

Why a thesis work on NIRS technique?

NIRS is promising the feasibility of diffuse optical methods employment as tools for assessing cognition and for imaging the brain in the neuroscience field. To realize their full potential, however, diffuse optical imaging methods need further development and implementation. In this PhD thesis work we will discuss the current methodological issues with diffuse optical imaging and the progress being made towards resolving some of them. We will also provide example results from activities carried on within the EU nEUROPt project. Specifically,

1. We will be about the discussion on defining the improvements brought about by *time resolved* trNIRS, with respect to the previous generation of *continuous wave* cwNIRS devices.

2. We will highlight the significant improvement in the quality of trNIRS signals provided by their separation in two different components, each of them either accounting for intra-cerebral or extracerebral compartment.

3. We will emphasize that partial volume error leads to an underestimate of the concentration changes. While this is well known, many papers still report quantitative units for concentrations changes, although only the relative units are accurate. We will also show that, generally, the relative accuracy is sufficient for brain activation studies.

4. We will discuss the strong presence of systemic physiological signals in the optical data, which interferes with estimates of the hemodynamic response to brain activation. We will then present examples of how straightforward signal processing can help to distinguish the different systemic physiological components from the brain activation signal. We will also show how to manipulate such annoying interferences, so as to ultimately turn to our advantage the presence of side systemic contributions and open a finer view on the tight interplays existing among physiological signals, thus enhancing our knowledge about the regulatory mechanisms of human body.

5. We will present our progress in the spatial-temporal correlation of trNIRS and EEG, EMG and ECG. Ultimately, the routine combination of trNIRS and the other signals will provide the unique chance to functionally identify the nature of neurovascular coupling, by assigning to any cortical neurovascular source further specification about its electrical and hemodynamic characteristics.

Bibliography

Bacon DS, Afifi MS, Griebel JA, Camporesi EM. Cerebrocortical oxygenation and ventilatory response during sustained hypoxia.RespirPhysiol. 1990 May-Jun;80(2-3):245-57.

Barbour, R.L., Graber, H.L., Pei, Y., Zhong, S., Schmitz, C.H., 2001. Optical tomographic imaging of dynamic features of dense-scattering media. J. Opt. Soc. Am. A, Opt. Image Sci. Vis. 18, 3018– 3036.

Buxton, R.B., Wong, E.C., Frank, L.R., 1998. Dynamics of blood flow andoxygenation changes during brain activation: the balloon model. Magn.Reson. Med. 39, 855– 864.

Colier, W.N., Quaresima, V., Oeseburg, B., Ferrari, M., 1999. Human motor-cortex oxygenation changes induced by cyclic coupled movements of hand and foot. Exp. Brain Res. 129, 457– 461.

Davis, T.L., Kwong, K.K., Weisskoff, R.M., Rosen, B.R., 1998. Calibrated functional MRI: mapping the dynamics of oxidative metabolism. Proc. Natl. Acad. Sci. U. S. A. 95, 1834–1839.

Edwards AD, Wyatt JS, Richardson C, Potter A, Cope M, Delpy DT, Reynolds EO. Effects of indomethacin on cerebral haemodynamics in very preterm infants. Lancet. 1990 Jun 23;335(8704):1491-5.

Ehlis AC, Bähne CG, Jacob CP, Herrmann MJ, Fallgatter AJ. Reduced lateral prefrontal activation in adult patients with attention-deficit/hyperactivity disorder (ADHD) during a working memory task: a functional near-infrared spectroscopy (fNIRS) study.J Psychiatr Res. 2008 Oct;42(13):1060-7.

Eschweiler, G.W., Wegerer, C., Schlotter, W., Spandl, C., Stevens, A., Bartels, M., Buchkremer, G., 2000. Left prefrontal activation predicts therapeutic effects of repetitive transcranial magnetic stimulation (rTMS) in major depression Psychiatry Res. Psychiatry Res. 99, 161– 172.

Fallgatter AJ, Strik WK. Reduced frontal functional asymmetry in schizophrenia during a cued continuous performance test assessed with near-infrared spectroscopy.Schizophr Bull. 2000;26(4):913-9.

Ferrari M, De Blasi RA, Safoue F, Wei Q, Zaccanti G. Towards human brain near infrared imaging: time resolved and unresolved spectroscopy during hypoxic hypoxia.AdvExp Med Biol. 1993;333:21-31.

Ferrari M, De Marchis C, Giannini I, Di Nicola A, Agostino R, Nodari S, Bucci G. Cerebral blood volume and hemoglobin oxygen saturation monitoring in neonatal brain by near IR spectroscopy.AdvExp Med Biol. 1986;200:203-11.

Ferrari M, Giannini I, Sideri G, Zanette E. Continuous non invasive monitoring of human brain by near infrared spectroscopy. AdvExp Med Biol. 1985;191:873-82.

Franceschini, M.A., Fantini, S., Thompson, J.H., Culver, J.P., Boas, D.A., 2003. Hemodynamic evoked response of the sensorimotor cortex measured non-invasively with near infrared optical imaging. Psychophysiology 40, 548–560.

Frostig, R.D., Lieke, E.E., Tso, D.Y., Grinvald, A., 1990. Cortical functional architecture and local coupling between neuronal activity and the microcirculation revealed by in vivo high-resolution optical imaging of intrinsic signals. Proc. Natl. Acad. Sci. U. S. A. 87, 6082– 6086.

Fukui, Y., Ajichi, Y., Okada, E., 2003. Monte Carlo prediction of near-infrared light propagation in realistic adult and neonatal head models. Appl. Opt. 42, 2881–2887.

Heekeren, H.R., Obrig, H., Wenzel, R., Eberle, K., Ruben, J., Villringer, K., Kurth, R., Villringer, A., 1997. Cerebral haemoglobin oxygenation during sustained visual stimulation—A near-infrared spectroscopy study. Philos. Trans. R. Soc. Lond., B Biol. Sci. 352, 743– 750.

Hirth, C., Obrig, H., Villringer, K., Thiel, A., Bernarding, J., Muhlnickel, W., Flor, H., Dirnagl, U., Villringer, A., 1996. Non-invasive functional mapping of the human motor cortex using near-infrared spectroscopy. NeuroReport 7, 1977–1981.

Hock C, Villringer K, Heekeren H, Hofmann M, Wenzel R, Villringer A, Müller-Spahn F. A role for near infrared spectroscopy in psychiatry?AdvExp Med Biol. 1997;413:105-23. Review.

Hoge, R.D., Atkinson, J., Gill, B., Crelier, G.R., Marrett, S., Pike, G.B., 1999. Linear coupling between cerebral blood flow and oxygen consumption in activated human cortex. Proc. Natl. Acad. Sci. U. S. A. 96, 9403– 9408.

Hoshi Y. Functional near-infrared spectroscopy: potential and limitations in neuroimaging studies.Int Rev Neurobiol. 2005;66:237-66. Review.

Hoshi, Y., Kobayashi, N., Tamura, M., 2001. Interpretation of near-infraredspectroscopy signals: a study with a newly developed perfused rat brainmodel. J. Appl. Physiol. 90, 1657–1662.

Huettel, S.A., Song, A.W., McCarthy, G., 2003. Functional Magnetic Resonance Imaging. Sinaur Associates Inc., Sunderland, MA.

Huppert, T.J., Hoge, R.D., Diamond, S.G., Franceschini, M.A., Boas, D.A., 2006. A temporal comparison of BOLD, ASL and NIRS haemodynamic responses to motor stimuli in adult humans. NeuroImage 29, 368– 382.

Huppert, T.J., Hoge, R.D., Diamond, S.G., Franceschini, M.A., Boas, D.A., 2006. Atemporal comparison of BOLD, ASL and NIRS haemodynamic responses tomotor stimuli in adult humans. NeuroImage 29, 368–382.

Huppert, T.J., Hoge, R.D., Franceschini, M.A., Boas, D.A., 2004. A temporal comparison of simultaneously acquired BOLD fMRI and near infrared spectroscopy (NIRS) hemodynamic response functions. Neuro-Image, Suppl. 1, 24.

Jackson PA, Reay JL, Scholey AB, Kennedy DO. DHA-rich oil modulates the cerebral haemodynamic response to cognitive tasks in healthy young adults: a near IR spectroscopy pilot study. Br J Nutr. 2011 Oct 3:1-6.

Jasdzewski, G., Strangman, G., Wagner, J., Kwong, K.K., Poldrack, R.A., Boas, D.A., 2003. Differences in the hemodynamic response to eventrelated motor and visual paradigms as measured by near-infrared spectroscopy. NeuroImage 20, 479–488.

JobsisFF. Noninvasive, infrared monitoring of cerebral and myocardial oxygen sufficiency and circulatory parameters. Science 1977;198:1264-7.

Kita Y, Gunji A, Inoue Y, Goto T, Sakihara K, Kaga M, Inagaki M, Hosokawa T. Self-face recognition in children with autism spectrum disorders: A near-infrared spectroscopy study.Brain Dev. 2011 Jun;33(6):494-503.

Kleinschmidt, A., Obrig, H., Requardt, M., Merboldt, K.D., Dirnagl, U., Villringer, A., Frahm, J., 1996. Simultaneous recording of cerebral blood oxygenation changes during human brain activation by magnetic resonance imaging and near-infrared spectroscopy. J. Cereb. Blood Flow Metab. 16, 817– 826.

Kleinschmidt, A., Obrig, H., Requardt, M., Merboldt, K.D., Dirnagl, U., Villringer, A., Frahm, J., 1996. Simultaneous recording of cerebral blood oxygenation changes during human brain activation by magnetic resonance imaging and near-infrared spectroscopy. J. Cereb. Blood Flow Metab. 16, 817– 826.

Kwong, K.K., Belliveau, J.W., Chesler, D.A., Goldberg, I.E., Weisskoff, R.M., Poncelet, B.P., Kennedy, D.N., Hoppel, B.E., Cohen,M.S., Turner, R., Cheng, H.-M., Brady, T.J., Rosen, B.R., 1992. Dynamic magnetic resonance imaging of human brain activity during primary sensory stimulation. Proc. Natl. Acad. Sci. U. S. A.

Lin, F.H., McIntosh, A.R., Agnew, J.A., Eden, G.F., Zeffiro, T.A., Belliveau, J.W., 2003. Multivariate analysis of neuronal interactions in the generalized partial least squares framework: simulations and empirical studies. NeuroImage 20, 625– 642.

MacIntosh, B.J., Klassen, L.M., Menon, R.S., 2003. Transient hemodynamicsduring a breath hold challenge in a two part functional imagingstudy with simultaneous near-infrared spectroscopy in adult humans.NeuroImage 20, 1246–1252.

Malonek, D., Dirnagl, U., Lindauer, U., Yamada, K., Kanno, I., Grinvald, A., 1997. Vascular imprints of neuronal activity: relationships betweenthe dynamics of cortical blood flow, oxygenation, and volume changes following sensory stimulation. Proc. Natl. Acad. Sci. U. S. A. 94, 14826– 14831.

Malonek, D., Grinvald, A., 1996. Interactions between electrical activit and cortical microcirculation revealed by imaging spectroscopy: implications for functional brain mapping. Science 272, 551– 554.

Matsuo, K., Kato, T., Fukuda, M., Kato, N., 2000. Alteration of hemoglobin oxygenation in the frontal region in elderly depressed patients asmeasured by near-infrared spectroscopy. J. Neuropsychiatry Clin. Neurosci. 12, 465–471.

Meek, J.H., Elwell, C.E., Khan, M.J., Romaya, J., Wyatt, J.S., Delpy, D.T., Zeki, S., 1995. Regional changes in cerebral haemodynamics as a result of a visual stimulus measured by near infrared spectroscopy. Proc. R. Soc. Lond., B 261, 351–356.

Minagawa-Kawai, Y., Mori, K., Hebden, J.C., Dupoux, E., 2008. Optical imaging of infants' neurocognitive development: recent advances and perspectives. Dev. Neurobiol. 68, 712–728.

Moosmann, M., Ritter, R., Krastel, I., Brink, A., Thees, S., Blankenburg, F., Taskina, B., Obrig, H., Villringer, A., 2003. Correlates of alpha rhythm in functional magneticresonance imaging and near infrared spectroscopy. Neuroimage 20, 145–158.

Nishimura Y, Takizawa R, Muroi M, Marumo K, Kinou M, Kasai K. Prefrontal cortex activity during response inhibition associated with excitement symptoms in schizophrenia.Brain Res. 2011 Jan 25;1370:194-203.

Obrig, H., Hirth, C., Junge-Hulsing, J.G., Doge, C., Wolf, T., Dirnagl, U., Villringer, A., 1996. Cerebral oxygenation changes in response to motor stimulation. J. Appl. Physiol. 81, 1174– 1183.

Obrig, H., Neufang, M., Wenzel, R., Kohl, M., Steinbrink, J., Einhaupl, K., Villringer, A., 2000. Spontaneous low frequency oscillations of cerebral hemodynamics and metabolism in human adults. NeuroImage 12, 623–639.

Ogawa, S., Tank, D., Menon, R., Ellermann, J., Kim, S.-G., Merkel, H., Ugurbil, K., 1992. Intrinsic signal changes accompanying sensory stimulation: functional brain mapping with magnetic resonance imaging. Proc. Natl. Acad. Sci. 89, 5951–5955.

Ohi K, Hashimoto R, Yasuda Y, Kiribayashi M, Iike N, Yoshida T, Azechi M, Ikezawa K, Takahashi H, Morihara T, Ishii R, Tagami S, Iwase M, Okochi M, Kamino K, Kazui H, Tanaka T, Kudo T, Takeda M. TATA box-binding protein gene is associated with risk for schizophrenia, age at onset and prefrontal function.Genes Brain Behav. 2009 Jun;8(4):473-80.

Okada, F., Takahashi, N., Tokumitsu, Y., 1996. Dominance of the dnondominantT hemisphere in depression. J. Affect Disord. 37, 13–21.

Okada, F., Tokumitsu, Y., Hoshi, Y., Tamura, M., 1994. Impaired interhemispheric integration in brain oxygenation and hemodynamics in schizophrenia. Eur. Arch. Psychiatry Clin. Neurosci. 244, 17–25.

Prince, S., Kolehmainen, V., Kaipio, J.P., Franceschini, M.A., Boas, D., Arridge, S.R., 2003. Time-series estimation of biological factors in optical diffusion tomography. Phys. Med. Biol. 48, 1491–1504.

*Reif A, Schecklmann M, Eirich E, Jacob CP, Jarczok TA, Kittel-Schneider S, Lesch KP, Fallgatter AJ, Ehlis AC. A functional promoter polymorphism of neuronal nitric oxide synthase moderates prefrontal functioning in schizophrenia.*Int J Neuropsychopharmacol. *2011 Feb 1:1-11.*

*Roche-Labarbe N, Zaaimi B, Berquin P, Nehlig A, Grebe R, Wallois F. NIRS-measured oxy- and deoxyhemoglobin changes associated with EEG spike-and-wave discharges in children.*Epilepsia. *2008 Nov;49(11):1871-80.*

Ruben, J., Wenzel, R., Obrig, H., Villringer, K., Bernarding, J., Hirth, C., Heekeren, H., Dirnagl, U., Villringer, A., 1997. Haemoglobin oxygenation changes during visual stimulation in the occipital cortex. Adv. Exp. Med. Biol. 428, 181–187.

Sakatani, K., Chen, S., Lichty, W., Zuo, H., Wang, Y.P., 1999. Cerebral blood oxygenation changes induced by auditory stimulation in newborn infants measured by near infrared spectroscopy. Early Hum. Dev. 55, 229– 236.

Sander T.H., Liebert A., Burghoff M.,Wabnitz H.,Macdonald R., Trahms L., 2007, Cross-correlation analysis of the correspondence between magnetoencephalographic and near-infrared cortical signals.Methods Inf Med, 46:164-168.

Sato, H., Takeuchi, T., Sakai, K.L., 1999. Temporal cortex activation during speech recognition: an optical topography study. Cognition 73, B55– B66.

*Schecklmann M, Romanos M, Bretscher F, Plichta MM, Warnke A, Fallgatter AJ. Prefrontal oxygenation during working memory in ADHD.*J Psychiatr Res. *2010 Jul;44(10):621-8.*

Sheth, S.A., et al., 2004. Linear and nonlinear relationships between neuronal activity, oxygen metabolism, and hemodynamic responses. Neuron 42, 347-355.

*Shinba T, Nagano M, Kariya N, Ogawa K, Shinozaki T, Shimosato S, Hoshi Y. Near-infrared spectroscopy analysis of frontal lobe dysfunction in schizophrenia.*Biol Psychiatry. *2004 Jan 15;55(2):154-64.*

*Shinba T, Nagano M, Kariya N, Ogawa K, Shinozaki T, Shimosato S, Hoshi Y.Near-infrared spectroscopy analysis of frontal lobe dysfunction in schizophrenia.*Biol Psychiatry. *2004 Jan 15;55(2):154-64.*

Siegel, A.M., Culver, J.P., Mandeville, J.B., Boas, D.A., 2003. Temporalcomparison of functional brain imaging with diffuse optical tomographyand fMRI during rat forepaw stimulation. Phys. Med. Biol. 48,1391– 1403.

*Sokol DK, Markand ON, Daly EC, Luerssen TG, Malkoff MD. Near infrared spectroscopy (NIRS) distinguishes seizure types.*Seizure. *2000 Jul;9(5):323-7.*

Steinbrink, J., Villringer, A., Kempf, F., Haux, D., Boden, S., Obrig, H., 2006. Iluminating the BOLD signal: combined fMRI-fNIRS studies. Magn. Reson. Imag. 24, 495–505.

Steinbrink, J., Villringer, A., Kempf, F., Haux, D., Boden, S., Obrig, H., 2006. Iluminatingthe BOLD signal: combined fMRI-fNIRS studies. Magn. Reson. Imag. 24, 495–505.

Steinhoff BJ, Herrendorf G, Kurth C. Ictal near infrared spectroscopy in temporal lobe epilepsy: a pilot study. Seizure. *1996 Jun;5(2):97-101.*

Strangman, G., Culver, J.P., Thompson, J.H., Boas, D.A., 2002. A quantitative comparison of simultaneous BOLD fMRI and NIRS recordings during functional brain activation. NeuroImage 17, 719–731.

*Taelman J, Vanderhaegen J, Robijns M, Naulaers G, Spaepen A, Van Huffel S. Estimation of muscle fatigue using surface electromyography and near-infrared spectroscopy.*AdvExp Med Biol. *2011;915:353-9.*

Takizawa R, Hashimoto K, Tochigi M, Kawakubo Y, Marumo K, Sasaki T, Fukuda M, Kasai K. Association between sigma-1 receptor gene polymorphism and prefrontal hemodynamic response induced by cognitive activation in schizophrenia.ProgNeuropsychopharmacolBiol Psychiatry. 2009 Apr 30;33(3):491-8.

Thirion, B., Faugeras, O., 2003. Dynamical components analysis of fMRI data through kernel PCA. NeuroImage 20, 34– 49.

Toronov, V., Walker, S., Gupta, R., Choi, J.H., Gratton, E., Hueber, D., Webb, A., 2003.The roles of changes in deoxyhemoglobin concentration and regional cerebralblood volume in the fMRI BOLD signal. NeuroImage 19, 1521–1531.

Toronov, V., Webb, A., Choi, J.H., Wolf, M., Michalos, A., Gratton, E., Hueber, D., 2001. Investigation of human brain hemodynamics by simultaneous near-infrared spectroscopy and functional magnetic resonance imaging. Med. Phys. 28, 521– 527.

Toronov, V., Webb, A., Choi, J.H., Wolf, M., Michalos, A., Gratton, E.,Hueber, D., 2001. Investigation of human brain hemodynamics bysimultaneous near-infrared spectroscopy and functional magneticresonance imaging. Med. Phys. 28, 521– 527.

Villringer A. Understanding functional neuroimaging methods based on neurovascular coupling. AdvExp Med Biol. 1997;413:177-93.

Villringer, A., Chance, B., 1997. Noninvasive optical spectroscopy and imaging of human brain function. Trends Neurosci. 20, 435–442.

Walsh, V., Cowey, A., 2000. Transcranial magnetic stimulation and cognitive neuroscience. Nat Rev Neurosci 1, 73–79.

Watanabe E, Maki A, Kawaguchi F, Yamashita Y, Koizumi H, Mayanagi Y. Noninvasive cerebral blood volume measurement during seizures using multichannel near infrared spectroscopic topography.J Biomed Opt. 2000 Jul;5(3):287-90.

Weber P, Lütschg J, Fahnenstich H. Cerebral hemodynamic changes in response to an executive function task in children with attention-deficit hyperactivity disorder measured by near-infrared spectroscopy.J DevBehavPediatr. 2005 Apr;26(2):105-11.

Weishaupt, D., Kchli, V.D., Marincek, B., 2008. How Does MRI Work? An Introduction to the Physics and Function of Magnetic Resonance Imaging. Springer–Verlag, Berlin Heidelberg. Wilcox, T., Bortfeld, H., Woods, 89, 5675– 5679.

Wolf, M., Ferrari, M., Quaresima, V., 2007. Progress of near-infrared spectroscopy and topography for brain and muscle clinical applications. J. Biomed. Opt. 12 062104-1-14.

Wolf, M., Wolf, U., Toronov, V., Michalos, A., Paunescu, L.A., Choi, J.H., Gratton, E., 2002. Different time evolution of oxyhemoglobin anddeoxyhemoglobin concentration changes in the visual and motor cortices during functional stimulation: a near-infrared spectroscopy study. NeuroImage 16, 704– 712.

Ye, J.C., Tak, S.H., Jang, K.E., Jung, J.W., Jang, J.D., 2009. NIRS-SPM: statisticalparametric mapping for near-infrared spectroscopy. NeuroImage 44, 428–447.

Yu G, Shang Y, Zhao Y, Cheng R, Dong L, Saha SP. Intraoperative evaluation of revascularization effect on ischemic muscle hemodynamics using near-infrared diffuse optical spectroscopies.J Biomed Opt. 2011 Feb;16(2):027004.

Zhang, Y., Brooks, D.H., Franceschini, M.A., Boas, D.A., 2004. Eigenvector-based spatial filtering for reduction of physiological interference in diffuse optical imaging. J. Biomed. Opt.

Protocols

During the first year of the PhD course, part of the efforts were addressed to the creation of a small database of computerized audio-visual tests for neuropsychological assessment. This battery was initially created by using a specific licensed software environment (Presentation®, NeourobehaviouralSystems Inc, Albany, CA), while afterwards some of the algorithms were translated into MATLAB code for a larger diffusion to clinics, and for a better sharing with other research groups.

The availability of computerized routines offers some advantages, which have been irremissible in our research activity:

- The possibility to synchronize the behavioral task (i.e. subjects' cognitive activity) to the NIRS hardware;
- The possibility to synchronize the task to more than one recording device, thus allowing multimodal data recording for a direct comparison of NIRS tracks with signals acquired by other techniques;
- The possibility of event-related data processing (i.e., the processing of tracks with reference to the protocol design, to rest and activity time intervals, to the timing of the endogenous or exogenous stimuli, etc.)

Last, the majority of computerized tests were built as a precise replica of some published versions of the same tests. Though, in the case of The Divided Attention Test (Zimmermann and Fimm, 1992), a modified version was created, due to some limitations declared by the same authors. In this last case, a validation trial was set up, before using the modified test for data acquisition.

2.1 The Continuous Performance Task

The task consisted in watching a sequence of alphabetical letters, randomly presented in the central portion of a computer screen. The subject was seated in front of the screen. He had to click the left mouse button as fast as he could, whenever the letter X appeared (Rosvold et al., 1956). Letters were presented with inter stimulus interval (ISI) of 1, 2 or 4 s and remained on the screen for 250 ms (stimulus duration). A total of 234 letters were presented, with probability of critical stimulus set at 15%. The activation task was organized in 6 blocks, each of them lasting 91 s and containing 39 letters. Activation blocks were interleaved by rest intervals lasting 90 s. An initial baseline lasting 2 min and a final recovery period lasting 8 min were also recorded at the beginning and at the end of the test respectively, for a total protocol duration of 20 min. During baseline and recovery, the subjects were presented a meaningless image (differently oriented geometrical lines)to which no response was required (Fig.2.1).
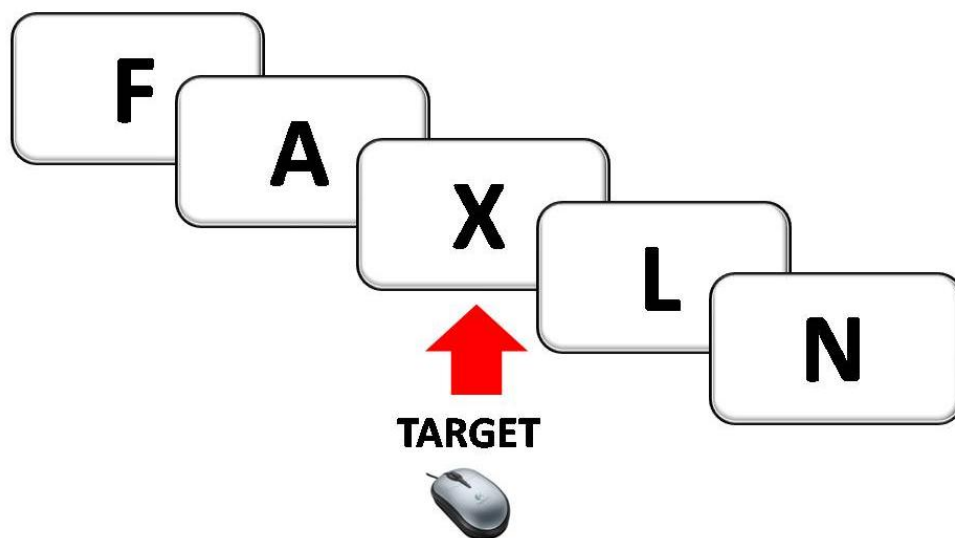
Fig.2.1. CPT test for sustained attention assessment. Subjects have to press the left mouse button whenever X letter appears on the computer screen.

2.2 The Conners' Continuous Performance Task

This second task was based on the 'not-X' version of the Continuous Performance Test (CPT), often called the Conners' CPT (Conners, 1994). The same test described above (Fig.2.1), with a different letter randomization, was presented. Different instructions were yet given: in this case, the subject had to click the left mouse button as fast as he could whenever a letter appeared and not to press any key at the appearance of the target letter X. This version of the CPT was specifically created at the purpose to study response-retention, and is usually administered whenever a deficit in inhibition is suspected (Ballard, 2001).

2.3 The N-back Task

Each participant was given a computerized variant of the n-back task using letters of the English alphabet as memoranda (Cohen et al., 1997). N-back task is a verbal memory test which provides four levels of memory load (0-, 1-, 2-, and 3-back), presented in a factorial design. It yields a total of eight task blocks (4 conditions, repeated twice). For each difficulty modality, computerized lists of 30 stimuli were constructed and then presented in a pseudorandom order, making up a total of 240 intermingled letters shown to the subject. A block of a single condition lasted 67 s, consisting of 5 s presentation of task instructions (e.g., "2-back letter task"), followed by 2 s pause and then 30 stimuli (250 ms presentation of a stimulus, followed by a 1750 ms blank-screen interstimulus interval - ISI). Each block of a single condition was presented separately and between the blocks a rest of 30 s was given. 60 s baseline and 60 s recovery were acquired at the start and at the end of the test, for a total acquisition time of 16 min.

At the end of the first four blocks (0-, 2-, 1-, and 3-back), in the middle of the test, subjects saw the word REST for approximately 90 s before the same four blocks, in different order (2-, 1-, 3-, and 0-back) began, providing a supplementary rest period. On each trial, subjects observed stimuli presented in the centre of a computer screen (Presentation software, by Neurobehavioral Systems). Letters were presented in a 24-point Helvetica font. Subjects responded to each stimulus presentation by pressing the left or right button on the mouse held in their right hand. To respond to a stimulus as a target, subjects pressed the button under their index finger (left button); to respond to a stimulus as a non-target, they pressed the button under their middle finger (right button) (Cohen et al., 1994). In the 0-back condition, the target letter was any letter that matched the one specified during the instructions given at the beginning of the block (in this test was letter "A"). In the 1-back condition, the target was any stimulus identical to the immediately preceding stimulus. In the 2-back and 3-back conditions, the target was any stimulus identical to the stimulus presented two or three trials prior, respectively (Fig.2.2). Stimuli were targets on 20% of trials, at all levels of load (every condition).

Subject performance during recording was monitored in terms of reaction time and accuracy (number of target letters identified correctly). Any correct reaction to the stimulus (both target and non-target) was a *commission*; any incorrect answer to the stimulus was a *commission error*. Any missing response (to both target and non-target stimuli) was an *omission error*.

Prior to beginning the experimental task, all participants were trained on the task and were given a pre-testing session to ensure that they had satisfactory understanding of the instructions.

It is well established that *n*-back task utilizes executive functions (Cohen et al., 1994), and that this functions are located in prefrontal cortex (Luria, 1980).

2.4 The Modified Divided Attention Test

The Divided Attention Test (TDA) used in this study is a modification of a computerized attention test battery developed by Zimmermann and Fimm (1992). The original test was modified in order to improve its difficulty, because of the behavioural results of the original version reported in Loose et al. (1993).
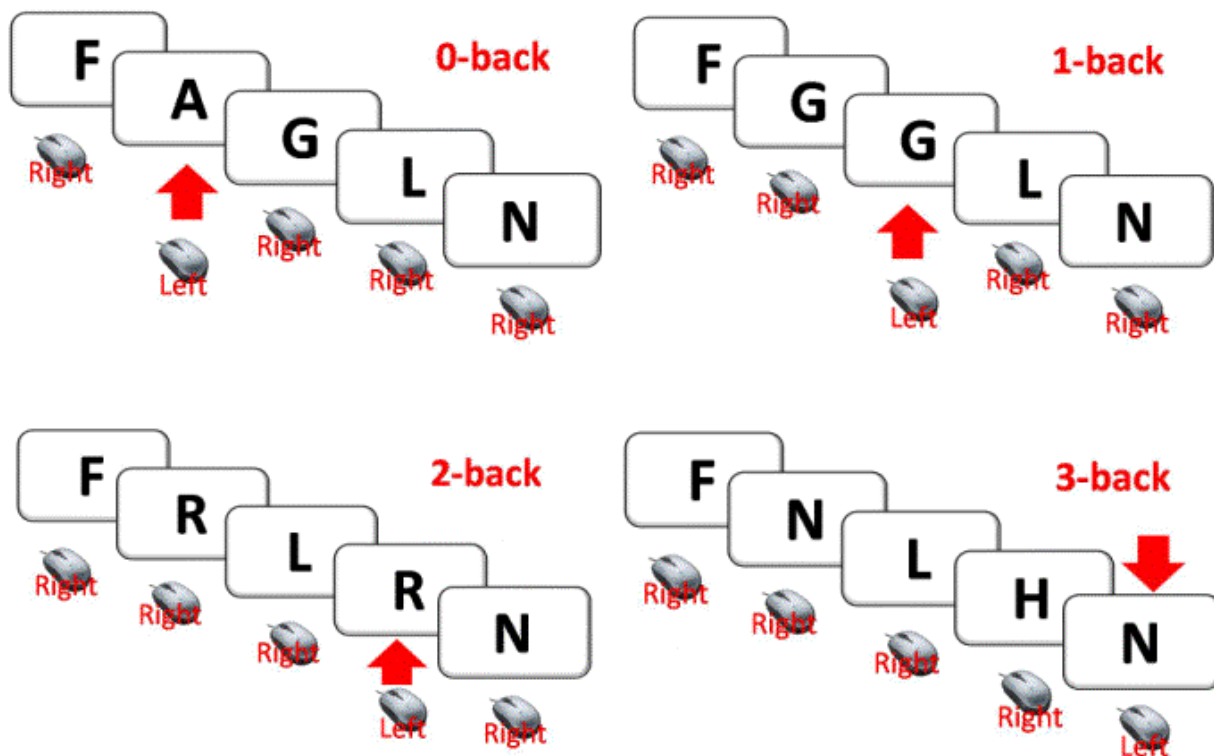
Fig.2.2. N-back test for attention and working-memory assessment. 0-back condition allows the evaluation of pure attention; higher loads require increasing working memory resources for both delay and recall.

Our test was composed by a 86 seconds baseline rest period followed by five blocks of task (165 seconds each) alternated with four 85 seconds rest periods. At the end of the test a 300 seconds recovery period was provided.

Each block of task was composed by 60 couples of auditory and visual stimuli. The auditory stimulus consisted of two frequency tones, low or high (1000 or 1500 Hz). Each tone lasted 100 ms. Target auditory stimulus was represented by two stimuli of different frequency. The subjects were asked to press a button with the middle finger of the right hand as quickly as possible when an auditory target stimulus was presented.

The visual stimulus consisted of seventeen white crosses in a black background. The target stimulus occurred when a cross was replaced with a white circle. The subjects were asked to press a button with the right index finger to recognize it. The visual stimulus was presented simultaneously with the second frequency tone and it lasted for 1,5 seconds. The interstimulus interval was 1,05 seconds. Figure 2.3 shows a schematic representation of the test.Each block of task was composed by 5 target visual or auditory stimuli and 55 non-target ones. Target auditory and visual stimuli were never presented at the same time. The test was presented on a computer screen using the software Presentation (Neourobehavioural Systems Inc, Albany, CA) and the subjects were provided with earphones in order to hear the frequency tones.
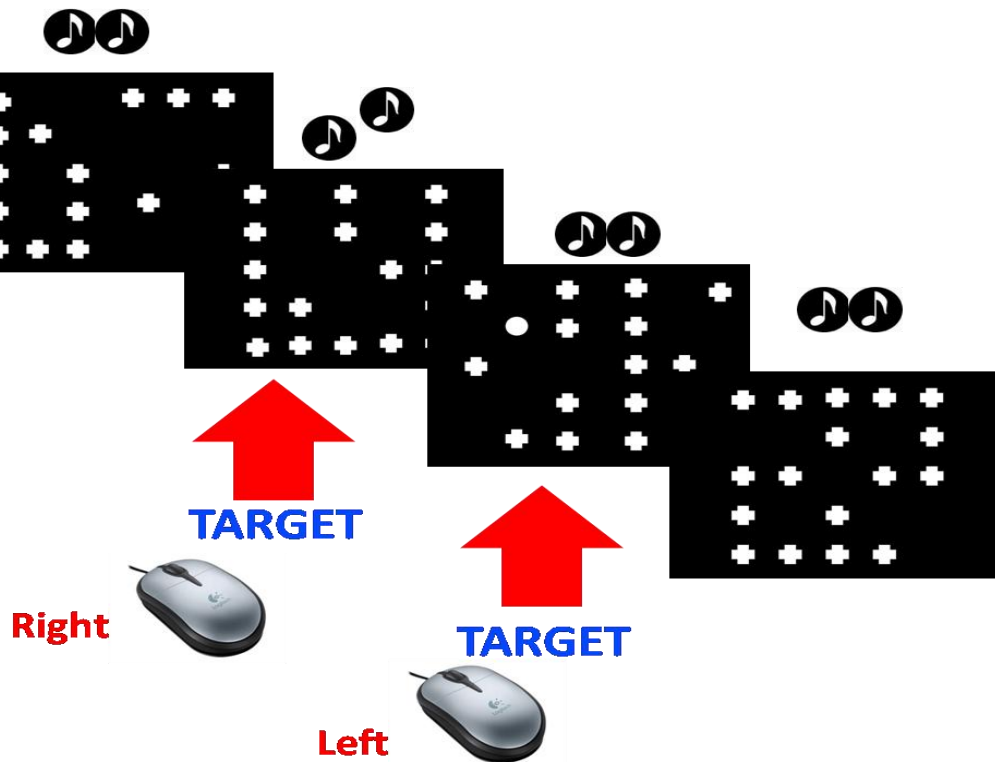
2.5 The Handgrip Task

The subjects were seated on a comfortable chair with their upper limbs laid on the table and with an elbow angle of 90 degrees. A 17" touch-screen monitor was placed in front of them. The test consisted in 3 conditions: (1) handgrip with the right hand, (2) handgrip with the left hand and (3) alternated handgrip, using both the hands.

The first condition started with 75 s initial baseline. Then, one activity period lasting 30s followed, in which subjects were asked to perform some handgrip movements with the right hand, at the frequency of approximately 2 Hz. Then, 30s rest was designed. This combination of 30s activation and 30s rest periods was repeated 10 times. Afterwards, 60s final rest ended the test.

This structure was maintained for the left handgrip condition. In this case, during the 10 activation periods, the subjects performed handgrip movements with their left hand.

Last, the third condition was built as follows. Itstarted with 75 s initial baseline. Then, one activity period lasting 30s followed, in which subjects were asked to perform some handgrip movements with the right hand, at the frequency of approximately 2 Hz. During the following 30s period, they were asked to perform the handgrip movements with the left hand, at the same frequency. This combination of 30s right handgrip and 30s left handgrip periods was repeated 10 times. No resting periods were done between task blocks. Afterwards, 60s final rest ended the test.

2.6 The Valsalva Maneuver

The subjects were seated on a comfortable chair.After a ten minutes habituation period at rest, a baseline period of spontaneous vasomotion was considered (10 minutes at rest). At the end of this baseline recording period, all subjects were asked to execute a forced expiratory Valsalva Maneuver (VM) for 15 seconds. The VM is performed by doing a moderately forceful attempted exhalation against a closed airway (i.e. with nose and mouth shut). Then the recovery baseline followed for 10 minutes, before the end of the experiment. VM is a test of autonomic nervous control of the heart.

Bibliography

Ballard J. C., "Assessing attention: comparison of response-inhibition and traditional continuous performance tests," J ClinExpNeuropsychol. Jun;**23**(3):331-50 (2001).

Cohen J.D., Forman S.D., Braver T.S., Casey B.J., Servan-Schreiber D., and Noll D.C., "Activation of prefrontal cortex in a nonspatial working memory task with fMRI," Hum. Brain Mapp. 1: 293–304, (1994).

Cohen J.D., Perlstein W.M., Braver T.S., Nystrom L.E., Noll D.C., Jonides J., and Smith E.E., "Temporal dynamics of brain activation during a working memory task," Nature. 386: 604–608, (1997).

Conners C.K., "The Conners continuous performance test," Toronto, Canada: Multi-Health Systems, (1994).

Loose R., Kaufmann C., Auer D.P., Lange K.W. 2003. Human prefrontal and sensory cortical activity during divided attention tasks, Human Brain Mapping 18:249-259.

Luria A.R., "Higher cortical funtions in man," New York: Basic Books; (1980).

Rosvold, H. E., Mirsky, A. F., Sarason, I., Bransome Jr., E. D., & Beck, L. H. (1956). A continuous performance test of brain damage. Journal of Consulting and Clinical Psychology, 20, 343–350.

Zimmermann P., Fimm B. 1992. Handbuch der testbatterie sur Aufmerksamkeitsprüfung [Manual for the attention assessment test battery], Psytest, Herzogenrath.

Methods

>>KeyPoints

> near infrared Spectroscopy is an **optical method** based on the measurement of photons transmitted in biological media. Its functioning is based on the exploitation of the optical absorbance and the scattering properties of tissues.

> HbO, HHb and HbT can be extracted by applying the **Lambert-Beer Law** and some layered model of the head.

> **Time resolved NIRS** acquires the temporal response of the tissue following the injection of a brief light pulse.

> Near infrared spectroscopy signal can be processed by means of **General Linear Model**, in order to statistically verify and localize HbO, HHb and HbT activations.

> Biological data can be pre-processed and **integrated** by means of GLM, in order to study interactions with NIRS signal.

The Near-Infrared (NIR) range of the light spectrum is an open window on the living tissues. Indeed, after Jöbsis observations, we nowadays know that light in the Near-Infrared frequencies has an increased ability to penetrate biological media. By the exploitation of the optical absorbance and the scattering properties of tissues, optical methods can thus help in the assessment of brain functionality. Being the retrieved information directly related to changes in the tissue optical parameters, it mainly embeds hemodynamics, while it fails in accounting for electrical phenomena.

Specifically, one of the major targets of Near-Infrared light is hemoglobin, on its turn very closely related to the cerebral vascular response. Near Infrared Spectroscopy, indeed, can discern between oxygenated and deoxygenated hemoglobin, thus providing in the latter case a signal very similar to BOLD information obtained by means of fMRI technique.

The development of software tools for NIRS data processing is recent, if compared to fMRI applications. Many efforts have been made in order to provide the research community with some comprehensive tools. Nevertheless, a complete standardization of procedures has still to be reached. In the present chapter, we will summarize the NIRS working principle and the model for hemoglobin signal extraction from light. Then a description of General Linear Model for NIRS data processing will be presented, together with one implementation. Last, some advanced GLM processing for data integration will be described.

3.1 NIRS working principle

The measurement of tissue oxygen saturation and tissue hemoglobin content in the brain is determined by computing the difference in intensity between a transmitted (I_0) and received (I) light, delivered at specific wavelengths.
According to the Lambert-Beer law, each layer of tissue absorbs a certain amount of light:

$$dI = -\mu_a I dz \tag{1}$$

Where *dz* is a distance, and μ_a is a tissue-specific constant, named absorption coefficient (cm^{-1}) and depending on the wavelength λ. Then:

$$\frac{dI}{I} = -\mu_a dz \tag{2}$$

$$\int_{I_0}^{I_l} \frac{dI}{I} = \int_l -\mu_a dz \tag{3}$$

$$ln\frac{I_1}{I_0} = -\mu_a l \tag{4}$$

being l (cm) the distance travelled by the light beam through the medium.
According to the Lambert-Beer law, though, μ_a can be seen as the inverse of the average path length travelled by a photon before being absorbed. Thus, μ_a can be regarded as the product of the cromophores concentration C (mol/l) and the molar extinction coefficient ε (cm^{-1}M^{-1}).

$$\mu_a = C\varepsilon \tag{5}$$

On the other hand, light travelling through living tissues comes across more than one cromophore. In this case, the contribution of each cromophore has to be taken into account, and the total absorption coefficient becomes a linear combination of many specific absorptions:

$$\mu_a = C_1\varepsilon_1 + C_2\varepsilon_2 + ... \tag{6}$$

Consequently, attenuation measurements have to be done at many wavelengths, so as to obtain concentration values of all the cromophores.
Last, the adimensional parameter A, called *absorbance*, is defined. Its definition is usually introduced for equations simplification:

$$A = ln\frac{I_0}{I_1} = \mu_0 l \tag{7}$$

When probing the brain, lights comes across hemoglobin. This latter can be either bonding oxygen (oxygenated hemoglobin or HbO) or not (deoxygenated hemoglobin or HHb). HbO and HHb have to be considered as two different cromophores, because NIRS can discern between them. It follows that two operating wavelength are needed, in order to later extract NIRS information, specifically for HbO and HHb.
Equation (6) becomes in this case:

$$\mu_a = \mu_a^{HbO} + \mu_a^{HHb} \qquad (8)$$

And thus:

$$\mu_a(\lambda) = C_{HbO}\mu_{HbO}(\lambda) + C_{HHb}\mu_{HHb}(\lambda) \qquad (9)$$

Highlighting the dependence on the wavelength.
For two different wavelengths, a system of two equations is obtained:

$$\begin{cases} A_1 = \left(C_{HbO}\varepsilon_{HbO}(\lambda_1) + C_{HHb}\varepsilon_{HHb}(\lambda_1)\right) \cdot l \\ A_2 = \left(C_{HbO}\varepsilon_{HbO}(\lambda_2) + C_{HHb}\varepsilon_{HHb}(\lambda_2)\right) \cdot l \end{cases} \qquad (10)$$

And in the matrix form:

$$\begin{bmatrix} A_1/l \\ A_2/l \end{bmatrix} = \begin{bmatrix} \varepsilon_{HbO}(\lambda_1) & \varepsilon_{HHb}(\lambda_1) \\ \varepsilon_{HbO}(\lambda_2) & \varepsilon_{HHb}(\lambda_2) \end{bmatrix} \begin{bmatrix} C_{HbO} \\ C_{HHb} \end{bmatrix} \qquad (11)$$

By solving the system, HbO and HHb concentrations are easily obtained:

$$\begin{bmatrix} C_{HbO} \\ C_{HHb} \end{bmatrix} = \begin{bmatrix} \varepsilon_{HbO}(\lambda_1) & \varepsilon_{HHb}(\lambda_1) \\ \varepsilon_{HbO}(\lambda_2) & \varepsilon_{HHb}(\lambda_2) \end{bmatrix}^{-1} \begin{bmatrix} A_1/l \\ A_2/l \end{bmatrix} \qquad (12)$$

Transmission of light at a given wavelength through tissue depends on a combination of reflectance, scattering, and absorptive effects.
- Reflectance is a function of the angle of the light beam and the regularity of the tissue surface. This decreases with increasing wavelength, thus favoring transmission of NIR vs. visible light.
- Scattering is a function of tissue composition and number of tissue interfaces.
- Absorption is determined by the molecular properties of substances within the light path.

Above 1300 nm, water (H_2O) absorbs all photons over a pathlength of a few millimeters with a secondary peak between 950 and 1050 nm, whereas below 700 nm, increasing light scattering and more intense absorption bands of hemoglobin prevent effective transmission. In the 700–1300 nm range, NIR light penetrates biological tissue several centimeters (McCormick et al., 1991).
Within the NIR range, the primary light-absorbing molecules in tissue are metal complex chromophores: hemoglobin, bilirubin, and cytochrome. The absorption spectra of deoxyhemoglobin (HHb) ranges from 650 to 1000 nm, oxyhemoglobin (HbO) shows a broad peak between 700 and 1150, and Cytochrome oxidase aa3 (Caa3) has a broad peak at 820–840 nm (Fig. 3.1) (Jobsis, 1977). The wavelengths of NIR light used in commercial devices are selected to be sensitive to these biologically important chromophores and generally utilize wavelengths between 700 and 850 nm where the absorption spectra of HHb and HbO are maximally separated and there is minimal overlap with H_2O. The isobestic point (wavelength at which oxy- and deoxy-hemoglobin species have the same molar absorptivity) for HHb/HbO is 810 nm. The isobestic absorption spectra can be utilized to measure total tissue hemoglobin concentration.
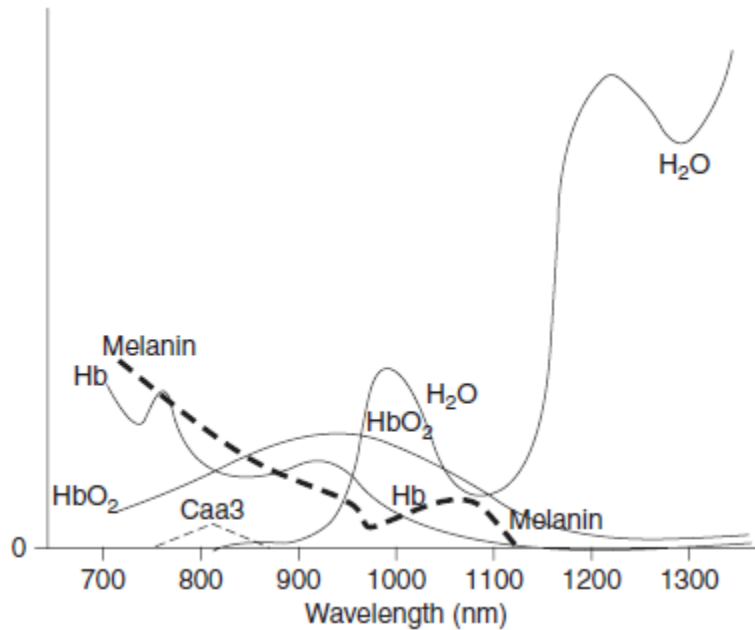
Fig. 3.1. Absorption spectra for oxygenated hemoglobin (HbO), deoxygenated hemoglobin (HHb), Caa3, melanin, and water (H_2O) over wavelengths in NIR range. Note the relatively low peak for Caa3. Commercial cerebral NIRS devices currently utilize wavelengths in the 700–850 nm range to maximize separation between HHb and HbO. The presence of melaninas found in human hair can significantly attenuate HHb, HbO, and Caa3 signals.

Due to the scattering events, the photons do not maintain the original direction, and the resurfacing from the plane of injection is highly probable. This implies that the injected photons travel through the so called "banana shape" path, re-emerging from the scalp at a certain distance (few centimeters) far from the site of injection (Fig.3.2)
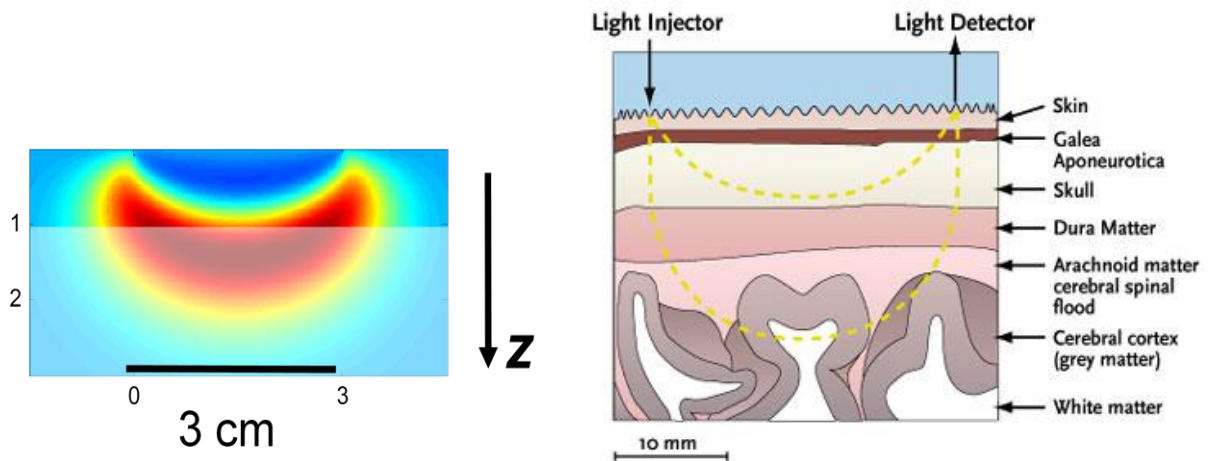
Fig. 3.2. "Banana shape" path travelled by photons in the human head: simulation (left) and schematic representation (right)

Since A is measured directly and ε has been determined for various tissue chromophores, absolute chromophore concentration C is thus inversely proportional to the optical pathlength. However, photon pathlength cannot be measured directly due to reflection and refraction in the various tissue layers involved. Unless pathlength can be determined, only relative change in chromophore concentration can be assessed. Modeling and computer simulation can be used to estimate photon tissue pathlength. By using successive approximation, an analysis algorithm can be calibrated to provide a measure of absolute

change of chromophore concentration, as utilized by some continuous wave commercial devices.

In order to measure absolute tissue chromophore concentrations, a different approach is used, based on radiative transport theory and using frequency-domain NIRS (fd-NIRS) or time-resolved NIRS (tr-NIRS) analyses to determine tissue absorption coefficients (μ). Theoretically, approaches such as fd-NIRS or tr-NIRS avoid the need for actual photon pathlength determination (Lakowicz and Berndt, 1990; Matcher et al., 1994). Fundamental to tr-NIRS technique is that pulsing light is delivered to the cortex. The emerging light is then referred to the previous light pulse injected, and the determination of the optical pathlength can be estimated on the basis of photons delay.

Since tissue chromophore concentration can be measured absolutely, there is no requirement for determination of optical pathlength (Kurth and Thayer, 1999). This approach has been shown to yield reasonable fidelity using an in vitro model of human skull and brain, but hemoglobin concentration <6 g/dl^{-1} yields errors of ~15% and increasing skull thickness produces errors as high as 32% (Kurth and Thayer, 1999). Accordingly, some correction for extracerebral tissue must still be made even with such 'absolute' measurements.

3.2 NIRS techniques

Several types of NIRS equipment, based on different methods, are commercially available. They measure the concentrations of HHb, HbO and the total hemoglobin HbT. If the Caa3 is also taken into account, then measurements with three wavelengths have to be done. Instruments with two wavelengths do not evaluate the Caa3 contribution. Three types of instruments are in use according to the measurement method: continuous wave (or continuous intensity), time resolved and frequency domain (or intensity modulated). For comprehensive details, see (Delpy and Cope, 1997).

3.2.1 Continuous wave NIRS

This technique is based upon the measurement of light attenuation change in the scanned tissue. It uses a source of monochromatic light emitting at constant intensity (*continuous wave*), and measures the intensity of the transmitted light, which can change over time. The value of the attenuation coefficient for a given wavelength is derived from a ratio between the measured and the injected light intensities (Fig.3.4left). As previously exposed, having to estimate the concentrations of two cromophores, two wavelengths are necessary in order to complete a system with two equations.

The majority of NIRS commercial devices are based on continuous wave technology. Its handiness, simplicity, low cost and low repetition frequency are the qualities which have brought to the diffusion of in vivo Near-Infrared Spectroscopy. This technique remains the most widespread and used, being the first released and the most liked.

Nevertheless, this technique holds the big limitation that the transmitted light cannot be linked back to the injected light, that is, the time relationship (delay) between injected and transmitted light is unavoidably lost. This implies that multilayer analysis cannot be carried out (unless using a multi-distance approach), and the homogeneity of the medium has to be assumed. Moreover, one other limitation of this methodology is that the contributions of scattering and absorption are mixed together in the amount of light coming out of the tissue.

3.2.2 Time-resolved NIRS

This technique is based on the injection of single pulses of light, each one followed by the measurement of the temporal distribution of the back scattered photons emerging from the tissue. Thus, tr-NIRS acquires the temporal response of the tissue following the injection of a brief light pulse (Fig.3.4right).

Time resolved NIRS technique needs the use of a system for single photons counting, called "Time-Correlated Single Photon Counting" (TCSPC): it consists of a detector, which records the arrival of single photons and holds in memory their time of flight in relation to a reference pulse. From this information, a histogram with arrival time distribution of the photons is derived (Fig.3.3). The histogram depicts the impulse response of the tissue, for a given source-detector distance. Its shape and temporal delay, measured by starting from the injection time, depends on the optical properties of the medium under measurements. Using a theoretical model for photon migration (Contini et al., 1997) in interpolating the histogram, it is possible to obtain values of absorption and scattering coefficients.

The temporal distribution of detected photons at a distance *d* from the injection point will result delayed, attenuated and broadened. In a first approximation, the delay is a consequence of the time spent by the photons to cross the medium. The broadening of the distribution is due to the different paths (caused by multiple scattering phenomena) traveled by the photons going from the source to the detection point. Finally, attenuation takes its origin in the absorption, decreasing the probability for a photon to be detected. The transmitted photons reach the detector earlier than the diffused ones; the diffused photons, covering longer paths in crossing entirely the material, take consequently more time before coming through the opposite surface (Fig.3.3).

Time resolved reflectance curve is dependent on many factors. Among them, we can list the source-detector distance, the scattering component, and the absorption level. At the increase of the source-detector distance, an increase of the delay time of temporal photon distribution onset and a decrease on the number of detected photons is observed. A similar behavior is observed at the increase of scattering component. Absorption has influence on signal intensity as well as on the descending slope of the curve, but has not influence on the temporal position of the onset.

Thus, by knowing the geometric parameters of the medium, it is possible to estimate scattering and absorption values starting from the position of the peak and the descending slope of the time resolved reflectance curve. More reliable estimation could be obtained by fitting a theoretical model to the data.
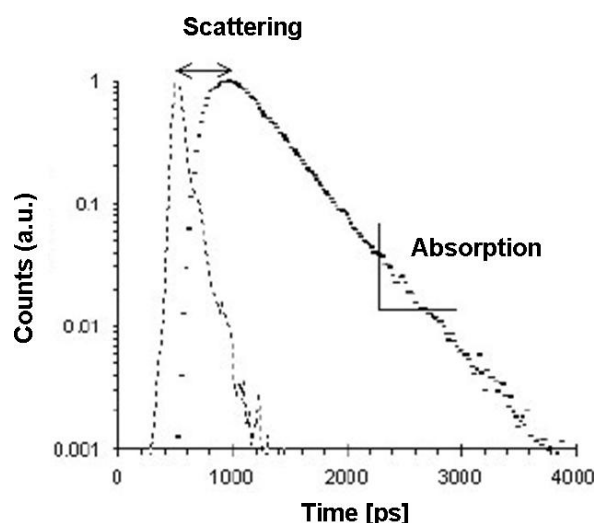

Fig. 3.3. Injected and detected light pulses in a high diffusive medium.

28

3.2.3 Frequency domain NIRS

Last, frequency domain spectroscopy uses intensity-modulated light and applies concepts from diffusion theory to determine both light absorption, due to alterations in HbO and HHb, and scattering characteristics, based on a two-layer tissue model (Rolfe, 2000; Delpy & Cope, 1997). This technique relies on the concept that light comes across attenuation of oscillations and phase shifting, while travelling through the living tissues. By analyzing light attenuation and phase shift of the transmitted light, with respect to the injected, it is thus possible to retrieve information about the cromophores concentrations (Fig.3.4center). This technique, although still used in some laboratories, has never been used during this PhD course, and will not be discussed further.

Most of the commercial instruments utilize continuous wave (cw) light. In combination with the modified Lambert-Beer law, it allows to measure changes in HHb and HbO. In a biological tissue, though, quantification of the NIRS signal remains difficult. Different methods have been proposed to improve the resolution. One of them is the spatially resolved spectroscopy (SRS), which uses cw light and a multi-distance approach. With this method the rSO_2 (the absolute ratio of HbO to the total Hb content-HbT), can be evaluated (Suzuki et al., 1999), and some rough separation between intra-cortical and extra-cortical NIRS signals can be performed.

A further distinction among the instruments can be made. The simplest are the photometers, which use single-distance and cw light, usually with one sensor channel).

The oximeters are more sophisticated: they use multi-distance (SRS) techniques with cw and usually two sensors (channels). For details, see (Ferrari et al., 2004; Delpy and Cope, 1997; Rolfe, 2000). Recently several groups have begun to use multi-channel cw imaging systems generating images of a larger area of the subject's head with high temporal resolution up to 10 Hz or more (Ferrari et al., 2004; Miura et al., 2001; Obrig and Villringer, 2003; Quaresima et al., 2001 and 2002).
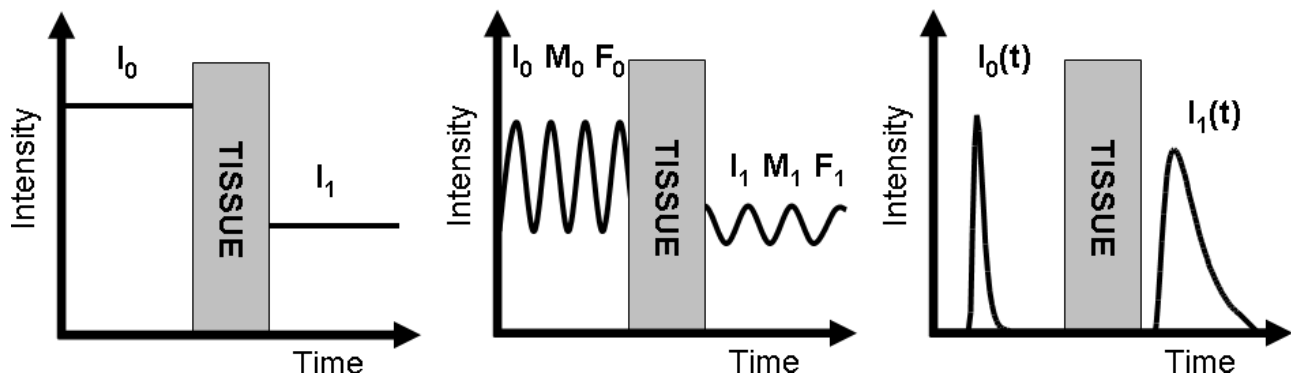
Fig. 3.4. Left: in continuous wave NIRS the value of the attenuation coefficient for a given wavelength is derived from a ratio between measured light intensity and injected light intensity. Center: in frequency domain NIRS cromophores concentrations are retrieved by studying the attenuation of light oscillations and light phase shift. Right: time resolved NIRS acquires the temporal response of the tissue following the injection of a brief light pulse.

3.3 Hardware

The time-of-flight resolved NIRS system, designed and built by the Dipartimento di Fisica of Politecnico di Milano, is based on pulsed semiconductor lasers at two wavelength 690 nm and 820 nm, on an injection optics which multiplies the source channels and on four independent detection chains based on time correlated single photon counting scheme for

a total of up to 16 detection channels. This system is part of a more complex apparatus in which the NIRS instrument synchronizes and controls all the experimental setup: a personal computer for stimuli presentation and another PC for on-line analysis and the acquisition of bio-signals. In the following scheme, injection fibers (in orange) are connected to four receivers each (in white) (Fig.3.5).

Each detector records the amount of light coming from a subset of neighbouring sources, with each source-detector pair called a channel. To identify the source associated with a given detected signal the sources are illuminated sequentially.

In this way, measurements can be taken at a rate of several Hz, typically between 1 and 10 Hz, enabling the time course of the hemodynamic response to be accurately charted.

3.3.1 Hardware description

Two pulsed diode lasers, operating at frequencies of 690 nm and 820 nm, with 80 MHz repetition rate and 1 mW average power (PDL, Picoquant GmbH, Germany), are used as light sources. The laser heads are connected to multimode graded index fibers (50/125 µm) by means of a home-made coupler which combines a neutral density attenuator (J54-082, Edmund OptiK GmbH; Germany), with variable attenuation in the range 0-80 dB, and a standard FC fiber optics coupler. Multimode graded index optical fibers (50/125 µm) with different lengths and a 2x2 fused fiber optic splitter (VISNIR5050, OZ Optics, Canada) are used to time multiplexing the laser pulses at the different wavelengths, and to create two independent channels. In each channel a 1x16 fiber optic switch (F-SM19, PiezoJena GmbH, Germany) creates up to 16 independent sources or injection points, therefore 32 sources are available.

Four parallel detection chains accomplish acquisition of time-resolved reflectance curves. The parallel use of the four detection and acquisition lines enables a total of 32 independent detectors. Fiber optic bundles, 1.5 m-length (Loptek GmbH, Germany), are used for light collection from human tissue.

The system is controlled by a personal computer (Pentium IV 3.5 GHz, 2 Gb RAM), which hosts the acquisition boards and allows data storage. Personalized software, written in C language is used to control the instrument. The software is interfaced to a micro-controller unit (dsPIC30F6014, Microchip Technology Inc., AZ) which is used for the hardware control of the instrumentation. The micro-controller unit generates trigger signals for the synchronization of data acquisition by the TCSPC boards and of the sequential activation of the sources. The instrument response function (IRF) obtained by filling all the propagating modes of the bundle has a FWHM of approximately 500 ps. A detailed description and characterization of the system can be found in Contini *et al.*, (2006).

The system is also interfaced with dedicated software (Presentation, Neurobehavioral Systems Inc, Albany, CA) for precise stimulus delivery and experimental control program.

3.3.2 Signal extraction

For each wavelength λ a reference time domain fNIRS curve $R_0(t;\lambda)$ is derived by averaging the tracks recorded during the initial baseline period. Fitting of $R_0(t;\lambda)$ yields the reference absorption value $\mu_{a0}(\lambda)$. Then, at each recording time *T* during the experiment, changes in the absorption coefficient are derived (Nomura et al., 1997) as

$$\Delta\mu_a(\lambda;T) = -\frac{1}{vt}\ln\left(\frac{R(t;\lambda;T)}{R_0(t;\lambda)}\right)$$

(13)

where v is the speed of light in the medium, t is the arrival time of photons, and $R(t, \lambda, T)$ is the time domain fNIRS curve at the recording time T. To enhance the contribution from deep layers and to remove possible disturbances caused by superficial layers, a correction method based on the use of late time windows (t = 1750-2500 ps) is also applied (Contini et al., 2007; Aletti et al., 2010). It is well known that depth information in time domain fNIRS is encoded in the time-of-flight of photons (Selb, 2005; Steinbrink et al., 2001; Del Bianco et al., 2002): early photons probe the superficial layers of the head, while late photons have a higher probability to visit deeper layers (Fig.3.6). Finally, the absorption coefficient is then derived from corrected late gate intensities as

$$\mu_a(\lambda;T) = \mu_{a0}(\lambda) + \Delta\mu_a(\lambda;T) \qquad (14).$$

HbO and HHb concentrations are derived by Lambert Beer law, taking the assumption that these compounds are the main chromophores contributing to absorption in the employed wavelength range, and also assuming that other chromophore concentrations (*i.e.* water, lipid, etc.) is unlikely subjected to relevant modifications, Then, total hemoglobin content (HbT = HHb+HbO) is calculated.
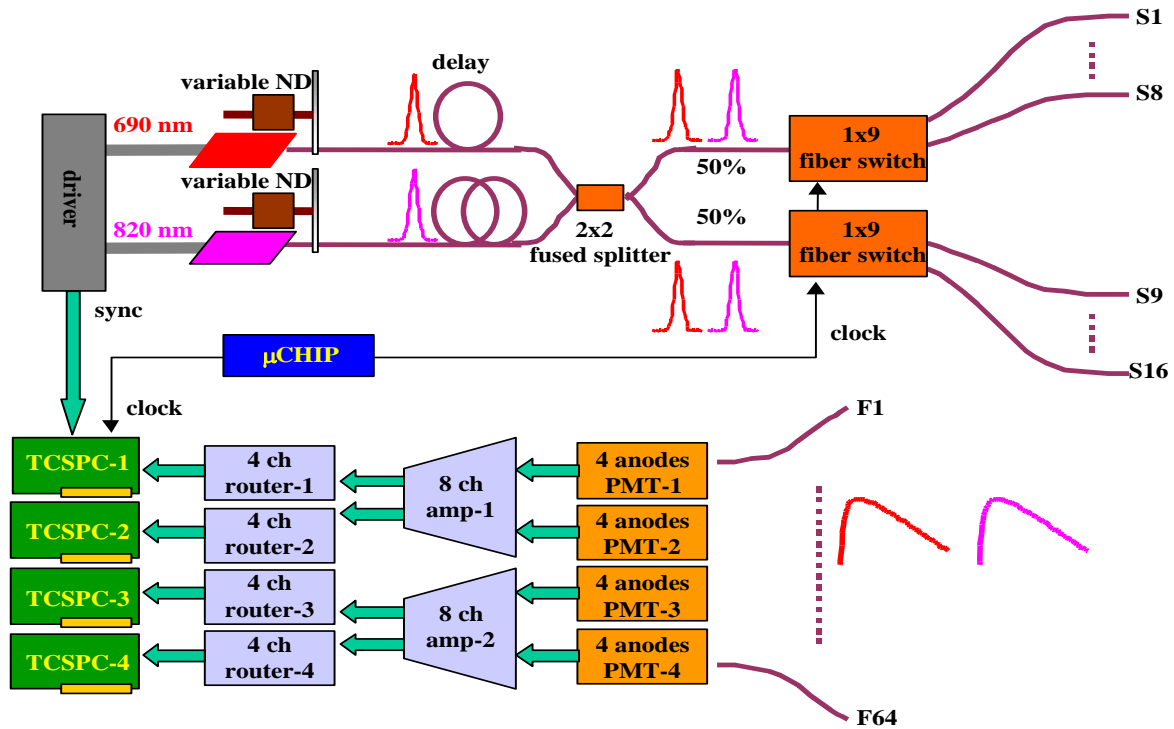
Fig. 3.5: Schene of time-of-flight NIRS device assembled by the Dipartimento di Fisica of Politecnico di Milano.

3.4 NIRS probe

Optical fibers of the tr-NIRS are fixed on a flexible cushioning material (neoprene, Fig. 3.7). The cushioning preserves fiber positioning over time, thus optimizing light injection. Sensors are also inserted into the cushioning, with excellent optical coupling. Fibers positioning over the scalp is accurately designed prior to any recording campaign, in order to meet the specific requirements of each acquisition protocol. In our experiments the goal was to monitor either the prefrontal cortex or the motor areas. The probe geometry was

accordingly modified. In all cases, two probes were used, for the two brain hemispheres. As a general rule, injection fibers were surrounded by four or more collection fibers at a distance of 2.5 cm.
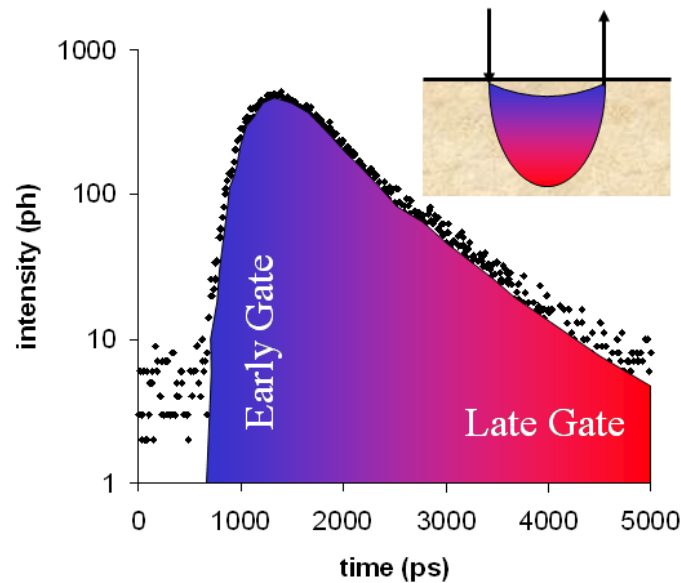
Fig. 3.6: Impulse response of time-of-flight NIRS device: early photons have travelled through the superficial tissue layers, while late photons most probably have reached the brain cortex.
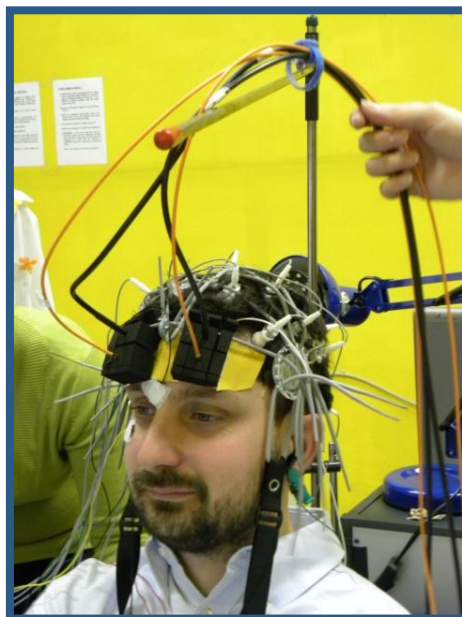
Fig. 3.7: NIRS probe positioning, during a combined EEG/NIRS acquisition. NIRS probes are placed prefrontally. 10/20 EEG montage is also shown. Courtesy of Davide Contini, Dipartimento di Fisica, Politecnico di Milano.

3.5 Pre-processing

Pre-processing of the optical data usually starts with a channel by channel assessment of the quality of the data in order to immediately discard those channels affected by poor scalp coupling or instrumentation problems. There are three types of noise to consider

when processing NIRS data: instrumentation, motion (especially from the infants), and physiological oscillations. Motion artifacts are usually characterized by abrupt changes in the signals occurring simultaneously in several channels—quite distinctive from the usual slow and smooth hemodynamic response. A secure design of the head gear or probe can reduce the presence of such artifacts, although it is unlikely to completely solve the problem.

In contrast to movement artifacts, low frequency oscillations such as vasomotion, can mimic in frequency and magnitude the hemodynamic response to stimulation (as demonstrated by Elwell et al., 1999; Katura et al., 2006; Taga et al., 2000). This can be overcome by careful design of the paradigm and the rate of stimulus presentation to minimize the possibility of coupling between functional activation and spontaneous cerebrovascular oscillations. In addition, in adults there is evidence of stimulus related changes in systemic parameters (e.g. heart rate, blood pressure, skin blood flow) (Obrig et al., 2000;Tachtsidis et al., 2008). Options for decoupling these systemic vascular changes and the cerebral hemodynamic response include the acquisition of systemic data by means of an independent measurement system, the sampling of multiple volumes with NIRS so that measurements at the surface layer (with small source-detector separations) can be subtracted from measurements at the cortex level (larger source-detector separations) (Saager and Berger, 2008), the gating of photons in time resolved NIRS measurements (Aletti et al., 2010), or the calculation of higher statistical moments (Steinbrink et al., 2001).

Traditionally, and due to the limited number of channels available in the first fNIRS systems, analysis of NIRS data has been based on time series processing, with standard t-tests to evaluate the significance of stimulus-correlated changes in the signals, or repeated measures analysis of the variance (ANOVA) to compare the shape (in time) of the response to different stimuli and/or groups of participants. Simultaneous acquisition of data from these multiple channel arrays has enhanced the potential of NIRS by opening the field to data reconstruction of functional images (Gibson et al., 2005). Indeed, the similarities between fMRI and optical experimental designs are being exploited and analysis techniques usually applied to fMRI are being adapted to optical data such as statistical parametric mapping techniques based on the general linear model (GLM) (Koh et al., 2007; Ye et al., 2009).

Being a relatively novel technique, it has been common practice for different groups using NIRS to develop their own analysis procedures and software. As an increasing number of research groups use optical topography for a wide range of functional studies that differ in their degree of complexity, age range, cortical region of interest, optode geometries and system configurations, it is paramount that we adopt a standard and robust analysis methodology (Schroeter et al., 2004). Several freeware packages are available for the analysis of optical signals, each with the flexibility to accommodate different system configurations (HomER, Huppert et al., 2009; fOSA, Koh et al., 2007; NIRS-SPM, Ye et al., 2009). However some unification and standardization of data analysis is now beneficial for the research community.

3.6 GLM method

In this section we now show the potentialities of the application of General Linear Model to NearInfrared Spectroscopy data. GLM has been widely used in the fMRI field (Friston et al., 1995), and ample literature on the method is available for the research community.

By means of contrasting each mathematical function (i.e. regressor) against the background, GLM highlights possible correlations existing between the single regressor and the dynamics embedded inside the data. It follows that we can make assumptions about certain dynamics possibly present inside the data, we can then create specific regressors modelling our hypothesis, and GLM can verify the hypothesis by providing a statistical map depicting the consistency of correlation at any point of the map.

The reader will now understand that the GLM procedure has no theoretical limitation with respect to application in the NIRS field. Given the smaller number of data voxels and the higher sampling frequency, the method can be adapted for the NIRS studies.

According to GLM, a time series for a given channel is modelled as a linear combination of L regressors (known functions) plus an error term:

$$\underset{(t\times 1)}{Y} = \underset{(t\times L)}{X}\underset{(t\times 1)}{\beta} + \underset{(t\times 1)}{\varepsilon} \tag{15}$$

X (txL matrix) is called the design matrix (DM), each column is a regressor and t is the number of time points. Each column L of matrix X contains the predicted hemodynamic response for one experimental block over time t. β is the vector of the unknown parameters, one for each regressor, weighting (i.e. quantifying) the contribution of each predictor (i.e. regressor) for modelling the functional time series (i.e. columns of matrix Y), and it serves as the parameter set for subsequent hypothesis testing. Errors ε are assumed to have normal distribution with zero mean and covariance $\sigma^2 V$, where σ^2 represents variances, and V is the temporal correlation matrix (identical at all voxels).

Origin for correlation on error terms can be found in cardiac, respiratory and vasomotor effects. The ordinary least squares estimation of the parameters is:

$$\hat{\beta} = \left(X^T X\right)^{-1} X^T Y \tag{16}$$

inference is then performed by testing the predictor variables through the T-statistic:

$$T = \frac{\hat{X}(r)}{\sqrt{C_{\hat{X}}(r)}} \tag{17}$$

Where $\hat{X}(r)$ is the product of the transposed contrast vector with the response signal strength, and $C_{\hat{X}}(r)$ is the error variance.

3.7 GLM processing procedure

Currently, GLM data processing is performed by means of software and toolboxes, created by research groups working in the statistics and fMRI imaging fields. In the last few years, however, a few free toolboxes specifically conceived for NIRS data processing have been released. Among them we can mention fOSA (University College of London), nilab (Charitè Berlin) and NIRS-SPM v.3.1 software (KAIST lab - Ye et al., 2009).

The main steps of fNIRS data processing by means of GLM-based software are now described, based on NIRS-SPM v.3.1 graphical interfaces.

1) All the software, toolboxes or routines require some data conversion. fOSA and NIRS_SPM now include some plugin software which allows for the conversion of NIRS data acquired with the most common commercial NIRS devices (Shimadzu, Hitachi, etc…). For prototype NIRS devices, the user needs to create routines for data conversion.

2) The second step usually consists in the visual inspection of raw NIRS data. Even though this step can be easily done in any environment (MATLAB, C, etc…) during pre-processing, software often include some interfaces for the "time course" inspection and processing. Be this step performed by means of a toolbox or not, it is of paramount importance to rule out artefacts before applying GLM to NIRS data.

3) Then, the design matrix needs to be created, usually by entering the onset instants and the durations of each test block (condition) inside a dialog box. In doing so, some mathematical functions (regressors) modelling the signal are generated, to make up the matrix of modelling functions (design matrix) (Fig.3.8).
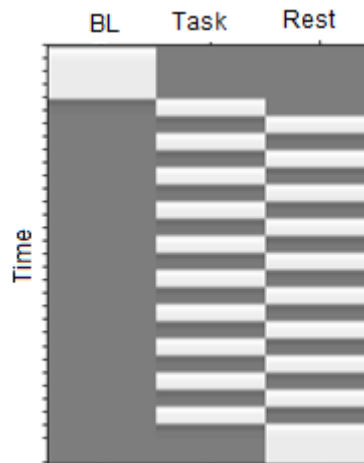
Fig.3.8 Design matrix: regressors (columns) model the conditions (activity blocks) of the test. Time runs from top to bottom.

4) Then, a decision has to be taken about whether NIRS data need to be detrended or not. Some software include made-on-purpose algorithms, conceived for the preservation of the signal oscillations related to the task block design, while clearing away the slower dynamics (Ye et al., 2009) (Fig.3.9).
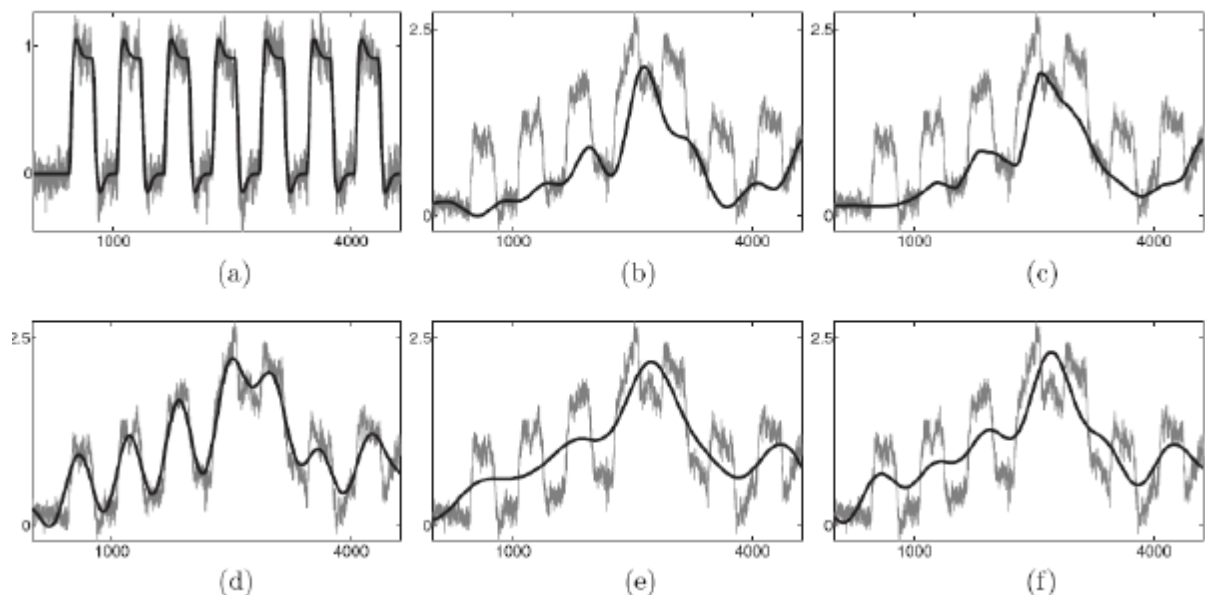
Fig. 3.9. The detrending result based on Wavelet-MDL vs. the conventional methods. (a) A synthetic hemodynamic response (black line) and a noise added signal (gray line). (b) The overall simulated signal (gray line) and a ground-truth trend. Trend estimates using (c) Wavelet-MDL, (d) FIR with cutoff frequency 0.02 Hz, (e) FIR with cutoff freuquency 0.015 Hz, and (f) DCT with cutoff frequeucy 0.015 Hz. Wavelet-MDL gives a closer estimate for the unknown trend (Jang et al., 2009)

35

5) Next, correction for serial correlations can also be done, to be sure that GLM will be correctly applied. If there were no corrections for temporal autocorrelation in NIRS data, statistical inference would produce inflated results, as the actual number of degrees of freedom is lower than the number of observations (i.e., scans). Two options can be chosen to address this problem:
   - Precoloring method (Worsley and Friston et al., 1995): in this method the intrinsic temporal correlations are swamped by an imposed temporal correlation structure, by smoothing the data with a temporal filter that will attenuate high frequency components; hence this is a 'low-pass filter'. The shape of this filter can be either Gaussian or HRF. Differences between these two are slight but, since the transfer function of HRF is in the frequencies of modeled neuronal signals, the HRF is preferred. The choice of the right hemodynamic response function (HRF) to be convolved with the mathematical functions forming the design matrix needs to be done: a bunch of possible templates can be used.
   - Prewhitening method (Bullmore et al., 1996; Plichta et al., 2006, 2007; Koh et al., 2007): this method attempts to regress out the unknown autocorrelations (AR(1) – model).
   Either temporal smoothing (precoloring) or AR(1) (prewhitening) should be chosen, not both. In our experimental data set, we found that precoloring is more appropriate for estimating temporal correlation of NIRS data than the prewhitening method.

6) The estimation procedure is then run for each subject of the study. The β unknown parameters are then estimated (see section 3.6).

7) Contrasts are defined, in order to extract the hemodynamic activation associated with the experimental block modelled by a certain regressor. The value of T-statistics is estimated for each NIRS channel, at the single subject level (see section 3.6).

8) Before mapping the statistically significant activations, though, it is necessary to register the NIRS channel positions over an MRI brain atlas, or over the structural MRI reconstruction of the subject (Fig.3.10).

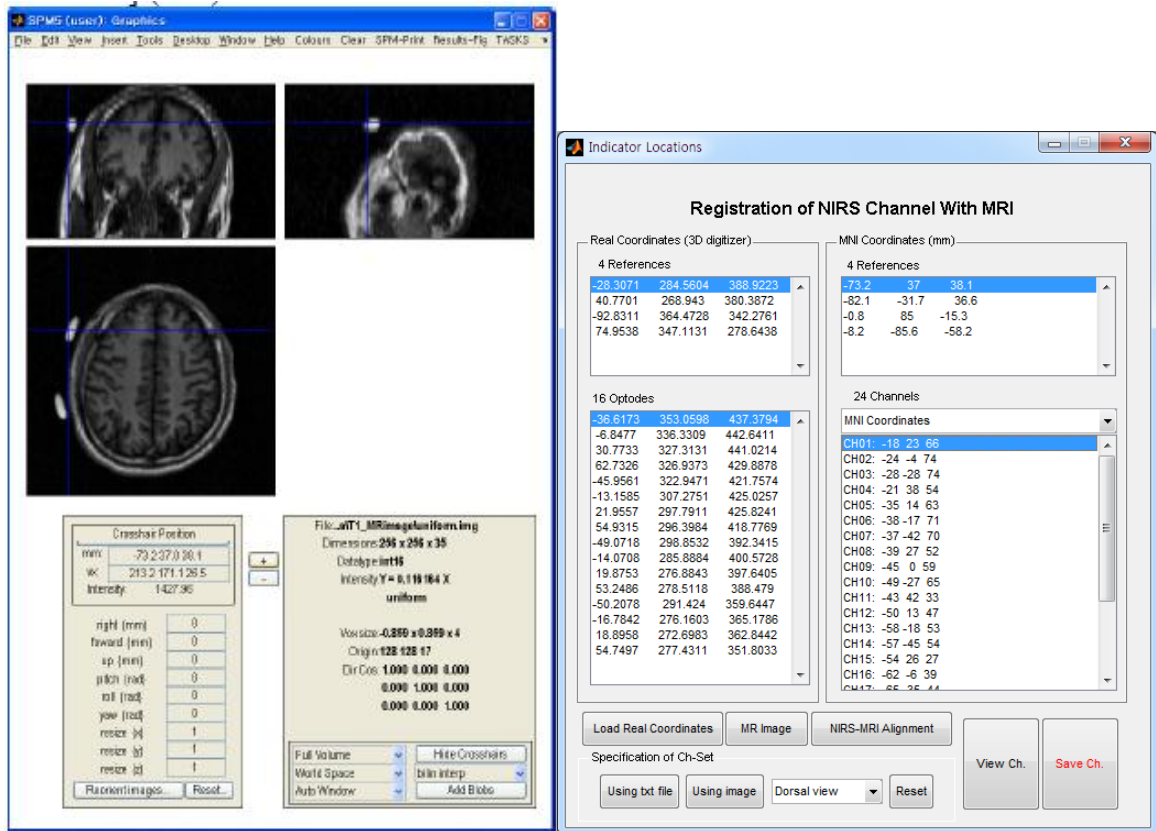**Fig. 3.10. Registration of NIRS channels over the structural MRI (or brain atlas). Software interface of NIRS_SPM toolbox.**

9) Afterwards, NIRS channel positions can be projected over the three-dimensional reconstruction of the brain cortex, obtained through MRI (Fig.3.11), according to the atlas or MRI coordinates.
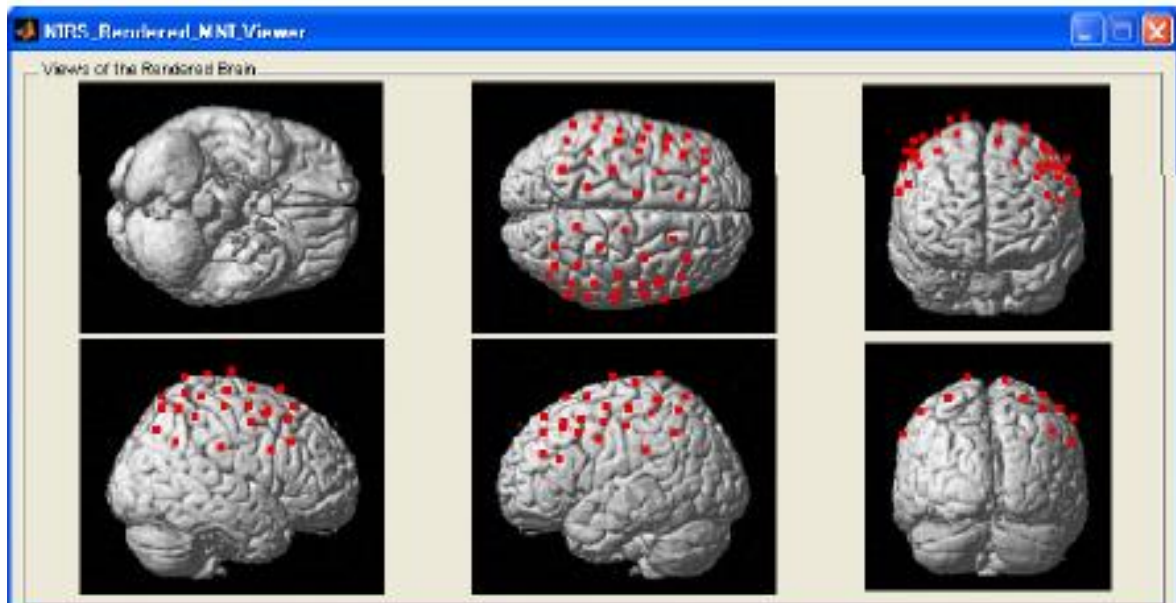

Fig.3.11. Projection of NIRS channels over the subject's (or atlas) brain cortex

10) Last, the interpolated map of the values of the T-statistics can be created and projected over the cortex (Fig.3.12left). A statistical threshold (based on p-value) can be set (Fig.3.12right). Thresholded activations can be plotted by means of uncorrected p-value, or by some other values of p, obtained after statistical corrections.

More specifically, the NIRS signal analysis requires the excursion probability of the inhomogeneous Gaussian random field that is generated by the interpolated samples from sparsely and irregularly distributed optode measurements. Even though the excursion probability for an inhomogeneous Gaussian random field is extremely difficult to calculate in general, some studies for a confidence region have been carried out, and some corrective methods have been proposed (Sun, 1993). Utilizing corrections, the resolution of maps localization can be improved for HbO, HHb, and HbT.
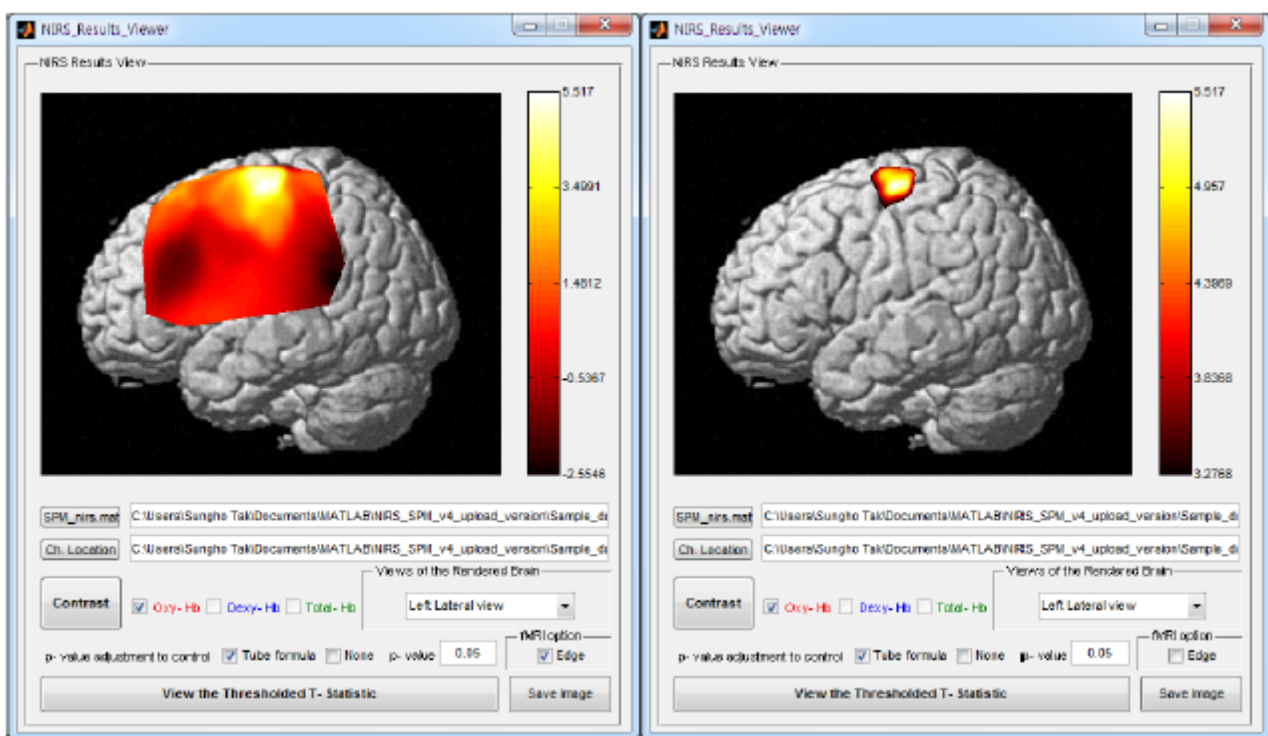
Fig.3.12. Left: Map of the t-statistics values for HbO activation. Unthresholded. Right: The same map, thresholded at p<0.05. Single subject results are shown

Then, the procedure can be repeated at the group level, for the second level analysis. Activation maps can be obtained for the whole group of subjects under investigation.

3.8 GLM for data modeling and data integration

GLM is primarily used in fMRI studies for modeling the task design. GLM, indeed, allows to create functions (i.e. regressors) modelling the alternating time intervals in which the subject under examination has to either accomplish some activity or stay still, in a resting attitude. This is a very common experimental architecture, which is usually referred to with the terms "block design task". Separate mathematical functions are created, in order to separately account for either resting periods, single activity conditions, or combinations of conditions. Correlations existing between any condition and the data can then be

inspected. We applied the procedure to NIRS data, and we assessed the feasibility of GLM approach in the case of spectroscopy data.

One step further, we can apply GLM for the study of the relationships standing between different biological data. Indeed, in the case that a polygraphy is available, and there is some suspicion of "cross-talk" between couples of signals and/or body systems, it is at least reasonable to attempt some modelling of biological data in order to create "polygraphic" regressors to be tested for correlations with NIRS data. In other words, some biological information can be used to create functions, testing for correlations with NIRS data. The amount of information shared among NIRS and other biological data can then be highlighted, with great potential advantage for our knowledge of physiological and pathological modulatory phenomena.

3.8.1 Task Design Analysis

We now present one application of GLM for the task design analysis of an handgrip task. During this task, the subjects under examination were repeatedly asked to do some handgrip with one hand. The task procedure is fully described in chapter 2, and we just recall here that it was made up of one initial baseline period, followed by ten intervals in which the subjects performed the handgrip task; these ten periods were interleaved by resting periods of the same duration. A final resting period ended the test. For the task design analysis, a design matrix was used (Fig.3.13left) containing three regressors modeling: (1) the baseline recorded at the beginning of the test, (2) the activation blocks of the handgrip test, and (3) the rest periods interleaving the activation blocks. Contrast arrays were designed to investigate: (1) the relationship between the motor (i.e. handgrip) activation and rest, and (2) the relationship between the motor activation and the baseline. The interpolated T-statistic maps were obtained for each subject first (1st level analysis), and then for each of the group of subjects (2nd level analysis). Fig.3.13left shows that each regressor was in fact an on/off function, having values equal either to 1 (in white), meaning "on", when modelling the condition of interest or to 0 (in black), meaning "off", being silent during the time intervals not involved in the condition of interest. Figure 3.13right shows the statistic map (activation areas calculated for $p<0.05$) obtained by contrasting the regressor modelling activation vs. the regressor modelling the rest intervals. An area of hemodynamic activation is found over the brain motor areas, contralateral to the side of handgrip movement.

3.8.2 "EEG informed" analysis

In the case that a suspicion exist about the possible presence inside NIRS data of some contribution from neuroelectrical phenomena, it is possible to model electroencephalographic activity so as to build "EEG regressors" for statistical testing.

This can theoretically be done either in the case we want to rule out the existence of any relationship between the ongoing EEG activity in the brain and some specific hemodynamic response we are eliciting in the cortex by means of certain tasks, or in the case we are interested in the investigation of the interplays existing between the electrical and hemodynamic events occurring in the cortex (i.e. the so called "neurovascular coupling"). In both cases, EEG signal needs to come across some pre-processing steps before entering the design matrix in the form of "regressors".

Fig.3.14 resumes the processing steps we applied in order to create EEG regressors to be inserted inside the design matrix. First, the EEG signal was filtered (0.5-48 Hz) and downsampled to 100Hz.
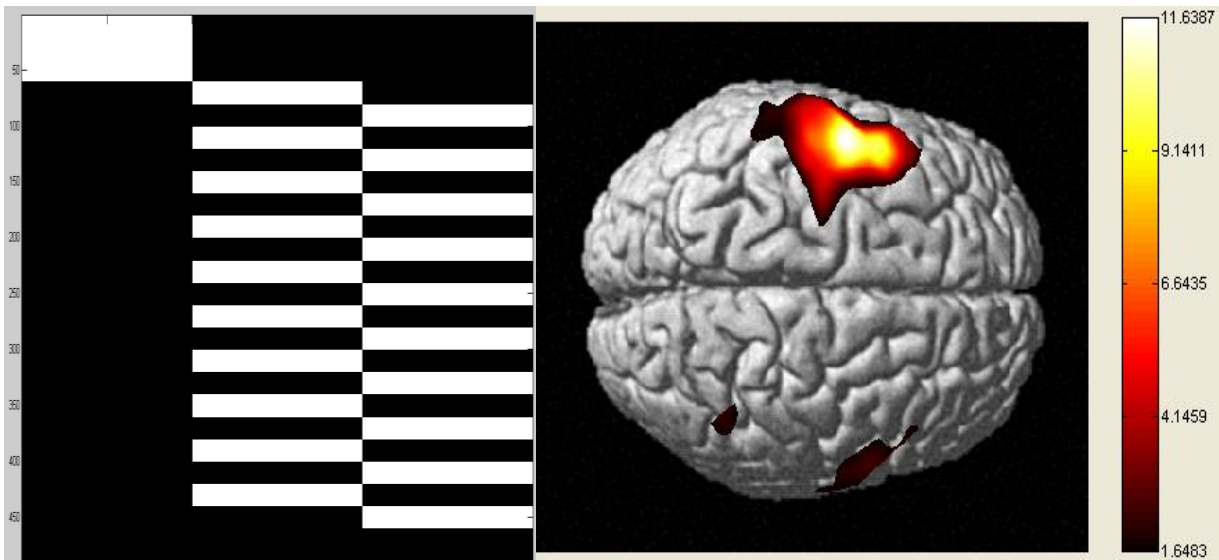
Fig.3.13: (left) Design matrix for the modeling of the block design of the task: regressors, from left to right, modelthe initial baseline condition, the activation blocks andthe rest period. Time runs from top to bottom.(right)HbO statistic map (p<0.05) for one subject performing a right handgrip task. This map was obtained by contrasting the regressormodelling activation vs. the regressormodelling the rest intervals.
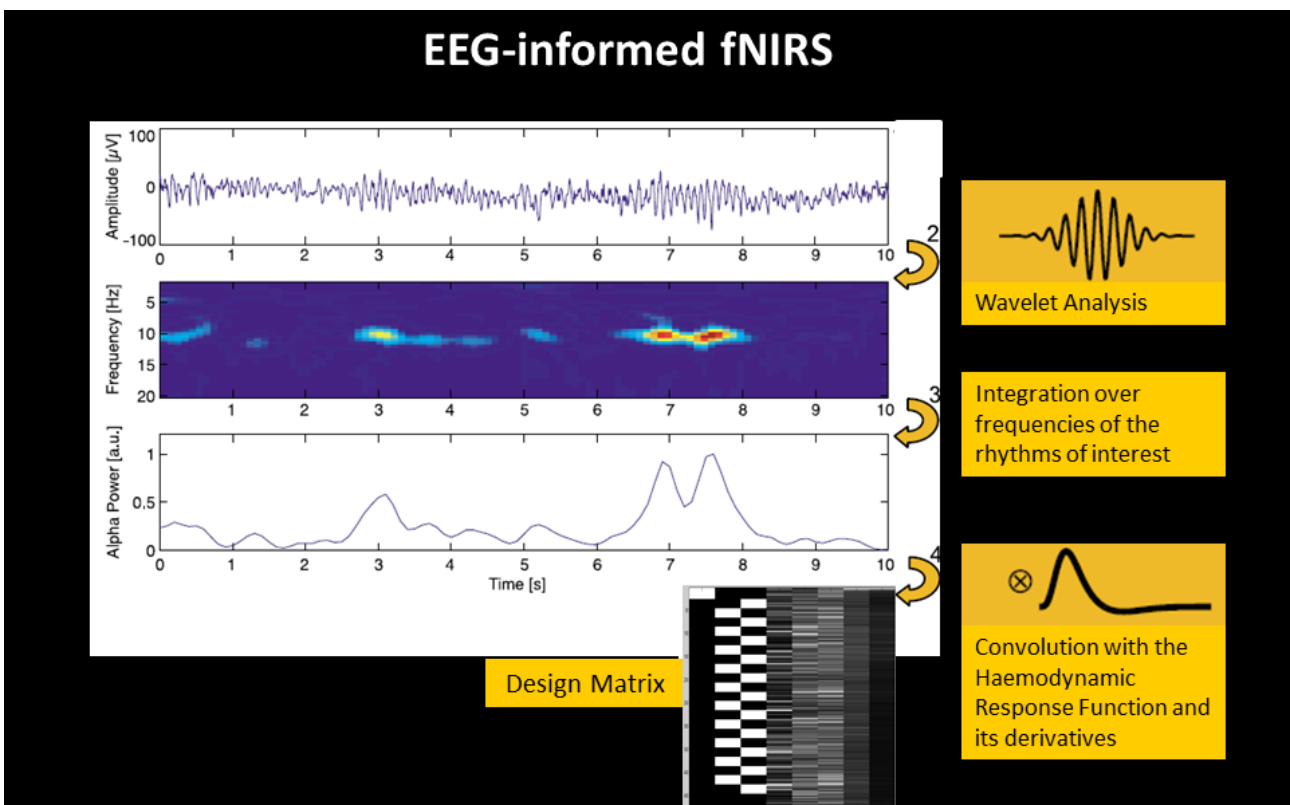
Fig. 3.14 "EEG informed" method for fNIRS data processing: EEG signal was decomposed into its contributions over frequency and time. Then, an integration over the frequencies of specific brain rhythms was performed, so to make up the five correspondent EEG power tracks. Such tracks were then convolved with the canonical HRF and finally entered inside the design matrix.

Then, it underwent wavelet analysis. By means of a Morlet mother wavelet, the EEG signal was decomposed into its contributions over frequency and time. Then, an integration over

the frequencies of specific brain rhythms (delta=0.5-4Hz, theta=4-8Hz, alpha=8-13Hz, beta=13-30Hz and gamma=30-48hz) was performed, so to make up the five correspondent EEG power tracks. Such tracks were convolved with the canonical Hemodynamic Response Function (HRF) and finally entered inside the design matrix.

After having obtained EEG regressors, modeling neuroelectrical power in each specific frequency band, they were included both in a broader design matrix, also containing the regressors modeling the task design (Fig.3.15left), and in a specific design matrix, containing EEG regressors only (Fig.3.16left).
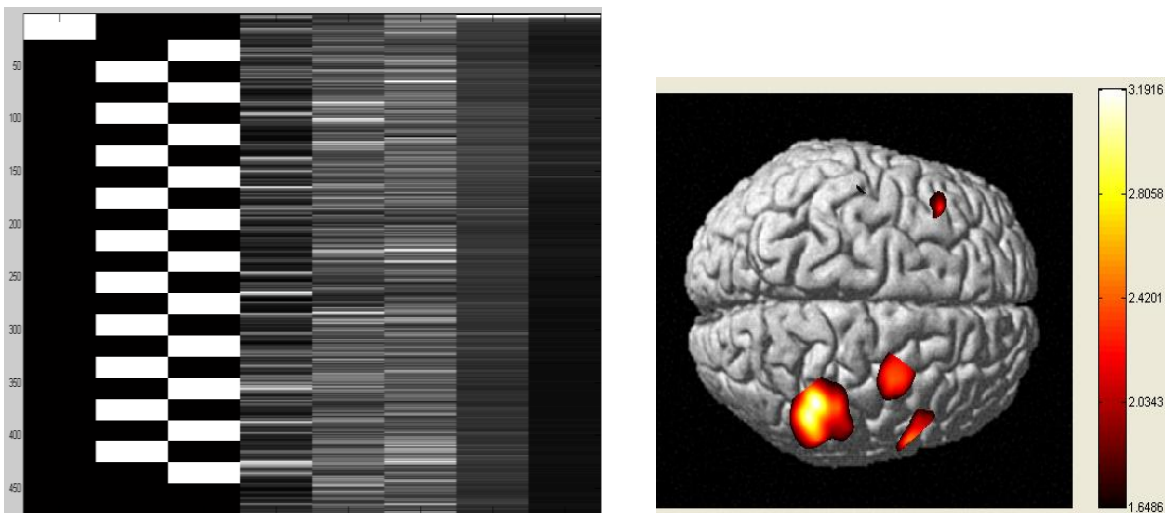
Fig.3.15 (left) Design matrix made up of regressors modeling, from left to right, the baseline period, activation blocks, rest periods, and five electroencephalographic rhythms (delta, theta, alpha, beta and gamma bands). Time runs from top to bottom.(right) The image showsthe HHb activation resulting from contrasting the regressor modeling EEG power in the alpha frequency band at 1st level analysis (one healthy subject). Contrast was set for EEG alpha rhythm. Significance was set at p-val<0.05.
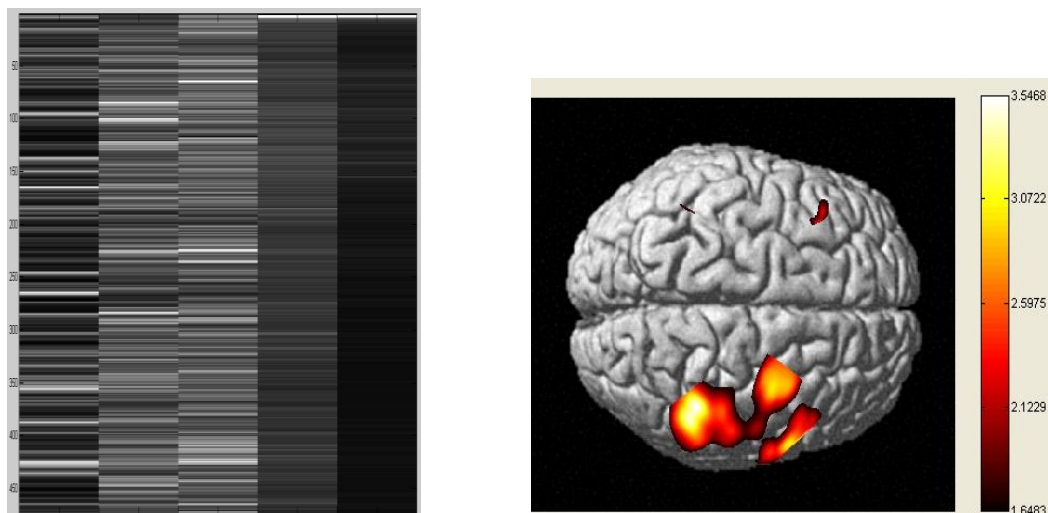
Fig.3.16: (left) Design matrix made up of regressors modelingthe five electroencephalographic rhythms (delta, theta, alpha, beta and gamma bands) only. Time runs from top to bottom. (right) The image showsthe HHb activation resulting from contrasting the regressor modeling EEG power in the alpha frequency band at 1st level analysis (one healthy subject). Contrast was set for EEG alpha rhythm. Significance was set at p-val<0.05.

The observation of Fig.3.15 right and fig.3.16 right brings about an important remark: the images, indeed, are very similar, but not identical. The reason for the similarity is almost trivial: being the two maps the statistical topography of the same contrast (i.e. of the

correlation between the same data with the same regressor), we clearly expect the statistically significant area of correlation to be the same. The subtle difference, though, could not be equally straightforward: the reason of such slight difference has to be traced back to the construction of the design matrix. Indeed, the adding of regressors is never costless. Due to slight "competition" of regressors, modeling either the task design or the EEG rhythms, in capturing some shared dynamics, some statistical power had to be shared as well. In other words, by adding regressors, we always add the chances that some data dynamics are simultaneously captured by more than one regressor, thus splitting the statistical power in all the contrasts sharing the correlation. We can thus infer the general rule that, by adding regressors, the single contrasts tend to loose part of the associated statistical power. The more relevant is the "competition" of regressors in modeling data dynamics, the heavier will be the statistical power lost.

3.8.3 "EMG informed" analysis and "polygraphy informed" analysis

A specific comment is needed for electromyography. Indeed, in the case of motor task, such as the present handgrip task, EMG can be used to model the task blocks, and thus substituting the "task blocks" regressor. As a results, the design matrix will include (Fig.3.17left): (1) one on/off regressor modeling the baseline, (2) one regressor modeling the task by means of "pre-processed EMG" and (3) one on/off regressor modeling the rest periods. EMG pre-processing consisted in high-pass filtering and in extracting the envelope of EMG dynamics. Values were normalized before being entered in the design matrix.

Obviously, the substitution of "task blocks" regressor with "EMG" regressor remains possible also in the case of more complex design matrixes, such as the one depicted in fig.3.17right, comprising baseline and rest on/off regressors, EMG and EEG rhythms.
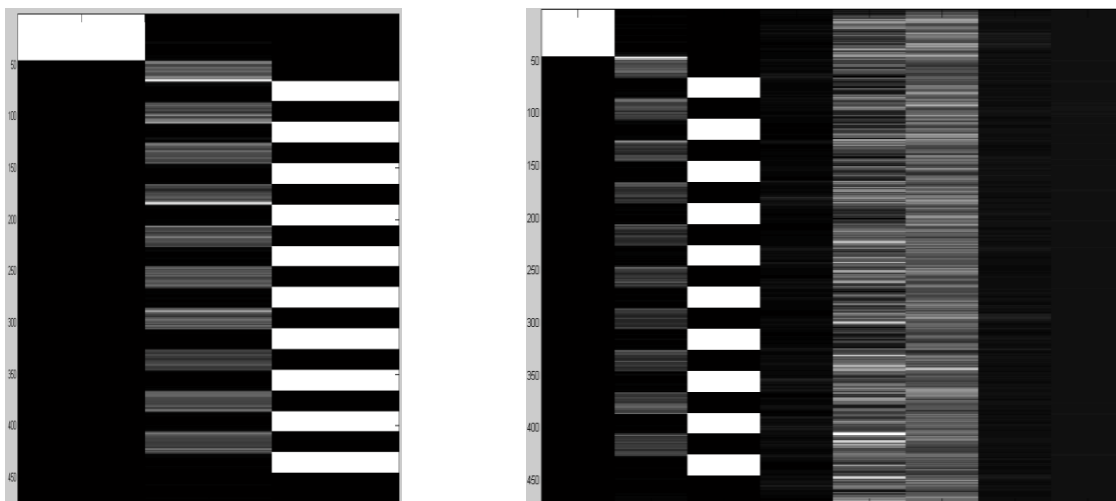
Fig.3.17: (left) Design matrix for the modeling of the task through electromyogram: regressors, from left to right, model the initial baseline condition, the activation blocks and the rest period. The activation blocks are modeled by means of the pre-processed electromyographic track (EMG). Time runs from top to bottom. (right)Design matrix comprising baseline and rest on/off regressors, EMG and EEG regressors.

The assumption leading to the substitution of the "task blocks" regressor with the "pre-processed EMG" regressor is that EMG captures the real muscular activity generated by the handgrip task. EMG, then, can be regarded as the real measurement of the handgrip activity, in terms of muscular contractions executed while performing the movements of the hand. Being the most direct measure of muscular activity, EMG can thus be considered the best descriptor of handgrip movements.

In figure 3.18 an example is shown, illustrating the ability of EMG regressor to focus the cortical area involved in motor execution. Indeed, the "task blocks" regressor (left) highlights a region with the same location, but broader extension, if compared to the "pre-processed EMG" regressor (right). EMG seems then to be capable of more specific and focused detection of the neural networks involved in movement, with respect to on/off regressors modeling the task. This observation is clearly valid only in the case the comparison is made with the same hemoglobin species and the same threshold for the statistical significance. It is also useful to underline that, even if the contrast of EMG implies some sort of search for correlations between the electrical activity of the muscle and the hemodynamic activation in the brain, such correlation cannot be regarded as neurovascular coupling, at least in the most traditional definition, as the electrical activation refers to the effectors, and not to the central nervous system.
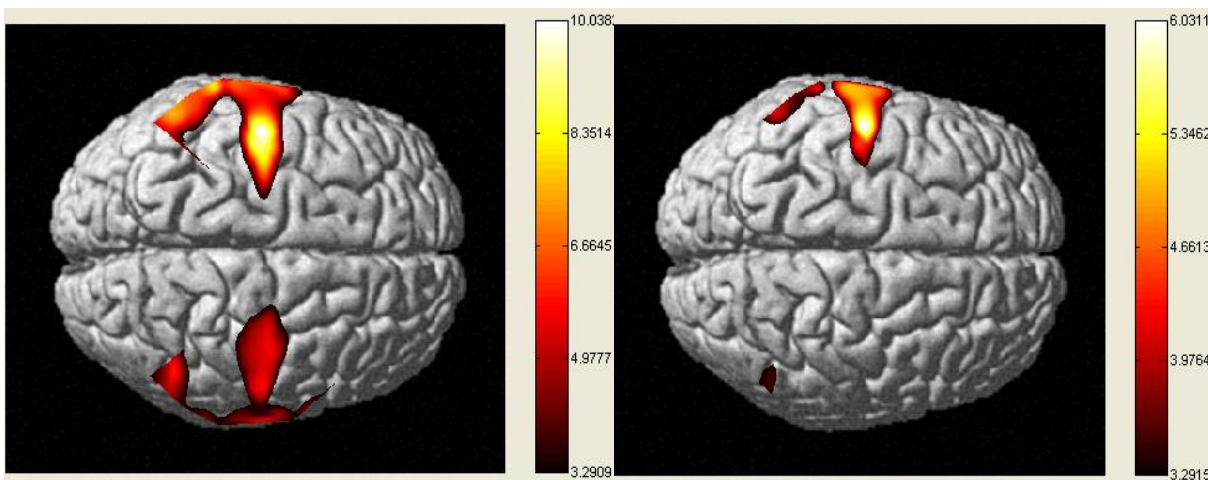
Fig.3.18: (Left) The image shows the HbO activation resulting from contrasting the on/off "task blocks" regressor vs. the initial baseline at 1st level analysis (one healthy subject). Significance was set at p-val<0.05. (Right) The image shows the HbO activation resulting from contrasting the "pre-processed EMG" regressor vs. the initial baseline at 1st level analysis (one healthy subject). Significance was set at p-val<0.05.

3.8.4 "ECG informed" analysis

Last, we would like to mention the possibility to include the electrocardiographic activity (ECG) inside the design matrix. The electrocardiographic track was pre-processed as follows, before being inserted inside the design matrix. The ECG track was automatically processed by means of a made-on-purpose MATLAB routine, searching for R peaks. For any heart beat, the R peak was identified. The routine consisted in an adapted version of the "Pan & Tompkins" algorithm, performing a bandpass filtering first, then derivative filtering, squaring and moving-window integration (for the method description, see Pan and Tompkins, 1995). Beat-to beat time differences were then calculated as the difference in time between two subsequent R peaks. We then obtained the so called RR series. The RR series was averaged over each block of task, giving as a results 11 mean values of RR intervals. The 11 values were then normalized between 0 and 1. The normalized RR block sequence was finally entered inside the design matrix, and provided the fourth regressor shown in fig.3.19.

The ECG regressor was not applied in the previously mentioned motor handgrip task, because we did not expect any modification of the ECG due to the task. Indeed, the
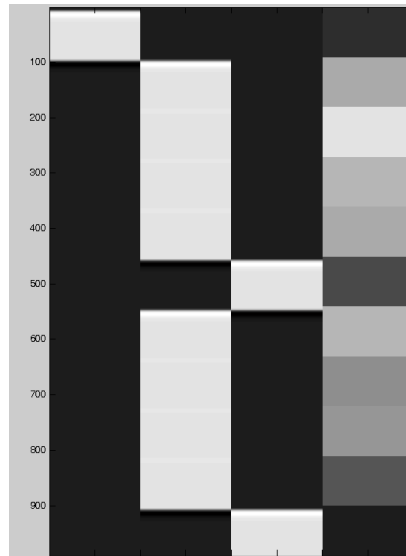
Fig.3.19: Design matrix including electrocardiogram: regressors, from left to right, model the initial baseline condition, the activation blocks, the rest period and the normalized interbeat-interval series (RR series). Time runs from top to bottom.
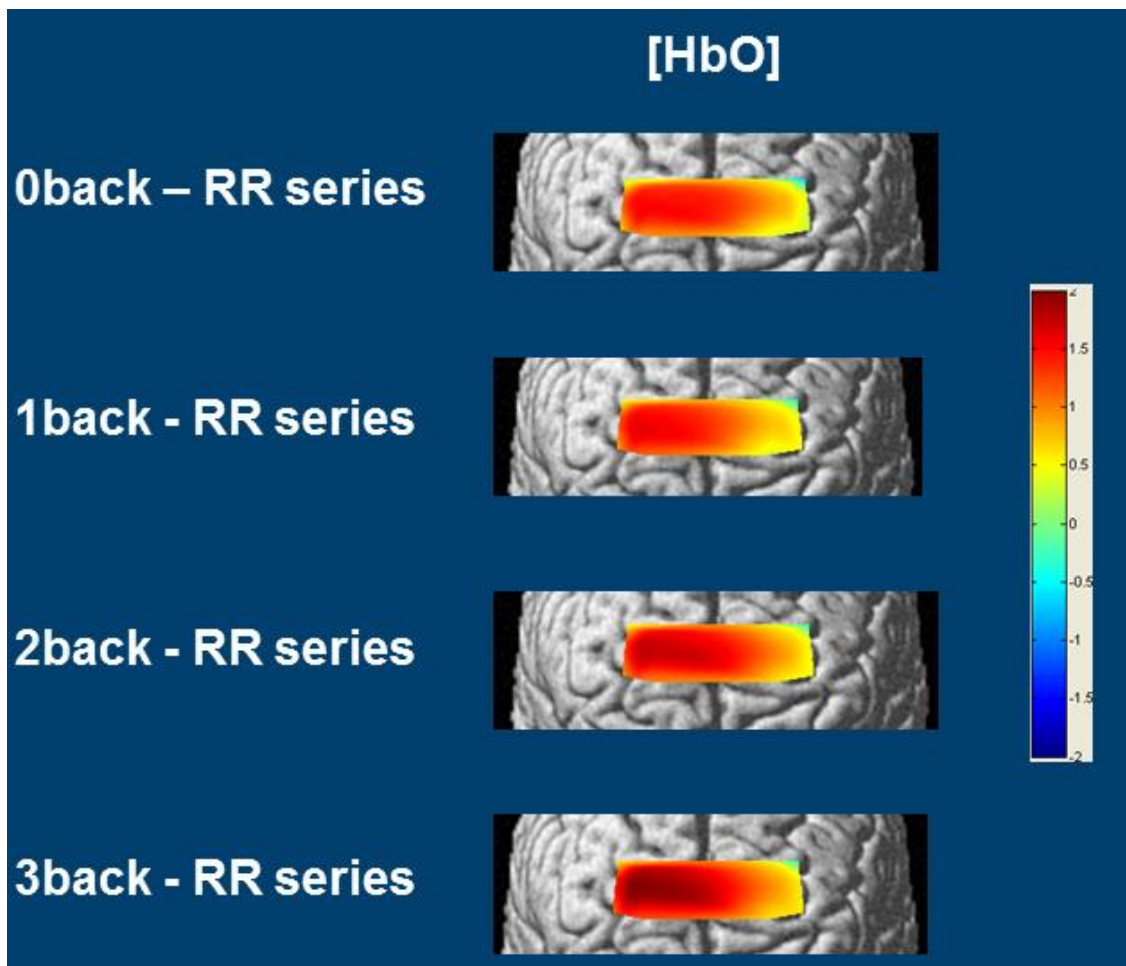
Fig.3.20: The image shows the statistical maps of HbO activation resulting from contrasting the ECG regressor vs. the initial baseline during a working memory task with graded cognitive loads. This is a frontal view. A 1st level analysis (one healthy subject) is shown here. Significance was not thresholded here.

handgrip of one hand, being the subject seated in a comfortable chair, is usually not demanding enough for a modification of the ECG to happen. On the other hand, this regressor was applied for the analysis of tests implying some stressful situation, due to the difficulty, rapidity or emotional involvement of the task. Indeed, apart from pathological statuses, it is well known that ECG is conditioned by the subject's emotional state.

In fig.3.20 some statistical maps are shown, which depict the correlation between NIRS data and the ECG regressor. They were obtained while processing NIRS data recorded during the "n-back" working memory task (see chapter 2 for details) with graded levels of cognitive requirement. The cognitive effort increases from top to bottom of the image, being the "0-back" the pure attentive condition (least demanding), and the "3-back" the hardest mnemonic condition (most demanding). It can be observed that the statistical power increases with the task demand, proving that a more stressful situation indices stronger conditioning on ECG and hemoglobin dynamics.

Bibliography

Aletti F, Re R, Pace V, Contini D, Molteni E, Cerutti S, Bianchi AM, Torricelli A, Spinelli L, Cubeddu R, Baselli G. *Deep and surface hemodynamic signal from functional time resolved transcranial near infrared spectroscopy compared to skin flowmotion. ComputBiol Med. 2011 Jul 8.*

Bullmore, E., Brammer, M., Williams, S.C., Rabe-Hesketh, S., Janot, N., David, A., Mellers, J., Howard, R., Sham, P., 1996. *Statistical methods of estimation and inference for functional MR image analysis Magn Reson Med 35, 261-277.*

Contini D., A. Torricelli, A. Pifferi, L. Spinelli, and R. Cubeddu, *"Novel method for depth-resolved brain functional imaging by time-domain NIRS," in: Diffuse Optical Imaging of Tissue , Brian W. Pogue, RinaldoCubeddu, Editors , Proc. SPIE 2007;Vol. 6629, 662908, (2007).*

Contini D., A. Torricelli, A. Pifferi, L. Spinelli, F. Paglia, and R. Cubeddu, *"Multi-channel time-resolved system for functional near infrared spectroscopy," Opt Expr. 14, 5418-5432, (2006).*

Del Bianco S., F. Martelli, and G. Zaccanti, *"Penetration depth of light re-emitted by a diffusive medium: theoretical and experimental investigation," Phys. Med. Biol. 47, 4131-4144 (2002)*

Delpy DT, Cope M. *Quantification in tissue near-infrared spectroscopy. Philosophical Transactions of the Royal Society of London, Series B- Biological Sciences 1997; 352(1354): 649-659*

Delpy DT, Cope M. *Quantification in tissue near-infrared spectroscopy. Philos Trans R Soc Lond B Biol Sci 352: 649–659, 1997.*

Elwell, C.E., Springett, R., Hillman, E., Delpy, D.T., 1999. *Oscillations in cerebral haemodynamics: implications for functional activation studies. Adv. Exp. Med. Biol. 471, 57–65.*

Ferrari M, Mottola L, Quaresima V. *Principles, Techniques, and Limitations of Near Infrared Spectroscopy. Can J Appl Physiol 2004; 29(4): 463-487*

Germon TJ, Evans PD, Barnett NJ, Wall P, Manara AR, Nelson RJ. *Cerebral near infrared spectroscopy: emitter-detector separation must be increased. Br J Anaesth 1999; 82: 831–7.*

Gibson, A., Hebden, J., Arridge, S., 2005. *Recent advances in diffuse optical imaging. Phys. Med. Biol. 50, R1–R43.*

Huppert, T.J., Diamond, S.G., Franceschini, M.A., Boas, D.A., 2009. *HomER: a review of time-series analysis methods for near-infared spectroscopy of the brain. Appl. Opt. 48, D280–D298.*

Jang, K. E., Tak, S. H., Jung, J. W., Jang, J. D., Jeong, Y., and Ye, J. C., 2009, *Wavelet-MDL detrending for near-infrared spectroscopy (NIRS)," Journal of Biomedical Optics, vol. 14, no. 3, pp. 1-13, May/June 2009.*

Jobsis FF. *Noninvasive, infrared monitoring of cerebral and myocardial oxygen sufficiency and circulatory parameters. Science 1977; 198: 1264–7*

Katura, T., Tanaka, N., Obata, A., Sato, H., Maki, A., 2006. *Quantitative evaluation of interrelations between spontaneous low-frequency oscillations in cerebral hemodynamics and systemic cardiovascular dynamics. NeuroImage 31, 1600 1592.*

Koh, P. H., Glaser, D. E., Flandin, G., Kiebel, S., Butterworth, B., Maki, A., Delpy, D. T., Elwell, C. E., November 2007. *Functional optical signal analysis: a software tool for nearinfrared spectroscopy data processing incorporating statistical parametric mapping. J. Biomed. Opt. 12, 1–13.*

Koh, P.H., Glaser, D.E., Flandin, G., Kiebel, S., Butterworth, B., Maki, A., Delpy, D.T., Elwell, C.E., 2007. *Functional optical signal analysis: a software tool for nearinfrared spectroscopy data processing incorporating statistical parametric mapping. J. Biomed. Opt. 12 064010-1083-3668.*

Kurth CD, Thayer WS. A multiwavelength frequency-domain near-infrared cerebral oximeter. Phys Med Biol 1999; 44: 727–40.

Lakowicz JR, Berndt K. Frequency-domain measurements of photon migration in tissues. ChemPhysLett 1990; 166: 246–52

Matcher SJ, Cope M, Delpy DT. Use of the water absorption spectrum to quantify tissue chromophore concentration changes in near-infrared spectroscopy. Phys Med Biol 1994; 39: 177–96

McCormick PW, Stewart M, Goetting MG, Balakrishnan G. Regional cerebrovascular oxygen saturation measured by optical spectroscopy in humans. Stroke 1991; 22: 596–602

McCormick PW, Stewart M, Goetting MG, Dujovny M, Lewis G, Ausman JI. Noninvasive cerebral optical spectroscopy for monitoring cerebral oxygen delivery and hemodynamics. Crit Care Med 1991; 19: 89–97

Miura H, McCully K, Hong L, Nioka S, Chance B. Regional difference of muscle oxygen saturation and blood volume during exercise determined by near infrared imaging device. Jpn J Physiol. 2001 Oct;51(5):599-606.

Nomura Y., O. Hazeki, and M. Tamura, "Relationship between time-resolved and non-time-resolved Beer-Lambert law in turbid media," Phys. Med. Biol. 42, 1009-1023, (1997).

Obrig H, Villringer A. Beyond the visible - imaging the human brain with light. J. Cereb. Blood Flow & Metab. 2003; 23: 1-18

Obrig, H., Neufang, M., Wenzel, R., Kohl, M., Steinbrink, J., Einhaupl, K., Villringer, A., 2000. Spontaneous low frequency oscillations of cerebral hemodynamics andmetabolism in human adults. NeuroImage 12, 639 623.

Ohmae E, Ouchi Y, Oda M, et al. Cerebral hemodynamics evaluation by near-infrared time-resolved spectroscopy: correlation with simultaneous positron emission tomography measurements. Neuroimage 2006; 29: 697–705

Pan J. and Tompkins W.J. 1985, A Real-Time QRS Detection Algorithm, IEEE Trans. on Biomed. Eng., BME-32(3):230-236

Plichta, M. M., Heinzel, S., Ehlis, A. C., Pauli, P., Fallgatter, A. J., April 2007. Model-based analysis of rapid event-related functional near-infrared spectroscopy (NIRS) data: A parametric validation study. NeuroImage 35, 625–634.

Plichta, M., Herrmann, M., Baehne, C., Ehlis, A., Richter, M., Pauli, P., Fallgatter, A., 2006. Event-related functional near-infrared spectroscopy (fNIRS): Are the measurements reliable? Neuroimage 31 (1), 116–124.

Quaresima V, Ferrari M. Cerebral oximetry. J Neurosurg. 2001 May;94(5):864-6.

Quaresima V, Ferrari M. Quantitation of muscle oxygenation by near-infrared spectroscopy methods. Eur J Appl Physiol. 2002 Jan;86(3):283-4; author reply 285-6.

Rolfe P. In vivo near-infrared spectroscopy. Annu Rev Biomed Eng 2000; 2: 715-754 Sato N, Hagihara B, Kamada T, Abe H. Anal Biochem 1976; 74: 105-117

Rolfe P. *In vivo near-Infrared spectroscopy. Annu Rev Biomed Eng 2: 715–754, 2000*

Saager, R., Berger, A., 2008. Measurement of layer-like hemodynamic trends in scalp and cortex: implications for physiological baseline suppression in functional near-infrared spectroscopy. J. Biomed. Opt. 13, 034017.

Schroeter, M.L., Bucheler, M.M., Muller, K., Uludag, K., Obrig, H., Lohmann, G., Tittgemeyer, M., Villringer, A., Cramon, D.Y., 2004. Towards a standard analysis for functional near-infrared imaging. NeuroImage 21, 283–290.

Selb J., "Improved sensitivity to cerebral hemodynamics during brain activation with a time-gated optical system: analytical model and experimental validation," Journal of Biomedical Optics, Vol. 10, No. 1, 11013, (2005).

Steinbrink J., H. Wabnitz, H. Obrig, A. Villringer, and H. Rinneberg, "Determining changes in NIR absorption using a layered model of the human head," Phys. Med. Biol. 46, 879-896, (2001).

Steinbrink J., Wabnitz H, Obrig H, Villringer A, and Rinneberg H. Determining changes in NIR absorption using a layered model of the human head. Phys. Med. Biol. 46, 879-896, 2001.

Sun, J., Loader, C., 1994. Simultaneous confidence bands for linear regression and smoothing. Ann. Statist 22 (3), 1328–1345.

Suzuki S, Takasaki S, Ozaki T, Kobayashi Y. A tissue oxygenation monitor using NIR spatially resolved spectroscopy. Proc SPIE 1999; 3597: 582-592

Tachtsidis, I., Leung, T.S., Devoto, L., Delpy, D.T., Elwell, C.E., 2008. Measurement of frontal lobe functional activation and related systemic effects: a near-infraredspectroscopy investigation. Adv. Exp. Med. Biol. 614, 397–403.

Taga, G., Konishi, Y., Maki, A., Tachibana, T., Fujiwara, M., Koizumi, H., 2000. Spontaneous oscillation of oxy- and deoxy- haemoglobin changes with a phasedifference throughout the occipital cortex of newborn infants observed using non-invasive optical topography. Neurosci. Lett. 282, 104 101.

Watzman HM, Kurth CD, Montenegro LM, Rome J, Steven JM, Nicolson SC. Arterial and venous contributions to near-infrared cerebral oximetry. Anesthesiology 2000; 93: 947–53

Worsley, K. J., Friston, K. J., 1995. Analysis of fMRI time-series revisited again NeuroImage 2, 173–181.

Ye, J.C., Tak, S.H., Jang, K.E., Jung, J.W., Jang, J.D., 2009. NIRS-SPM: statistical parametric mapping for near-infrared spectroscopy. NeuroImage 44, 428–447.

Validation Study

>>KeyPoints

> Time resolved NIRS can separate **intra-cerrebral and extra-cerebral** contributions of HbO, HHb and HbT

> Timer resolved NIRS allows for the study of systemic autonomic and local vasomotor regulation

> NIRS can be used in combination with Laser Doppler in neurology, albeit some cautions must be applied.

One open issue in the assessment of the relationship between the NIRS signal and the functional response of the prefrontal cortex is the need for an accurate and reliable disentanglement of systemic hemodynamic changes from functional changes, being the latter related to cortical activations in response to proper stimuli or tasks and the former referable to cardiovascular (CV) autonomic and local regulation. Models based on time-resolved measures have been recently proposed, in order to separate skin flow confounding effects from cortical activity, which can be traced back to early and late photons, respectively (Liebert et al., 2004; Contini et al., 2006).

However, a few assumptions underlying these models still need more evidence in their support, since their validation has been mainly carried out by comparing the information extracted from fNIRS and fMRI measurements. An alternative option may be the assessment of the optical response of different layers of the head, from the pre-frontal cortex up to the more superficial layers of the forehead and temples skin. To fulfil this purpose, prefrontal cortex hemodynamics can be monitored by fNIRS, while flowmotion of the superficial layers of the forehead and temples skin can be measured by laser Doppler flowmetry (LDF) (Sheperd & Oberg, 1990).

LDF provides continuous, non invasive measurements of microcirculatory blood flow, or vasomotion, or flowmotion, in the skin surface LDF is able to investigate blood flow through arterioles, capillaries and venules in a volume of approximately 1 mm^3 and penetrating to a depth of 1-2 mm.

4.1 Previous works

Stefanovska and co-workers (1999) extracted the dynamics of local hemodynamics carried by the LDF signal, also pointing out the relationship with the classical CV spectral bands. Since local hemodynamics are characterised by oscillations in the VLF (Very Low Frequency) band of the CV spectrum, experimental measurements with LDF have to be performed over sufficiently long intervals. By following the footsteps of the methodological and physiological observations reported in Stefanovska et al., (1999), other researchers, were able to extract from LDF recordings the information related to local hemodynamics and vasomotor regulation in conditions of severe stress of the whole cardiovascular system. Such stress consisted in strong systemic stimuli which drive the main rhythms of hemodynamic variability through the autonomic nervous system (Kvernmo et al., 1998; Serne' et al., 2002;Urbancic-Rovan, 2004; Rossi et al. 2004, 2005a, 2005b, 2006; Kvandal et al., 2006; Landsverk et al., 2007).

Stauss et al. (1998) were able to focus on the sympathetic activity in the LDF signal in the low frequency (LF) band of the CV variability spectrum, and to compare its analysis with power spectral analysis of systemic signals (ECG, respiration, arterial blood pressure). This was done by applying spectral computation approaches based on the FFT algorithm and thus showing how skin vasomotion can be sympathetically induced to respond at a frequency around 0.1 Hz in humans.

These previous findings can motivate the use of LDF to disentangle the contribution to local variability by peripheral autoregulation from autonomic driven variability under systemic stimuli, therefore suggesting that LDF may help detecting the disturbances carried by surface flowmotion to the functional component of the NIRS measurement.

To our knowledge, the simultaneous use of NIRS and LDF devices for the direct validation of the functional information carried by the NIRS signal was previously proposed in an invasive study on piglets (Klaessens et al., 2003). In their study, Klaessens and coworkers chronically placed LDF probes on the dura to verify that the content of information in the fNIRS signal, which is supposed to be related to the activation of the prefrontal cortex of the brain, is not disturbed by the noise due to local autoregulation phenomena which contribute to the flowmotion or vasomotion signal detected by the LDF.

4.2 Our contribution

In the present PhD thesis, a different approach to the contemporaneous use of LDF and NIRS recordings for the validation of the functional information content of the NIRS signal is proposed and applied to an experimental protocol with the following goals:
1. to achieve a better physiological comprehension of the cross-talks among CV regulation under stimulation of the autonomic nervous system (ANS), brain autoregulation, and functional response;
2. to validate fNIRS time resolved technique, with respect to its informational content;
3. to perform better confounding effect cancellation in tr-NIRS data due to skin flowmotion.

The experimental recordings which were analyzed in this work included a time resolved, frontopolar (Fp2), fNIRS and two laser Doppler flowmetry (LDF) measurements.

Prior to the experimental protocol of autonomic stimulation for the disentanglement of the hemodynamic effects due to cortex functional response and surface skin flowmotion, a preliminary protocol was necessary in order to determine if either device could be a source

of noise and disturbance This testing phase of the experimental setup that would have been used for this work allowed to determine the distance between the two LDF probes and the NIRS optode used.

4.3 Signal processing and analysis

Artifact free, stationary segments approximately 5 min long were selected in pre-Valsalva Maneuver (pre-VM) and post-VM epochs of the acquired data (a description of the Valsalva Maneuver is provided in Chapter 3) .

Early and late, HbO and HHb concentration samples were extracted from fNIRS recordings. LDF signals were acquired with a 32 Hz sampling frequency while fNIRS functional parameters with a 1 Hz sampling frequency to improve single photon counting and photodetector efficiency. Time series of the flowmotion signals were extracted from the LDF raw signals, which were downsampled to 4 Hz, by means of an antialising low-pass filter. This was done in order to limit the bandwidth of the signal to the regulatory mechanisms of interest, from the very slow local vasomotor phenomena related to vascular autoregulation up to the respiratory and heartbeat frequencies. In addition, the time series derived from the right and left LDF raw measurements were averaged.

Analysis included time correlation during VM, spectral and correlation analysis during pre-VM and post-VM in the very low frequency band (VLF, frequencies (f) < 0.04 Hz), in the autonomic bands (LF, 0.04 Hz < f < 0.15 Hz; HF, 0.15 < f < 0.5 Hz), and in the band where the dominating phenomenon is the pulse (0.8 < f < 2 Hz).

As regards the cross-correlation analysis, the cross-correlation function was computed in three different epochs: pre-Valsalva (1200 samples), Valsalva (50 samples) and post-Valsalva (1200 samples).

Power spectral analysis of pre-VM and post-VM time series were performed by autoregressive (AR) parametric model estimation, and also by non parametric approaches (Fourier transform and Welch modified periodogram)

4.4 Statistical analysis

All statistics were performed using R statistical software and Matlab Statistical Toolbox. For the time interval preceding VM, the statistical analysis was carried out by applying parametric t-paired test to correlation data of the paired LDF channels; a Wilcoxon rank sum nonparametric test was used to assess significant differences between LDF and fNIRS data. Differences between two groups (e.g. pre-VM vs.VM; post-VM vs. VM and pre-VM vs. post-VM) were analyzed using paired 2-tailed Student's t test if Kolmogorov-Smirnov null hypothesis of normal distribution could not be rejected. The level of significance was set to p=0.05. Normalized correlation coefficients between LDF and fNIRS during VM and power contents in the VLF and ''autonomic'' band were instead compared using Wilcoxon sum rank non parametric test in order to get more robust statistics being the population not normally distributed (Kolmogorov– Smirnov, p<0.05). Regression analysis was applied to quantify the correlation between the spectral power of LDF and fNIRS time series in the VLF band and in the autonomic band (LF+HF). Also, cross- correlation analysis was carried out to assess the correlation between VLF, LF, and HF normalized powers in the spectra of the left and right temples laser Doppler flowmotion signals. Boxplots were derived to compare medians and averages of different populations

through paired Student t-test. Wilcoxon sum-rank nonparametric test was applied to the second phase-protocol data.

4.5 Phantom trials

The recordings during the experimental protocols included a time resolved, frontopolar (Fp2), fNIRS measurement and two laser Doppler flowmetry (LDF) measurements, with the LDF optodes placed on the left and right temples at a distance longer than 3 cm from the fNIRS optode. This optimal distance was determined by phantom trials, aimed at minimizing the optical interference between the two sources of signal, notably the disturbance produced by the LDF emitter on the NIRS probe. The fNIRS optodes were also equipped with sharp filters cutting the LDF light out; nonetheless, uncorrupted measures required the 3 cm minimum distance.

4.6 Preliminary experiment

Eight healthy volunteers (HV, age 25±2), sitting comfortably in a quiet, conditioned (temperature 23±2 °C), dimly lit room were required to perform a Valsalva Manoeuvre (VM) for a duration of 15 s. The VM was preceded by a 10 minute long pre-VM epoch of baseline recordings in conditions of spontaneous hemodynamic variability, and by a 10 minute long recovery period after Valsalva, to assess the spontaneous vasomotor variability and the recovery after the strong stimulation provided by VM, respectively. All subjects, who voluntarily enrolled in the study after signing the informed consent authorization, were non-smokers and had no history of cardiovascular or respiratory disorder. Alcohol, caffeine and any drugs were not taken for a half day before the experiments.

A laser Doppler flowmeter (780 nm 1 mW) (Perimed AB,Sweden), connected to a laptop equipped with a data acquisition system (Perimed Systems, Inc.,Sweden) was used to record the temple skin flowmotion measured in relative units (Arbitrary Perfusion Units). Two coaxial probes (Perimed AB, Sweden) were placed on the right and left temple with double-sided tape. Prior to the beginning of the protocol, the subjects adapted to the environment where the experiment was carried out, sitting on an armchair for at least ten minutes after placing the LDF and NIRS probes on their head. Baseline recordings of spontaneous vasomotion and in conditions of spontaneous hemodynamic variability were then acquired for 10 minutes at rest. At the end of this baseline recording period all subjects were asked to execute a forced expiratory maneuver (VM) for 15 seconds. Then recovery recordings followed for 10 minutes.

The goal of this preliminary study was to ascertain a high coherence between the two distant LDF signals during both a 15 s VM and the pre and post-VM stationary periods. This was considered a pre-requisite for the two LDF signals to provide with a sufficiently reliable measure of skin flow of the forehead and temples This flow, indeed, was assumed to be representative of the surface hemodynamic signal in correspondence of the pre-frontal cortex, the perfusion of which can be detected by a NIRS device.

Correlation analysis between LDF channels (left temple, right temple) before the VM provided the correlation coefficient range of microcirculation perfusion at rest (0.65±0.85). During recovery following the VM, the coefficient decreased to (0.45±0.85) (p<0.01) (Fig.4.1). Pre-VM r-coefficient values were higher than post-VM in 7 subjects out of 8

(Table 4.1). During VM, higher values of correlation between the two LDF channels were found (0.96±0.02, p<0.001).
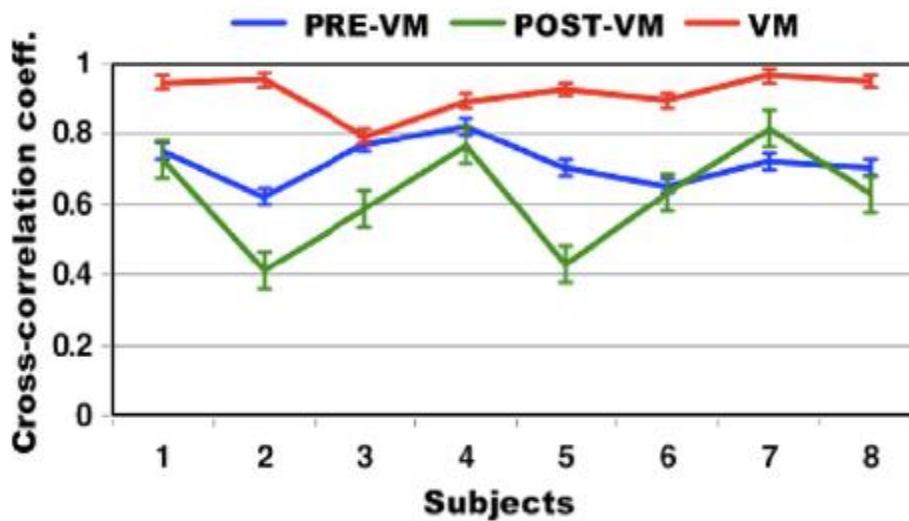

Figure 4.1. Cross-correlation coefficients between left and right-temple skin flow signals in pre-VM, during Valsava, and post-VM periods in the 8 subjects participating in the preliminary protocol. (Errorbars indicate standard error).

Subject #	Pre-VM (p-value)	VM (p-value)	Post-VM (p-value)
1	0.75 $p<0.01$	0.94 $p<0.001$	0.73 $p<0.01$
2	0.62 $p=0.08$[a]	0.95 $p<0.001$	0.41 $p=0.12$[a]
3	0.77 $p<0.01$	0.79 $p=0.07$[a]	0.59 $p=0.09$[a]
4	0.82 $p<0.01$	0.89 $p<0.01$	0.77 $p<0.05$
5	0.70 $p<0.01$	0.92 $p<0.001$	0.43 $p=0.07$[a]
6	0.65 $p=0.05$	0.89 $p<0.01$	0.63 $p<0.05$
7	0.72 $p<0.01$	0.96 $p<0.001$	0.81 $p<0.01$
8	0.70 $p<0.01$	0.95 $p<0.001$	0.63 $p=0.05$

[a] Not significant correlations.

Table 4.1 Coefficients of correlation between LDF signals recorded from left and right temples. During VM correlation is significant in 7 out of 8 subjects (p<0.01).

4.7 Autonomic stimulation experiment

The NIRS optode was placed on the forehead, slightly to the right of the frontal suture, in Fp2 position, while the LDF probes were placed on the left and right temples at a distance longer than 3 cm from the fNIRS optode.
The experimental set-up and the protocol were the same of the preliminary protocol (10 minutes of spontaneous variability recordings, 15 seconds of forced expiratory Valsalva maneuver, 10 minutes of recovery to baseline). Thirteen healthy volunteers (age 28±2) were enrolled and gave their informed consent to participate in the study.

All 13 subjects enrolled in the main experiment (simultaneous recording of LDF signals on the left and right temple, fNIRS recording on the forehead, in Fp2 position) displayed similar responses to VM, with particularly distinguishable and repeatable patterns in the averaged LDF signal and in the surface HbO dynamics (respectively red and black tracings in fig. 4.2).
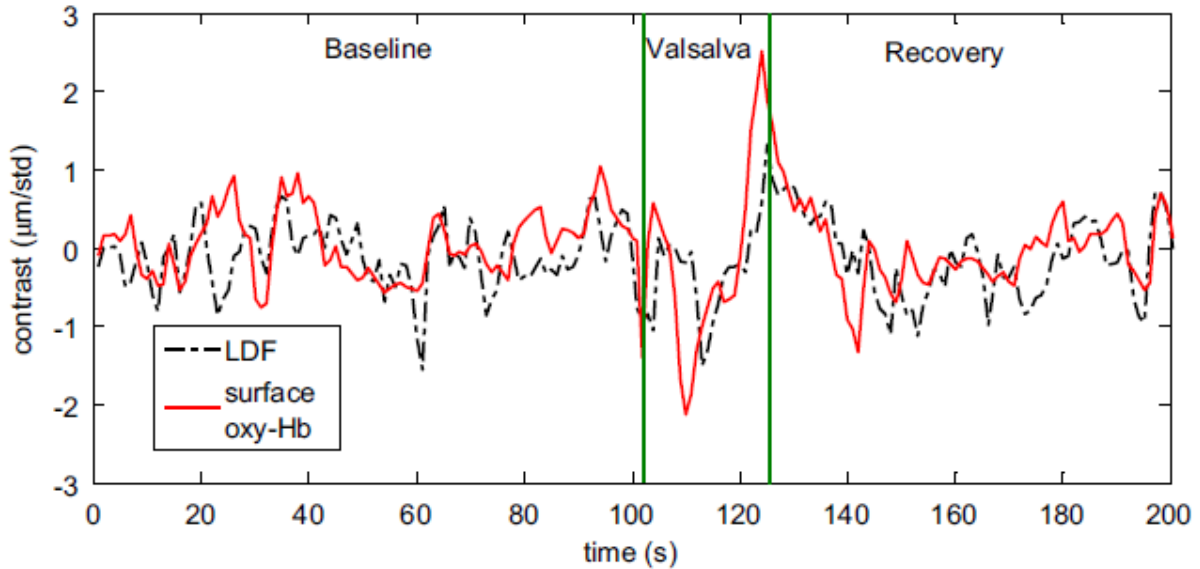
Figure 4.2. Grand average of LDF (black) and NIRS surface oxy-Hb (red) signals showing common patterns in their time course during the protocol. Green lines mark VM onset and offset.

Both transients showed an undershoot during the deep inspiration preparing the Valsalva onset and a marked overshoot during the forced expiration. After the Valsalva offset (15 s after the onset), surface HbO concentration fell more rapidly (~13 s) than the LDF signal (~18 s).

Intra cerebral fNIRS signals, calculated from the late photons measurements, showed different dynamics: the fast rising spike appearing at the VM onset, and typical of forced expiratory VM maneuver in LDF and superficial HbO, faded in deep fNIRS dynamics (Fig.4.3).
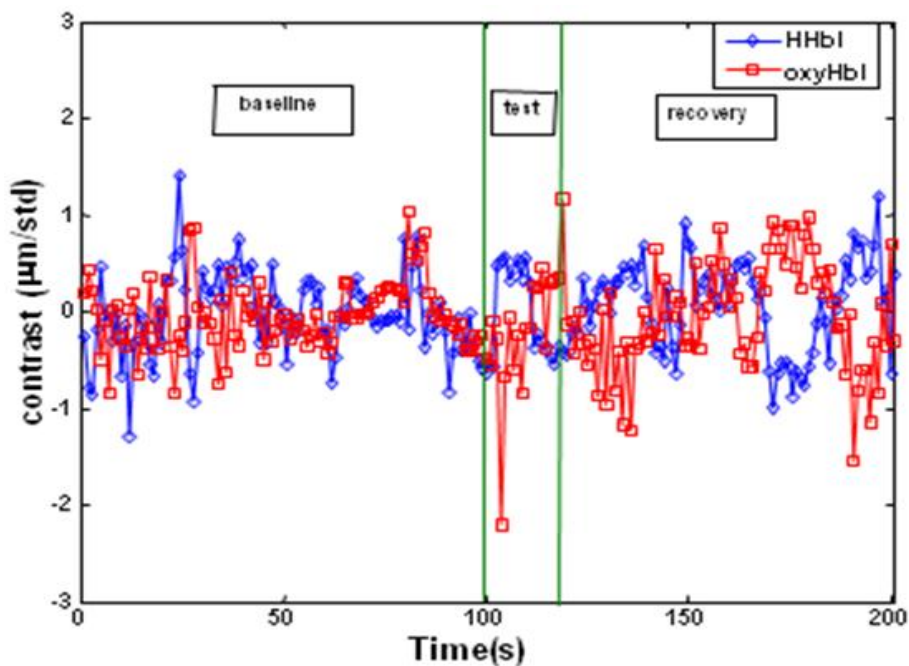
Figure 4.3. Grand average of NIRS cortical oxy-Hb (red) and deoxy-Hb (blue) measurements, referred to late photons measures of intracerebral haemodynamics.

High correlation (r>0.9) was found during VM between LDF and all fNIRS signals; however, after scaling it (Fig.4.4) by fNIRS signal rms (i.e., fNIRS rms correlated to LDF),

54

significantly higher values (0.04±0.010 surface HbO; 0.01±0.006 surface HHb) were obtained for surface signals compared to cortical ones (0.02±0.008 cortex HbO; 0.009±0.0015 cortex HHb). Similarly, higher r coefficients were found for HbO compared to HHb.
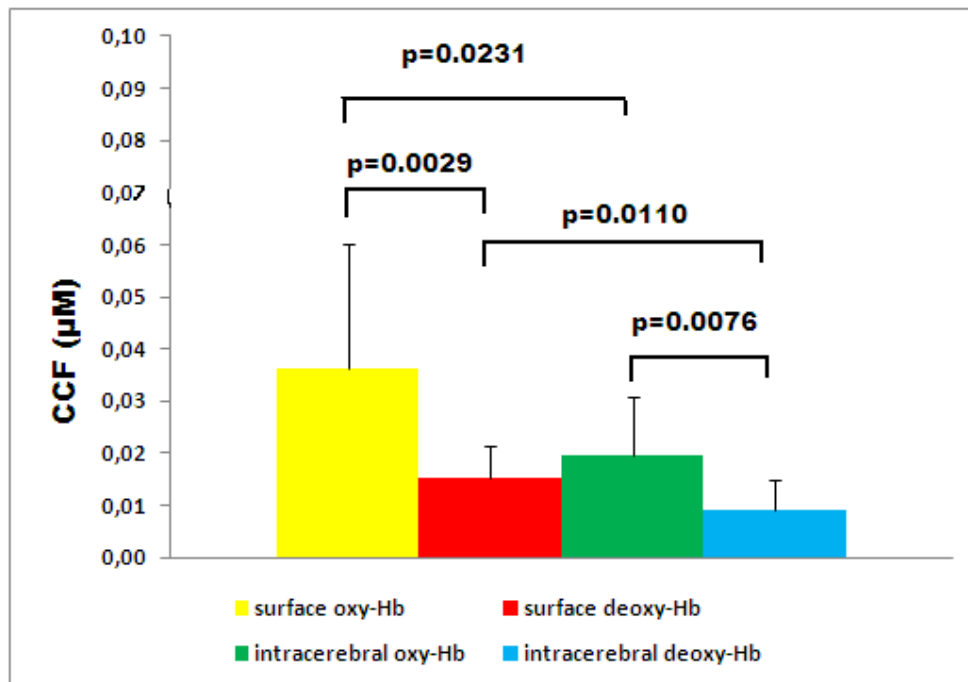
Figure 4.4. Cross-correlation coefficients rescaled by rms of surface and cortex oxy-Hb and deoxy-Hb. Oxy-Hb value is significantly higher than deoxy-Hb value; extracerebral oxy-Hb values are significantly higher than intracerebraldeoxy-Hb values.

During pre and post-VM, the spectral analysis of LDF and fNIRS time-series revealed the presence of a large VLF component and significant activity in the LF (vasomotor) and HF (respiratory) band (Fig.4.5). The poorly correlated power, however, did not allow a separate analysis of LF and HF bands so that these least were unified in a single autonomic "LF+HF" band.

In pre-VM and post-VM, both LDF and fNIRS displayed VLF and LF+HF activity, but low correlations (0.1<r<0.2) were found in both bands between fNIRS and LDF signals.

Power coherence calculation confirmed VLF band-related power to be the main common power component of surface skin flowmotion signal detected by LDF and extracerebral HbO obtained through fNIRS, both before and after VM (Fig.4.6 left).

The power of VLF and LF+HF band did not vary significantly post Valsalva maneuver both in LDF and extra-cerebral HbO signals (Fig.4.6 right). The prevalent power content in the VLF band was consistent with the typically slow rhythms of peripheral microvascular hemodynamics (Stefanovska et al., 1999) which characterize the vasomotion phenomena detected by the LDF signal.
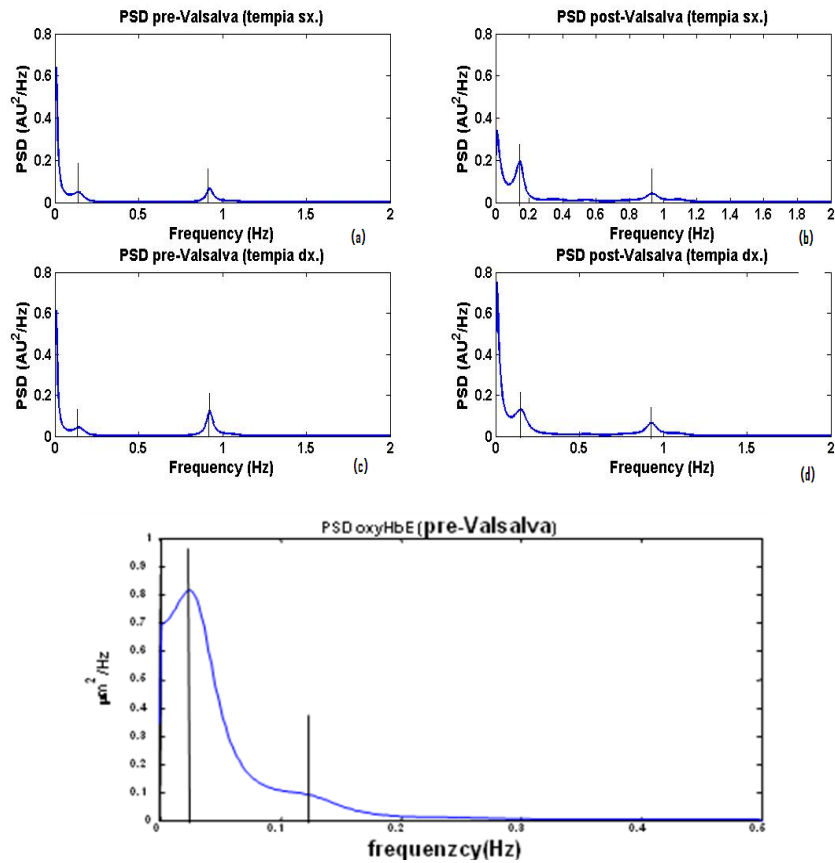
Figure 4.5. Power spectra of LDF (a,b,c,d) and fNIRS signals during pre-Valsalva (left) and post-Valsalva (right) for one subject. Spectral analysis confirms the overlapping of LF and HF bands.
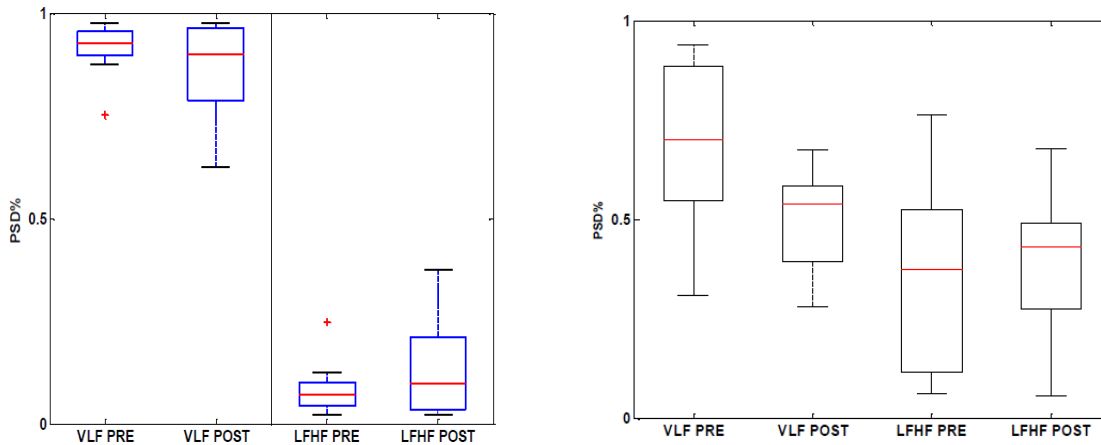
Figure 4.6. Left: box-plot of total VLF and LF+HF power of LDF before and after VM. Right: box-plot of total VLF and LF+HF power of superficial HbO before and after VM.

4.8 Interpretation

The phantom trials and the preliminary experiments were useful to analyze the cross-talk between the two instruments used for the main experimental protocol presented in this

chapter. The phantom trials allowed to determine that, because of the different power emitted by the laser Doppler flowmeter and the near-infrared spectroscope, the optimal set-up would entail placing the two LDF probes on the opposite sides of the forehead, with the NIRS optode placed in correspondence to the medial portion of the frontal lobe".

Subsequently, the preliminary test on the information carried by the two LDF signals collected on the two temples showed that the vasomotion related dynamics detected by the two signals were highly correlated and comparable. Given that it would be virtually impossible to thoroughly map the entire forehead by an empiric approach aimed at finding the potential discrepancies in local vasomotor responses, our approach basically revealed the affinity in the information conveyed by the two LDF recordings, thus suggesting that the vasomotor and autoregulation typical dynamics of the two measurement sites could be considered homogeneous. Moreover, Tsuji et al. (2000), and Brady et al. (2007) found one peak of coherence between NIRS signal and arterial blood pressure in neonates and between NIRS and Laser-Doppler signal in piglets respectively, at frequencies lower than 0.04 Hz. The spectral analysis presented in this work seems to match these previous findings.

The results of the preliminary experiment suggested that the strong hemodynamic perturbation induced by Valsalva provocative test generated: a) first, a sharp synchronization of central and peripheral oscillations during a forced expiratory maneuver, indicated by the high value of correlation between the two LDF channels; b) a desynchronization of oscillatory rhythms following the VM, which characterized the recovery epoch.

The main experiment was aimed at investigating the potential correlation between the so-called "early photons" detected by the NIRS device and referred to the surface response, and the LDF signals. A first element of interest was brought by the comparable patterns in the time domain shown by both the LDF and the extra-cerebral NIRS. Our results confirmed previous findings obtained by Themelis et al. (2007), who observed good correlation between the information captured by the laser Doppler system and the time continuous NIRS device during the evaluation of the scalp influence in the measurement of the arterial oscillations originating in the brains of piglets. In addition, the normalized cross-correlation coefficients (fig. 4.4) further emphasized the relationship between surface hemodynamics related to local flowmotion and the component of the NIRS data which are interpreted as unrelated to either the functional cortical activation and hemodynamics.

The importance of these findings mainly consists in the effectiveness of the LDF signal in supporting a validation of the statistical hypothesis underlying the definition of the "early photons" detected by the NIRS optode as representative of the extra cortical areas of the frontal skull. The results presented in this chapter appear rather compelling in showing that the model-based separation of time-resolved NIRS early (superficial) and late (deep) photons is able to cancel, or at least buffer, the surface confounding effects.

Although one of the limitations of the current protocol might be the ability of the LDF to investigate a volume of the forehead comparable, in depth, to the surface portion that is meant to be included in the extra-cerebral NIRS signal acquisitions, it was also clearly emphasized that the comparable patterns and the cross-correlation between the LDF grand average and the extra-cerebral NIRS supported the hypothesis that early photons dynamics are strongly influenced by surface skin vasomotion. This may partly depend on hemodynamic changes unrelated to cortical variations in blood flow. The ensuing interpretation, thus, is that this dependency could be ascribed to systemic changes, which are especially significant under the drive of strong hemodynamic provocations such as a Valsalva maneuver.

Obrig et al. (2003) have shown that systemic changes may appear in the extra-cerebral compartment and can influence NIRS measurements. On the other hand, Stefanovska et al. (1999) showed that the skin blood vasomotion related information conveyed by the LDF is subject to systemic drives and stimuli. Our results were consistent with these previous reports: although the measured local flow dynamics basically reflects the effect of vasomotion on peripheral resistance and flow in a much limited peripheral district of the arterial tree, and although the microcirculation is not innervated by sympathetic fibers as larger caliber vessels, the drive of the beating heart, of respiration, and of global control of circulation is in part conveyed to the peripheries by the pulsating arterial wave, whose dynamic features are largely buffered by peripheral compliances.

4.9 Outcome

In this chapter we aimed at demonstrating the feasibility of combined fNIRS and LDF optical measures and we confirmed the effectiveness of time resolved fNIRS in separating deep from surface signals during provocative maneuvers like a Valsalva. Our experimental and analytical approach was able to propose simple approaches to the validation of the interpretation of late photons detected by the NIRS signal as representative of functional and hemodynamic cortical activation, as well as to show a method to accurately remove or attenuate surface physiologic noise from the hemodynamic contribution coming from the cortex.

One of the physiological issues that remains open is whether autonomic control affects the deep cortical hemodynamics more than simple systemic provocative tests, such as Valsalva. Further autonomic tests might shed light on the difference in variability between surface and cortex fNIRS signals, and between pre-VM and post-VM responses.

Considering the potential significance of the fNIRS in portraying the functional activation of the prefrontal cortex, it might also be useful to further investigate the relationship between surface flowmotion and deep recordings in presence of simple functional tasks, such as finger tapping; in this case, the separation of the relevant confounding effects, which can be elicited by the likely side effects due to a contemporaneous autonomic activation whose role is still be to clarified, might prove instrumental in correctly characterizing the functional content of deep fNIRS as a reliable measurement of cortical activation.

Bibliography

Brady KM, Lee JK, Kibler KK, Smielewski P, Czosnyka M, Easley RB, Koehler RC, Shaffner DH. Continuous time-domain analysis of cerebrovascular autoregulation using near-infrared spectroscopy. Stroke. 2007 Oct;38(10):2818-25.

Contini D et al., A multi-channel time-resolved system for functional near infrared spectroscopy, Opt Expr 14, 5418-5432, 2006.

Klaessens et al., Monitoring cerebral perfusion using near-infrared spectroscopy and laser Doppler flowmetry, Physiological Measurement, 2003

Kvandal P, Landsverk SA, Bernjak A, Stefanovska A, Kvernmo HD, Kirkeboen KA. Low-frequency oscillations of the laser Doppler perfusion signal in human skin. Microvasc Res 2006;72(3):120-127.

Kvernmo HD, Stefanovska A, Bracic M, Kirkeboen KA, Kvernebol K. Spectral analysis of the Laser Doppler perfusion signal in human skin before and after exercice. Microvascular research 1998,56:173-182.

Landsverk SA, Kvandal P, Bernjak A, Stefanovska A, Kirkeboen KA. The effects of general anesthesia on human skin microcirculation evaluated by wavelet transform. AnesthAnalg 2007;105(4):1012-1019.

Liebert et al., Time-resolved multidistance near-infrared spectroscopy of the adult head: intracerebral and extracerebral absorption changes from moments of distribution of times of flight of photons, Appl. Optics, 3037-3047, 2004.

Obrig et al., Beyond the visible- imaging the human brain with light, J Cereb Blood Flow Metab., 1-18, 2003

Rossi M, Bertuglia S, Varanini M, Giusti A, Santoro G, Carpi A. Generalised wavelet analysis of cutaneous flowmotion during post-occlusive reactive hyperemia in patients with peripheral arterial obstructive disease. Biomed Pharmacother 2005a;59:233-239.

Rossi M, Carpi A, Di Maria C, Galetta F, Santoro G. Spectral analysis of Laser Doppler skin blood flow oscillations in human essential arterial hypertension. Microvascular research 2006, 72:34-41.

Rossi M, Maurizio S, Carpi A. Skin blood flowmotion response to insulin iontophoresis in normal subjects. Microvasc Res 2005b;70:17-22.

Rossi M, Ricco R, Carpi A. Spectral analysis of skin Laser Doppler blood perfusion signal during cutaneous hyperemia in response to acetylcholine iontophoresis and ischemia in normal subjects. ClinHemorheolMicrocirc 2004;31:303-310.

Serne' EH, Ijzerman RG, Gans ROB, Nijveldt R, de Vries G, Evertz R, Donker AJM, Stehouwer CDA. Direct evidence for insulin-induced capillary recruitment in skin of healthy subjects duringphysiological hyperinsulinemia. Diabetes 2002;51:1515-1522.

Sheperd& Oberg, Laser Doppler flowmetry, 1990.

Stauss HM, Anderson EA, Haynes WG, Kregel KC. Frequency response characteristics of sympathetically mediated vasomotor waves in humans. Am J Physiol. 1998 Apr;274:H1277-83.

Stefanovska A et al., Wavelet analysis of oscillations in the peripheral blood circulation measured by laser Doppler technique, IEEE Trans. Biomed. Med. Eng., 1230-1239, 1999.

Themelis G., D'Arceuil H., Diamond S.G., Thaker S., Huppert T.J., Boas D.A., andFranceschini M.A. Near-infrared spectroscopy measurement of the pulsatile component of cerebral blood flow and volume from arterial oscillations J Biomed Opt. 2007 Jan-Feb;12(1):014033.

Tsuji M, Saul JP, du Plessis A, Eichenwald E, Sobh J, Crocker R, Volpe JJ. Cerebral intravascular oxygenation correlates with mean arterial pressure in critically ill premature infants. *Pediatrics.* 2000;*106*:625–632.

Urbancic-Rovan K, Stefanosvka A, Bernjak A, Azman-Juvan K, Kocijancic A. Skin blood flow in the upper and lower extremities of diabetic patients with and without autonomic neuropathy. J Vasc Res 2004;41:535-545.

Results

In this chapter we will present and discuss some results dealing with the major issues still open in the Near Infrared Spectroscopy field. In the first section, we will present some general results about a campaign testing 13 healthy people for motor cortex activation. Motor activation rises one of the broadest hemodynamic responses we can elicit in the brain. By inducing such a strong response, we could then test some mathematical and statistical methods for NIRS data processing and integration. We will briefly present here one case study showing how we can exploit methods such as General Linear Model for the deep investigation of refined physiological phenomena, and for the speculation about modulatory effects and interplays among the body systems. In the second section we will provide results about studies aiming at the disentanglement of issues related to NIRS working principle and hardware design. In this section we will explore some technical peculiarities, advantages and limitations of time resolved NIRS devices, which will be further discussed in Chapter 7.

The third section will move towards neuroscience applications, as it will show how NIRS data can be useful to study neurovascular coupling. A polygraphic study will be described, in which delays occurring between electroencephalographic, hemodynamic and electrocardiographic signals were computed, and the correlations between these biological signals disentangled. The last part will provide one specific example about the employment of time resolved NIRS for the distinction of cognitive abilities and for the quantitative evaluation of cognitive load. We will see that, while the former task is made feasible by tr-NIRS, the latter remains the next obstacle to put down.

>> KeyPoints

> The application of **General Linear Model** to NIRS data highlighted some modulatory effect induced by the experimental task in hemoglobin dynamics

> The application of **"biologically informed"** General Linear Model to NIRS data allowed the disentanglement of some relationships between different body compartments. EMG, alpha and beta EEG rhythms were found to correlate with the hemodynamic response elicited by a motor task.

> Time resolved NIRS makes feasible the separation of **intra-cerebral and extra-cerebral contributions** embedded in NIRS signals. Intra-cerebral contributions prevalently show the cortical hemodynamics, while extra-cerebral contributions prevalently display systemic effects acting in skin flowmotion.

> Time resolved NIRS was also employed for the study **of neurovascular coupling** during cognition. Activation of several systems was observed, each one characterized by a different time delay: neural electrical response was sudden, autonomic response was then risen, and a slower hemodynamic response was induced last.

> The combined employment of time resolved NIRS and General Linear Model processing succeeded in identifying **distinctive patterns** of cortical activation for two different neurophysiological categories: attention and working memory. Unfortunately, though, the distinction of cognitive loads could not be done on the basis of tr-NIRS recordings.

5.1 Data Integration

5.1.1 Background

Near-infrared spectroscopy has already been used to assess human motor-cortex oxygenation changes in response to self-paced movements as well as movement imagery. Indeed, motor tasks rise a huge activation in the brain, easily captured by NIRS. Wriessnegger et al. (2008) used a 24 channel NIRS-system for the study of sixteen healthy subjects performing a simple right and left hand tapping task and a kinesthetic movement imagery. All subjects showed significant increases in HbO during both tasks compared to the resting period, but with different onset latencies of oxygenation. During left and right movement imagery, the HbO concentration increased about 2 s later compared to real movement execution. Furthermore, the oxygenation found was bilaterally represented for both tasks but with temporal differences. Shibuya et al. (2008) examined six healthy, right-handed subjects during handgrip. The subjects performed a 3-min handgrip task with increasing intensity in a ramp-like manner. Contralateral motor cortex oxygenation increased significantly from 100 to 180 s after the start of the motor task compared with the baseline value. They also found that there is a delayed oxygenation in ipsilateral primary motor cortex area compared with contralateral side during a unimanual dominant-hand motor task. Holper et al. (2009), on the other hand, reported that fNIRS detects oxygenation changes in relation to task complexity during finger-tapping, and that activation areas are broader in the case of bimanual tasks. Recently, Nambu et al. (2009) performed the first single-trial reconstruction of finger-pinch forces from human motor-cortical activation by applying near-infrared spectroscopy, and Holper et al. (2011) could finally discriminate between motor imagery and execution by means of fNIRS recordings.

In our study, we applied the handgrip motor protocol (described in chapter 2) to 13 healthy subjects. Our aim was the investigation, at group level, of the topographic differences in brain activation elicited by right, left and bimanual handgrip, and captured by time resolved NIRS. Furthermore, we explored the feasibility of "biologically informed" GLM analysis of NIRS handgrip data, aiming at extracting augmented information.

5.1.2 Data recording

A 19 channels EEG was recorded with Ag/AgCl electrodes placed according to the international 10/20 system (Jasper, 1958). Common ground was used as reference. Two additional bipolar electrodes were used for the collection of eye movements (EOG), other two bipolar electrodes were placed on the chest of the subjects to collect the ECG signal, and four to collect EMG from the arms. All the EEG and EMG recordings were performed by means of a 32-channel AC/DC amplifier (SAM-32, Micromed Italy) and its data acquisition software (QuickBrain System). The A/D sampling rate was 256 Hz. Each electrode impedance was below 5 KΩ. A prototypical sixteen-channels time resolved NIRS device (Dipartimento di Fisica, Politecnico di Milano) was employed for HbO, HHb and HbT acquisitions. The system was provided also of suitable probes (made of Velcro stripes and custom-made plastic holders) for positioning of the injection fibers and of the detection bundles on the central areas, C3 and C4 standard locations. The NIRS signals were sampled at 1 Hz. The previously described instruments have been synchronized so that the recording of the signals started automatically with the beginning of the test and all the signals (NIRS, EEG, EMGand ECG).

Brain fMRI was also acquired for each subject during a separate session, and only for the right handgrip condition.

"Biologically informed" GLM data processing was run on data, according to the detailed description given in chapter 3.

5.1.3 Group analysis

At a group level, fNIRS activations resulted to be contralateral to the side of movement: Task block analysis GLM confirmed the hypothesis that HbO, HHb and HbT were located in the left hemisphere in the case of right handgrip task (Fig.5.2), in the right hemisphere when the left handgrip was performed (Fig 5.3), and bilaterally in the case of alternated handgrip task (Fig 5.4). In all cases, activations resulted to be located over the motor areas, centered in C3 and C4 standard electroencephalographic positions. fMRI analysis confirmed the NIRS findings, showing a location compatible with the one highlighted by NIRS for the right handgrip activation (Fig. 5.1).
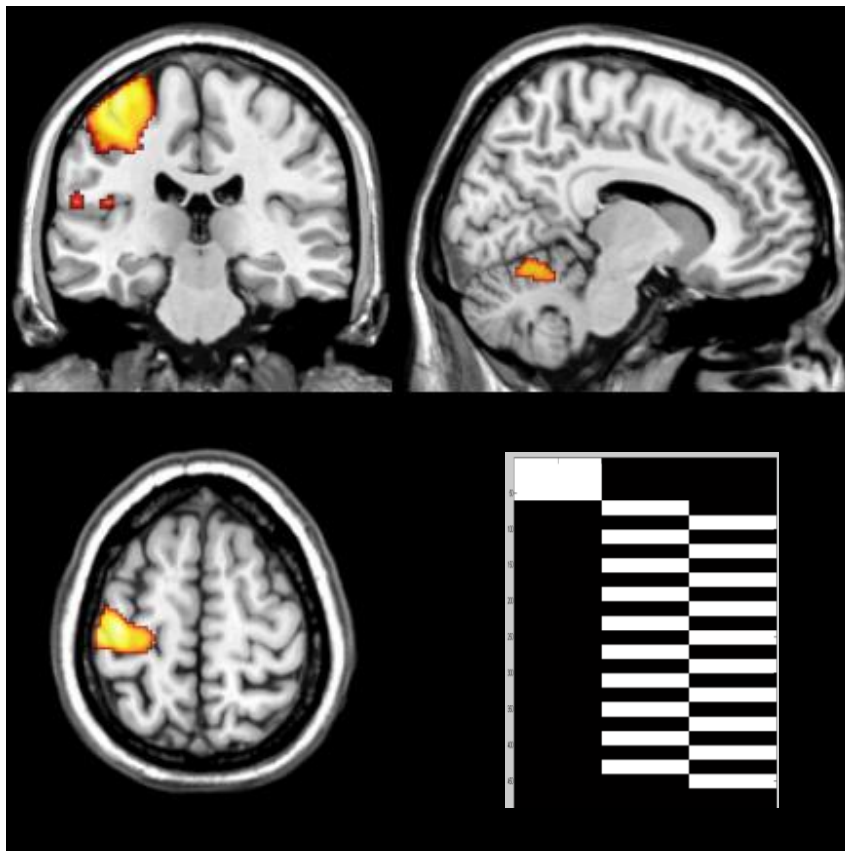
Fig.5.1: The fMRI images show the BOLD activation corresponding to the motor areas involved in a right handgrip task. Activation results from contrasting the task block design regressor. Images were obtained at 2nd level analysis (group analysis of thirteen healthy subjects). Significance was set at p-val<0.05. Regressors refer to the design matrix depicted in the bottom right corner.
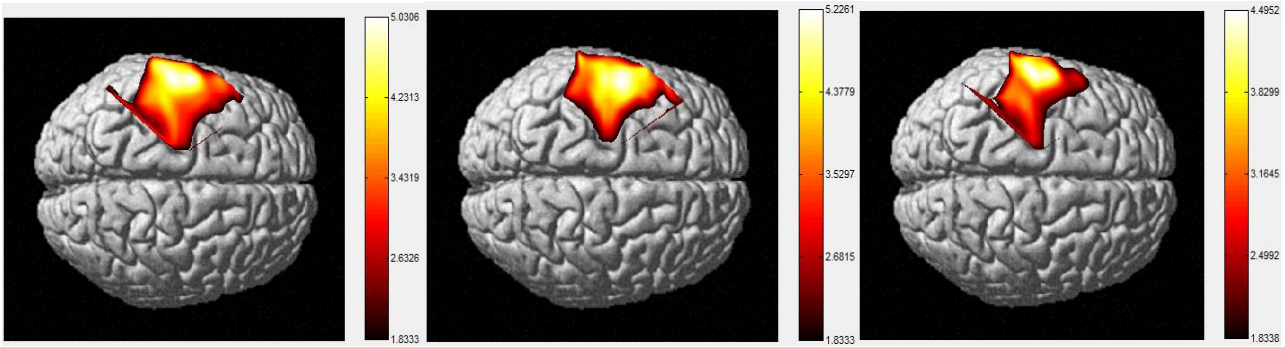
Fig.5.2: The images show (from left to right) the HbO, HHb and HbT activations resulting from contrasting the task block design of a right handgrip task. Images were obtained at 2nd level analysis (group analysis of thirteen healthy subjects). Significance was set at p-val<0.05.
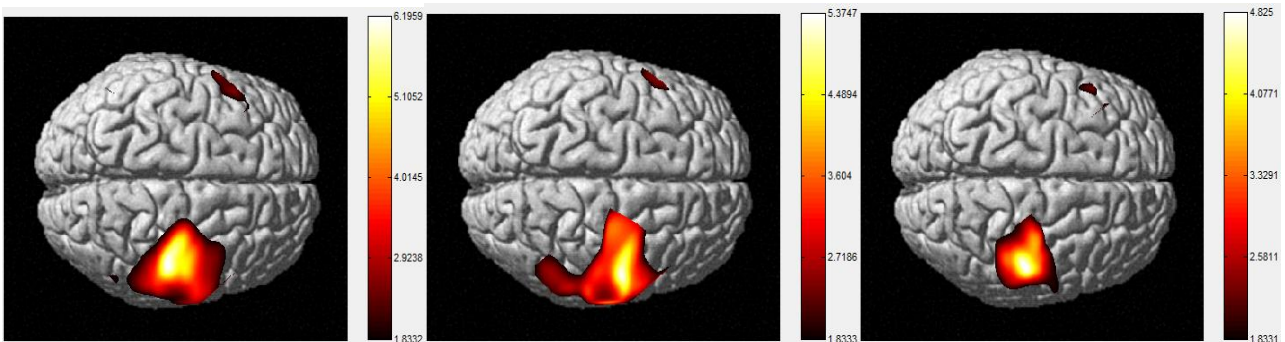
Fig.5.3: The images show (from left to right) the HbO, HHb and HbT activations resulting from contrasting the task block design of a left handgrip task. Images were obtained at 2nd level analysis (group analysis of thirteen healthy subjects). Significance was set at p-val<0.05.
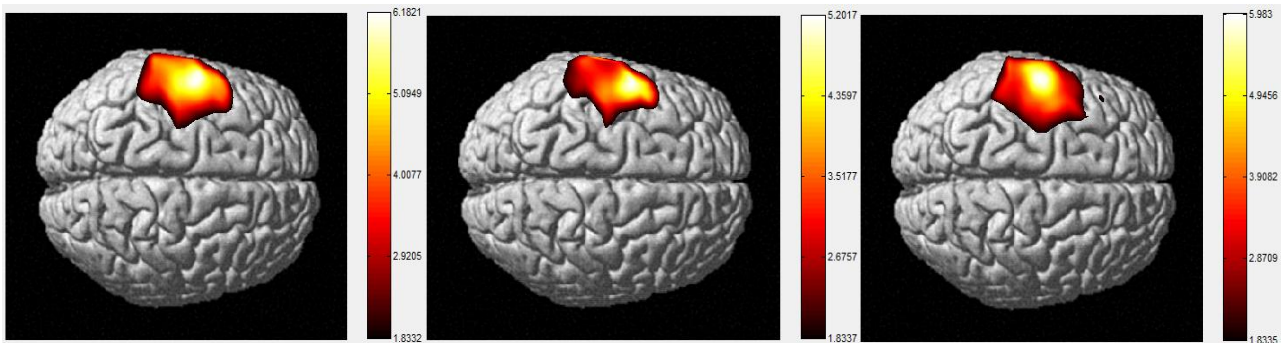
Fig.5.4: The images show (from left to right) the HbO, HHb and HbT activations resulting from contrasting the right handgrip task vs. the left, in an alternating handgrip task. Images were obtained at 2nd level analysis (group analysis of thirteen healthy subjects). Significance was set at p-val<0.05.

5.1.4 Data integration study

Then, "biologically informed" GLM processing (see chapter 3 for the full description of processing steps) was done at the single subject level (1st level analysis). Results about one subject are described here.

Single subjects showed the contralateral pattern of motor activation observed in the 2nd level group analysis, in all cases confirming the evidences provided by the group maps. Nevertheless, while HbO and HbT always provided statistically significant activation spots (Fig.5.5), HHb activation often resulted negligible for single subjects (not shown).

Fig.5.5: (Left) The image showsthe HbO activation resulting from contrasting the task block design of a right handgrip task (1st level analysis of one healthy subjects). Significance was set at p-val<0.05. **(Right)** The image showsthe HbO activation resulting from contrasting the task block design of a left handgrip task (1st level analysis of one healthy subjects). Significance was set at p-val<0.05.

Fig.5.6: (Left) The image showsthe HbO activation resulting from contrasting the task block design of a right vs. left, alternated handgrip task (1st level analysis of one healthy subject). Significance was set at p-val<0.05. **(Right)** The image showsthe HHb activation resulting from contrasting the task block design of a right vs. left, alternated handgrip task (1st level analysis of one healthy subject). Significance was set at p-val<0.05.
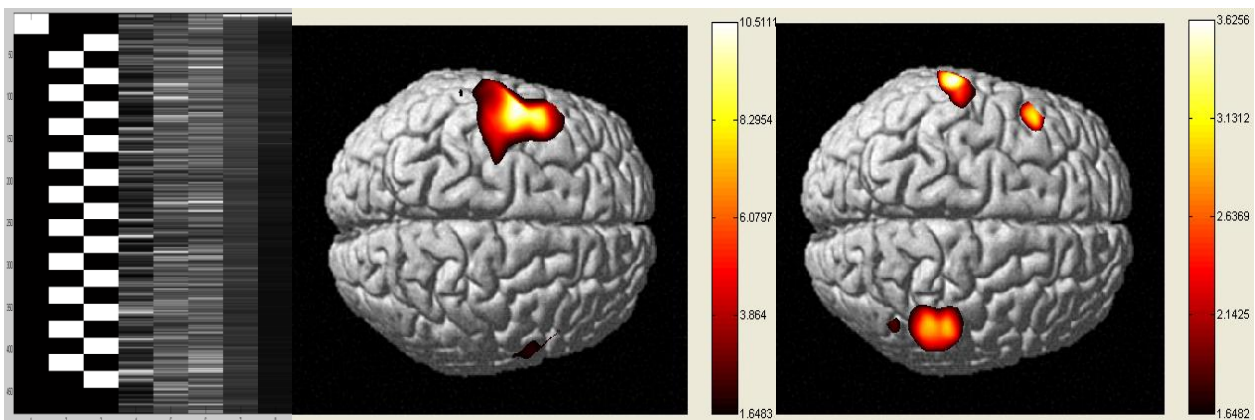
Fig.5.7: (Left) "EEG informed" design matrix containing on/off regressors modeling the task design and five regressors modeling five EEG rhythms. **(Middle)** The image showsthe HbO activation resulting from contrasting the task block design of a right handgrip task (1st level analysis of one healthy subject) in the "EEG informed" design matrix. Significance was set at p-val<0.05. **(Right)** The image showsthe HbO activation resulting from contrasting the alpha regressor of a right handgrip task (1st level analysis of the same healthy subject). Significance was set at p-val<0.05.

In the case of alternated handgrip, though, by contrasting the right vs. left hemispheres, also HHb activation showed up very robust and statistically significant HHb activation over the motor areas, for the majority of subjects. One example is shown (Fig.5.6).

The employment of "EEG informed" GLM provided results consistent with those previously observed by applying the task block analysis. Fig. 5.7middle displays HbO activation highlighted by contrasting the task regressor inside the "EEG informed" design matrix. The activation spot is very similar to the one depicted in fig.5.5left, which was obtained from the same NIRS data, by using the "task block analysis" design matrix only.

Fig.5.7right shows that the "EEG informed" GLM could also provide some spots of neurovascular coupling, where HbO proved to be correlated with alpha rhythm. Correlations were also found for HbO and beta rhythm, and for HHb and alpha and beta rhythms (results are not shown).

It is important to point out that, in "EEG informed" GLM processing, the choice of the EEG channel to be modeled was extremely important: indeed, by substituting the track recorded from C3 channel with the one acquired over C4, the estimated areas of coupling between EEG and NIRS signals dramatically changed. This problem was obviously absent for the modeling task block regressors.

Fig.5.8 shows that the employment of C3 track provided in this case broader and more realistic areas than those highlighted by C4 track. Indeed, the images show the HbO activations extracted from the alternated handgrip condition, in which the right hand is the dominant one, and then the left hemisphere candidates to be dominant with respect to the left one. Consequently, the use of contralateral C3 track, located over the left hemisphere, optimized the capture of EEG dynamics connected with movements.
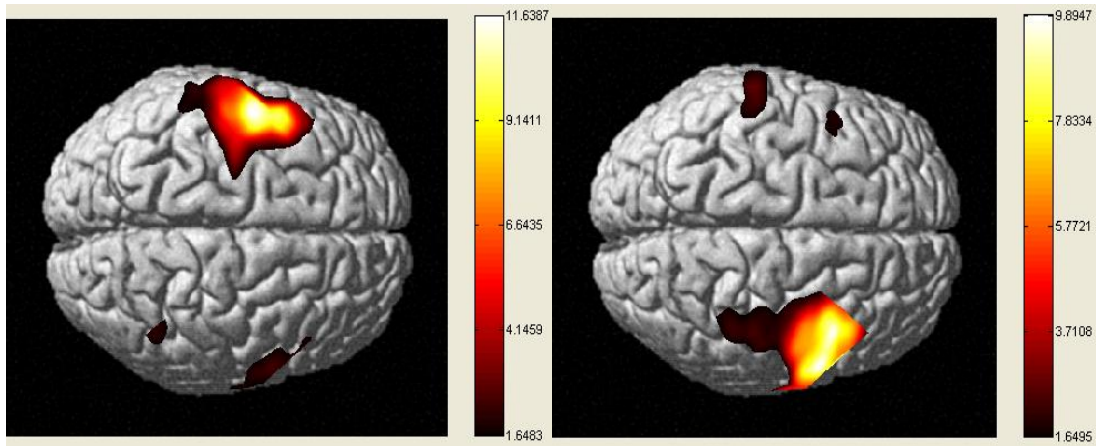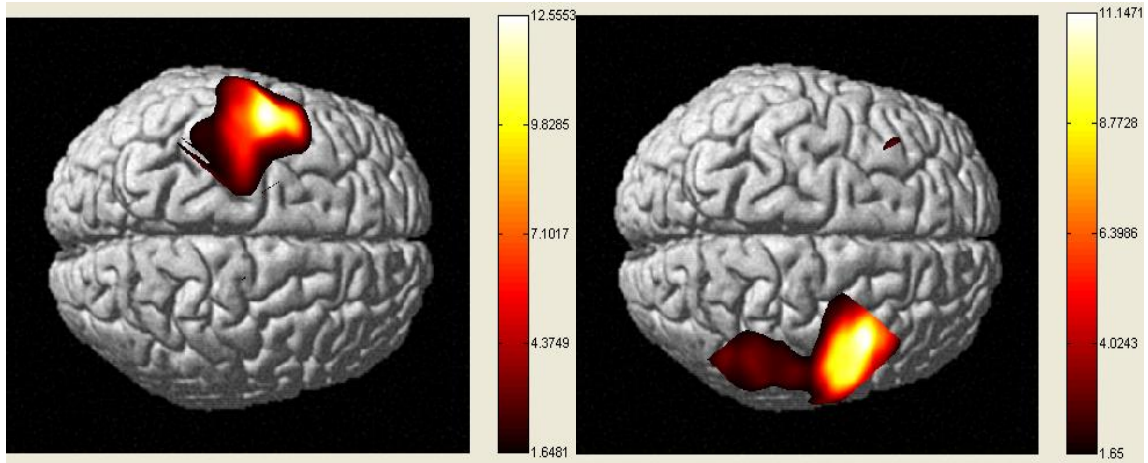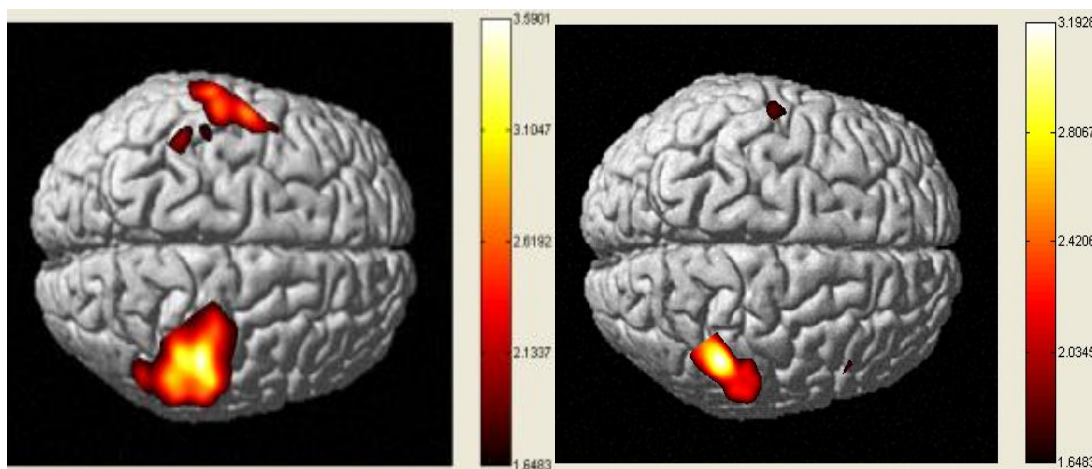

Fig.5.8: (Left) The image shows the HbO activation resulting from contrasting the EEG beta regressor of a right vs. left handgrip task (1st level analysis of the same healthy subject). The EEG regressors were extracted from C3 EEG channel, placed over the left cortex. Significance was set at p-val<0.05. The "EEG informed" design matrix was used.(Right) The image shows the HbO activation resulting from contrasting the EEG beta regressor of a right vs. left handgrip task (1st level analysis of the same healthy subject). The EEG regressors were extracted from C4 EEG channel, placed over the right cortex. Significance was set at p-val<0.05. The "EEG informed" design matrix was used.

Fig.5.9middle and fig.5.8left were obtained from the same data.Fig.5.9middle, though, was extracted by means of the "Only EEG" design matrix during GLM processing. The reader can observe that the result is similar, albeit not identical. Slight differences have to be traced back to the parasitic contribution of the "Task block" regressors to the disentanglement of correlations (see chapter 3 for further discussion), when using the design matrix shown in fig.5.7left. Fig.5.9right depicts the pattern of correlation existing between HHb and alpha rhythm: this map is referred to the alternated handgrip condition, and is highly subject-specific. All the subjects, indeed, showed some kind of neurovascular

pattern, correlating HHb and alpha rhythm; nevertheless, patterns revealed great inter-subject variability.

Fig.5.10 depicts the activation pattern put into evidence by correlating the NIRS signal with the electromyographic derivation from the moving arm. A focal, broad and robust activation pattern is highlighted for the three hemoglobin species: HbO, HHb and HbT. For many subjects of our study, EMG proved to be a very powerful and specific regressor for the extraction of activation patterns of handgrip.
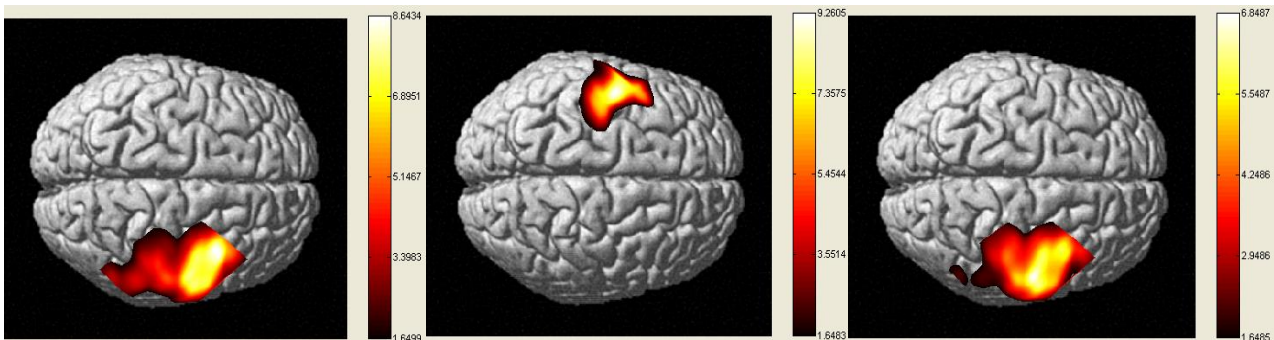
Last, the "poligraphy informed" GLM processing provided very similar replicas of all the information previously extracted: we were able to obtain, by means of this last design matrix, the same neurovascular patterns previously extracted through "EEG informed" and "EMG informed" approaches. Fig 5.11middle and fig.5.11right display the "poligraphy informed" results analogous to those shown in fig.5.9. The reader will notice that, in these last images, some statistical improvement has been obtained, due to the substitution of the "task block" regressors with the more performing "EMG" regressors, modeling the ongoing handgrip movement.

All considered, we can conclude that the "biologically informed" approach allowed for a deep investigation and specification of the subject's neurovascular coupling patterns, and

also provided augmented information to the investigators. Importantly, the origin and nature of couplings could be ascertained, thus opening a new door on the identification of phenomena driving the insurgence of hemodynamic response.
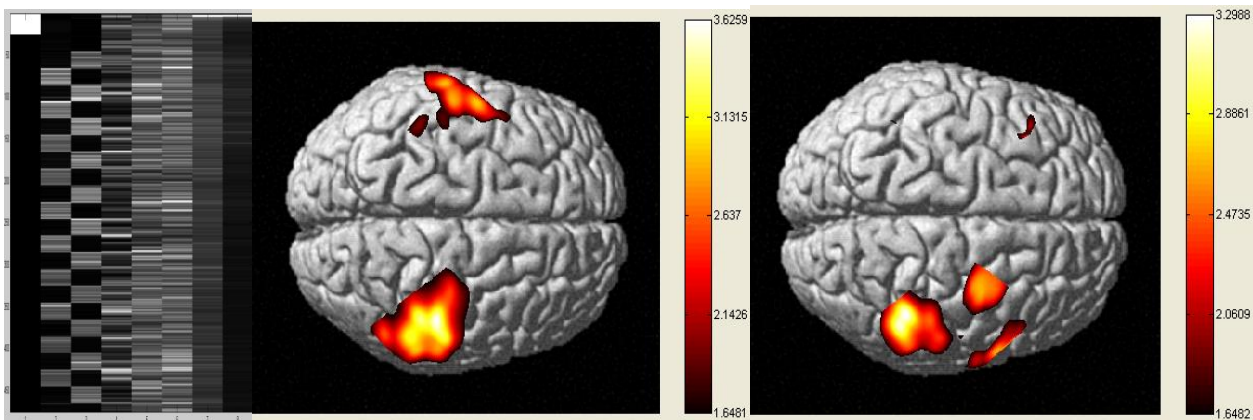
Fig.5.11: (Left) "Poligraphy informed" design matrix containing regressors modeling EMG and EEG rhythms. (Middle) The image shows the HbO activation resulting from contrasting the EEG beta regressor of a right vs. left handgrip task (1st level analysis of the same healthy subject). The EEG regressors were extracted from C3 EEG channel, placed over the left cortex. Significance was set at p-val<0.05. (Right) The image shows the HbO activation resulting from contrasting the EEG alpha regressor of a right vs. left handgrip task (1st level analysis of the same healthy subject). The EEG regressors were extracted from C4 EEG channel, placed over the right cortex. Significance was set at p-val<0.05.

5.2 Technical and methodological issues

5.2.1 Background

The response dynamics of HbO and HHb have been shown to differ, depending on the stimulus paradigm. For motor paradigms, previous fNIRS studies have demonstrated an earlier response in HbO when compared to the dynamics of the HHb decrease. Despite the existence of wide literature ascribing this evidence to neurovascular coupling (i.e. synchronous electrical and metabolic phenomena in one area of the brain – see section 5.3 of the present chapter for further discussion), it was demonstrated that this may depend partly on hemodynamic changes unrelated to the cortical increase in blood flow (Boden et al., 2007).

Secondly, it has been shown that, in contrast to other neuroimaging methods, the NIRS signal is highly sensitive to extracerebral blood volume changes. Our hypothesis is that these changes may be caused by systemic variations, on their turn potentially explained by a difference in autonomic response. Systemic hemodynamic variations are thus extremely relevant to NIRS and motivate the present study.

The main limitation of NIRS technique resides in the fact that signals contain contributions from both the brain and the overlying tissues. Extra-cerebral contributions to the NIRS signal cannot be easily differentiated from truly cortical signals unless advanced NIRS technology (such as time-resolved imaging) is applied. Therefore, a proper instrumental design, combined with advanced methods of data analysis, must be applied to differentiate intracerebral from extracerebral contributions (Liebert et al., 2004). Indeed, continuous wave NIRS per se does not allow for this differentiation: some multi-distance approaches have been attempted, consisting in capturing the emerging light at multiple interoptode distances from the source, but results are discouraging.

By exploiting the fact that time-resolved measurements are based on a temporal approach, according to which, on average, photons detected after long times of flight

probe deeper tissue layers than early photons, a statistical separation of surface and deepness contributions is made feasible.

In this work, a cognitive visual "n-back task" for working memory stimulation was used, aiming at rising a broad prefrontal hyper-oxygenation. In our work, we have been following the goal of isolating intra-cortical and extra-cortical information during the physiologic working memory effort by studying, with a multi-channel time-of-flight NIRS,"early photons" and "late photons" contributions.

5.2.2. NIRS recordings and data processing

An 8-channels time-resolved NIRS device was used for recordings. Two optical probes were placed over the forehead around Fp1 and Fp2 position (EEG 10/20 standard). A one-derivation ECG was recorded in the meanwhile. A General Linear Model (GLM) approach was applied for data analysis by means of NIRS-SPM v.3.1 software (Ye et al., 2008). An hemodynamic response function (HRF) low-pass filter and the wavelet-MDL detrending algorithm (4 coefficients) were applied. No correction for serial correlations was performed. A first design matrix was used, containing regressors modeling: (1) the activation blocks of the cognitive test, (2) rest periods interleaving the activation blocks, (3) the baseline recorded just before the beginning of the test and (4) the heart rate instantaneous values obtained from ECG. Contrast arrays were designed to investigate the relationships between: (1) the cognitive activation and rest, (2) the cognitive activation and the baseline and (3) the cognitive activation and the heart rate. A second design matrix was created, aiming to the modelling of: (1) each cognitive load provided by the test, (2) the baseline recorded just before the beginning of the test and (3) the heart rate instantaneous values obtained from ECG. Contrast arrays were designed to investigate the relationships between: (1) each cognitive load and the baseline and (2) adjacent cognitive loads. The interpolated t-statistic maps were obtained for each subject first (1st level analysis), and then for each of the two groups (2nd level analysis), and for both the intra-cerebral and extra-cerebral compartments.

Additional correlations were calculated between fNIRS signals and heart rate for each subject, for both the fNIRS districts (intra-cerebral and extra-cerebral compartments), and for the quantities HbO and HHb. This was done in order to assess possible relationships between the cardiac information and the hemodynamic data collected over the head.

Nineteen healthy males took part in the present study, with a mean age of 27.15 years (SD 2.01 years, range 23-30 years). Seventeen subjects were right handed. The participants were screened thoroughly for neurological symptoms: they all did not show neuro-psychological illness; cognitive level, attentive capability and memory skills were in a normal state.

5.2.3 Results

Behavioral results

The 19 subjects committed an average of 1,58 errors (SD=0,69) in the *n*-back task, thus falling in the normality range. On average, they committed 0,77 errors during the 0-back condition, 1,28 errors during the 1-back, 2,14 during the 2-back and 2,15 during the 3-back. They answered correctly to the target in 511 ms (SD=36). More specifically, reaction times on targets were 464 ms for the 0-back condition, 508 for the 1-back, 540 ms for the 2-back and 535 ms for the 3-back.

GLM results

In this study, General Linear Models were applied to both intra-cerebral and extra-cerebral fNIRS data. Intra-cerebral information were obtained by extracting the "late photons" contribution from the fNIRS signals, while extra-cerebral information were obtained by operating in the "early photons counting" mode. Contrasting the regressor modelling the task periods against the one capturing the baseline activity, a widespread significant increase in HbO ($p<0.05$) was found all over the frontal cortex probed by the fNIRS device; analogously, HbO increase was sensed in the surface tissues, but the involved area was much smaller (Fig.5.12). HHb was found to change as well; GLM, though, attested a significant modification of this parameter inside the cortex only. HbT significantly increased during the task in both the probed districts: the superficial one (skin and skull) and the cortex.

The contrast between the task periods and the interleaved rest intervals provided no significance of hemodynamic changes: neither for HbO, nor for HHb and HbT. P-values were similar for intra-cerebral and extra-cerebral compartments.

The contrast between the task periods and the subjects' heart rate reached no significance for both intra-cerebral and extra-cerebral data. Thus, we could not rule out for the heart rate a modulation effect induced by the task and/or the cognitive load. Moreover, p-values were remarkably different for intra-and extra-cerebral compartments. This last element led to further and specific investigation (above).

Last, contrasts between each cognitive load (0, 1, 2 and 3-back) and the baseline period were studied. All the loads contrasted against the baseline showed a significant HbO increase confined to the right hemisphere. HbT was found to significantly raise during the 1, 2 and 3-back loads with respect to the baseline condition ($p<0.05$). Importantly, all these results about loads were observed for the intra-cerebral compartment only, while the processing of extra-cerebral data provided no significant result (p-val set at 0.05). HHb changes never reached significance in both the compartments. (Further analysis will be described in section 5.4.).

Correlation results

Correlations between fNIRS signals and heart rate globally showed very low values. For most channels, small and negative values of correlation for HbO and heart rate were found in both the surface and deepness compartments. In spite of this, t-test assessed significant different correlations in the two districts for five channels out of eight (Fig. 5.13).
Correlations between HHb and heart rate showed very low values. For all the channels, values of correlation for HHb and heart rate were positive in the intra-cerebral district. At the surface this result was not confirmed, due to six negative values out of eight. Indeed, t-test assessed significant different correlations in the two districts for six channels out of eight (Fig. 5.14).
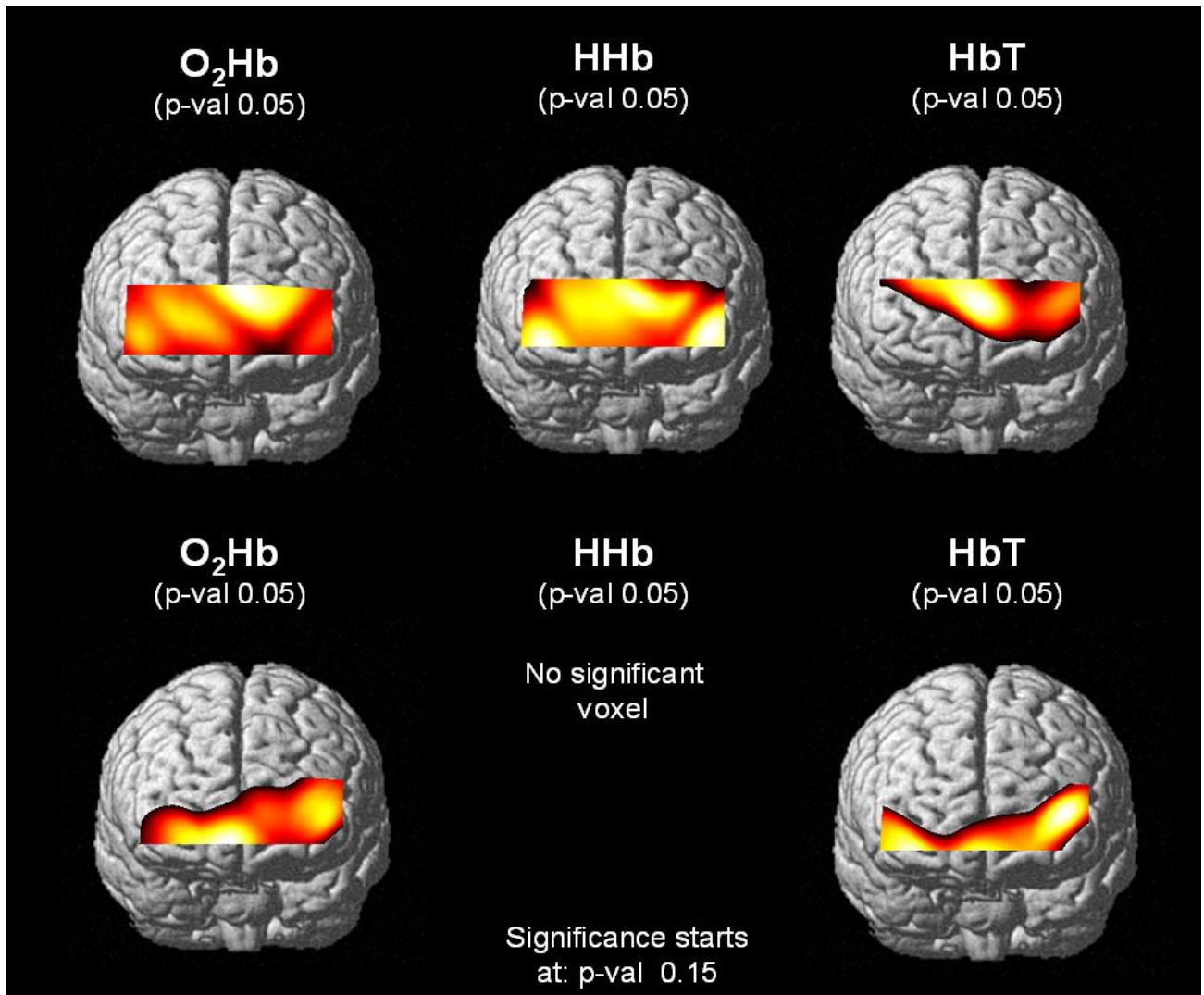
Fig. 5.12. Second level analysis of fNIRS data. Here the activation provided by the _n_-back task is contrasted against the baseline period. Maps at the top of the figure show information extracted from the intra-cerebral compartment. Significant bilateral changes in HbO, HHb and HbT were found. Extra-cerebral fNIRS information (bottom) evidenced increase in HbO and HbT as well, but HHb change did not reach statistical significance.

Surface 0.011971 ± 0,34121	Surface -0,059999 ± 0,28819	Surface -0,180640 ± 0,35239	Surface -0,250590 ± 0,33321
Deepness -0,127540 ± 0,23002	Deepness -0,200750 ± 0,23624	Deepness -0,074450 ± 0,21094	Deepness -0,077850 ± 0,25747
Surface -0,193500 ± 0,25790	Surface -0,049748 ± 0,22600	Surface -0,217800 ± 0,25432	Surface 0,044955 ± 0,35068
Deepness -0,111080 ± 0,25521	Deepness -0,122800 ± 0,20815	Deepness -0,159880 ± 0,24997	Deepness -0,147890 ± 0,18971

Fig. 5.13. Correlations between HbO data and heart rate at each of the eight probe channels. Full colours point out channels which passed the t-test for the separation of cognitive and systemic effects.

Surface	Surface	Surface	Surface
0,011971	-0,059999	-0,180640	-0,25059
±0,38921	±0,34869	±0,37260	±0,33787
Deepness	Deepness	Deepness	Deepness
0,043661	0,116690	0,120900	0,167160
±0,24100	±0,26110	±0,29239	±0,30189
Surface	Surface	Surface	Surface
-0,193500	-0,049748	-0,217800	0,044955
±0,38810	±0,43651	±0,34007	±0,39809
Deepness	Deepness	Deepness	Deepness
0,149790	0,120430	0,082801	0,066384
±0,25965	±0,24422	±0,28554	±0,22020

Fig. 5.14. Correlations between HHb data and heart rate at each of the eight probe channels. Full colours point out channels which passed the t-test for the separation of cognitive and systemic effects.

5.2.4 Outcome

In the present work, possible differences between intra-cerebral and extra-cerebral contributions to NIRS signal were investigated; moreover, links between behavioral processes and changes in vagally-controlled heart rate has been the focused.

Response to stressors is a primary source of transient, vagally-induced cardiac slowing during information processing, and a conditioning factor for both peripheral and central blood perfusion. Pharmacological blockade studies have established that this heart rate slowing is controlled by vagal activation. Individual differences in such responses have been shown to relate to the amplitude of cardiovascular responses to both cognitive and motor tasks (Jennings et al., 2002).

Correlations (rho and p-value) were calculated between fNIRS signals and heart rate for each subject, for both the fNIRS districts (intra-cerebral and extra-cerebral compartments), and for the quantities HbO and HHb. This was done in order to ascertain possible relationships between the cardiac information and the hemodynamic data collected over the head. Moreover, we tested the hypothesis that cardiac variability could be mirrored differently inside the intra-cerebral and extra-cerebral hemodynamics, as the former should mainly account for cognitive activation, while the latter should mainly be modulated by autonomic effects. Heart ratevariability, indeed, is largely -though not exclusively- related to vagal function.

Nowadays it is known that the autonomic nervous system continuously adjusts cardiovascular parameters in anticipation of the person's actions (Jennings et al., 2002).

Sympathetic activation increases cardiac force and direct vascular output to active tissue. As a consequence, it often induces a relatively heightened level of metabolic support, together with the rising of blood pressure. Nevertheless, sympathetic activation can co-occur with the vagal activation that slows the heartbeat. Indeed, the baroreceptors located in the carotid artery sense increases in pressure and initiate a vagally-mediated decrease in heart rate.

Functionally, the slowing of the heart beat permits a greater time for the heart to fill, such that the next cardiac cycle will be relatively enhanced in both volume and force, meanwhile preserving blood pressure.

Motor activation alternating with rest is accompanied by an autonomic response mirrored in systemic effects such as an increase in heart rate (Franceschini et al., 2003) which lead to extracerebral changes in oxy-hemoglobin concentration (Obrig et al., 2003).

As n-back task contains different cognitive loads, heart rate was partially modulated by the different difficulty stages, and modification of the informative content was observed inside the heart rate data. Franceschini (2003) and coauthors demonstrated heart rate to be

positively correlated to the magnitude of the blood flow response in cortical areas independent of the stimulus processing.

Similarly, a strong correlation between type of paradigm and systemic activation was shown by Moody et al. (2003). Obrig et al. (2003) could recently show, for a sensorimotor paradigm, that these changes might also appear in the extra-cerebral compartment and can influence NIRS measurements.

In conclusion, evidence about the feasibility of disentangling cardiovascular contribution inside fNIRS in cognitive tasks was provided here. Moreover, this work relaunches the benefit of extracting the autonomic contribution from hemodynamic data for the eduction of clearer functional information. Importantly, the intra-cerebral and extra-cerebral contributions to NIRS data revealed the presence of different information content.

5.3 Neurovascular Coupling

5.3.1 Background

Neurovascular coupling refers to the relationship between local neural activity and subsequent changes in cerebral blood flow (CBF) (Roy and Sherrington, 1890).Indeed, it has been shown that brain activity is associated with focal cortical hyperemia, that is, the changes of neural electrical activity are coupled with a functionally induced focal cortical hyper-oxygenation (Sheth et al., 2004). Despite hemodynamic and electrical activities have been widely investigated individually (Uludag et al., 2004), interesting physiological concerns could only be clarified by considering them conjointly. Unfortunately, the considerable differences existing between hemodynamic and electrical signals, their different physiological nature and time dynamics make it difficult to investigate neurovascular coupling as a whole.

Given this two-faced nature of neurovascular coupling, both electrophysiological and hemodynamic techniques are needed for investigation (Shibasaki, 2008). Despite fMRI is the gold standard for studying the hemodynamic transients in the brain (Attwell and Iadecola, 2002), it shows many drawbacks:it derives contrast only from changes in deoxyhemoglobin because of its paramagnetic properties, it has a low temporal resolution, and it cannot capture the electrical correlates of neurovascular phenomena.In the present study, we used Near-Infrared Spectroscopy and electroencephalographic techniques.

In previous studies it has been demonstrated that the performance of a cognitive task involves the response of several physiological districts, such as Central Nervous System (CNS), Autonomic Nervous System (ANS) and Cerebro-Vascular System (CVS) (Tanida et al., 2007; Tanida et al., 2004; Moosmann, 2003; Obrig et al., 1996). Despite the earliest studies about neurovascular coupling were designed as repeated tasks for the subsequent recording of different measurements, the simultaneous employment of different measurement techniques proved to be advantageous, as the experimental conditions are arduously controlled and reproduced among different test sessions in cognitive protocols (Telkemeyer et al., 2011; Wallois et al., 2011).

Literature reports a small number of studies investigating neurovascular coupling in cognitive task using EEG and NIRS techniques simultaneously. Obrig and his group (Koch et al., 2008; Syré et al., 2003; Obrig et al., 2002) compared visually evoked potentials (VEP) with evoked NIRS signals, finding a decrease in VEP component amplitude, closely coupled to a decrease in the amplitude of oxygenation parameters (HbO, HHb). Combining EEG and NIRS measurements, Izzetoglu et al. (2007) investigated the

response to external stimuli using a cognitive visual oddball paradigm, finding an increase in ERP and oxygenation signals amplitude after the stimulus presentation, while Moosman et al. (2003) investigated the common information shared by the two signals in the occipital cortex, working out the cross-correlation between alpha rhythm and concentration changes of HHb and finding that alpha activity is associated with a metabolic deactivation. Sander et al. (2007) found that time-resolved NIRS (tr-NIRS) signals had an onset delay of about 5 s, if compared to the magnetoencephalographic (MEG) tracks. These results, though, were found on two subjects only -of which only one was reported- and were calculated for EEG and tr-NIRS recordings and for a motor task. Although preliminary, these evidences point out the slower rise and drop of the tr-NIRS signals, with respect to electromagnetic techniques. The same research group also simultaneously monitored neuronal and vascular signal changes in patients in the subacute state of ischemic stroke, highlighting comparable findings (Leistner et al., 2011).

In the present study, neurovascular coupling has been induced by means of a bimodal audiovisual task of divided attention. Divided attention is the most demanding attentional process, and results in the ability to divide the attentive resources among two or more information sources or stimuli (Sarter and Turchi, 2002).

The present work specifically aims at clarifying the time relationship between electroencephalographic and hemodynamic correlates of neurovascular coupling, and at quantifying the degree of information shared by EEG and NIRS HbO and HHb signals during a divided attention task involving visual and auditory resources. In order to obtain further information about the hemodynamic response and to study the activation of ANS elicited by the execution of the cognitive task, an additional electrocardiographic (ECG) derivation was recorded.

5.3.2 NIRS, EEG and ECG acquisition

A 19 channels EEG was recorded with Ag/AgCl electrodes placed according to the international 10/20 system (Jasper, 1958). Common ground was used as reference. Two additional bipolar electrodes were used for the collection of eye movements (EOG), and other two bipolar electrodes were placed on the chest of the subjects to collect the ECG signal. All the EEG recordings were performed by means of a 32-channel AC/DC amplifier (SAM-32, Micromed Italy) and its data acquisition software (QuickBrain System). The A/D sampling rate was 256 Hz. Each electrode impedance was below 5 KΩ. A prototypical two-channels time resolved NIRS device (Dipartimento di Fisica, Politecnico di Milano) was employed for HbO, HHb and HbT acquisitions. The system was provided also of suitable probes (made of Velcro stripes and custom-made plastic holders) for positioning of the injection fibers and of the detection bundles on the forehead tissue, 0.7 cm under the Fp1 and Fp2 standard locations. The NIRS signals were sampled at 1 Hz.

The previously described instruments have been synchronized so that the recording of the signals started automatically with the beginning of the test and all the signals (NIRS, EEG and ECG) and the behavioural data recorded by Presentation were time aligned.

Sixteen healthy volunteers (8 males, 8 females) took part in the present study. Mean age was 25,63 (SD 3,81 years, age range 19-34 years) and all the subjects were self-reported right handed. None of them had a life time or family history of neurological or psychiatric illness, all of them were declared normal vision and hearing. They underwent the Divided Attention Test (TDA) described in in Chapter 2.

5.3.3 NIRS, EEG and ECG data analysis

EEG analysis

Raw EEG data were digitally band pass filtered between 0,5 and 48 Hz. Then they underwent Laplacian Surface Operator for the improvement of the spatial localization of neuronal activity, according to the method described in Foffani et al. (2004). The data were then cleaned by ocular and muscular artifacts by means of Independent Component Analysis (ICA) (Makeig et al., 1996) and downsampled at 128 Hz.

The EEG frequency analysis was then implemented through an autoregressive (AR) batch modeling according to the Yule-Walker estimation procedure. The AR estimation was performed on the electrode Fz with time windows of 2 s length with 50% overlap, in order to obtain a stationary signal (Baselli et al.,1987). Each time window underwent Anderson's test to evaluate the whiteness of the residual and the optimum order was chosen according to the Akaike Information Criterion. According to the method, through pole estimation, the spectrum is divided into bell-shaped curves and the characteristics of power and frequency of each spectral component are extracted from the position and residual of each pole. The calculation of spectral power was made following the procedure described in Zetterberg (1969). The spectral peaks were divided, according to their central frequency, into the characteristic EEG rhythms (0,5-3 Hz Delta, 3-8 Hz Theta, 8-13,5 Hz Alpha, 13,5-30 Hz Beta, 30-48 Hz low Gamma).

The chosen time windows length lead us to obtain one power value for each second, so that the EEG power signal could be directly compared and correlated with NIRS signal.

RR series analysis

From the ECG bipolar derivation acquired simultaneously with the EEG signal the inter-beat interval (RR) series were extracted through the Pan and Tompkins (1985) algorithm. The RR series were then splined to calculate one value every second of activity, in order to obtain the same sampling rate of EEG and NIRS signals.

An example of the acquired signals can be observed in Fig. 5.15. The reader should note that in the top panel an example of raw EEG signal is presented within an interval of 10 s, while the other panels show the whole time course of the signals during the task.

NIRS data analysis

After the observation of raw signals, two main contributions in the NIRS signals were isolated, by using a low pass Chebychev IIR filter with 6 coefficients, pass band 0,002 Hz and stop-band 0,003 Hz, with 30 dB maximum ripple amplitude.

One component, in low frequency, was late deemed to be due to the sustained attention condition required by the test, whereas a second contribution, in the higher frequencies, was later attributed to the modulation caused by the switching between test and rest periods. An example of LF and HF for HbO and HHb signals can be observed in Fig. 5.16, if comparing top and bottom panels.
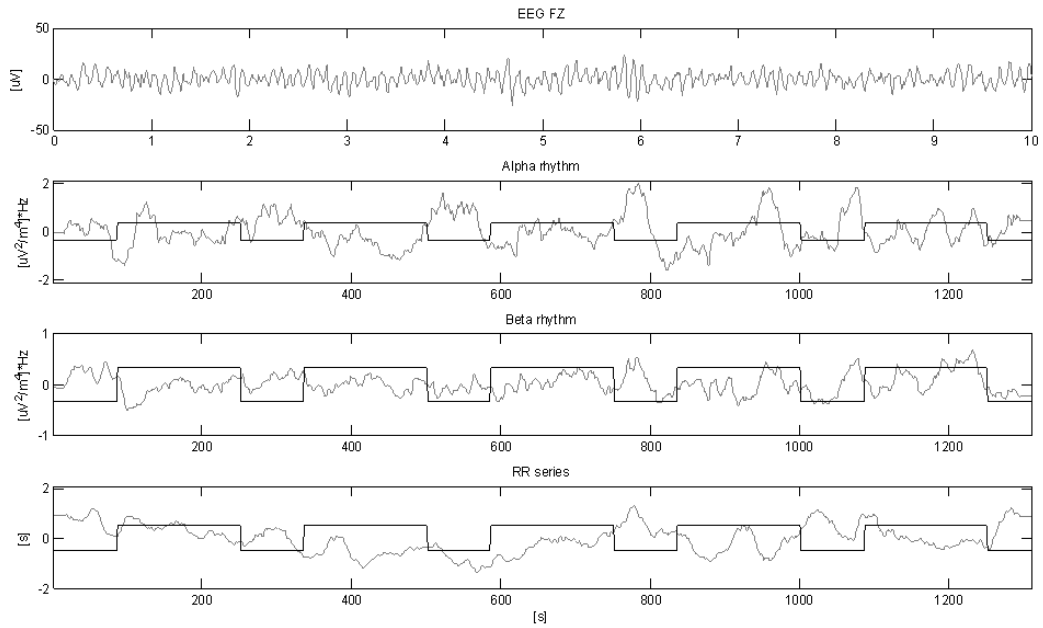
Fig. 5.15. From top: Raw EEG signal, within 10 s duration; power of Alpha and Beta rhythm; RR series. For all the signals except the first one the whole time course during the task is presented. The square wave overlapped to the signals represents the block task. The signals are shown for subject 01.
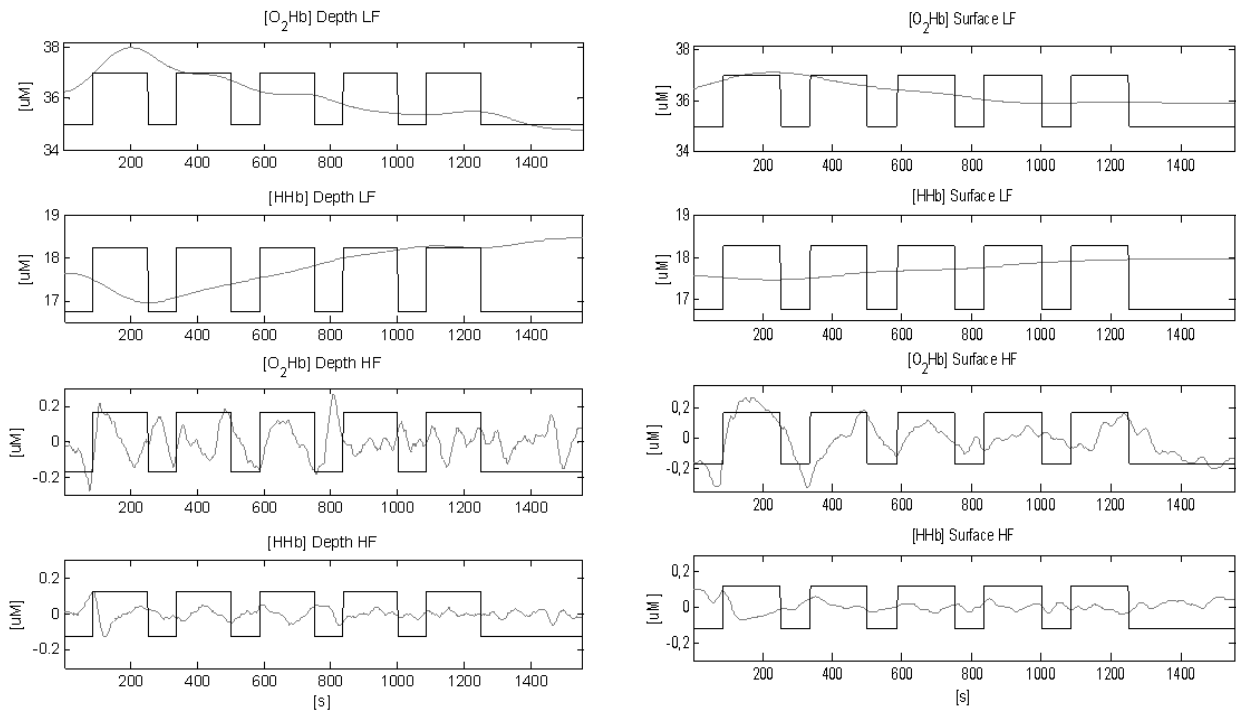
Fig. 5.16. From top: [HbO], [HHb] Low Frequency time course, [HbO], [HHb] High Frequency time course. Left panel: depth signals, Right panel: surface signals. All the signals shown belong to subject 13.

Correlations

The quantification of neurovascular coupling was made by means of Cross Correlation Function (CCF). CCF was applied, firstly, between each signal and the task, and then between couples of signals. As shown in the upper part of Table 5.1, the signals which

76

underwent CCF with the task were: Alpha and Beta EEG power rhythms (on Fz electrode), the RR series, HbO and HHb high frequency (HF) depth and surface NIRS signals. The task was modeled as a square wave: test intervals corresponded to crests, while rest periods corresponded to hollows.

Then CCF was evaluated between couples of signals: Alpha power rhythm – RR series, Alpha power rhythm - HbO and HHb HF depth signals, RR series - HbO and HHb HF depth and surface signals, as shown in the lower part of Table 5.1.

Before undergoing correlation, all the signals (except for the task) were moving average filtered with a 29 samples window and time re-aligned, in order to reduce signals variability due to noise. All the signals were also cut to the same length (from 86 seconds before the beginning of the test to 60 seconds after its end). Their mean value was subtracted, and then they were divided by the standard deviation before entering correlation function.

The temporal shift between each couple of signals for which the CCF reached the maximum absolute value was calculated, the CCF for that shift was then extracted and the p-value was evaluated. Depending on the couple of signals under processing, a maximum or minimum value of correlation was considered.
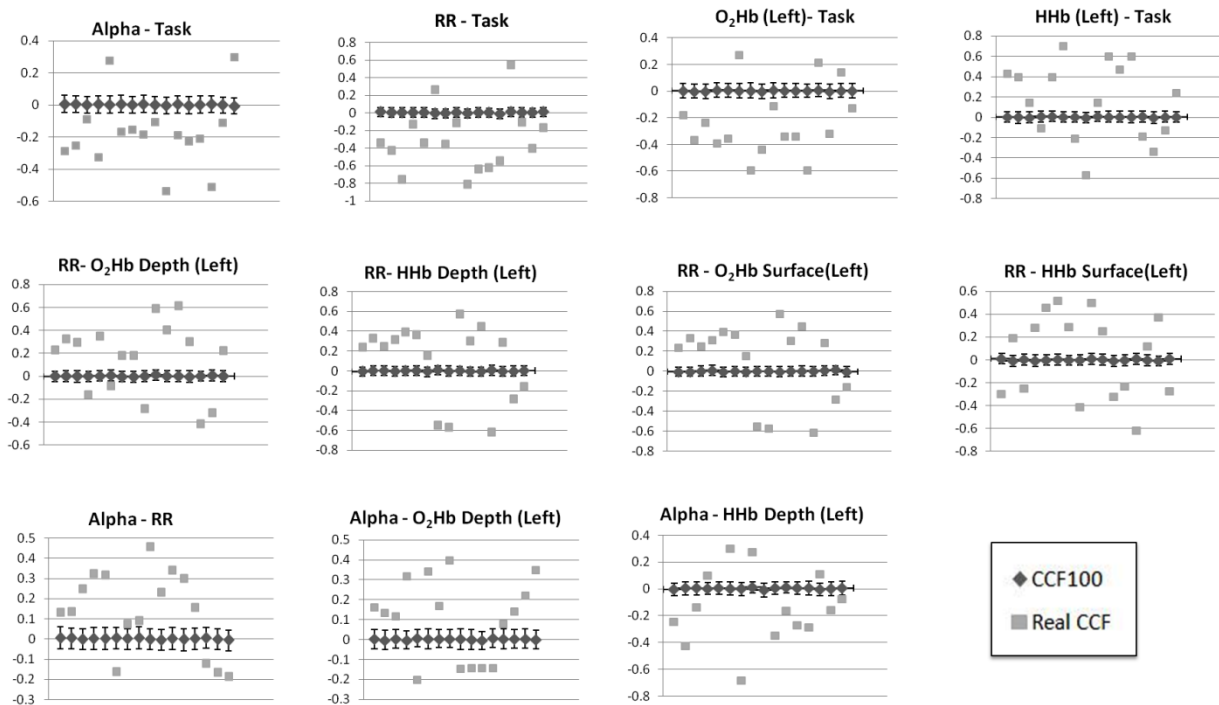
Fig. 5.17. Results of CCF100 evaluated on all the couples of signals. In each panel black diamonds represent, for all the subjects, mean±SD of 100 surrogate correlations (i.e. CCF100), while gray squares indicate real CCF for the corresponding subject. For CCFs that include NIRS signals, only results derived by left pad are presented, but results of right one can be considered analogous.

Significance of CCF

Results for all the CCFs computed between couples of signals were compared with the mean CCF value obtained by n different correlations, each of them deriving from the application of CCF between one signal from the considered couple and a surrogate modification on the second signal, always different at any of the n iterations. In so doing, we obtained n surrogate signals for testing each one of the correlations, for each one of the couples (see Table 5.1).

This analysis was conceived for testing the CCF between each signal and the task (by creating surrogates of the considered physiological signal) and also for testing CCF between couples of signals (by randomizing alternatively one of the two signals).

The surrogate series were obtained by randomizing the values of the signal (i.e. by shuffling the samples of the signal, and thus preserving its length, mean and SD) for n-times. For each subject, the mean value of the n CCFs between surrogates and the task, $M_n \pm$ its SD, was compared with the value of the real CCF calculated for the same signal from the same subject. If the real CCF value was lower than $M_n - SD$ or higher than $M_n + SD$ (i.e. real CCF value stood outside the range $CCF_n \pm SD$), it was assumed that the real CCF value is significant.

In order to achieve a good convergence of M_n, the number of iterations n was chosen to be 100. To indicate that, the notation CCF_{100} will be used. Results can be examined in Fig. 5.17, for all the subjects.

5.3.4 Results

Behavioural Results

The 16 subjects committed an average of 0,13±0,49 Visual Omission errors (0,13 missing answers on 15 visual target stimuli), 0,47±0,63 Auditory Omission errors (0,47 missing answers on 15 auditory target stimuli) and 11,63±24,42 Commission errors (all kinds), corresponding to 11,63 wrong answers during all the divided attention test. They answered to the visual target stimuli in 649,55±129,27 ms and to the auditory target stimuli in 698,14±141,30 ms.

EEG Results

The correlation between Alpha rhythm and the task, modeled as a square wave, showed a general negative trend (14 out of 16 subjects). Indeed Alpha power increased for this group of subjects during the resting periods. The mean CCF value among these subjects was -0,23±0,17, p<<0,001.

The correlation between Beta rhythm and the task showed a positive trend for 8 subjects and a negative trend for the others eight. Even though for 14 subjects out of 16 the mean delay of Beta rhythm with respect to the task resulted lower than 1s, which is a plausible time for the neuronal response onset, the different behaviour over the subjects made it impossible to identify a prevalent trend. Beta rhythm was then excluded from further analysis.

RR series Results

The RR series showed a strong modulation by the cognitive task, resulting from CCF values. An increasing trend throughout the whole test was evidenced, meaning that the cardiac frequency, after an increasing in the beginning of the test, slowly tends to recover to the baseline values. This slower trend was separated with a linear signal detrend before calculating the CCF.

Correlation with the task was negative for 14 out of 16 subjects (implying that RR period decreased during test periods and increased during the resting periods), with a mean value of -0,41±0,24, p<<0,001.

NIRS results

The low frequencies (LF) components of [HbO] and [HHb] depth signals were characterized by an increase of [HbO] and [HHb]. This trend in some cases lasted until the

end of the test (6 subjects for the right pad, 5 for the left one for HbO, 4 subjects for both right and left pad for HHb) while, in other cases, it had a recovery to the initial values (10 subjects for the right pad, 11 for the left one for HbO and 12 subjects for left and right pad for HHb).

Considering the course of both HbO and HHb signals, three different time courses were observed:

1. opposite trend (8 subjects for the right, 7 for the left pad), that means an increase in [HbO] and decrease in [HHb], or an opposite recovery,
2. similar trend (4 subjects for the right, 4 for the left pad), that means that the two signals either increased both, or decreased, or had the same kind of recovery.
3. different trend (neither opposite, nor similar, 4 subjects for the right, 5 for the left pad) of [HbO] and [HHb] signals.

The superficial signals showed the same singular trends, but it was not possible to work out a classification based on the observation of the two [HbO] and [HHb] signals together, because of their large variability among the subjects.

The CCF between signals and task was calculated only for HF components of the NIRS depth and superficial signals, being these latter those components in which the modulation induced by the blocks of task had been isolated. All the p-values resulted $p \ll 0.001$.

The correlation between the HbO depth signals and the square wave task showed a negative trend for 15 subjects on the right pad and 13 on the left. Mean values of CCF minima were, respectively, -0.26 ± 0.14 and -0.34 ± 0.15, with an average between the two pads of -0.30 ± 0.15.

The correlation between HHb depth signals and the square wave task showed a positive trend for 13 subjects on the right pad and 10 on the left. Mean value of CCF maxima was, respectively, 0.27 ± 0.15 and 0.41 ± 0.19, with an average between the two pads of 0.33 ± 0.23.

The correlation between HbO surface signals and the task was negative for 9 subjects on the right pad and 11 on the left, but it was inverted (e.g. negative for right pad and positive for left one and viceversa) on the two pads of 6 subjects.

The correlation of the HHb surface signals had a different sign on the two pads for half of the subjects. It showed a positive trend for 8 subjects on right and 10 on the left pad, but it resulted opposite over the two pads for 7 out of 16 subjects. Despite it was not possible to identify a strongly prevalent trend over the subjects, a positive correlation was considered as the most reliable one (as it was, at the same time, similar to the HHb depth signaland opposite to the HbO superficial prevalent trend). Thus all the CCFs between NIRS surface signals and the task reported $p \ll 0.001$, they showed a too large variability among the subjects and between the two pads of the same subject, with respect to the depth signal. For this reason, correlation between surface signals and the task were not considered reliable and their results will not be presented and discussed in the next sections.

Identification of a group of subjects.

Fig. 5.18 shows the Grand Average of signals (EEG Alpha and Beta rhythms, [HbO] and [HHb] depth NIRS depth signals, RR series) acquired from all the 16 subjects.
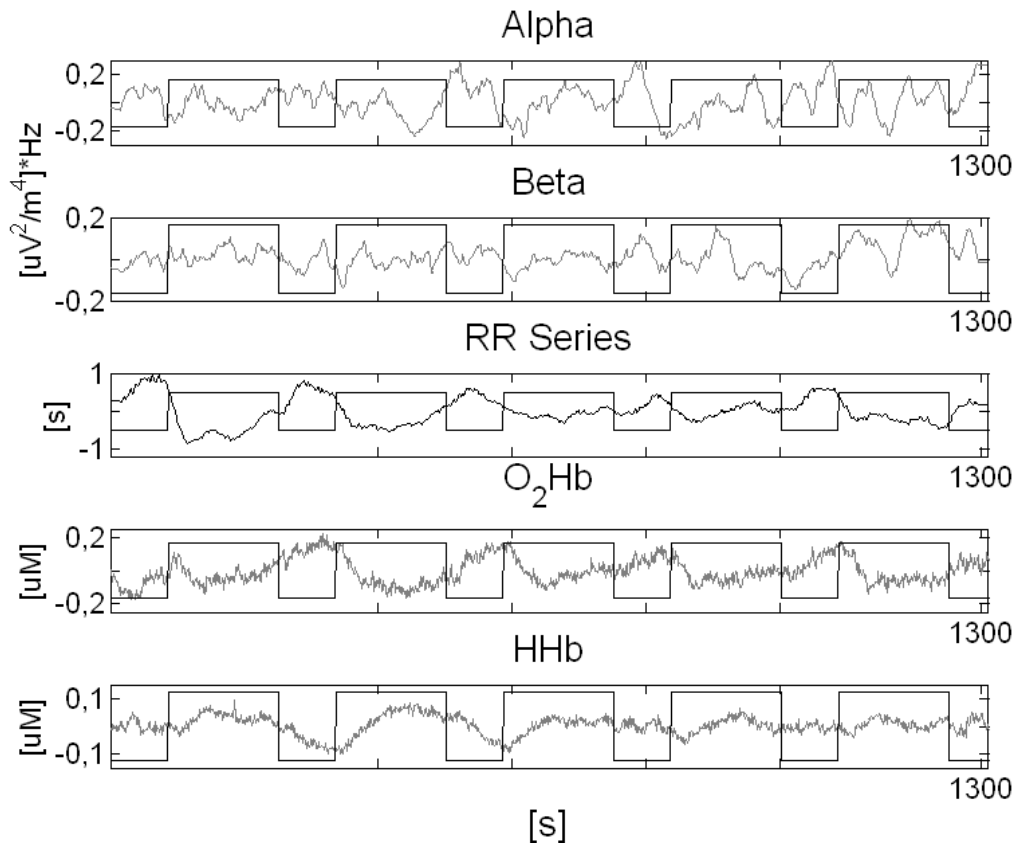
Fig. 1.18. Grand Averages of all the acquired signals from all the subjects. From top: power of Alpha and Beta rhythm, RR series, concentration of HbO and HHb depth signals.

From the observation of the correlations mentioned above a group of 8 subjects (50% of the investigated population) showing the same time course for all the correlations was identified. These subjects correspond to the identification codes 01, 04, 05, 07, 10, 14, 15, 16.

CCF results

Table 5.1 summarizes the results of CCF of both real signals and surrogates, for all the couples of signals for which it was computed. Results are presented as values averaged over the 8 subjects included in the group described above.

In the upper part of the table, results concerning correlations with the task are presented, while in the lower part the results of CCFs over couples of signals are shown.

CCF with the task is negative for Alpha rhythm, RR series and [HbO] and positive for [HHb]. The signs of the CCFs was always found to be consistent with the observations (e.g. if Alpha and RR correlated in a negative way with the task, then the correlation between them resulted positive).

Considering the surrogates series generated for each signal of each subject, it was found that, for each signal and for all the 16 subjects, the real CCF values stand out of the mean interval $CCF_{100} \pm SD$ assessed for the same signal of the same subject as shown in Fig.5.17. This additional analysis allowed to rule out that the correlation values found could be due to a casual relation.

Signals	Real CCF [mean±SD]			CCF$_{100}$ surrogates [mean±SD]			% signals passing the test (on 16 subj.)
Alpha - Task	-0.25	±	0.15	0.0002	±	0.004	100%
RR - Task	-0.48	±	0.20	0.0031	±	0.007	100%
HbO Depth - Task	-0.36	±	0.13	0.0024	±	0.004	100%
HHb Depth - Task	0.35	±	0.19	0.0006	±	0.005	100%
Alpha - RR	0.16	±	0.17	-0.0011	±	0.006	94%
Alpha - HbO Depth	0.20	±	0.17	0.0004	±	0.004	94%
Alpha - HHb Depth	-0.23	±	0.12	0.0025	±	0.005	91%
RR - HbO Depth	0.37	±	0.14	-0.0002	±	0.005	100%
RR - HHb Depth	-0.28	±	0.2	-0.0010	±	0.007	100%
RR - HbO Surface	0.23	±	0.23	-0.0017	±	0.0042	100%
RR - HHb Surface	-0.15	±	0.24	0.0002	±	0.0058	100%

Table 5.1. Real CCF and CCF100 results. The first column presents the couple of signal for which the CCF results are shown in the second column, in terms of mean ± SD. The mean results ± SD of CCF between the 100 surrogate signals are presented in the third column. It should be pointed out that correlations that include NIRS signals are made for both left and right pad, doubling the number of CCF evaluated.

The mean delay between each signal and the task was then evaluated, in order to identify the response delay of each physiological district (neuronal, systemic, hemodynamic) with respect to the divided attention task. As explained above, Beta signal was excluded from this analysis, as well as superficial NIRS data.

The mean delay among the 8 subjects and the correspondent values of CCF are shown in Table 5.2. Table 5.2 testifies that it is possible to identify a temporal cascade of responses: the activation of Alpha rhythm is almost instantaneous, and it is followed by RR series, that has an autonomic influence. Last, NIRS signals rise, thus attesting the contribution of the hemodynamic activity.

Signals	Delay [s]		
Alpha - Task	1.75	±	4.94
RR - Task	15.75	±	14.02
HbO - Task	19.69	±	21.27
HHb - Task	34.43	±	30.25

Table 5.2. Mean delay between each signal and the task. The first column presents the couple of signal for which the CCF results have been calculated, the second one presents the mean delay for which a maximum or minimum of correlation occurred in terms of mean ± SD.

The CCF among couples of signals was then calculated: Alpha and RR, Alpha and HbO, Alpha and HHb, RR and HbO, RR and HHb. Only NIRS depth signals were considered, except for the correlation with the RR series, for which the surface HbO and HHb signals were considered as well. Fig. 5.19 shows the mean results of CCF (±SD) between couples of signals.

The highest value of correlation was found between depth [HbO] and RR series followed by the value of CCF between depth [HHb] and RR series. Interestingly, all of these signals share a common cardiovascular origin, which will be discussed further.
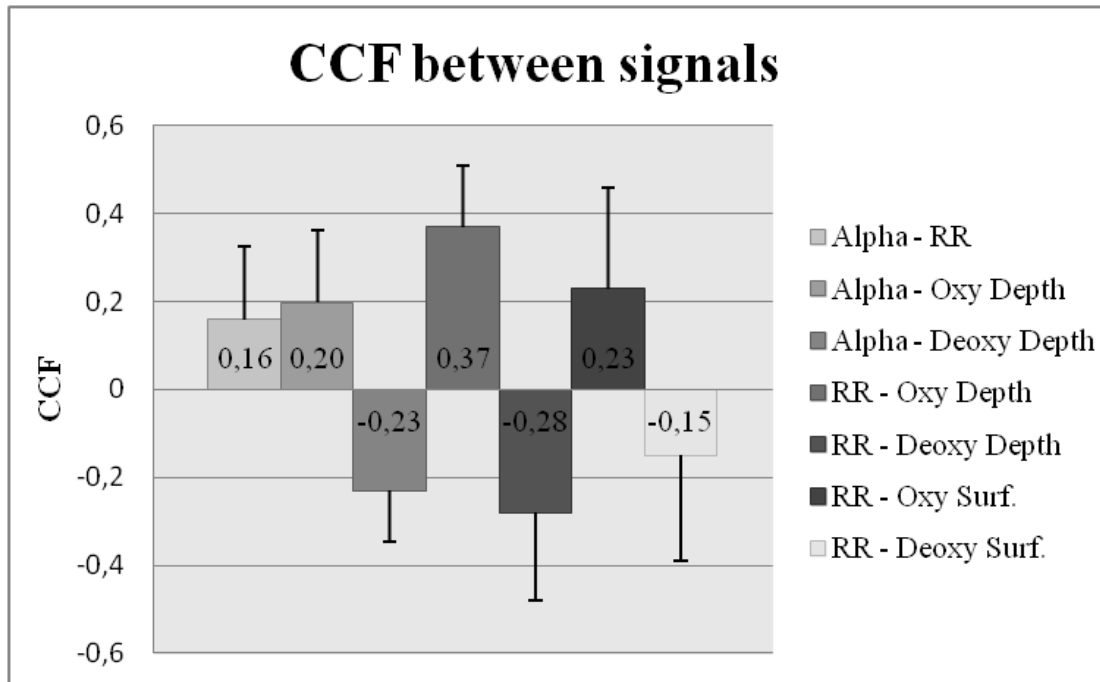
Fig. 5.19. Mean values of CCF among couple of signals. Correlations between alpha rhythm and depth HHb, between RR series and depth HHb and between RR series and surface HHb are negative.

5.3.5 Outcome

While performing electrical activity, neurons come across a number of cellular processes, such as the release and recycling of neurotransmitting molecules and the regulation of trafficking through the ionic channels (Riera and Sumiyoshi, 2010). All these activities require a large energy expenditure, biologically "translated" in a huge consumption of adenosine triphosphate (ATP). Albeit ATP can be synthesized through at least three different pathways in our body, the brain largely fosters the oxidative glucose metabolism. As this pathway is aerobic, cerebral metabolism ultimately relies on a constant supply of both glucose and oxygen. The provision of these two energy substrates is maintained by CBF, which delivers glucose and oxygen to neural tissue through the complex network of blood vessels in brain vascular system. Accordingly, within some seconds after the onset of a localized neural activity, increases in oxygen and glucose consumption are followed by an increase in CBF. This increment is larger than the concomitant increase in oxygen consumption (Fox & Raichle, 1986), resulting in a local increase of hemoglobin oxygenation. The rise in CBF is mainly achieved by arteriolar dilation inducing increased perfusion pressure downstream. Very recent observations support the hypothesis that red blood cells may act as sensors of local tissue hypoxia, through the oxygenation status of the hemoglobin, and initiate improved local perfusion to the tissue through hypoxic vasodilation (Thorn et al., 2011).Blood flow per capillary is increased mainly by an intensification in blood flow velocity, whereas capillary recruitment, i.e. opening and closing of capillaries, seems not to occur in the brain (Gobel et al., 1989; Villringer et al., 1994). These factors result in a local increase in [HbO] and a drop in [HHb] (Obrig et al., 1996), being the latter also the main basis of the fMRI BOLD contrast (Kwong et al., 1992; Ogawa et al., 1992; Frahm et al., 1992; Bandettini et al., 1992).

In our work, we simultaneously recorded EEG, ECG and NIRS signals during the performance of a bimodal task of divided attention. All the subjects were able to fully

accomplish the attentive request, as they could complete the task providing accuracy above 95% for all the conditions. On the other hand, some errors were made, indicating that subjects operated at the very limit of their attentive capabilities.

The first relevant result is the major modulation induced by the attentive task on alpha EEG rhythm. Such conditioning was not observed in the beta frequency range. Our findings are in agreement with Bollimunta et al. (2011), who found that visual attention reduces the magnitude of alpha oscillations as well as the level of alpha interactions in macaques, and Mo et al. (2011), who suggest that ongoing alpha oscillations in inferotemporal cortex may be part of the neuronal mechanism representing task-relevant information.

The RR series showed a strong modulation induced by the task, and an increasing trend during all the test, meaning that the cardiac frequency -after an increasing in the beginning of the test- slowly recovered to the baseline values. This result finds longstanding confirmations in literature (Somsen et al., 2004; Pagani et al., 1991; Steptoe and Sawada, 1989).

The LF components of NIRS depth signals showed an increase in HbO with a concurrent decrease in HHb in the divided attention task. This finding is fully consistent with previous literature (Kubo et al. 2008; Fallgatter and Strik, 1998) and with previous work of the research group (Butti et al., 2009).

The lack of reliability found for the surface contribution to NIRS signals has already been discussed elsewhere by our group (Aletti et al., 2011), and by recent literature (Takahashi et al., 2011): the surface component of NIRS signals, measured over the forehead, proved indeed to be affected by a skin flowmotion contribution, in its turn dependent on a strong systemic drive, while the deep cortical NIRS signal did not appear to be tainted by surface vasomotor activity, but rather autoregulation dynamics were dominant with respect to autonomic control of circulation.

Surrogate analysis confirmed that all the correlation values presented in Table 5.1, although low in value in some cases, can be accepted. As expected, the highest correlation values were obtained for the relationship between RR series and the task, and between RR and NIRS depth signals; in other words, the cognitive task primarily influenced the signals of cardiovascular nature. This evidence can be interpreted as a consequence of an high emotive involvement during the task blocks.

Correlation between RR series and Alpha rhythm showed lower values. This result seems plausible, due to the different origin of the two signals (ANS and CNS respectively). This result also agrees with the well-established notion that there is very little mirroring of the cardiac activity in EEG signals.

Furthermore, the time courses of NIRS depth signals and Alpha rhythm show the presence of neuronal desynchronization (reduction in Alpha power), reduction in HbO concentration and increase in HHb during the test period. These results could globally be interpreted as "metabolic saving", according to which synchronized membrane oscillations are energetically advantageous. An increase in synchronization during rest periods (i.e. periods of decreased metabolic consumption) becomes straightforward. The higher correlation between Alpha rhythm and [HHb], with respect to Alpha and [HbO], was also reported by Moosman et al. (2003).

Table 5.2 resumes the activations induced by the divided attention task. Activation of several systems was observed, each one characterized by a different time delay: neural electrical response was sudden (delay of Alpha rhythm with respect to the task was less than 2 s), autonomic response was then risen (mean delay of RR series 15.75 s) and a slower hemodynamic response (mean delay of HbO around 20 s, around 30 s for HHb) was finally induced. Globally, the task elicited a cascade of responses, in which time delays could be quantified.

The correlations between couples of signals showed that the different responses to the task were interdependent: a desynchronization of Alpha rhythm, a reduction in HbO concentration and an increase in HHb concentration and Heart Rate were doubtless observed during test blocks. These phenomena mirror metabolic consumption, and proved to reverse during rest periods. For these reasons, we can infer that the cognitive task is effectively the generator of the neuronal, autonomic and hemodynamic responses.

Last, despite the findings described above, some limitations of the study need to be highlighted too: (i) The two-channel NIRS device provided a limited head coverage, only probing the frontopolar area, (ii) the synchronous placement of EEG electrodes and NIRS emitters and receivers could not be done with respect to any standard or guidelines and (iii) signals showed high inter-subject variability, which could only be handled by arbitrarily restricting the discussion to a subgroup of subjects who showed concordant results.

5.4 Cognitive load

5.4.1 Background

In this study we applied a working memory protocol to healthy subjects at the aim of assessing the possibility to discern different cognitive categories and different cognitive loads by means of time resolved Near Infrared Spectroscopy instrumentation.

Working memory (WM) is the cognitive function resulting from the active short-term memory system that guides and controls humans' behaviour. It allows the temporary storage and the further recollecting of information (McAfoose & Baune, 2009). Importantly, it is a limited-capacity resource, which thus can easily saturate under extremely stressful conditions, excessively rapid streams of information and in disproportionately complex environmental settings. Psychophysiology demonstrated sustained activity in the frontal and parietal brain areas while information is held in mind (Funahashi, 2006; Klingberg, 2006; Petrides, 2005). Visual WM, specifically, involves the concerted activity of a distributed neural system, including anterior areas in prefrontal cortex (PFC) and the visual cortex posteriorly (Pessoa & Ungerlieder, 2004). Within the visual cortex, ventral stream areas are selectively involved in object vision, whereas dorsal stream areas are involved in spatial vision (Munk et al., 2002). This domain specificity appears to extend forward into PFC, with ventrolateral areas involved mainly in WM for objects and dorsolateral areas involved mainly in WM for spatial locations (Funahashi, 2006; Petrides, 2005; Curtis, 2006). Moreover, interactions between the inferior temporal neocortex, PFC and parietal cortex likely support WM maintenance via an attention-based mechanism, enhancing the relevant information among irrelevant background noise (Hopf et al., 2006; Tomasi et al., 2006).Overlap of the cerebral networks of WM and attention has been demonstrated in targeted comparisons (Corbetta et al., 2002). Specifically, superimposition of activation was observed in the frontal midline and in a part of the right and inferior frontal gyrus in fMRI studies (Mayer et al., 2007). As a result, competition for processing resources that are shared by the WM and attention systems can lead to a severe limitation of neural processing capabilities. One major bottleneck of information processing, indeed, arises from the common demands on neural resources shared between visual WM and attention during the encoding stage.Some regions in the left PFC and in the inferior temporal cortex have shown selective responsiveness to cognitive load during a WM task (Mayer et al., 2007). Areas selectively responsive to high attentional demand have been highlighted by Mayer et al. (2007) within the right prefrontal and bilateral occipital cortex. Consequently,

they inferred a hemispheric specialization with left PFC selectively responsive to WM load and right PFC selectively responsive to attentional demand. On the other hand, some evidences suggests that medial temporal lobe (MTL) and the PFC serve complementary roles for WM processes: whereas the PFC appears to be predominantly important for WM maintenance of familiar items such as words or numbers, the MTL may play a role for maintenance of unfamiliar novel items (Axmacher et al., 2008). In addition, it has been recently shown that multi-item memory processing depends on the organization of item representations by the same MTL (Axmacher et al., 2008). Recently, Rissman et al. (2008) have put forward that two neural circuits may dynamically trade off to accommodate the particular mnemonic demands of the task: some evidences credit the establishment of interactions between frontal gyrus and fusiform face area, mediating maintenance of information at lower cognitive loads, and the involvement of hippocampus, supporting the retention when a higher effort is needed. Besides, Jaeggi et al. (2003) have specifically investigated the modulation effect induced by the mnemonic demand of the task on the activation in the PFC. By showing that activation increases with memory load in the PFC, even in the case that the capacity of the WM's central executive system is exceeded, they definitively uncoupled neural activation from behavioural accuracy measures and performance.

In this context, multichannel fNIRS can measure cortical activation during cognitive processing without interfering with task procedure; indeed, it has been successfully employed in protocols evaluating psychological and emotional pressure (Ito et al., 2011) and in pediatric studies (Sanefuji et al., 2011).Schreppel et al. (2008) investigated the effects of interference resolution processes on activation of the PFC in a WM task by means of fNIRS. Shibuya-Tayoshi et al. (2007) and Nakahachi et al. (2010) employed fNIRS devices to obtain a mapping of the activation of the PFC during the visuospatial WM Trail Making Test. They reported bilateral activation, primarily in the PFC. Lee et al. (2008) examined qualitatively distinct types of error trials during the execution of a delayed WM task to further specify the behavioural and neural difference between errors that arise from a loss of mental representation versus those which arise from the encoding of an incorrect stimulus; they applied both fNIRS and fMRI for a comparison of activations. To our knowledge though, none of these studies have ever investigated the capabilities of fNIRS devices to detect hemodynamic changes due to variation in cognitive load. Despite fMRI and positron emission tomographic (PET) studies have deeply fathomed out the matter (Jaeggi et al., 2003; Jolles et al., 2010; Nyberg et al., 2009; Rypma et al., 2002; Vanderberghe et al., 1997), the applicability of easy to use noninvasive optical instrumentation could open the investigation to much broader cohorts.

The present study mainly introduces two items of novelty with respect to the literature mentioned above: i) the employment of NIRS devices in the investigation of the modulatory effect risen in the frontal hemodynamic pattern by means of a stimulation with differential cognitive load and ii) the use of time domain fNIRS (based on high repetition rate light sources and picosecond detection of photon time-of-flight) to improve depth sensitivity to cortical hemodynamic changes (Liebert et al., 2004; Quaresima, 2005; Selb, 2005; Steinbrink et al., 2001).

The aims of this work were: (i) to determine whether multichannel time domain fNIRS is capable to discern differences in frontal patterns of activation due to pure attentional and WM tasks; (ii) to assess time domain fNIRS sensitivity in detecting modulation effects induced by the mnemonic demand of a cognitive task with graded levels of difficulty. This was done by focusing on frontal cortical activation during a n-back task with different stages of memory requirement.

5.4.2 Materials and Methods

Data recordings

A prototypical eight-channels time resolved NIRS device (Dipartimento di Fisica, Politecnico di Milano) was employed for HbO, HHb and HbT acquisitions. The system was provided also of suitable probes (made of Velcro stripes and custom-made plastic holders) for positioning of the injection fibers and of the detection bundles on the forehead tissue.The optical probe was placed over the head in order to cover the underlying prefrontal cortex and light sources were centered (according to the international 10-20 system for the EEG electrode placement) at the Fp1 and Fp2 for left and right sides, respectively. The NIRS signals were sampled at 1 Hz.

To enhance the contribution from deep layers and to remove possible disturbances caused by superficial layers, a correction method based on the use of late time windows ($t = 1750\text{-}2500$ ps) was also applied (Contini et al., 2007; Aletti et al., 2011). HbO and HHb concentrations were then derived by Lambert Beer law, and total haemoglobin content (HbT = HHb+HbO) was calculated.

Finally, low frequency and high frequency components were extracted from the hemodynamic data by using a digital filter. The choice was that of 9th order digital Chebyshev filter (MATLAB®) with the stop-band 30 decibels down. Transition frequency was selected as the inverse of the period of the task modulation.

Statistics

To examine whether there were statistically significant changes in fNIRS signals, amplitude analysis on the HbO, HHb and HbT measures was performed. A t-test was conducted for assessing differences between fNIRS data acquired over the two hemispheres (right vs. left). Then, repeated measures ANOVAs were conducted, with two within-group factors: Condition (rest and loads) and Channel. Post-hoc analyses were performed with pairwise ANOVAs. A *P*-value of 0.05 was considered to be statistically significant. The Greenhouse-Geisser procedure was used to correct for sphericity violations, where necessary.

T-tests were also conducted on behavioural data, in order to assess differences in performance between conditions. All the statistical analyses were performed with NCSS Statistical Software (NCSS Statistical & Power Analysis Software, http://www.ncss.com).

Generalized Linear Model

Both low and high frequency components of HbO, HHb and HbT time courses (time series) were analysed with the Generalized Linear Model (GLM). The task was modelled as a series of consecutive boxcar regressors, each one marking with a unit value a single condition (e.g. two activation periods with the same cognitive load) and with a zero value all the remaining part of the task. The timing of the regressors was chosen accordingly to the different activities performed during the experiment. The GLM was applied separately for HbO, HHb and HbT data. The employed Hemodynamic Response Function was the same for HbO, HHb and HbT data (Ye et al., 2009). First level analysis (i.e. on single subjects) was performed first. Activated areas were extracted by setting uncorrected p-value of the t-statistics at 0.05.

Inferential procedures at a second level (e.g. about activated channels over all subjects) were then performed, by setting uncorrected p-value of the t-statistics at 0.001, and the DM was accordingly modified.

Contrast matrix was designed for a direct comparison of: (1) activation during the two task periods and rest condition with respect to the reference (whole test) (see fig.5.20 – left), (2) activation during each cognitive load and rest condition with respect to the load/rest immediately harder/easier (see fig.5.20 – right), (3) activation during each cognitive load and rest condition with respect to the reference (whole test) (again, see fig.5.20 – right).

Cerebral activation is indicated by positive T-values in the HbO and HbT time-series, and by negative T-values for HHb. The results from these second level analyses were plotted as statistical parametric maps in NIRS_SPM (Ye et al., 2009), which illustrate the brain regions where increased or decreased HbO, HHb and HbT correlate with the stimulation protocol over time.

Pearson Product Moment Correlation Coefficient at lag 1 of basal fNIRS signals is not significantly different from zero for both HbO and HHb series, if the p-value is set at 0.05. Then, no corrections for serial correlations were applied in the GLM employed in the present work.
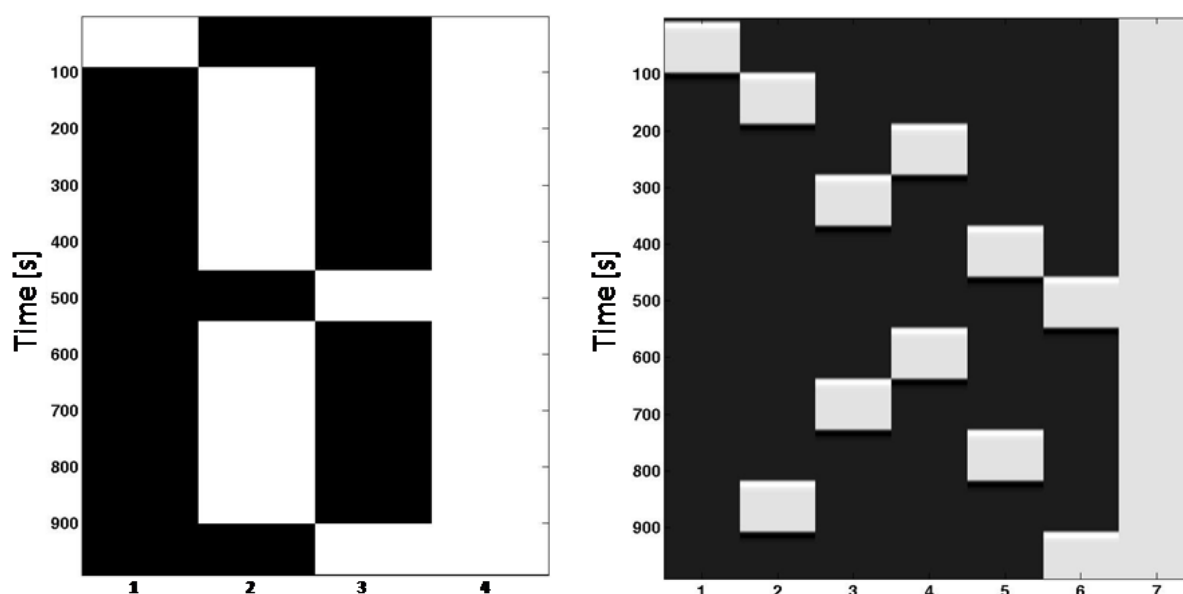
Fig.5.20. Design matrix DM1, modeling baseline, task and rest (left): time course proceeds from top to bottom, while baseline, task, rest, and "reference" functions are aligned from left to right. Design matrix DM2, modeling baseline, the four cognitive loads and rest (right): time course proceeds from top to bottom, while baseline, 0-, 1-, 2- and 3-back, rest, and "reference" functions are aligned from left to right.

Subjects

Nineteen healthy volunteers, comparable for age (mean 27.15 years, SD 2.01 years, range 23-30 years) and school attendance (mean: 19.9 years, SD: 1.2 years, range 17-21 years) participated in the experiment. Seventeen subjects were right-handed. The neuropsychological status of each participant was assessed by means of an unpublished adapted Italian version of the "Neuropsychological History Questionnaire" (Greenberg, 1994). They all had normal vision and had no history of psychiatric disorders. None of them showed any neuropsychological illness; cognitive level and attentive capability were normal; none of them had any first-degree relatives with a psychiatric illness. They all underwent the "n-back" working memory task described in chapter 2.

5.4.3 Results

Behavioural results

The 19 subjects committed an average of 1,58 errors (SD=0,69) in the *n*-back task, thus falling in the normality range (Cohen et al., 1997). On average, they committed 0,77 errors during the 0-back condition, 1,28 errors during the 1-back, 2,14 during the 2-back and 2,15 during the 3-back. They answered correctly to the target in 511 ms (SD=36). More specifically, reaction times on targets were 464 ms for the 0-back condition, 508 for the 1-back, 540 ms for the 2-back and 535 ms for the 3-back. A statistically significant difference was found for errors committed at the four different cognitive loads ($p < 0.05$), as well as for reaction times, grouped for the same four loads ($p < 0.05$).

fNIRS results

Results emerging from time domain fNIRS acquisitions show that variations of HbO remained positive in the PFC, over both the hemispheres and during the entire test (fig. 5.21). Activation level increased during the first half of the test, reaching a peak in the central part of it; then, activation remained stable during the second part of the task, with a final and further increase in the last recovery period. In addition to the large, persistent changes described hitherto, transient and less prominent changes were observed, time locked to the active blocks presentation.

Variations of HHb globally stayed in a range of negative values throughout the test. Right channels showed an initial decrease and an ensuing increase in value, which moved towards the restoration of the rest value; left channels exhibited an initial decrease of HHb as well, with a delayed recovery.
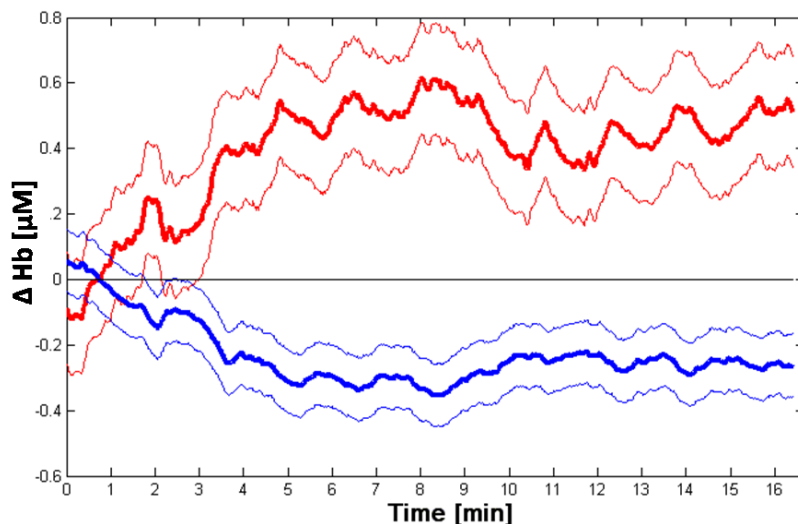
Fig. 5.21. Time course of HbO (red line) and HHb (blue line). Averages (thick line) and standard deviations (thin line) over the population of the study (all channels). HbO increased during the first half of the test, and its values remained high; HHb values tended to decrease, reaching a stable equilibrium very early during the test.

Globally, larger variations of HbO and HHb were found over the right frontal area, with respect to the contralateral hemisphere. This hemispheric lateralization, visually discerned on raw data, was later confirmed by statistical analysis: t-test indeed confirmed the statistical difference between the average signals from right and left channels for both HbO

and HHb. The prevalence of activation on the right side was then assessed, i.e., right PFC showed higher HbO increases than the left one.

Moreover, repeated-measures ANOVA test conducted on HHb revealed a strong effect of time ($p < 0.001$) and of time-by-channel interaction ($p < 0.001$); while a main effect of channel was not observed ($p > 0.05$). The effect of time is paramount: the task generated a strong hemodynamic response throughout its entire duration, presenting a momentary decrease only in correspondence of the central rest period. Standard deviation increased with time within both parts of the task, thus testifying a greater uniformity of behaviour among subjects during the "early" response to the task (and then a more pronounced inter-subject variability for the long-term response). Repeated-measures ANOVA test conducted on HbO attested a significant main effect of time and of time-by-channel interaction ($p<0.001$). Effect of channel was not statistically significant ($p>0.05$).

To tentatively discriminate between the tonic contribution to activation, due to subject's involvement in the cognitive challenge, and the phasic cerebral activity, which is more specifically linked to the working memory effort, low and high frequency components were extracted from the fNIRS signals. The two contributions were separately considered, with reference to the performance of the cognitive task (Fig. 5.22).

As mentioned in the previous section, high frequency components of the signals were first analysed by means of DM1 (fig. 5.20 left), and then statistical t-maps were calculated for the analysed group of volunteers using the T-value parameters. These interpolated maps were obtained through the resolution of the complete GLM at group level. Each map represents the distribution associated to a specific contrast between two regressors. Response of the PFC to task presentation is given in figure 5.23a, for HbO, HHb and HbT respectively. The temporal trend noted above is confirmed by these activity maps. The task originated a strong metabolic response, leading to an increasing difference between parameters values registered during the test and during the baseline period. The test, indeed, was characterized by a strong and steady activation. Contrarily to the initial baseline period, the interleaved and final recovery periods could not provide any significant deactivation, if compared to the task. Modifications are spread over the PFC, attesting a general involvement on the frontal lobe due to this task. Some hemispheric lateralization to the right is found for HHb, while HbO and HbT show their activation foci medially.

High frequency components were then analyzed by means of DM2 (fig.5.20 - right) for a load-by-load signal analysis. Results seem to suggest that high frequency activity underwent a modulation induced by the task presentation sequence, thus following the alternation of task/rest blocks (Fig 5.22 and 5.24c). Due to this characteristic, this component should be the one which mostly represents the real cortical activity related to the WM effort. In figure 5.23b, 0-back (pure attentive) condition is contrasted against baseline. Maps of HbO, HHb and HbT are presented. HHb shows a strongly significant right lateralization. HbO and HbT maps attest a different distribution of cerebral oxygenation over the PFC during the lightest period of the task, showing a peak of statistics medially.

Figures 5.23c, 5.24a and 5.24b show the pseudocolour representations of the t-statistic values of HbO, HHb and HbT courses (high frequency signals) for 1-back, 2-back and 3-back loaded conditions respectively, contrasted with the baseline. At any load, HHb shows a strong activation, considerably lateralized over the right hemisphere. HbO also shows activation, though more uniform and medially located. Spatial distribution of HbT shows a mild lateralization to the left, more pronounced in the 1-back and 3-back conditions.
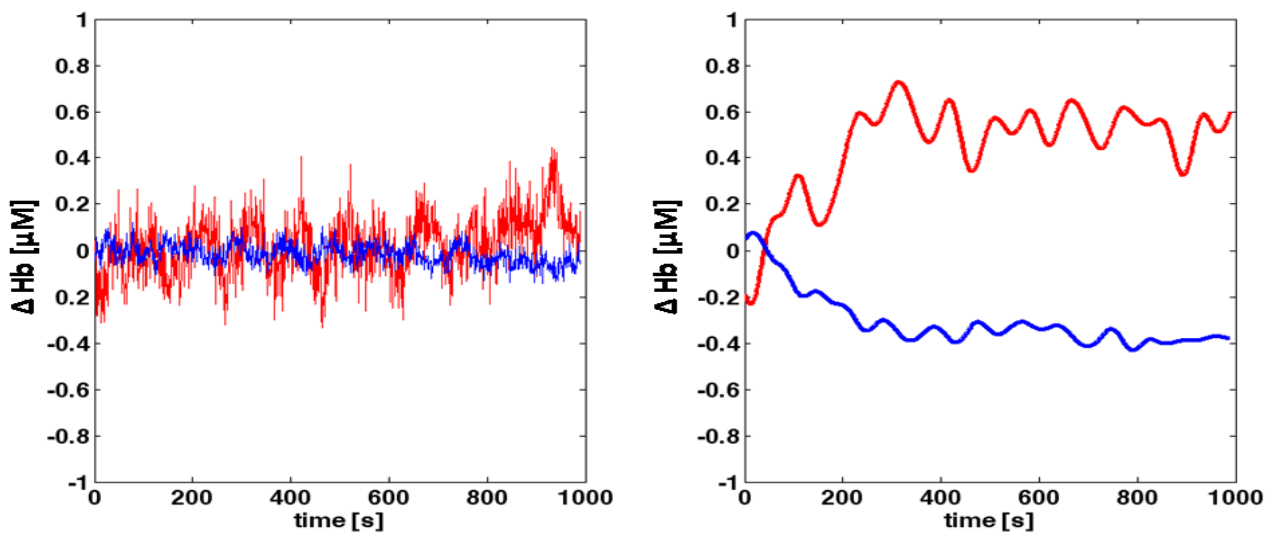
Fig. 5.22 Time course of high-frequency (left) and low-frequency (right) contributions of HbO (red line) and HHb (blue line) during the working memory task. As an example, signals belonging to subject n°8 are shown. Channels are averaged.

The study of neighbouring loads has provided us with congruent results: contrasts between 0-back (pure attentional) and higher loads (working memory conditions) highlighted significant differences in activation pattern (see figure 5.24c for an example of activation pattern resulting from contrast between the pure attentional and the easy WM conditions). Contrasts between different WM loads (1-back vs. 2-back, 1-back vs. 3-back, etc.) showed a trend of difference in activation patterns in the left hemisphere, which though was not significant.

GLM was finally run for "low frequency data" (by means of both DM1 and DM2). Maps revealed a faint activation of HbO in the 1-back and 2-back conditions. Surprisingly, HHb proved to be significant at every task load, if contrasted with baseline. A poor right lateralization was still detected for HHb: though omnipresent, it provided no statistical significance.

During the employment of GLM, the variance of model residuals was calculated, for both DM1 and DM2. Table 5.3 resumes our findings.
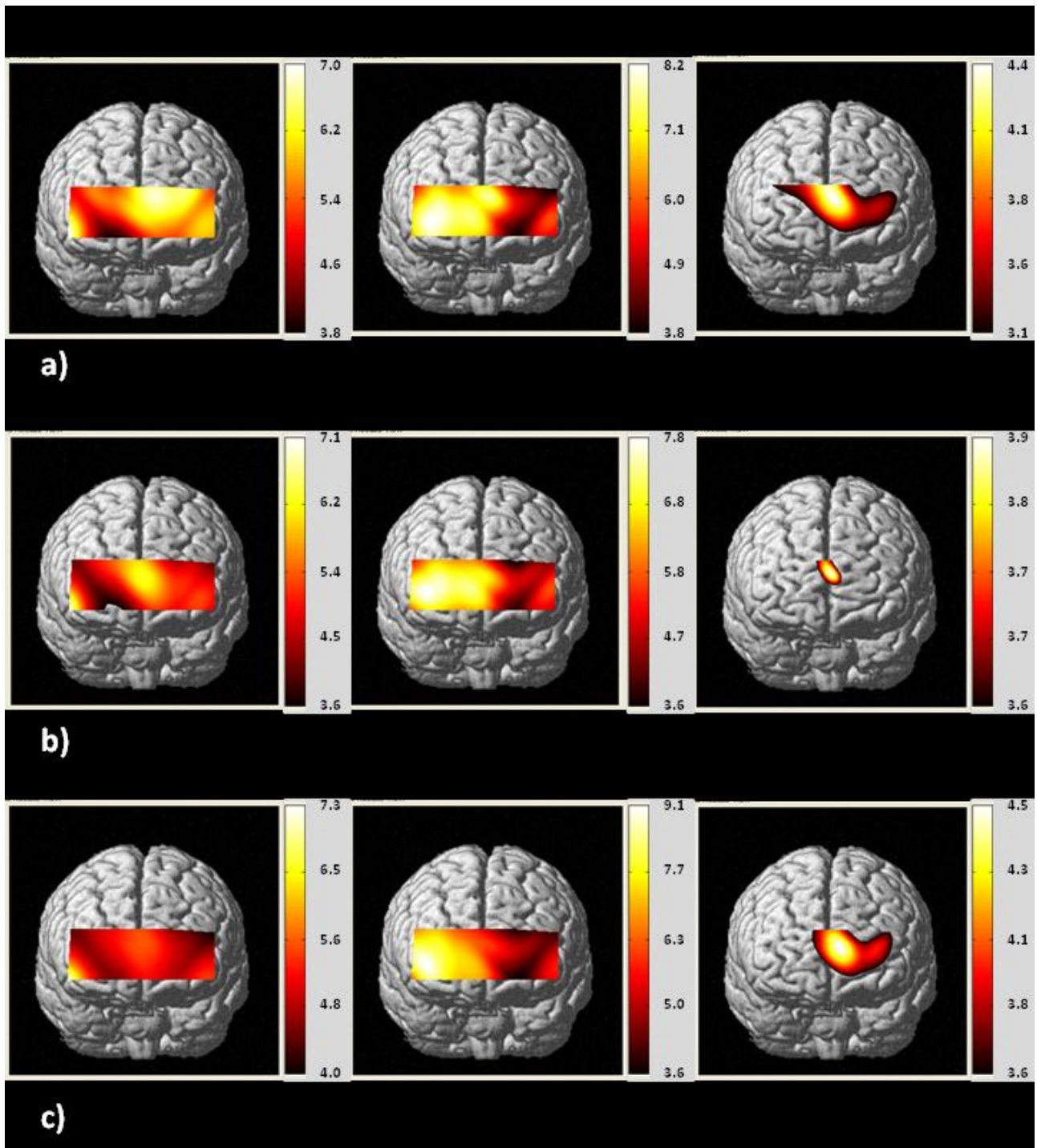
Fig. 5.23. Cortical activation during WM task: high frequency signals. The activation maps are obtained from t-statistic values, assessed by a second level analysis of the GLM model. From left to right: HbO,HHb and HbT maps are presented. a) Each map depicts the significant difference between task condition and baseline. b) Significant difference between the 0-back condition and baseline. c) Significant difference between the 1-back condition and baseline. (p-val<0.001 for all maps).
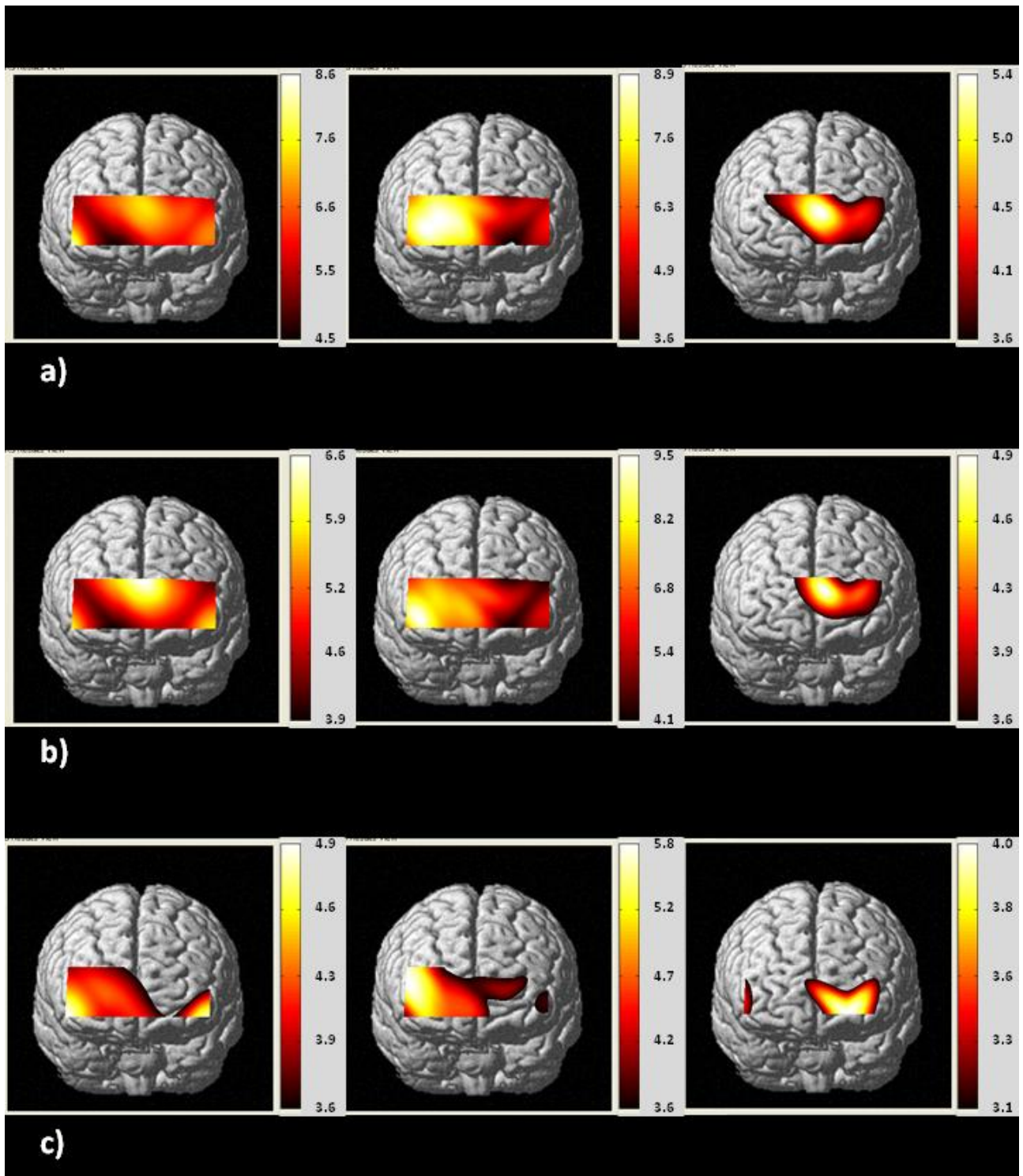
Fig. 5.24. Second level analysis of the GLM model: high frequency signals. From left to right: HbO, HHb and HbT maps are presented. a) Each map depicts the significant difference between the 2-back condition and baseline. b) Each map depicts the significant difference between the 3-back condition and baseline. c) Each map depicts the significant difference between the 1-back condition and 0-back. (p-val<0.001 for all maps).

5.4.4 Outcome

Both pure attentional effort and executive functions engagement (such as WM) are known to activate the dorsolateral PFC (Funahashi, 2006; Klingberg, 2006, Petrides, 2005). In spite of this, attention and higher cognitive faculties differ phenomenologically, and cannot be regarded as the same process. Rather, attention is nowadays intended to serve as an underlying process on which the other cognitive activities can graft and develop. It is then possible that physiological differences existing between attention and higher processes are mirrored in some unlikeness in the dynamics and extension of PFC activation (Tomasi et al., 2006). *N*-back task decouples attentional and mnemonic contributions to the global cognitive effort, and in addition allows the investigation of cortical activation during incremental cognitive exertion and –eventually– fatigue.

WM errors may arise from a failure to encode the target, from loosing internal representations during maintenance or from an incorrect coding of the target held in mind (Lee et al., 2008). The first case prevents the subject's brain from entering the maintenance step of memory, potentially causing a lack of PFC activation with respect to correct trials; the third case is for sure not affected by the risk of an absence of activation demand, generating an incorrect recollection; the second case clearly consists of a trade-off between the previous two cases. N-back task requires a constant encoding load: velocity of encoding never changes among conditions. The difficulty of the task is modulated by the maintenance request only. For this reason, if subjects perform correctly during the 0-back condition, a decay of PFC activation due to encoding performance can be excluded and – importantly – any change in PFC activation can be attributed to maintenance only. In our study, all subjects performed very well during the 0-back condition, and they proved to be able to afford even the most difficult (3-back) condition of the task.

fNIRS activation studies have demonstrated that cognitive tasks generally cause increases of HbO and HbT associated with decreases of HHb in the prefrontal cortex (Hock et al., 1995; Hock et al., 1997; Hoshi & Tamura, 1997; Hoshi, 2003; Sakatani et al., 1998). The increases of HbO and HbT reflect the occurrence of redundant regional cerebral blood flow (rCBF) increases in response to neuronal activation, and the decrease of HHb is caused by evoked-rCBF rises which exceed the increases in oxygen consumption during neuronal activity (Fox & Raichle, 1986). Our results totally agree with these previous findings, as it is shown in fig. 5.21. It has been reported that cortical activation results in an overshoot of regional blood supply that is disproportionately larger than the increase in oxygen demand (Fox & Raichle, 1986). This phenomenon is known as the "physiological uncoupling" of oxygen metabolism and blood supply. Augmented arterial blood flow into the cerebral cortex washes away deoxygenated haemoglobin more rapidly, resulting in a decrease in HHb with an increase in HbO (Villringer & Chance, 1997; Hoshi et al., 2001). In this study, an explanation by the above mechanism is applicable.

The relative HbO concentration in frontal brain tissue increased significantly and bilaterally during the performance of the n-back test, compared with a resting condition. This result can be interpreted as an expression of increased cerebral perfusion as a consequence of an activated brain metabolism during the task. Simultaneously, HHb showed a progressive reduction. This latter effect is consistent with an enhanced HHb draining, secondary to hyper-perfusion.

During a two-channel fNIRS registration of a continuous performance test in healthy subjects, a significant frontal HbO increase was found, compared with a baseline at rest, by Fallgatter and Strik (1998). This result is generally interpreted as an enhanced perfusion of the frontal lobes consistent with attentive local activation. Lee et al. (2008) reported an increase for both HbO and HHb in a WM task performed by healthy people.

Data of the present study seem not to support this evidence, as we found an increase in HbO with a concurrent decrease in HHb in the n-back task for WM assessment, as in Toichi et al. (2003) where an increase in HbO with a concurrent decrease in HHb in tasks of higher cognitive function (i.e. WM) is reported. Furthermore, Lee et al. (2008) also observed an increase of both HbO and HHb in tasks of pure attention and a lack of increase in HbT in some subjects during tasks of higher cognitive processing, which we could not observe in our data. They hypothesized that the cerebral metabolic rate of oxygen consumption during tasks of attention may be higher than that during tasks of higher cognitive processing and, consistently with this interpretation, they proposed the change in HHb to be a physiological marker discriminating between attention and higher cognitive processing. The origin of such discrepancies can be founded in the differences in the technologies employed: continuous wave NIRS, used in Toichi's and Lee's works, could provide data more affected by the superficial systemic contribution.

Rather, our results totally agree with recent studies by Shibuya-Tayoshi et al. (2007) and Nakahachi et al. (2010), who found a bilateral HbO increase prefrontally. Interestingly, a widespread, powerful right HHb activation is constantly present in GLM maps throughout the test. fNIRS literature can only provide partial confirmations of this result.

The analysis of contrasts between neighbouring loads has revealed that 0-back (pure attentional) condition and higher load conditions (WM) elicit significantly different activation patterns in the PFC (fig. 5.24c for an example). This is consistent with the difference existing between the two cognitive categories at a neural level. Besides, contrasts between different WM loads (1-back vs. 2-back, 1-back vs. 3-back, etc.) showed differences in activation patterns which were maximal in the left hemisphere, even though not significant: the left lateralization is consistent with previous results produced by Mayer et al. (2007) in an fMRI study, while the lack of significance between loads can be related to the scanty statistical power associated with the modulation of PFC activation, which is not comparable with a newly generated activation focus. However, as the attentive background is constant throughout the test of our study, the result appears to be specific for the demands of the augmented memory load, and not due to the general effects of attention, perception and motor response. In recent years, Linden et al. (2003) found that PFC responds to WM load beyond the capacity of the parietal–premotor network. Therefore, WM load-selective activation in the PFC might fit within the framework postulating that this brain region subserves extra-mnemonic processes of top–down control over posterior regions where information is actually stored (Curtis & D'Esposito, 2003; Postle, 2006). This is in agreement with the continuous increase of PFC activation through loads seen in our study.

Last, comparing fig.5.23b with fig. 5.23c, 5.24a and 5.24b, it can clearly be seen that the overlap of the cerebral networks of WM and attention observed in the frontal midline by Mayer et al. (2007) likely finds confirmation in the present study. Fig. 5.23b, indeed, shows a HbO midfrontal pattern due to attention only, which match literature. Other confirmations can be found in Hopf et al. (2006) and Tomasi et al. (2006).

During the employment of GLM for the analysis of high and low frequency data, the variance of model residuals was calculated, for both DM1 and DM2. Table 5.3 resumes our findings. In all cases, DM2 proved to perform a better description of data, thus providing lower residuals. This result confirms that a better modelling of data is obtained if the different conditions administered during the task are separately taken into account inside the linear model.

DM	contribution	O$_2$Hb	HHb	tHb
DM1	High frequency	0.0730+0.0193	0.0160+0.0067	0.0477+0.0127
DM1	Low frequency	0.0121+0.0194	0.0031+0.0065	0.0071+0.0128
DM2	High frequency	0.0707+0.0079	0.0156+0.0027	0.0464+0.0045
DM2	Low frequency	0.0113+0.0079	0.0029+0.0027	0.0066+0.0045

Tab. 5.3. Variances of the GLM residuals. In the columns (from left to right) design matrices are listed, together with frequency contributions and values of the variance of GLM residuals for oxygenation, deoxygenation and total haemoglobin signals. All values are obtained in the form of mean value and standard deviation from the whole population. In all cases, DM2 proved to perform a better description of data, thus providing lower residuals.

Last we point out that, as we considered the presence of the inter-hemispheric fissure, some spatial undersampling occurred in the medial area, and thus we cannot completely rule out small shifts in localizing the medial activations, due to spatial interpolation. This fact, albeit marginal, could be considered one limitation of our study.

In conclusion, the present investigation by multichannel time domain fNIRS supports the results from fMRI studies, showing an enhanced frontal lobe perfusion during performance of the n-back task. Overlapping activation for attention-demanding visual search and WM was observed in distributed frontal regions; nevertheless, the combined employment of time-resolved and GLM processing succeeded in identifying distinctive patterns of cortical activation for the two different neurophysiological categories under investigation (attention and short-term memory). Indeed, a subset of regions, in the right prefrontal cortex, showed an additive increase in HbO activation passing from attentional demand to WM effort.

In conclusion, the present study (1) successfully explored the capability of fNIRS (and more specifically time domain fNIRS) to detect and characterize the prefrontal patterns of activation risen by attention and WM, and (2) contributed to highlight the advantages deriving from a multiple application of GLM to fNIRS data. On the other hand, a statistically significant distinction of cognitive load could not be reached.

Bibliography

Aletti F, Re R, Pace V, Contini D, Molteni E, Cerutti S, Bianchi AM, Torricelli A, Spinelli L, Cubeddu R, Baselli G. Deep and surface hemodynamic signal from functional time resolved transcranial near infrared spectroscopy compared to skin flowmotion. Comput Biol Med. 2011 Jul 8.

Attwell, D., and Iadecola, C. (2002). The neural basis of functional brain imaging signals. Trends in neurosciences 25, 621-625.

Axmacher N., DP. Schmitz, T. Wagner, CE. Elger, and J. Fell, "Interactions between medial temporal lobe, prefrontal cortex, and inferior temporal regions during visual working memory: a combined intracranial EEG and functional magnetic resonance imaging study," J Neurosci. Jul 16;28(29):7304-12, (2008).

Banaji M., A. Mallet, CE. Elwell, P. Nicholls, and CE. Cooper, "A Model of Brain Circulation and Metabolism: NIRS Signal Changes during Physiological Challenges," PLoS Comput Biol 4(11): e1000212, (2008).

Bandettini PA, Wong EC, Hinks RS, Tikofsky RS, Hyde JS. Time course EPI of human brain function during task activation. Magn Reson Med. 1992 Jun;25(2):390-7.

Baselli G., Cerutti S., Civardi S., Lombardi F., Malliani M., Merri M., Pagani M., Rizzo G. 1987, Heart rate variability signal processing: A quantitative approach as an aid to diagnosis in cardiovascular pathologies, International Journal of Bio-Medical Computing, 20(1): 51-70

Boas DA., AM. Dale, and MA. Franceschini, "Diffuse optical imaging of brain activation: approaches to optimizing image sensitivity, resolution, and accuracy," Neuroimage. 23 Suppl 1:S275-88, (2004).

Boden S, Obrig H, Köhncke C, Benav H, Koch SP, Steinbrink J. The oxygenation response to functional stimulation: is there a physiological meaning to the lag between parameters? Neuroimage. 2007 May 15;36(1):100-7.

Bollimunta A, Mo J, Schroeder CE, Ding M. Neuronal mechanisms and attentional modulation of corticothalamic α oscillations. J Neurosci. 2011 Mar 30;31(13):4935-43.

Butti M, Contini D, Molteni E, Caffini M, Spinelli L, Baselli G, Bianchi AM, Cerutti S, Cubeddu R, Torricelli A. Effect of prolonged stimulation on cerebral hemodynamic: a time-resolved fNIRS study. Med Phys. 2009 Sep;36(9):4103-14

Cohen JD., WM. Perlstein, TS. Braver, LE. Nystrom, DC. Noll, J. Jonides, and EE. Smith, "Temporal dynamics of brain activation during a working memory task," Nature. 386: 604–608, (1997).

Contini D., A. Torricelli, A. Pifferi, L. Spinelli, and R. Cubeddu, "Novel method for depth-resolved brain functional imaging by time-domain NIRS," in: Diffuse Optical Imaging of Tissue , Brian W. Pogue, Rinaldo Cubeddu, Editors , Proc. SPIE 2007;Vol. 6629, 662908, (2007).

Corbetta M., JM. Kincade, and GL. Shulman, "Neural systems for visual orienting and their relationships to spatial working memory," J. Cogn. Neurosci. 14, 508–523, (2002).

Curtis CE., "Prefrontal and parietal contributions to spatial working memory," Neuroscience 139:173–80, (2006).

Curtis CE., and M. D'Esposito, "Persistent activity in the prefrontal cortex during working memory," Trends Cogn. Sci. 7, 415–423, (2003).

Fallgatter AJ., and WK. Strik, "Frontal brain activation during the Wisconsin Card Sorting Test assessed with two-channel near-infrared spectroscopy," Eur Arch Psychiatry Clin Neurosci. 248(5):245-9, (1998).

Foffani G., Bianchi A.M., Cincotti F., Babiloni C., Carducci F., Babiloni F. et al, 2004. Indipendent component analysis compared to laplacian filtering as "Deblurring" techniques for event related synchronization/desynchronization, Methods Inf. Med.43(1):74-78.

Fox PT, Raichle ME. Focal physiological uncoupling of cerebral blood flow and oxidative metabolism during somatosensory stimulation in human subjects. Proc Natl Acad Sci U S A. 1986 Feb;83(4):1140-4.

Frahm J, Bruhn H, Merboldt KD, Hänicke W. Dynamic MR imaging of human brain oxygenation during rest and photic stimulation. J Magn Reson Imaging. 1992 Sep-Oct;2(5):501-5.

Franceschini, M.A., Fantini, S., Thompson, J.H., Culver, J.P., Boas, D.A., 2003. Hemodynamic evoked response of the sensorimotor cortex measured noninvasively with near-infrared optical imaging. Psychophysiology 40, 548–560.

Funahashi S., "Prefrontal cortex and working memory processes," Neuroscience. 139:251–61, (2006).

Göbel U, Klein B, Schröck H, Kuschinsky W. Lack of capillary recruitment in the brains of awake rats during hypercapnia. J Cereb Blood Flow Metab. 1989 Aug;9(4):491-9.

Highton D., C. Elwell, and M. Smith, "Noninvasive cerebral oximetry: is there light at the end of the tunnel?," Curr Opin Anaesthesiol. Oct;23(5):576-81, (2010).

Hillman EMC., "Optical brain imaging in vivo: techniques and applications from animal to man. Journal of Biomedical Optics," Vol. 12, No. 5, 051402, (2007).

Hock C., F. Müller-Spahn, S. Schuh-Hofer, M. Hofmann, U. Dirnagl, and A. Villringer, "Age dependency of changes in cerebral hemoglobin oxygenation during brain activation: a near-infrared spectroscopy study," J Cereb Blood Flow Metab. Nov;15(6):1103-8, (1995).

Hock C., K. Villringer, F. Müller-Spahn, R. Wenzel, H. Heekeren, S. Schuh-Hofer, M. Hofmann, S. Minoshima, M. Schwaiger, U. Dirnagl, and A. Villringer, "Decrease in parietal cerebral hemoglobin oxygenation during performance of a verbal fluency task in patients with Alzheimer's disease monitored by means of near-infrared spectroscopy (NIRS)--correlation with simultaneous rCBF-PET measurements," Brain Res. May 2;755(2):293-303, (1997).

Holper L, Biallas M, Wolf M. Task complexity relates to activation of cortical motor areas during uni- and bimanual performance: a functional NIRS study. Neuroimage. 2009 Jul 15;46(4):1105-13.

Holper L, Shalóm DE, Wolf M, Sigman M. Understanding inverse oxygenation responses during motor imagery: a functional near-infrared spectroscopy study. Eur J Neurosci. 2011 Jun;33(12):2318-28

Hopf JM., CN. Boehler, SJ. Luck, JK. Tsotsos, HJ. Heinze, and MA. Schoenfeld, "Direct neurophysiological evidence for spatial suppression surrounding the focus of attention in vision," Proc Natl Acad Sci U S A 2006;103:1053–1058, (2006).

Hoshi Y., "Functional near-infrared optical imaging: utility and limitations in human brain mapping. Psychophysiology," Jul;40(4):511-20, (2003).

Hoshi Y., and M. Tamura, "Near-infrared optical detection of sequential brain activation in the prefrontal cortex during mental tasks," Neuroimage. May;5(4 Pt 1):292-7, (1997).

Hoshi Y., N. Kobayashi, and M. Tamura, "Interpretation of near-infrared spectroscopy signals: a study with a newly developed perfused rat brain model," J Appl Physiol. May;90(5):1657-62, (2001).

Huppert TJ., RD. Hoge , SG. Diamond, MA. Franceschini, and DA. Boas, "A temporal comparison of BOLD, ASL, and NIRS hemodynamic responses to motor stimuli in adult humans," NeuroImage 29,368–382, (2006).

Ito H., H. Yamauchi, H. Kaneko, T. Yoshikawa, K. Nomura, and S. Honjo, "Prefrontal overactivation, autonomic arousal, and task performance under evaluative pressure: A near-infrared spectroscopy (NIRS) study," Psychophysiology. May 12, (2011).

Izzetoglu M, Bunce SC, Izzetoglu K, Onaral B, Pourrezaei K., 2007, Functional brain imaging using near-infrared technology., IEEE Eng Med Biol Mag. 2007 Jul-Aug;26(4):38-46.

Jaeggi SM., R. Seewer, AC. Nirkko, D. Eckstein, G. Schroth, R. Groner, and K. Gutbrod, "Does excessive memory load attenuate activation in the prefrontal cortex? Load-dependent processing in single and dual tasks: functional magnetic resonance imaging study," Neuroimage. Jun;19(2 Pt 1):210-25, (2003).

Jasper H.H., "The ten twenty electrode system of the International Federation. Electroencephal. Clin. Neurophys., vol. 10, pp. 371–375, 1958.

Jennings JR, van der Molen MW, Somsen RJ, Graham R, Gianaros PJ. Vagal function in health and disease: studies in Pittsburgh. Physiol Behav. 2002 Dec;77(4-5):693-8.

Jobsis FF., "Non invasive, infrared monitoring of cerebral and myocardial oxygen sufficiency and circulatory parameters," Science, Vol. 198 No. 4323, pp. 1264-1267, (1977).

Jolles, D.D., Grol, M.J., van Buchem, M.A., Rombouts, S.A., &Crone, E.A.Practice effects in the brain: changes in cerebral activation after working memory practice depend on task demands. NeuroImage, 52, 658–668. (2010).

Klingberg T., "Development of a superior frontal-intraparietal network for visuospatial working memory," Neuropsychologia. 44:2171–7, (2006).

Koch SP, Koendgen S, Bourayou R, Steinbrink J, Obrig H. Individual alpha-frequency correlates with amplitude of visual evoked potential and hemodynamic response. Neuroimage. 2008 Jun;41(2):233-42.

Kubo M, Shoshi C, Kitawaki T, Takemoto R, Kinugasa K, Yoshida H, Honda C, Okamoto M. Increase in prefrontal cortex blood flow during the computer version trail making test. Neuropsychobiology. 2008;58(3-4):200-10.

Kwong KK, Belliveau JW, Chesler DA, Goldberg IE, Weisskoff RM, Poncelet BP, Kennedy DN, Hoppel BE, Cohen MS, Turner R, et al. Dynamic magnetic resonance imaging of human brain activity during primary sensory stimulation. Proc Natl Acad Sci U S A. 1992 Jun 15;89(12):5675-9.

Lee J., BS. Folley, J. Gore, and S. Park, "Origins of spatial working memory deficits in schizophrenia: an event-related FMRI and near-infrared spectroscopy study," PLoS One. Mar 12;3(3):e1760, (2008).

Leistner S, Sander-Thoemmes T, Wabnitz H., Moeller M, Wachs M, Curio G, Macdonald R, Trahms L, Mackert BM. Non-invasive simultaneous recording of neuronal and vascular signals in subacute ischemic stroke. Biomed Tech (Berl). 2011 Apr;56(2):85-90. Epub 2011 Feb 7.

Liebert A, Wabnitz H, Steinbrink J, Obrig H, Möller M, Macdonald R, Villringer A, Rinneberg H. Time resolved multidistance near-infrared spectroscopy of the adult head: intracerebral and extracerebral absorption changes from moments of distribution of times of flight of photons. Appl Opt. 2004 May 20;43(15):3037-47.

Linden DEJ., RA. Bittner, L. Muckli, JA. Waltz, N. Kriegeskorte, R. Goebel, W. Singer, and MHJ Munk, "Cortical capacity constraints for visual working memory: dissociation of fMRI load effects in a fronto-parietal network," NeuroImage. 20, 1518–1530, (2003).

Makeig S., A. J. Bell, T. P. Jung, and T. J. Sejnowski, "Independent component analysis of electroencephalographic data", Adv. Neural Inf. Process. Syst., vol. 8, pp. 145–151, 1996.

Mayer JS., RA. Bittner, D. Nikolić, C. Bledowski, R. Goebel, and DE. Linden, "Common neural substrates for visual working memory and attention," Neuroimage. Jun;36(2):441-53, (2007).

McAfoose J., and BT. Baune, "Exploring visual-spatial working memory: a critical review of concepts and models," Neuropsychol Rev. Mar;19(1):130-42, (2009).

Mo J, Schroeder CE, Ding M. Attentional modulation of alpha oscillations in macaque inferotemporal cortex. J Neurosci. 2011 Jan 19;31(3):878-82.

Moody, M., Panerai,R.B., Eames, P.J., Potter, J.F., 2005. Cerebral and sistemi hemodynamic changes during cognitive and motor activation paradigms. Am. J. Physiol.: Regul., Integr. Comp. Physiol. 288, R1581–R1588.

Moosmann M, Ritter P, Steinbrink A, Thees S, Blankenburg F, Taskin B, Obrig H, Villringer A. Correlates of alpha rhythm in functional magnetic resonance imaging and near infrared spectroscopy. Neuroimage. 2003 Sep;20(1):145-58.

Munk MH., DEJ. Linden, L. Muckli, H. Lanfermann, FE. Zanella, W. Singer, and R. Goebel, "Distributed cortical systems in visual short-term memory revealed by event-related functional magnetic resonance imaging," Cereb. Cortex. 12, 866–876, (2002).

Nakahachi T., R. Ishii, M. Iwase, L. Canuet, H. Takahashi, R. Kurimoto, K. Ikezawa, M. Azechi, O. Kajimoto, and M. Takeda, "Frontal cortex activation associated with speeded processing of visuospatial working memory revealed by multichannel near-infrared spectroscopy during Advanced Trail Making Test performance," Behav Brain Res. Dec 20;215(1):21-7, (2010).

Nambu I, Osu R, Sato MA, Ando S, Kawato M, Naito E. Single-trial reconstruction of finger-pinch forces from human motor-cortical activation measured by near-infrared spectroscopy (NIRS). Neuroimage. 2009 Aug 15;47(2):628-37

Nyberg, L., Dahlin, E., Stigsdotter, N.A., &Backman, L.Neural correlates of variable working memory load across adult age and skill: dissociative patterns within the fronto-parietal network. Scandinavian Journal of Psychology, 50, 41–46. (2009).

Obrig H, Israel H, Kohl-Bareis M, Uludag K, Wenzel R, Müller B, Arnold G, Villringer A. Habituation of the visually evoked potential and its vascular response: implications for neurovascular coupling in the healthy adult. Neuroimage. 2002 Sep;17(1):1-18.

Obrig H., and A. Villringer, "Beyond the visible-imaging the human brain with light," Journal of Cerebral Blood Flow and Metabolism, Vol. 23, No. 1, pp. 1-18, (2003).

Obrig, H., Hirth, C., Junge-Hulsing, J.G., Doge, C., Wolf, T., Dirnagl, U., Villringer, A., 1996. Cerebral oxygenation changes in response to motor stimulation. J. Appl. Physiol. 81, 1174– 1183.

Obrig, H., Steinbrink, J., Villringer, A., 2003. The blushing brain: changes in brain colour indicate the functional state of the cerebral cortex. Med. Laser Appl. 18, 206–216.

Ogawa S, Tank DW, Menon R, Ellermann JM, Kim SG, Merkle H, Ugurbil K. Intrinsic signal changes accompanying sensory stimulation: functional brain mapping with magnetic resonance imaging. Proc Natl Acad Sci U S A. 1992 Jul 1;89(13):5951-5.

Pagani M, Mazzuero G, Ferrari A, Liberati D, Cerutti S, Vaitl D, Tavazzi L, Malliani A. Sympathovagal interaction during mental stress. A study using spectral analysis of heart rate variability in healthy control subjects and patients with a prior myocardial infarction. Circulation. 1991 Apr;83(4 Suppl):II43-51.

Pan J. and Tompkins W.J. 1985, A Real-Time QRS Detection Algorithm, IEEE Trans. on Biomed. Eng., BME-32(3):230-236

Pessoa L., and LG. Ungerleider, "Top–down mechanisms for working memory and attentional processes," In: Gazzaniga, M.S. (Ed.), The New Cognitive Neurosciences. MIT Press, Cambridge, pp. 919–930, (2004).

Petrides M., "Lateral prefrontal cortex: architectonic and functional organization," Phil Trans R Soc B. 360:781–95, (2005).

Postle BR., "Working memory as an emergent property of the mind and brain," Neuroscience 139, 23–38, (2006).

Pu S., T. Yamada, K. Yokoyama, H. Matsumura, H. Kobayashi, N. Sasaki, H. Mitani, A. Adachi, K. Kaneko, and K. Nakagome, "A multi-channel near-infrared spectroscopy study of prefrontal cortex activation during working memory task in major depressive disorder," Neurosci Res. Jan 14, (2011).

Quaresima V., "Bilateral prefrontal cortex oxygenation responses to a verbal fluency task: a multichannel time-resolved near-infrared topography study," Journal of Biomedical Optics. Vol. 10, No. 1, 011012, (2005).

Quaresima V., P. Giosuè, R. Roncone, M. Casacchia, and M. Ferrari, "Prefrontal cortex dysfunction during cognitive tests evidenced by functional near-infrared spectroscopy," Psychiatry Res. Mar 31;171(3):252-7, (2009).

Riera JJ, Sumiyoshi A. Brain oscillations: ideal scenery to understand the neurovascular coupling. Curr Opin Neurol. 2010 Aug;23(4):374-81.

Rissman J., A. Gazzaley, and M. D'Esposito, "Dynamic adjustments in prefrontal, hippocampal, and inferior temporal interactions with increasing visual working memory load," Cereb Cortex. Jul;18(7):1618-29, (2008).

Roy, C.S., and Sherrington, C.S. (1890). On the Regulation of the Blood-supply of the Brain. The Journal of physiology 11, 85-158 117.

Rypma, B., Berger, J.S., &D'Esposito, M.The influence of working-memory demand and subject performance on prefrontal cortical activity. Journal of Cognitive Neuroscience, 14, 721–731. (2002).

Sakatani K., Y. Xie, W. Lichty, S. Li, and H. Zuo, "Language-activated cerebral blood oxygenation and hemodynamic changes of the left prefrontal cortex in poststroke aphasic patients: a near-infrared spectroscopy study," Stroke. Jul;29(7):1299-304, (1998).

Sander T.H., Liebert A., Burghoff M.,Wabnitz H.,Macdonald R., Trahms L., 2007, Cross-correlation analysis of the correspondence between magnetoencephalographic and near-infrared cortical signals.Methods Inf Med, 46:164-168.

Sanefuji M., Y. Takada, N. Kimura, H. Torisu, R. Kira, Y. Ishizaki, and T. Hara, "Strategy in short-term memory for pictures in childhood: a near-infrared spectroscopy study," Neuroimage. Feb 1;54(3):2394-400, (2011).

Sarter M., Turchi J. 2002. Age and dementia –associated impairments in divided attention: psychological constructs. Animal models, and underlying neuronal mechanisms, Dementia and geriatric cognitive disorders, 13:46-58

Schecklmann M., M. Romanos, F. Bretscher, MM. Plichta, A. Warnke, and AJ. Fallgatter, "Prefrontal oxygenation during working memory in ADHD," J Psychiatr Res. Jul;44(10):621-8, (2010).

Schreppel T., J. Egetemeir, M. Schecklmann, MM. Plichta, P. Pauli, H. Ellgring, AJ. Fallgatter, and MJ. Herrmann, "Activation of the prefrontal cortex in working memory and interference resolution processes assessed with near-infrared spectroscopy," Neuropsychobiology. 57(4):188-93, (2008).

Selb J., "Improved sensitivity to cerebral hemodynamics during brain activation with a time-gated optical system: analytical model and experimental validation," Journal of Biomedical Optics, Vol. 10, No. 1, 11013, (2005).

Sheth, S.A., Nemoto, M., Guiou, M., Walker, M., Pouratian, N., and Toga, A.W. (2004). Linear and nonlinear relationships between neuronal activity, oxygen metabolism, and hemodynamic responses. Neuron 42, 347-355.

Shibasaki H. Human brain mapping: hemodynamic response and electrophysiology. Clin Neurophysiol. 2008 Apr;119(4):731-43.

Shibuya K, Sadamoto T, Sato K, Moriyama M, Iwadate M. Quantification of delayed oxygenation in ipsilateral primary motor cortex compared with contralateral side during a unimanual dominant-hand motor task using near-infrared spectroscopy. Brain Res. 2008 May 19;1210:142-7

Shibuya-Tayoshi S., S. Sumitani, K. Kikuchi, T. Tanaka, S. Tayoshi, and S. Ueno, "Activation of the prefrontal cortex during the Trail-Making Test detected with multichannel near-infrared spectroscopy," Psychiatry Clin Neurosci 61:616–21, (2007).

Somsen RJ, Jennings JR, Van der Molen MW. The cardiac cycle time effect revisited: temporal dynamics of the central-vagal modulation of heart rate in human reaction time tasks. Psychophysiology. 2004 Nov;41(6):941-53.

Steinbrink J., H. Wabnitz, H. Obrig, A. Villringer, and H. Rinneberg, "Determining changes in NIR absorption using a layered model of the human head," Phys. Med. Biol. 46, 879-896, (2001).

Steptoe A, Sawada Y. Assessment of baroreceptor reflex function during mental stress and relaxation. Psychophysiology. 1989 Mar;26(2):140-7.

Syré F, Obrig H, Steinbrink J, Kohl M, Wenzel R, Villringer A. Are VEP correlated fast optical signals detectable in the human adult by non-invasive nearinfrared spectroscopy (NIRS)? Adv Exp Med Biol. 2003;530:421-31.

Takahashi T, Takikawa Y, Kawagoe R, Shibuya S, Iwano T, Kitazawa S. Influence of skin blood flow on near-infrared spectroscopy signals measured on the forehead during a verbal fluency task. Neuroimage. 2011 Aug 1;57(3):991-1002.

Tanida M, Katsuyama M, Sakatani K. Relation between mental stress-induced prefrontal cortex activity and skin conditions: a near-infrared spectroscopy study. Brain Res. 2007 Dec 12;1184:210-6.

Tanida M., Sakatani K., Takano R., Tagai K.,2004, Relation between asymmetry of prefrontal cortex activities and the autonomic nervous system during a mental arithmetic task: nerainfrared spectroscopy study. Neuroscience Letters 36:69-74.

Telkemeyer S, Rossi S, Nierhaus T, Steinbrink J, Obrig H, Wartenburger I. Acoustic processing of temporally modulated sounds in infants: evidence from a combined near-infrared spectroscopy and EEG study. Front Psychol. 2011;1:62.

Thorn CE, Kyte H, Slaff DW, Shore AC. An association between vasomotion and oxygen extraction. Am J Physiol Heart Circ Physiol. 2011 Aug;301(2):H442-9.

Toichi M., and Y. Kamio, "Long-term memory in high-functioning autism: controversy on episodic memory in autism reconsidered," J Autism Dev Disord. Apr;33(2):151-61, (2003).

Tomasi D., T. Ernst, EC. Caparelli, and L. Chang, "Common deactivation patterns during working memory and visual attention tasks: an intra-subject fMRI study at 4 Tesla," Hum Brain Mapp. Aug;27(8):694-705, (2006).

Uludag, K., Dubowitz, D.J., Yoder, E.J., Restom, K., Liu, T.T., and Buxton, R.B. (2004). Coupling of cerebral blood flow and oxygen consumption during physiological activation and deactivation measured with fMRI. NeuroImage 23, 148-155.

Vandenberghe R, Duncan J, Dupont P, Ward R, Poline JB, Bormans G, Michiels J, Mortelmans L, Orban GA. Attention to one or two features in left or right visual field: a positron emission tomography study. J Neurosci. May 15;17(10):3739-50. (1997).

Villringer A, Planck J, Stodieck S, Bötzel K, Schleinkofer L, Dirnagl U. Noninvasive assessment of cerebral hemodynamics and tissue oxygenation during activation of brain cell function in human adults using near infrared spectroscopy. Adv Exp Med Biol. 1994;345:559-65.

Villringer A., and B. Chance, "Non-invasive optical spectroscopy and imaging of human brain function," Trends Neurosci. vol. 20, pp. 435-442, (1997).

Wallois F, Mahmoudzadeh M, Patil A, Grebe R. Usefulness of simultaneous EEG-NIRS recording in language studies. Brain Lang. 2011 May 3.

Wolf M., M. Ferrari, and V. Quaresima, "Progress of near-infrared spectroscopy and topography for brain and muscle clinical applications," J Biomed Opt. 12(6), 062104, (2007).

Wriessnegger SC, Kurzmann J, Neuper C. Spatio-temporal differences in brain oxygenation between movement execution and imagery: a multichannel near-infrared spectroscopy study. Int J Psychophysiol. 2008 Jan;67(1):54-63.

Ye JC, Tak S, Jang KE, Jung J, Jang J. NIRS-SPM: statistical parametric mapping for near-infrared spectroscopy. Neuroimage. 2009 Jan 15;44(2):428-47

*Zetterberg L.H. 1969, Estimation of parameters for a linear difference equation with application to EEG analysis, Mathematical Biosciences,5(3-4):**227-275***

Clinical Applications

The final aim of this PhD work is the exploitation of clinical employment of NIRS devices.

Specifically, in this section, two applications in the neurological field will be described and discussed.

Psychological features of neurologic patients often include avoidant personality, with associated obsessive compulsive traits, anxiety and depression. In clinical practice, this sometimes results in avoidant and passive attitudes toward health-care. Patients thus tend to minimize symptoms and to miss out periodical visits. As a consequence, reducing the invasiveness of cognitive assessment becomes of primary importance, as it potentially widens the accessibility of screenings to a larger number of reluctant patients and potentially increases the frequency of evaluative sessions.

As Functional Near InfraRed Spectroscopy (fNIRS) is a low-cost, portable and easy-to-use tool to non-invasively monitor changes in HbO, HHb and HbT concentrations in the human tissues, some work has been carried out during the PhD course in order to assess the feasibility of fNIRS cognitive investigations in Myotonic Dystrophy type 1 and Unverricht-Lundborg patients. The results we show encourage the employment of fNIRS as a complementary technique for the clinical evaluation of the functional cognitive activation of patients affected by Myotonic Dystrophy type 1, and encourage further research on cohorts affected by Unverricht-Lundborg epilepsy and other neurological and psychiatric diseases.

>>KeyPoints

> In the neurologic and psychiatric field, reducing the invasiveness of cognitive assessment becomes of primary importance, as it potentially widens the **accessibility** of screenings to a larger number of reluctant patients and potentially increases the frequency of evaluative sessions.

> continuous wave fNIRS could help in assessing the neurological outcome of patients affected by Myotonic Distrophy type 1 (DM1 or **Steinert syndrome**) and other neurologic diseases.

> time resolved fNIRS provided controversial results in a cohort of patients affected by progressive myotonic epilepsy type 1 (EPM1 or **Unverricht-Lundborg disease**).

>**General Linear Model** was applied in both the studies about DM1 and EPM1. The block design of the task was modelled by using some regressors, and the brain activations were extracted for single patients and groups (1st and 2nd level analyses)

> An "**EEG informed**" **version** of **General Linear Model** was created for EPM1 data. Cases about two patients are reported and discussed.

6.1 Myotonic Dystrophy type 1

6.1.1 Previous works

Myotonic dystrophy type 1 (DM1) is the most common form of adult muscular dystrophy, with a reported prevalence of 69 to 90 cases per million (Emery 1991). Three clinical pictures are distinguished, based on the age of onset and the predominant symptoms: a congenital, a juvenile and a classical or adult form (Meola and Sansone, 2007). In addition to neuromuscular symptoms, central nervous system (CNS) involvement in DM1 had been observed since the first descriptions of the disease.

Two distinct patterns of cognitive dysfunction can be singled out in DM1: in congenital form a global cognitive impairment is often reported, while patients with juvenile/adult onset frequently develop an aging-related decline of fronto-temporal cognitive function (Modono 2008; Meola et al., 2007; Harper, 2001). Importantly, the nexus between the severity of the muscular disease, the extent of intellectual impairment and the brain damage seems not to be plain, and correlation studies provide results hard to be disentangled (Caramia et al., 2010; Antonini et al., 2004; Malloy et al., 1990). For these reasons, the assessment of frontal cortex (dys)function in response to cognitive tasks appears to be crucial for the diagnostic process; and consequently, tools allowing a comfortable and thorough inspection of metabolic and perfusion integrity in frontal cortex are regarded with interest by neurologists.

Neuropsychological features in DM1 patients include difficulties on executive functions, visuospatial/constructive abilities, memory and even facial emotional recognition. The emerging neuropsychiatric patterns include avoidant personality, with associated obsessive compulsive, passive-aggressive and schizotypic trait; furthermore depression and anxiety are features most frequently associated with DM1. In addition, more that 50% of patients with classic DM1 are referred because of excessive daytime sleepiness. This sometimes results in serious impairments in occupational and social functioning, thus decreasing DM1 patients' quality of life. In clinical practice, patients tend to be either obsessive in their health-related care, continuously consulting their referring physician, or - more often- avoidant and passive in their attitudes toward health-care, thus tending to minimize symptoms and to miss out periodical visits. Clinical evaluation may thus require time and persuasion (Meola et al., 2007). As a consequence, reducing the invasiveness of cognitive assessment and prefrontal cortex (PFC) functional inspection becomes of primary importance, as it potentially widens the accessibility of screenings to a larger number of reluctant patients and potentially increases the frequency of evaluative sessions.

Over the last twenty years, neuroimaging studies have documented brain involvement specifically consisting of changes in cortical and subcortical structures, as well as hypoperfusion, hypometabolism, white matter lesions, ventricular dilatation, and global brain atrophy.

The analysis of regional gray matter (GM) loss with magnetic resonance (MRI) voxel based morphometry (VBM) technique revealed selective regional GM atrophy, prevailing in the parietal and frontal cortices, but also involving the temporal gyrus and occipital cortex (Antonini 2004), since the early stage of the disease (Akiguci 1999).

White matter (WM) alterations - similar to those seen in demyelinating disorders - have been detected by MRI (Ota et al., 2006; Giorgio et al., 2006; Chang et al., 1993; Huber et al., 1989) and were found to be correlated to psychomotor speed reduction (Weber et al., 2010), but not to GM loss (Antonini 2004). They are mainly observed in the frontal region

of the brain in adult DM1 forms, while they preferably install in the temporal region in congenital forms (Weber et al., 2010), but their role in the pathogenesis of the disease is not yet completely understood.

Decreases in cerebral glucose utilization and cerebral blood flow have also been observed during positron emission tomographic (PET) investigations (Meola et al., 1999; Chang et al., 1993; Fiorelli et al., 1992), with a prevalence of frontal and tempo-parietal regions (Weber et al., 2010; Romeo et al., 2010a; Romeo et al., 2010b). Functional neuroimaging with PET has demonstrated a common pattern of cerebral hypoperfusion, with rCBF reductions in the ventral and mesial aspects of the frontal lobes (orbitofrontal cortex) and in the temporal poles.

These studies have concurred to outline the two main neurological evidences of the disease: (1) patients manifest a marked cerebral hypoperfusion, chiefly occurring in the temporal and frontal neocortical regions (Chang et al., 1993), (2) DM1 disease is characterized by an impaired glucose penetration into many tissues, including the brain (Weber et al., 2010; Annane et al., 1998; Fiorelli et al., 1992).

To our knowledge, fNIRS has never been used in studies on DM1; nevertheless, its handiness, together with the possibility to provide direct assessment of the oxygen presence in the brain tissues, allow this technique to be the optimal candidate for the neurological screening and monitoring of loath or averse patients.

6.1.2 Our contribution

The goal of the present section is to report the assessment of NIRS applicability in the clinical environment, as an evaluation tool of DM1 patients' brain activation during the performance of controlled mental tasks. Specifically, our interest was focused on evaluating (1) the tolerability of NIRS device shown by DM1 patients and (2) NIRS sensibility in detecting alterations in cerebral blood perfusion in DM1 patients with respect to an healthy cohort. A continuous wave NIRS device was used in this study.

6.1.3 Clinical assessment

Fourteen subjects (2 males and 12 females) affected by genetically determined myotonic dystrophy type 1 participated in this study. The group included 3 congenital forms (all from maternal transmission), 2 juvenile forms and 9 adult onset form. The analysis of $(CTG)_n$ repeats was performed in leukocytes DNA after blood sampling, and patients were classified either E1 (n<500), E2 (500<n<1000) and E3 (n>1000). Disease duration, age at onset, educational level and neuromuscular status were recorded for all patients. Demographic, clinical and genetic data on all subjects are summarized in Table 6.1. The inclusion criteria were (1) molecular confirmation of the DM1 diagnosis (2) age between 16 and 70 years. The exclusion criteria were (1) a history of major psychiatric illness (according to DSM IV criteria), acquired brain injury or alcohol or drug abuse (2) motor impairment and coordination abilities insufficient to account for possible delay in neuropsychological tests administered. Functional muscle impairment in patients was quantified by the Muscular Impairment Rating Scale (MIRS; Matiheu et al 2001).

Seventeen healthy volunteers (8 males and 9 females), comparable for age and school attendance, participated in the experiment. They had a mean age of 27 years (SD 7 years). All subjects were right-handed and native Italian speakers. They all had normal vision and had no history of psychiatric disorders. None of them showed any neuropsychological illness; cognitive level and attentive capability were normal; none of them had any first-degree relatives with a psychiatric illness.

The study received the approval of the local Ethics Committee. Moreover, written informed consent was obtained from all volunteers (both healthy subjects and DM1 patients) after the examination and test procedure had been explained. The study was performed in accordance to all the statements contained in the Helsinki Declaration of 1975, as revised in 1983.

Pat code	age	sex	Inh	School years	CTG exp.	Form	Age atonset	Myot.phen.	MIRS
2	17	F		11	E3	C	1	2	3
8	14	F	1	8	E3	C	1	2	3
9	18	F	1	12	E3	C	1	2	2
4	19	F	1	11	E2	J	7	2	3
6	17	F	1	12	E2	J	8	2	2
1	45	F	1	6	E1	A	40	2	2
3	47	F	1	8	E2	A	30	2	2
5	42	F	2	13	E2	A	13	2	4
7	43	F		16	E1	A	34	2	2
10	60	F	1	6	E2	A	40	2	4
11	40	M		8	E2	A	20	2	3
12	36	M	2	11	E1	A	10	2	2
13	40	F	2	11	E2	A	25	2	3
14	35	F	2	13	E2	A	30	2	2
GLOBAL MEAN	33.8			10.4			18.1		2.6
GLOBAL SD	14.3			2.9			15.0		0.7

Tab.6.1: Demographic and clinical data. Columns from left to right report patients' code (Pat code), age, sex, mode of inheritance (Inh.: 1=maternal; 2=paternal), years of school attended, CTG expansion (CTG exp.: E1<500; 500<E2<1000; E3>1000), classification of pathology (A=adult, J=juvenile, C=congenital), age at the insurgence, classification of myotonic phenomenon (Myot. Phen.: 1=absent; 2=present) and Muscular Impairment Rating Scale (MIRS) (1= no sign; 2=minimal signs; 3= distal weakness; 4= proximal and distal weakness; 5= severe proximal weakness) evaluations.

Patient code	N er CPT	N er CON	VIQ	PIQ	FIQ	REY cop	REY mem	WMS Q.M.	CORSI
2	2	13	51	55	53				
8	11	20	84	71	75	−3.15	−2.41		−2.56
9	1	24	74	86	77				
MEAN	4.67	19.00	69.67	70.67	68.33	−3.15	−2.41	−	−2.56
SD	5.51	5.57	16.92	15.50	13.32	−	−	−	−
4	0	39	51	66	56	−7.34	−3.25	65	−1.94
6	5	21	91	84	85	−1.76	0.73		−0.5
MEAN	2.50	30.00	71.00	75.00	70.50	−4.55	−1.26	65.00	−1.22
SD	3.54	12.73	28.28	12.73	20.51	3.95	2.81	−	1.02
1	6	20	92	75	83				
3	1	1	78	81	77	−2.70	−2.34	74	0.75
5	1	4	111	131	121	0	−0.40	137	0.44
7	2	5	126	119	126	1.11	0.40	126	1.38
10	2	11	107	112	110				
11	1	15	89	70	79				
12	2	17	110	85	99	1.6	0.31	108	−1.36
13	3	3	103	87	95				
14	1	5	92	88	89				
MEAN	2.11	9.00	100.89	94.22	97.67	0.00	−0.51	111.25	0.30
SD	1.62	6.91	14.50	21.18	17.94	1.92	1.27	27.56	1.18
GLOBAL MEAN	2.71	14.14	89.93	86.43	87.50	−1.75	−0.99	102.00	−0.54
GLOBAL SD	2.89	10.44	21.63	21.10	21.41	3.07	1.63	31.58	1.47

Tab.6.2: Cognitive assessment results. Columns from left to right report patients' code, number of errors committed while performing the clinical CPT (N er CPT) and Conners' CPT (N er CON) tests, results of verbal IQ (VIQ), performance IQ (PIQ), full IQ (FIQ),Rey copy test performance (REY Q.I. cop), Rey memory test performance (REY Q.I. mem), Wechsler' Memory Scale score and Corsi test. Rey copy and memory performance and Corsi performance are listed in z-scores.

6.1.4 Neurocognitive assessment

Neurocognitive test were administered to patients by a psychologist, to evaluate mental function. The Wechsler Adult Intelligence Scale revised III (WAIS III) was administered to the adult DM1 patients and the Wechsler Intelligence Scale for children (WISC III) with the congenital form. Seven of them (1 congenital, 2 juvenile and 4 adults) had an additional cognitive assessment by Rey copy, Rey memory and Corsi tests, while five patients (1 juvenile and 4 adults) completed the Wechsler' Memory Scale scoring to specifically assess working memory.

All the DM1 patients and the healthy volunteers underwent a computerized Continuous Performance Test (CPT) and a Conners' Continuous Performance Test (Conners' CPT) (described in Chapter 2).

6.1.5 fNIRS data processing

The continuous wave fNIRS device used for this study was provided by Drexel University (Philadelphia, PA). The device allows for relative measures of blood oxygenation, with reference to a baseline value. It is comprised of a flexible probe that covers the forehead (Bozkurt et al., 2004). The sensors consists of 4 LED light sources and 10 photodetectors, giving 16 acquisition channels (Fig.6.1.a). NIRS sampling frequency was 1 Hz.

A generalized linear model (GLM) approach was applied for data analysis (Friston et al., 1995). Data processing was performed by means of NIRS-SPM v.3.1 software (Ye et al., 2009). An hemodynamic response function (HRF) low-pass filter was chosen. The wavelet-MDL detrending algorithm (4 coefficients) was applied, aiming at avoiding the removal of task-related oscillations. No correction for serial correlations was performed. A design matrix was used (Fig.6.1.b) containing three regressors modeling: (1) the activation blocks of the cognitive test, (2) rest periods interleaving the activation blocks and (3) the baseline recorded just before the beginning of the test. Contrast arrays were designed to investigate: (1) the relationship between the cognitive activation and rest, and (2) the relationship between the cognitive activation and the baseline. The interpolated t-statistic maps were obtained for each subject first (1st level analysis), and then for each of the two groups (2nd level analysis). GLM provides intrinsic statistical significance of the maps shown, and it allows the mapping of t-statistics with reference to a threshold, which we set at p-value = 0.05.

Statistical analysis

To highlight potential differences in behavioural performance between the healthy and the DM1 groups, we performed an Analysis of Variance (ANOVA) for group effect on committed errors. Pearson's linear correlation coefficient was computed between performance data (number of committed errors in either CPT or Conners' CPT) and scores obtained during the cognitive assessments (either IQ verbal, performance and full, REY QI copy, REY QI memory, WMS QM or Corsi QI).
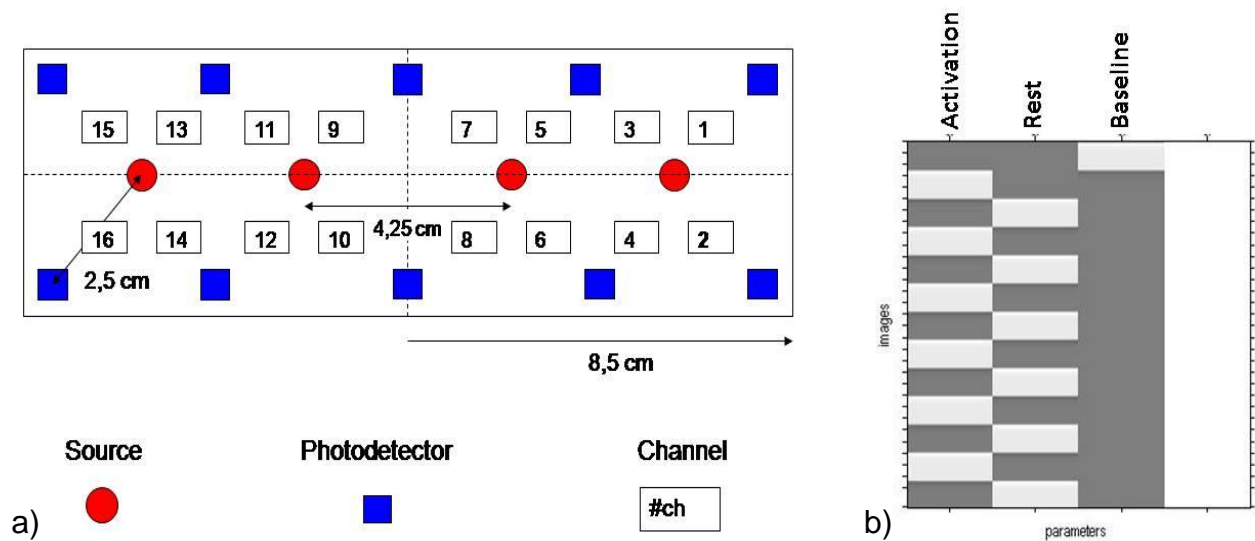
Fig.6.1: (a) Illustration of fNIR probe design: four sources emit light, which is then captured by 10 photodetectors, to give 16 channels; **(b)** design matrix: regressors modeling activation blocks, rest periods and initial baseline condition are shown. Time runs from top to bottom. The last column represents the default regressor.

6.1.6 Results

Neurocognitive evaluation

Table 6.2 illustrates some results obtained from the cognitive assessment of DM1 patients. IQ indexes were available for all the DM1 patients. Among the subjects with adult type DM1, IQs were globally within the normality range. Considering the subjects with juvenile form DM1, one (subj. 6) showed a borderline QI, while the other showed mental retardation (subj. 4). Last, none of the three congenital DM1 patients scored at least 75 in all the three evaluations, though only one of them (subj. 2) had a definitely poor performance.

A number of cognitive tests was administered, specifically aiming at evaluating memory performance in the DM1 cohort. Albeit we could administer the whole test battery to seven DM1 patients only, all the available results (listed in table 6.2) clearly hint worse memory performance in the congenital and juvenile forms with respect to the adult form.

With regard to behavioural results, on average the fourteen DM1 patents committed an average of 2.71 errors (SD=2.89) in the CPT task, and answered correctly to the target in 414.75 ms (SD=72.36 ms). During the Conners' test, the same subjects committed an average of 14.14 errors (SD=10.44), and answered correctly to the target in 384.30 ms (SD=92.32 ms) (Tab. 6.2).

The eighteen healthy subjects committed 1.67 errors (SD=1.12) in the CPT task, and answered correctly to the target in 383.48 ms (SD=68.45 ms). During the Conners' test, the same subjects committed an average of 5.78 errors (SD=3.27), and answered correctly to the target in 346.57 ms (SD=73.31 ms). ANOVA confirmed that DM1 patients performed worse than healthy group in both CPT (p-value=0.0378) and Conners' CPT (p-value=0.0043) tests.

Although performance in CPT test provided no significant correlation with the cognitive battery for DM1 patients, Conners' behavioural results (committed errors in Conners' test) provided significant negative correlations with three cognitive tests: Corsi QI (rho = -0.7936, p = 0.0331), IQ verbal (rho = -0.5598, p = 0.0374) and IQ full (rho = -0.5711, p = 0.0329). Moreover, IQ performance provided a similar correlation trend (rho = -0.5055, p = 0.0652) with Conners' errors, very close to significance.

fNIRS results

The analysis of fNIRS measures was performed after obtaining variations of HbO and HHb through the Modified Beer-Lambert Law. Figure 6.2 reports HbO and HHb tracks recorded for the healthy group during the CPT test. It shows the mean time course of HbO and HHb of channels placed over the left and right hemispheres (see Fig.6.1a for their identification). Variations of HbO remained positive in the PFC, over both the hemispheres and during all the test. The two hemispheres show a very similar course. Variations of HbO values repeatedly reached peaks of about 5 µM.

HHb initially stayed in a range of negative values, then turning into slightly positive only around the third activation block. Overall, HHb values swerved from constancy only slightly throughout the test.

DM1 patients' tracks obtained during the same CPT test show some major peculiarities (Fig.6.3). First, left channels globally recorded higher variations of HbO (significance of this difference could not be ascertained). HHb decreased in value only for few seconds at the beginning of the test, then moving towards positive variations, which exceeded 1 µM.

Figure 6.4 reports HbO and HHb tracks recorded for the healthy group during the performance of the Conners' test. The image displays a slight decrease of the HbO values, which suddenly turns in a large and enduring increase. HbO values reach the first peak of about 2 µM at 200 s from the beginning of the test (at the end of the first activation block). Variations in the same amplitude range are observed afterwards: around 400, 600, 800 and 1000 s. In a comparison between figure 6.2 and figure 6.4, a striking difference is seen in the values of HbO variations: the images clearly show that the Conners' test gives rise to smaller changes of HbO values, if compared to CPT task. HHb variations remain negative throughout the test, yet holding a tiny modulus. The right hemisphere globally shows slightly higher variations of HbO with respect to the left one (not significant). The same evidence is seen for HHb changes, which reach more negative values in the right hemisphere.

Figure 6.5 displays HbO and HHb variations obtained from DM1 patients during the Conners' test. HbO values are comparable with those reported for the healthy group. Nevertheless, a long-term transient of activation seems to be superimposed to local peaks of HbO variations. Predominance of activation is not observed here for the right hemisphere. HHb changes remain tiny in modulus and confined to the negative domain.

After HbO and HHb time courses were plotted, GLM statistics were applied to the data, in order to identify frontal cortical areas which showed statistically significant signal changes in response to the task stimulation.

Contrasting HbO, HHb and HbT values obtained during the activation blocks against those of the initial baseline, the healthy subjects showed a significant (p-val. < 0.05) increase in HbO over both the left and right PFC during the execution of the CPT test (Fig.6.6a), whereas the commitment in the Conners' task rose activation over the right PFC only (Fig.6.6b). A focused medial HHb increase was significant (p-val. < 0.05) during the CPT (Fig.6.6c), which appeared much more powerful and widespread over the whole rostral PFC area during the Conners' task (Fig.6.6d). HbT resulted significantly increased only during the CPT test (p-val. < 0.05), over the left hemisphere (not shown). No significant HbT increase was found for the healthy subjects during the Conners' test.
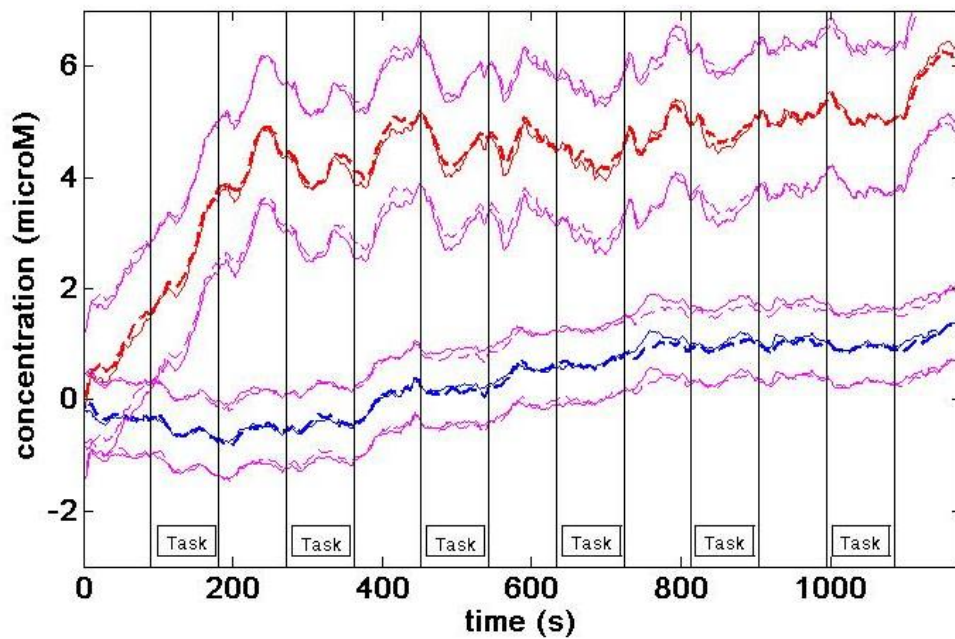
Fig.6.2: This image was obtained from the healthy group, while performing the CPT task. It shows the grand average of the mean time course (with standard deviation) of HbO (redlines) and HHb (blue lines) of channels placed over the left (dashed line) and right (solid line) hemispheres. HbO increases during the first part of the test, and then turns into a persisting hyper-oxygenation. Some modulation induced by task blocks can be observed.
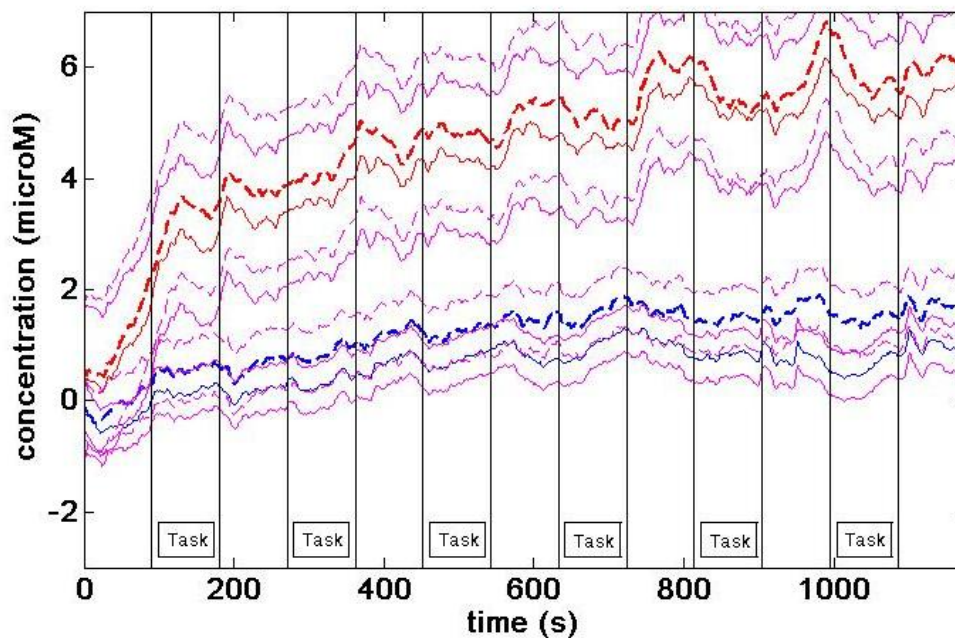

Fig.6.3: This image was obtained from the DM1 patients group, while performing the CPT task. It shows the grand average of the mean time course (with standard deviation) of HbO (red lines) and HHb (blue lines) of channels placed over the left (dashed line) and right (solid line) hemispheres.
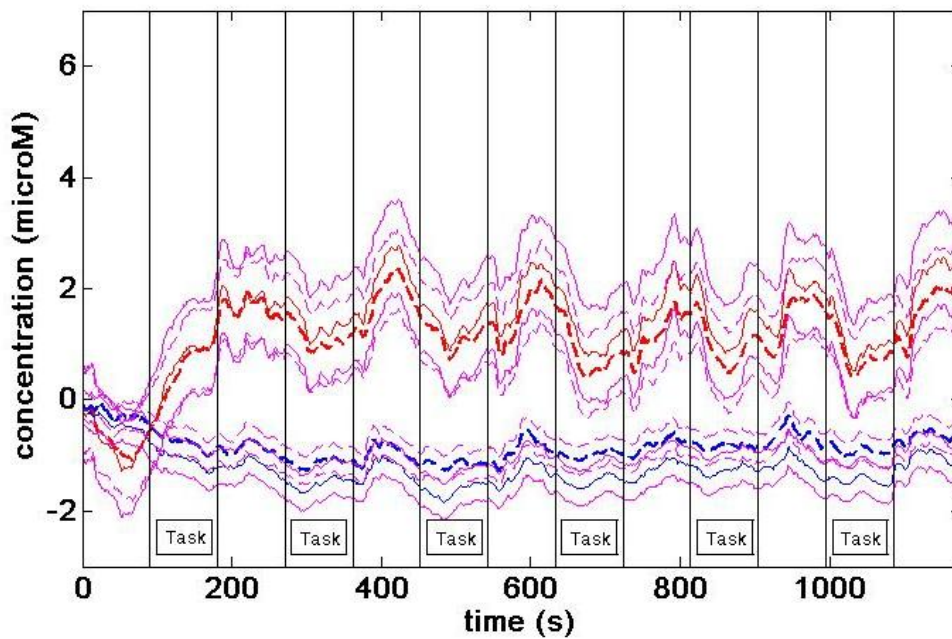
111

Fig.6.4: This image was obtained from the healthy group, while performing the Conners' test. It shows the grand average of the mean time course (with standard deviation) of HbO (red lines) and HHb (blue lines) of channels placed over the left (dashed line) and right (solid line) hemispheres. Hyper-oxygenation is induced, even though it is smaller than the one observed in CPT test (see fig. 6.2 for a comparison).
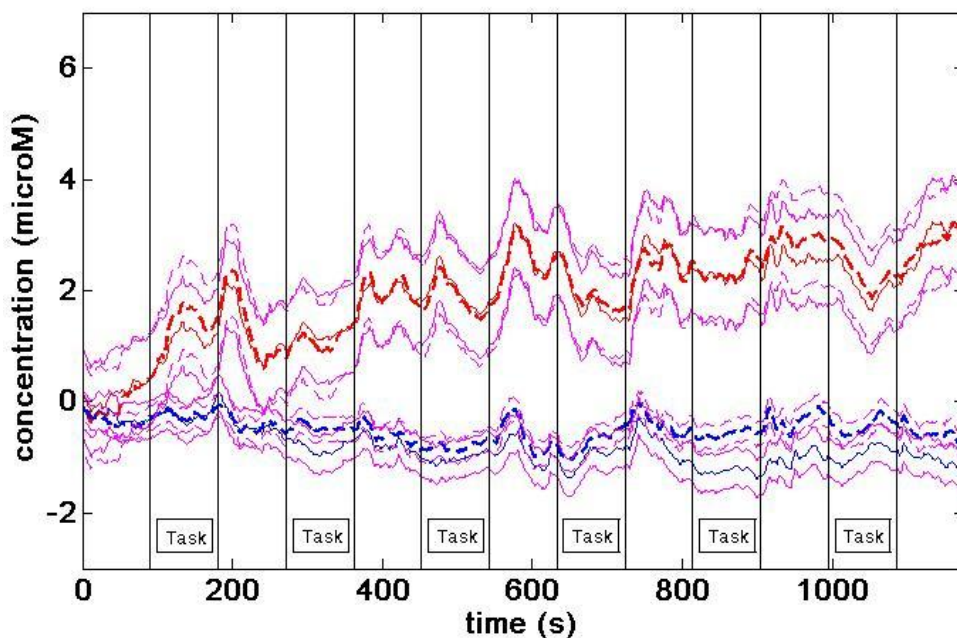

Fig.6.5: This image was obtained from the DM1 patients group, while performing the Conners' test. It shows the grand average of the mean time course (with standard deviation) of HbO (red lines) and HHb (blue lines) of channels placed over the left (dashed line) and right (solid line) hemispheres.

DM1 patients, instead, showed a significant (p-val. < 0.05) increase in HbO all over the PFC probed by the NIRS device during the execution of the CPT test (Fig.6.7a), with a right statistical maximum. Analogously, during the Conners' test, almost the whole

investigated area was activated (Fig.6.7b). Changes in HHb had no significance (p-val. > 0.05) in the CPT test, and a minimally spread right significance (p-val. < 0.05) during the Conners' test (not shown). An important, widespread HbT increase was found bilaterally (p-val. < 0.05) during the CPT test (Fig.6.8a) and the Conners' task as well (Fig.6.8b).
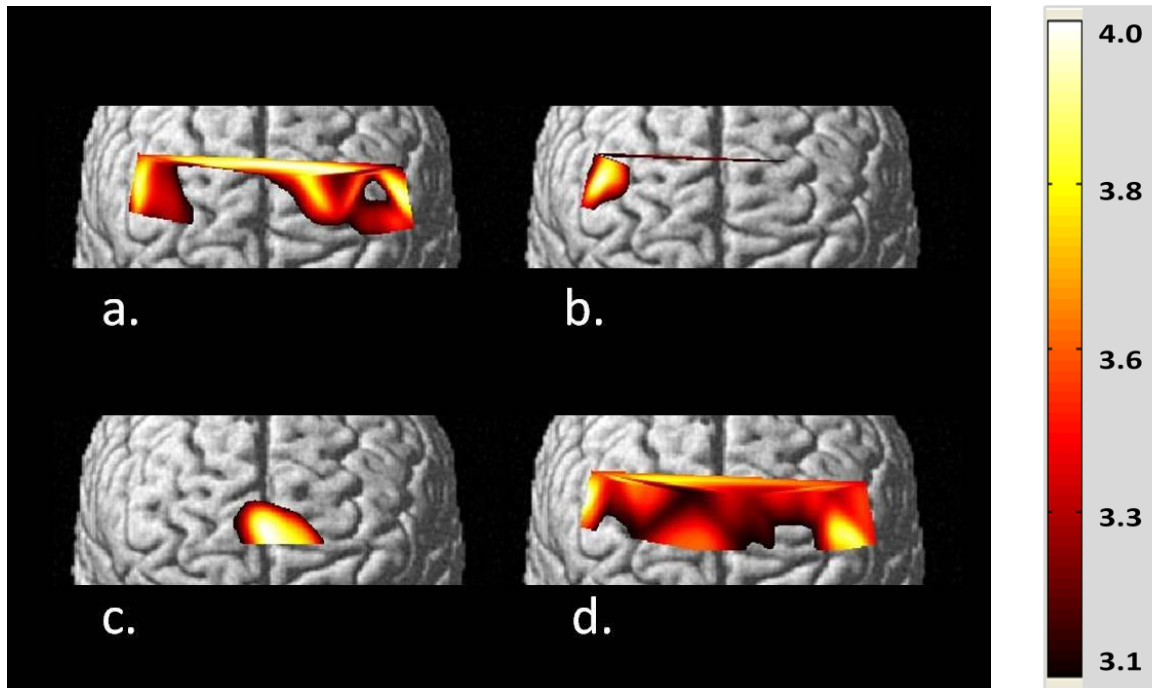

Fig.6.6: The image shows brain activation resulting from 2nd level analysis of the healthy group. Contrast was set between the activation blocks and the initial baseline. Significance was set at p-val<0.05. (a) HbO contrast during the CPT test, (b) HbO contrast during the Conners' test, (c) HHb contrast during the CPT test, (b) HHb contrast during the Conners' test.

Fig.6.7: The image shows brain activation resulting from 2nd level analysis of the DM1 patients group. Contrast was set between the activation blocks and the initial baseline. Significance was set at p-val<0.05. (a) HbO contrast during the CPT test, (b) HbO contrast during the Conners' test.

First level GLM analysis (i.e. single subject analysis) highlighted that patients affected by adult DM1 form had an activation pattern topographically comparable: six subjects out of nine displayed prominent right HbO activation, and five out of nine provided evidence of a clear bi-hemispheric pattern for HHb during CPT execution. Moreover, during Conners' test, the same patients provided a left or bilateral activation for both HbO and HHb in all but one subjects. The two patients affected by juvenile DM1 provided extremely high and broad frontal activation patterns for HbO, HHb and HbT in both tests, apparently diverging from the very poor cognitive performance. Congenital subjects provided strong activations for both tests in one case, and very low activation values in the two other subjects.
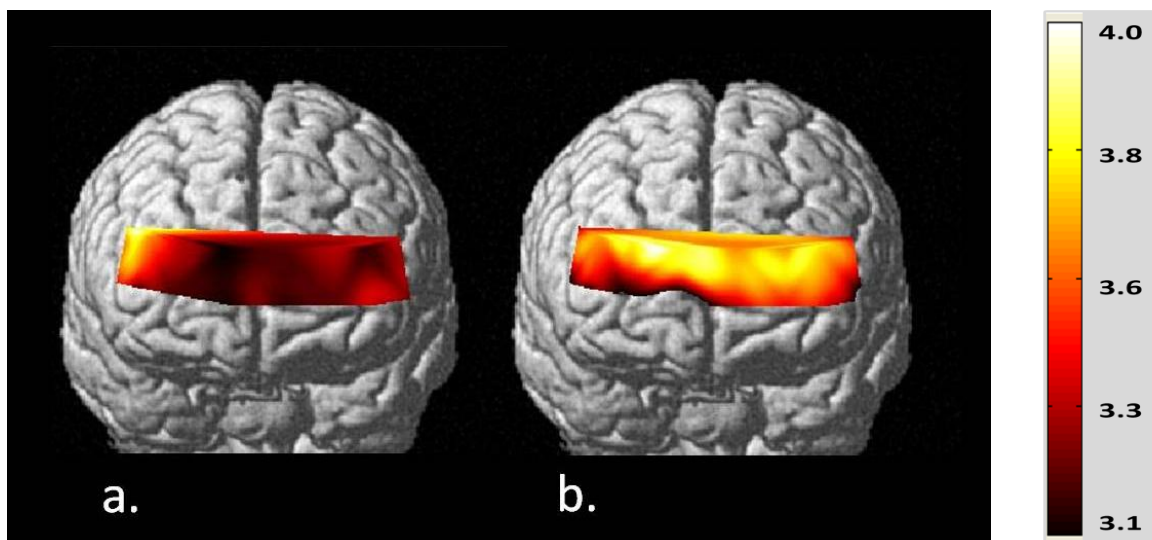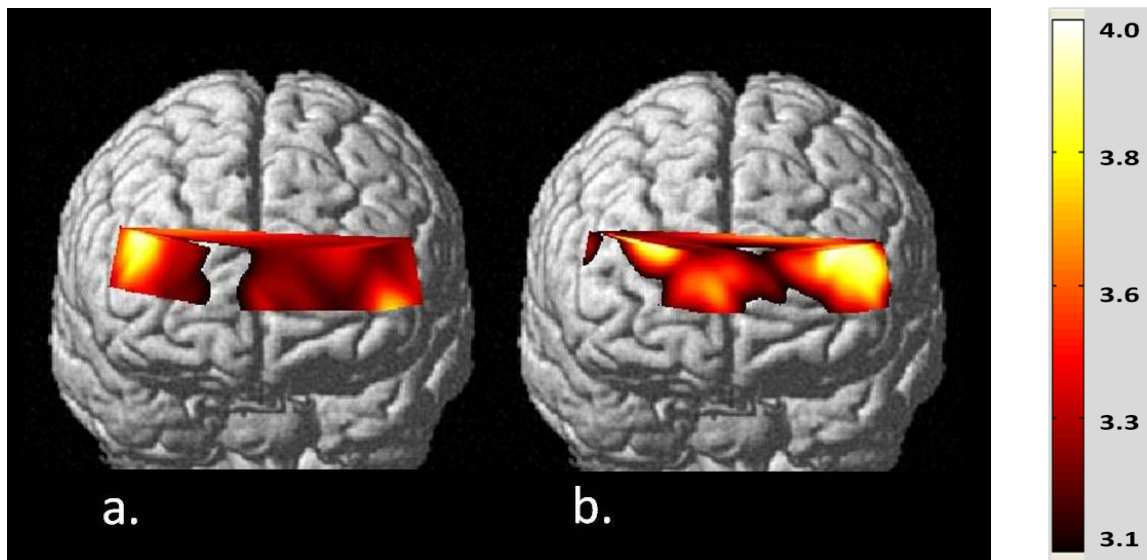

Fig.6.8: The image shows brain activation resulting from 2ⁿᵈ level analysis of the DM1 patients group. Contrast was set between the activation blocks and the initial baseline. Significance was set at p-val<0.05. (a) HbT contrast during the CPT test, (b) HbT contrast during the Conners' test.

6.1.7 Interpretation

In the present PhD work, a group of DM1 patients underwent a pure-attentive and an inhibitory computerized tasks. fNIRS data were acquired and processed by means of General Linear Model for the extraction of cortical activation patterns in the frontal area of the brain. The cohort was compared with a group of healthy subjects, who attended the same two tasks.

Overall, a clearly deficitary cognitive profile was encountered in several patients, especially among those affected by congenital and juvenile DM1 forms. Nevertheless, three subjects with adult type DM1 provided very good scoring through the entire cognitive assessment. These evidences are in agreement with previous findings and literature reviews (Meola et al., 2007).

Both recent imaging investigations on healthy subjects and lesional studies have demonstrated that a wide frontoparietal area is involved in sustained attention. The network primarily includes Brodmann's areas 9 and 11 and parietal cortical regions, mainly in the right hemisphere. Specifically, the activation comprises the right anterior cingulate, which is regarded as being the structure most closely involved in target identification and in attentive control coordination (Ogg et al., 2008; Sturm, 1999), the right dorsolateral prefrontal cortex (PFC) and the right inferior parietal lobulus. NIRS technique has provided an additional insight regarding how the PFC is activated in terms of hemodynamic

114

changes (Butti et al., 2009; Toichi et al., 2004; Fallgatter and Strik, 1997). Interestingly, tasks of attention, unlike those of higher cognitive processing, generally require significant subjective effort despite their relative simplicity and minimal response output. The hypothesis that the oxygen utilization of blood (i.e. the oxygen consumption relative to blood supply) during tasks of attention may be higher than that during inhibitory tasks seems to be confirmed in the present study (Fig. 6.2 to 6.5).

In most of the healthy subjects who participated in our study, HbO increased with a concurrent decrease in HHb during the activation of the PFC due to the Conners' task, while both HbO and HHb simultaneously increased during the activation due to the CPT test in both the hemispheres (Fig. 6.2 to 6.5). Interestingly, previous studies that examined the activation of the PFC due to typical tasks of attention reported an increase of both HbO and HHb in the PFC (Toichi et al., 2004; Fallgatter & Strik, 1997) as well. Moreover, the increase in HHb suggests increased oxygen consumption of the PFC during tasks of attention, which might be related to the disproportionately great subjective effort associated with sustained attention (Obrig et al., 2000). Toichi et al. (2004) found an increase in HbT during the CPT test, which was larger in the right than left hemisphere. He found a right hemisphere dominance in the activation of the PFC during the CPT. Besides, in some subjects, the decrease in HHb cancelled the increase in HbO, with no significant changes in HbT during the Conners' task. Our study confirms these previous findings, as some trend of HbT increase was found in healthy people during this task, but no significance was gained.

Since the late '80s, investigators have stressed the importance of right-hemisphere involvement in the pathogenesis of cognitive disturbances in MD patients (Malloy et al., 1990; Bird et al., 1983; Portwood et al., 1986), although no specific pathologic abnormalities in the right hemisphere had been detected. These right-hemisphere deficits were found to be strongly correlated with the decreased cerebral perfusion observed in the right temporal and right frontoparietal regions (Chang et al., 1993). More recently, it has been pointed out that the alterations in CBF observed in the frontal lobes may contribute in part to producing the attentive deficit seen in patients with DM1 (Weber et al., 2010; Meola et al., 1999; 2003).
In the healthy group, we have found a clear right predominance in activation during the Conners' task, while a bilateral increase of HbO was found for the CPT test (Fig.6.6). Conversely, DM1 patients showed statistical maxima in the right hemispheres for both the tasks, and a much more powerful and widespread activated area (Fig. 6.7). This fact could somehow indicate that DM1 subjects need some additional effort of the right hemispheres in order to perform cognitive tasks. Our hypothesis is that, as the cognitive effort physiologically hastens oxygen consumption, the difficulties in oxygen absorption due to DM1 pathology result in a stronger oxygen demand. The increase in HbT Fig. 6.8), mirroring the augmented cerebral blood flow (rCBF), could then represent the attempt at supplying more oxygen to the PFC, which nevertheless is not counterbalanced by the proper oxygen absorption and consumption, but rather causes oxygen accumulation. On the other hand, SPECT studies have previously highlighted brain hypoperfusion (Romeo et al., 2010; Chang et al., 1993) in DM1, pointing out a maximally severe reduction in rCBF in the right frontal and temporo-parietal association cortex. Thus, our results of increased HbT are not in complete agreement with those previously reported, as they suggest oxygen hypoabsorption rather than blood hypoperfusion.

PET has also revealed that carrier-mediated cerebral glucose transportation across the blood brain barrier is impaired in DM1. A reduction of 20% in cerebral metabolic rate of

glucose consumption (CMRGlu) was quantified in the same regions, and the existence of a link between the local reduction of metabolism and the cognitive symptoms was assessed (Meola et al., 1999). Last, it was shown that impaired glucose penetration takes place in a triplet repeats–dependent way (Romeo et al., 2010; Annane et al., 1998; Fiorelliet al., 1992). Interestingly, the involvement of frontal cortical areas in DM1 is in agreement with biomulecular, neuropsychological and functional data (Jiang et al., 2004). Recent results, though, put forward that an abnormal cortical glucidic uptake is mainly present in the left frontal lobe (Romeo et al., 2010).

Overall, the data presented here point out some modification of cerebral activation patterns in DM1 patients with respect to the healthy population. Nevertheless, some analogies can still be traced between adult DM1 pattern and healthy outline. Such analogies, though, are completely lost for juvenile and congenital DM1: in these last patients an extreme variability of patterns is highlighted, in any case profoundly divergent from physiology. Noticeably, severe hypo-oxygenation was detected for subj. 8 and 9, affected by congenital DM1; oppositely, subj. 2, affected by congenital DM1, and subj. 4 and 6, affected by juvenile DM1, provided an hyper-oxygenation pattern, probably indicating some compensatory effort to maintain function despite damage to cerebral circuits or to brain metabolism. Similar findings have been recently reported by Caramia et al. (2010) group during a motor study (fingertapping) in a cohort of 15 DM1 patients. Patients demonstrated greater activation than healthy people in several motor areas of the ipsilateral hemisphere of movement. The increased cortical and subcortical activation they observed in DM1 patients was deemed to be a consequence of the reorganization and redistribution that takes place in brain circuitry in response to brain tissue damage.

Last, it should be pointed out that none of the patients we have included in our analysis have impaired motor and coordination abilities sufficient to account for the results observed on the testing. Moreover, results crediting prefrontal activation cannot reasonably be ascribed to impaired motor abilities.

To our knowledge, this was the first study attempting to record fNIRS measurements from a cohort of DM1 subjects. In the present section, we discussed DM1 results obtained after group-level analyses, with respect to normality. Though, given the many-sided clinical manifestations of DM1, and the existence of three different forms, the reader should be aware that single-subject DM1 results showed a very high intra-subject variability, with some cases diverging consistently from the group-level results shown in figures 7 and 8. Moreover, we have already pointed out that at present fNIRS can provide limited spatial resolution, comparable to that one provided by electroencephalographic techniques, and can only probe cortical layers of the brain, being unable to reach the deeper structures. Despite these limitations, the progress of NIRS imaging technology and the increase of hardware reliability will for sure open the possibility of routinary single-subject fNIRS assessments in the future, providing beneficial spillover effect even in DM1. Last, the development of functional scales for the quantitative evaluation of perfusion and oxygenation patterns from fNIRS images will allow the study of correlations possibly existing between fNIRS information and neuropsychological assessment scores (i.e. between cortical oxygenation or perfusion and cognitive tests).

6.1.8 Outcome

Cognitive impairment is common in DM and is often among the major disabling components of the disease. The timely assessment of cognitive deficits is thus of primary importance in clinics. CNS tissue damage in DM1 patients may not be visible at conventional MR technique. On the other hand, functional neuroimaging techniques such

as PET/SPECT imaging and fMRI can provide valuable information regarding brain compromission (Sansone et al., 2007; Meola et al., 2003; Meola et al., 1999), at the cost of some uneasiness and patient's discomfort. The study described above supports the belief that fNIRS could help in assessing the neurological outcome of DM1 subjects in clinics, allowing a comfortable, uninvasive and relatively cheap assessment of some neurofunctional correlates of myotonic dystrophy.

6.2 Unverricht-Lundborg disease

6.2.1 Previous works

First described by Unverricht in 1891 (Unverricht, 1891) and by Lundborg in 1903 (Lundborg, 1903), Unverricht-Lundborg disease (ULD), or progressive myoclonic epilepsy type 1 (EPM1, OMIM254800) is an autosomal recessively inherited disorder, which is the most common cause for progressive myoclonus epilepsy. It is characterized by age of onset from 6 to 16 years, stimulus-sensitive myoclonus, and tonic–clonic epileptic seizures. In over half of the affected individuals the first symptoms are involuntary mioclonic jerks (Norio and Koskiniemi, 1979). The myoclonic jerks are action-activated and stimulus sensitive, and may be provoked by light, physical exertion, noise, and stress. They occur predominantly in the proximal muscles of the extremities and are asynchronous; they may be focal or multifocal and may generalize to a series of myoclonic seizures or even status myoclonicus (continuous myoclonic jerks involving a semiloss of consciousness). Some years after the onset, ataxia, incoordination, intentional tremor, and dysarthria develop. Individuals with EPM1 are mentally alert but show emotional lability, depression, and mild decline in intellectual performance over time. The diagnosis of EPM1 can be confirmed by identifying disease-causing mutations in a cysteine protease inhibitor cystatin B (*CSTB*) gene. Symptomatic pharmacologic and rehabilitative management, including psychosocial support, are the mainstay of EPM1 patients' care. EPM1 patients need lifelong clinical follow-up, including evaluation of the drug-treatment and comprehensive rehabilitation. So far, no obvious correlation has been found between the length of the expanded dodecamer repeat and the age of onset or disease severity.

The first application of Near-Infrared Spectroscopy to epilepsy dates back to 1996, when Steinhoff et al. (1996) published a pilot study on temporal lobe epilepsy. The aim was the investigation of the hemodynamic correlates of ictal activity in the epileptic brain, by means of NIRS. After that, however, three years more were needed in order to see other works published in the field: finally, between 1999 and 2000, Adelson et al. (1999) proposed NIRS as a tool for monitoring epileptic patients, Sokol et al. (2000) concentrated on the distinction of seizure types by using NIRS, and Watanabe et al. (2000) applied multichannel NIRS for the study of hemodynamic modifications over time, while the seizure is ongoing. Two years later, this latter also dealt with the localization of epileptic foci by using NIRS (Watanabe et al., 2002). Buchheim et al. (2004) then faced the observation of brain hemodynamics during absence seizures. Last, pediatric applications of adapted NIRS devices to epileptic children dealt with the measurement of hemodynamics during ictal activity (Haginoya et al., 2002; Arca Diaz et al., 2006) and spike-and-wave discharges (Roche-Labarbe et al., 2008; Wallois et al., 2009). Since 2010, a few studies synchronously applying NIRS and electroencephalography to the epileptic brain have been completing the picture (Nguyen et al., 2011; Lareau et al., 2011; Machado et al., 2011; Wallois et al., 2010).

6.2.2 Our contribution

The goal of this section is to present some data obtained by simultaneously applying electroencephalography and time resolved NIRS technology to the assessment of EPM1 brain hemodynamics during the performance of a handgrip motor task (see Chapter 2 for a detailed description of the protocol). Specifically, our interest was focused on evaluating (1) the tolerability of NIRS device shown by EPM1 patients, (2) the capability of time domain NIRS technology to successfully detect alterations in cerebral blood perfusion in EPM1 patients and (3) the possibility to extract "EEG informed" NIRS activations in the cortex. A time resolved NIRS device was used in this study, together with a MICROMED electroencephalographer. Eight patients underwent the protocol. Results obtained from two patients will be presented below, as single case studies.

6.2.3 Recruitment and fNIRS data processing

Eight subjects (6 males and 2 females) affected by genetically determined progressive myoclonic epilepsy type 1 participated in this study. Disease duration, age at onset, educational level and neuromuscular status were recorded for all patients. The exclusion criteria were (1) a history of major psychiatric illness (according to DSM IV criteria), acquired brain injury or alcohol or drug abuse (2) motor impairment and coordination abilities insufficient to account for possible delay in neuropsychological tests administered. Thirteen healthy volunteers (10 males and 3 females), comparable for age and school attendance, participated in the experiment. They all had no history of psychiatric disorders. None of them showed any neuropsychological illness; cognitive level and attentive capability were normal; none of them had any first-degree relatives with a psychiatric illness. The study received the approval of the Ethics Committee of Istituto Neurologico Besta.

The time resolved fNIRS prototype used for this study was provided by the Dipartimento di Fisica (Politecnico di Milano, Italy) (see Chapter 3 for a detailed description); tr-NIRS sampling frequency was 1 Hz. A MICROMED elecroencephalographer was also used for standard 10/20 EEG recording.

Generalized linear model (GLM) approach was applied for data analysis (Friston et al., 1995). Data processing was performed by means of NIRS-SPM v.3.1 software (Ye et al., 2009). An hemodynamic response function (HRF) low-pass filter was chosen. The wavelet-MDL detrending algorithm (4 coefficients) was applied, aiming at avoiding the removal of task-related oscillations. No correction for serial correlations was performed. The design matrix n°1 (DM1) was used (Fig.6.9.left) containing three regressors modeling: (1) the baseline recorded just before the beginning of the test, (2) the activation blocks of the motor test and (3) the rest periods interleaving the activation blocks. Contrast arrays were designed to investigate: (1) the relationship between the motor activation and rest, and (2) the relationship between the motor activation and the baseline. The interpolated t-statistic maps were obtained for each subject first (1st level analysis), and then for the patients' group (2nd level analysis – results not shown).

The design matrix n°2 (DM2) was then used (Fig.6.9.right) containing the same three regressors described above, and some additional regressors modelling five electroencephalographic frequency bands (delta, theta, alpha, beta and gamma rhythms). Contrast arrays were designed to investigate the relationship between the motor activation and the single brain rhythms. The interpolated t-statistic maps were obtained for each subject first (1st level analysis), and then for the patients' group (2nd level analysis – results not shown). GLM provides intrinsic statistical significance of the maps shown, and it allows the mapping of t-statistics with reference to a threshold, which we set at p-value = 0.05.
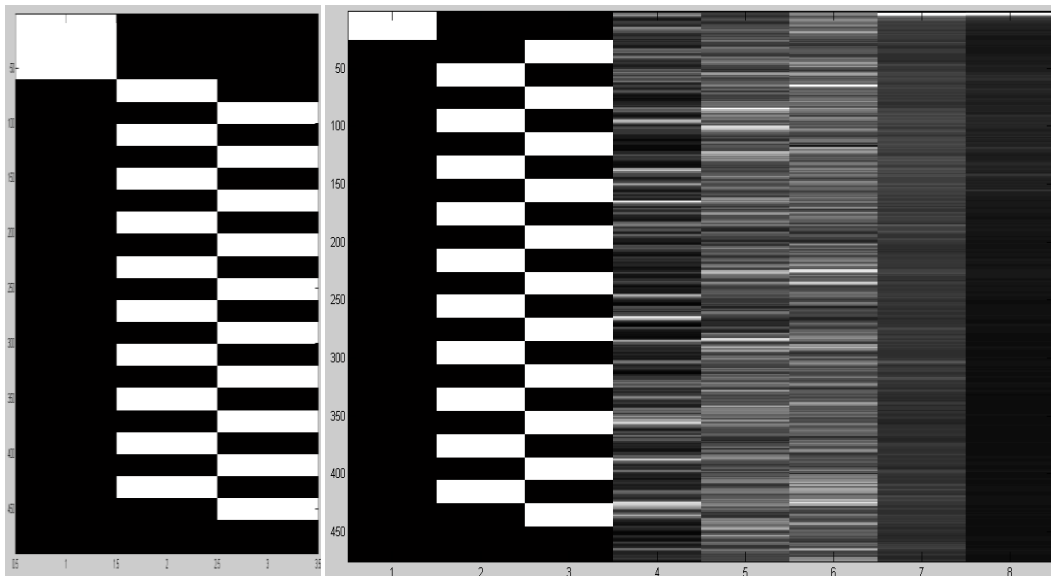
Fig.6.9: (left) design matrix 1 (DM1), with regressors modeling, from left to right, the baseline period, activation blocks and rest periods. Time runs from top to bottom. (right) design matrix 2 (DM2), with regressors modeling, from left to right, the baseline period, activation blocks, rest periods, and five electroencephalographic rhythms (delta, theta, alpha, beta and gamma bands). Time runs from top to bottom.

6.2.4 Case study 1

Processing of time resolved NIRS data by means of DM1 evidenced bilateral HbO activation while performing both right and left handgrip tasks. On the other hand, no HHb activations were evidenced for the same tasks. These results could not be confirmed by fMRI evidences, nor by electroencephalography. For the EPM1 subjects a physiological activation, contralateral to the moving hand, was indeed expected, at least for HbO (Fig6.10).
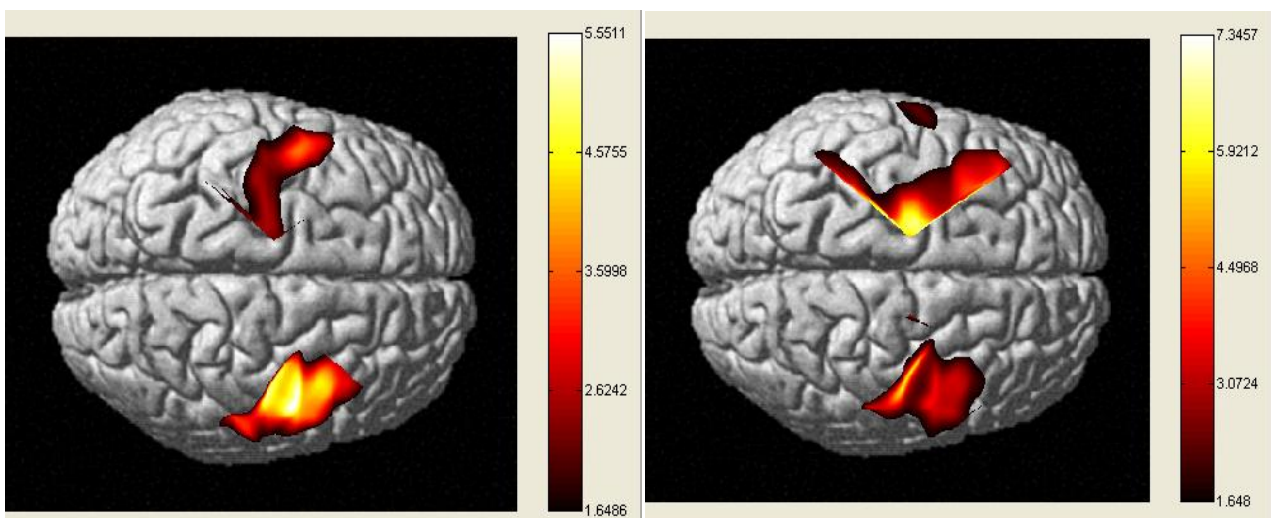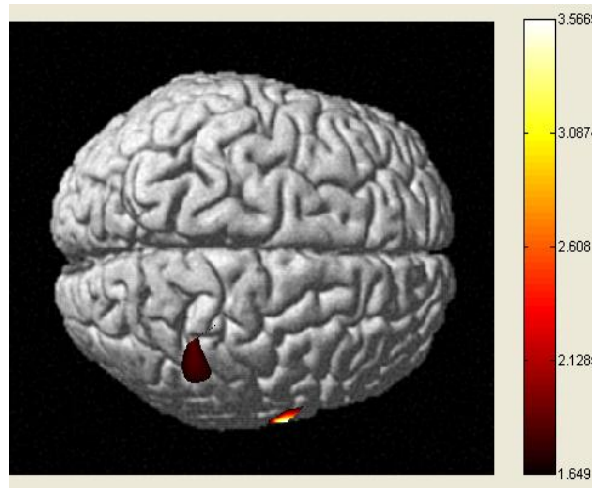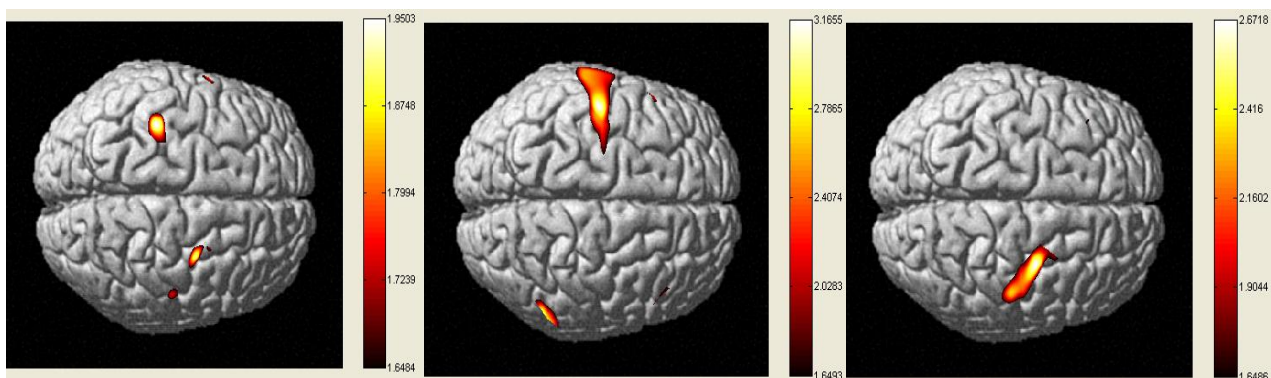

Fig.6.10: The images show HbObrain activation resulting from 1st level analysis of oneEPM1 patient. Contrast was set between the activation blocks and the rest intervals. Significance was set at p-val<0.05. (left) HbOcontrast while performing handgrip with the right hand;(right) HbO contrast while performing handgrip with the left hand.

The alternating (i.e. right vs. left) task unexpectedly showed very poor activation for this subject, and the same result was obtained for HHb. In the healthy subjects, the alternating task evidenced bilateral activation, located over the motor areas; moreover, the alternating task proved to be the most demanding condition in healthy subjects, eliciting the broadest hemodynamic activation over both the hemispheres. Such an activation could not be observed here (Fig.6.11).

Fig.6.11: The image shows HbO brain activation resulting from 1st level analysis of oneEPM1 patient (the same as in Fig.6.10). The patient performed an alternated handgrip task while alternating the use of the right and left hands. Contrast was set between the activation blocks (right vs. left). Significance was set at p-val<0.05.

"EEG informed" GLM provided the topography of hemodynamic activations correlated to electroencephalographic rhythms. Results were obtained for HbO, HHb and HbT, correlating with five EEG bands. In Fig.6.12 and fig.6.13 we report HbO activations obtained by contrasting alpha rhythm and beta rhythm regressors respectively. Alpha rhythm dispalyed correlation with HbO mainly in the left hemisphere for the right and left handgrips, while a right lateralization was evidenced for the alternating handgrip.

Fig.6.12: The images show the HbO activation resulting from contrasting the regressor modeling EEG power in the alpha frequency band at 1st level analysis (oneEPM1 patient, the same as in Fig.6.10). The patient performed right handgrip (left), left handgrip (middle) and alternated handgrip task (right image). Contrast was set between for EEG alpha rhythm. Significance was set at p-val<0.05.

Beta rhythm, on the other hand dispalyed a relevant correlation with HbO mainly in the right hemisphere for the right handgrip only. These last results need for sure further confirmation, as they were rather unexpected.
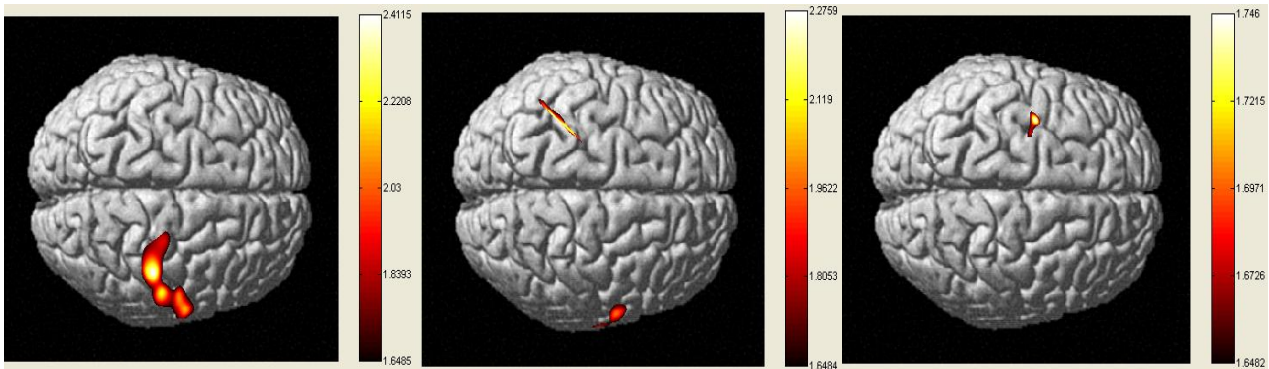
Fig.6.13: The images show the HbO activation resulting from contrasting the regressor modeling EEG power in the beta frequency band at 1st level analysis (oneEPM1 patient, the same as in Fig.6.10). The patient performed right handgrip (left), left handgrip (middle) and alternated handgrip task (right image). Contrast was set between for EEG beta rhythm. Significance was set at p-val<0.05.

6.2.5 Case study 2

Processing of time resolved NIRS data by means of DM1 evidenced bilateral HbO activation while performing all the tasks: right, left and alternated handgrip tasks. HHb activations were also evidenced for the same tasks, mainly bilateral. This pattern of activation, for sure broader than the one observed in the majority of the healthy subjects, could be compatible with the harder effort needed for the EPM1 subjects in order to perform the handgrip task, with respect to the healthy people (Fig.6.14 and 6.15).
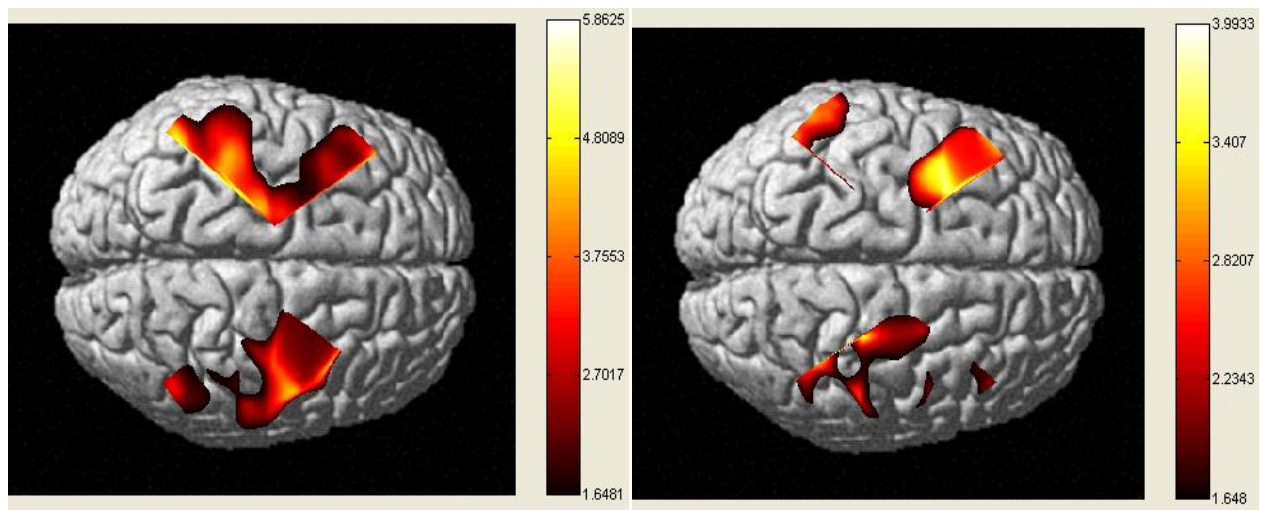

Fig.6.14: The images show HbO brain activation resulting from 1st level analysis of oneEPM1 patient. Contrast was set between the activation blocks and the rest intervals. Significance was set at p-val<0.05. (left) HbO contrast while performing handgrip with the right hand; (right) HbO contrast while performing handgrip with the left hand.
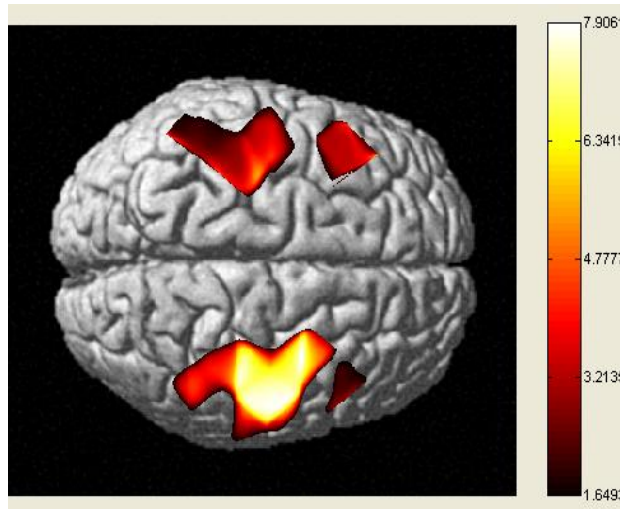
Fig.6.15: The image shows HbO brain activation resulting from 1st level analysis of oneEPM1 patient (the same as in Fig.6.14). The patient performed an alternated handgrip task while alternating the use of the right and left hands. Contrast was set between the activation blocks (right vs. left). Significance was set at p-val<0.05.

Fig.6.16: The images show the HbO activation resulting from contrasting the regressor modeling EEG power in the alpha frequency band at 1st level analysis (oneEPM1 patient, the same as in Fig.6.14). The patient performed right handgrip (left), left handgrip (middle) and alternated handgrip task (right image). Contrast was set between for EEG alpha rhythm. Significance was set at p-val<0.05.

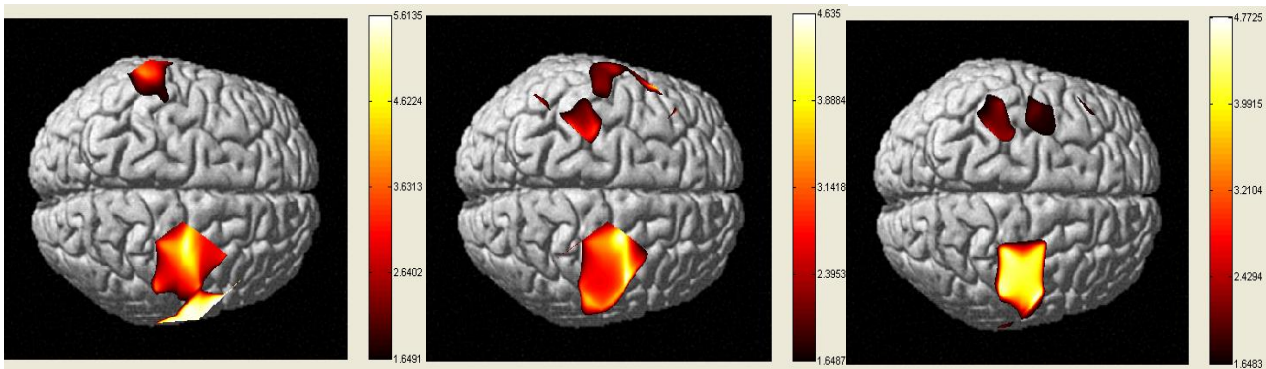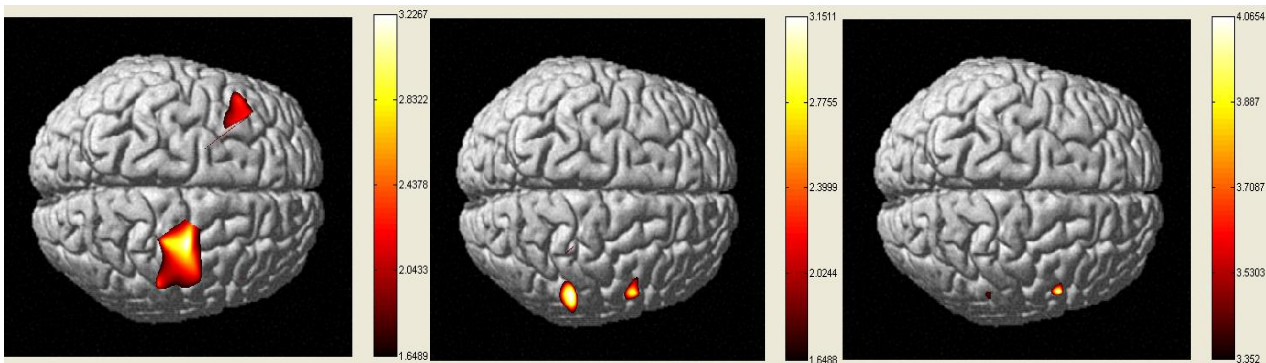**Fig.6.17: The images show the HbO activation resulting from contrasting the regressor modeling EEG power in the beta frequency band at 1st level analysis (oneEPM1 patient, the same as in Fig.6.14). The patient performed right handgrip (left), left handgrip (middle) and alternated handgrip task (right image). Contrast was set between for EEG beta rhythm. Significance was set at p-val<0.05.**

122

"EEG informed" GLM provided the topography of HbO, HHb and HbT activations correlated to electroencephalographic rhythms. In Fig.6.16 and fig.6.17 we report HbO activations obtained by contrasting alpha rhythm and beta rhythm regressors respectively. Alpha rhythm dispalyed correlation with HbO mainly in the right hemisphere for all the tasks: right, left and alternating handgrip (Fig.6.16). Beta rhythm dispalyed a relevant correlation with HbO mainly in the right hemisphere for the right handgrip only (Fig.6.17).

6.2.6 Interpretation and Outcome

The data obtained from the eight EPM1 patients showed high inter-subject variability; moreover – in some cases – NIRS signals were poor. This was mainly due to low photon countings, which badly affected the final signal quality. This matter was reported to the partners of Dipartimento di Fisica, who are now working on improved hardware solutions.

On the other hand, "EEG informed" GLM provided an extremely new tool for integrating EEG and NIRS data acquired from EPM1 patients. This method had never been attempted before in the NIRS imaging field.

The two case studies we reported showed the potentiality of "EEG informed" method: we could indeed evidence the feasibility of data integration. Hemodynamic activations could be highlighted by using a traditional approach, and then a more refined analysis allowed the identification of the electrical activity related to either HbO, HHb or HbT. In so doing, we could link any spot of metabolic activation to a specific electroencephalographic frequency band. Correlations of HbO with the alpha and beta EEG bands were shown. Apart from the clinical interpretation, which could not be reached due to hardware limitations, we could demonstrate the validity of "EEG informed" General Linear Model in providing further details about the hemodynamic phenomena in the brain.

Bibliography

Adelson PD, Nemoto E, Scheuer M, Painter M, Morgan J, Yonas H. Noninvasivecontinuous monitoring of cerebral oxygenation periictally using near-infrared spectroscopy: a preliminary report. Epilepsia. 1999 Nov;40(11):1484-9.

Annane D, Fiorelli M, Mazoyer B, Pappata S, Eymard B, Radvanyi H, Impaired cerebral glucose metabolism in myotonic dystrophy: a triplet-size dependent phenomenon. NeuromusculDisord 1998;8:39–45.

Antonini G, Mainero C, Romano A, Giubilei F, Ceschin V, Gragnani F, Morino S, Fiorelli M, Soscia F, Di Pasquale A, Caramia F. Cerebralatrophy in myotonic dystrophy: a voxel based morphometric study. JNeurolNeurosurgPsychiatry. 2004 Nov;75(11):1611-3.

Arca Diaz G, Cesaron E, Alfonso I, Dunoyer C, Yaylali I. Near infrared spectroscopy in the management of status epilepticus in a young infant. Eur JPaediatr Neurol. 2006 Jan;10(1):19-21.

Avrahami E., Katz A., Bornstein N., Korczyn A. D., Computerized tomographic findings of brain and skull in myotonic dystrophy. J NeurolNeurosurg Psychiatry. 1987;50:435-438.

Balasubramanyam A, Iyer D, Stringer JL, Beaulieu C, Potvin A, Neumeyer AM, et al. Developmental changes in expression of myotonic dystrophy protein kinase in the rat central nervous system. J CompNeurol 1998;394:309 –325.

Ballard J.C., "Assessing attention: comparison of response-inhibition and traditional continuous performance tests," J ClinExpNeuropsychol. Jun;23(3):331-50 (2001).

Bird TD, Follett C, Griep E. Cognitive and personality functions in myotonic muscular dystrophy. J NeurolNeurosurg Psychiatry 1983;46:971–980.

Bozkurt A., Onaral B. Safety assessment of near infrared light emitting diodes for diffuse optical measurements BioMedical Engineering OnLine2004, 3:9

Brook JD, McCurrach ME, Harley HG, et al. Molecular basis of myotonic dystrophy: expansion of trinucleotide (CGT) repeat at the 3_ end of a transcript encoding a protein kinase family member. Cell 1992;68:799–808.

Buchheim K, Obrig H, v Pannwitz W, Müller A, Heekeren H, Villringer A, Meierkord H. Decrease in haemoglobin oxygenation during absence seizures in adult humans. NeurosciLett. 2004 Jan 9;354(2):119-22.

Butti M, Contini D, Molteni E, Caffini M, Spinelli L, Baselli G, Bianchi AM, Cerutti S, Cubeddu R, Torricelli A. Effect of prolonged stimulation on cerebral hemodynamic: a time-resolved fNIRS study. Med Phys. 2009 Sep;36(9):4103-14.

Caramia F, Mainero C, Gragnani F, Tinelli E, Fiorelli M, Ceschin V, Pantano P, Bucci E, Barra V, Bozzao L, Antonini G. Functional MRI changes in the central motor system in myotonic dystrophy type 1. MagnReson Imaging. 2010 Feb;28(2):226-34. Epub 2009 Aug 19.

Censori B, Provinciali L, Danni M, Chiaramoni L, Maricotti M, Foschi N, Brain involvement in myotonic dystrophy: MRI features and their relationship to clinical and cognitive conditions. ActaNeurolScand 1994;90:211–217.

Chang L, Anderson T, Migneco OA, Boone K, Mehringer CM, Villanueva-Meyer J, et al. Cerebral abnormalities in myotonic dystrophy. Cerebral blood flow, magnetic resonance imaging, and neuropsychological tests. Arch Neurol 1993;50:917–923.

Chang L., Ernst T., Osborn D., Seltzer W., Leonido-Yee M., Poland RE. Proton spectroscopy in myotonic dystrophy. Correlations with CTG repeats. Arch Neurol 1998;55:305-311.

Conners C. K., "The Conners continuous performance test," Toronto, Canada: Multi-Health Systems, (1994).

Di Costanzo A, Di Salle F, Santoro L, Bonavita V, Tedeschi G. Brain MRI features of congenital- and adult-form myotonic dystrophy type 1: case– control study. NeuromusculDisord 2002;12:476–483.

Dyken PR, Harper PS. Congenital dystrophia myotonica. Neurology 1973;23:465– 473.

Fallgatter, A. J., &Strik, W. K. (1997). Right frontal activation during the continuous performance test assessed with near-infrared spectroscopy in healthy subjects. Neuroscience Letters, 223, 89–92.

Fiorelli M, Duboc D, Mazoyer BM, Blin J, Eymard B, Fardeau M, et al. Decreased cerebral glucose utilization in myotonic dystrophy. Neurology 1992;42:91–94.

*Friston K.J., Holmes A.P., Worsley K.J., Poline J.P., Frith C.D., and Frackowiak R.S.J., "Statistical parametric maps in functional imaging: a general linear approach," Hum Brain Mapp **2**(4), 189-210 (1995).*

Giorgio A, Dotti MT, Battaglini M, Marino S, Mortilla M, Stromillo ML, Bramanti P, Orrico A, Federico A, De Stefano N. Cortical damage in brains of patients with adult-form of myotonic dystrophy type 1 and no or minimal MRI abnormalities. J Neurol. 2006 Nov;253(11):1471-7.

Haginoya K, Munakata M, Kato R, Yokoyama H, Ishizuka M, Iinuma K. Ictalcerebral haemodynamics of childhood epilepsy measured with near-infraredspectrophotometry. Brain. 2002 Sep;125(Pt 9):1960-71.

Harper PS. Myotonic dystrophy, 2nd edition. Philadelphia: Saunders; 1989.

Huber SJ, Kissel JT, Shuttleworth EC, Chakeres DW, Clapp LE, Brogan MA. Magnetic resonance imaging and clinical correlates of intellectual impairment in myotonic dystrophy. Arch Neurol 1989;46:536 –540.

Irani F, Platek SM, Bunce S, Ruocco AC, Chute D. Functional near infrared spectroscopy (fNIRS): an emerging neuroimaging technology with importantapplications for the study of brain disorders. ClinNeuropsychol. 2007Jan;21(1):9-37.

Jiang H, Mankodi A, Swanson M. Myotonic dystrophy type 1 is associated with nuclear foci of mutant RNA, sequestration of muscleblind proteins and deregulated alternative splicing in neurons. Hum Mol Genet (2004) 13:3079–3088

Jobsis FF. Non invasive, infrared monitoring of cerebral and myocardial oxygen sufficiency and circulatory parameters, Science, Vol. 198 No. 4323, 1977, pp. 1264-1267.

Kuo HC, Hsiao KM, Chen CJ, Hsieh YC, Huang CC. Brain magnetic resonance image changes in a family with congenital and classic myotonic dystrophy. Brain Dev 2005;27:291– 296.

Lareau E, Lesage F, Pouliot P, Nguyen D, Le Lan J, Sawan M. Multichannelwearable system dedicated for simultaneous electroencephalography/near-infraredspectroscopy real-time data acquisitions. J Biomed Opt. 2011 Sep;16(9):096014.

León-Carrion J, Damas-López J, Martín-Rodríguez JF, Domínguez-Roldán JM, Murillo-Cabezas F, Barroso Y Martin JM, Domínguez-Morales MR. The hemodynamics of cognitive control: the level of concentration of oxygenated hemoglobin in the superior prefrontal cortex varies as a function of performance in a modified Stroop task. Behav Brain Res. 2008 Nov 21;193(2):248-56.

Lundborg H. (1903) Die progressive Myoclonus-Epilepsie (Unverricht's Myoclonie). Almqvist and Wiksell, Uppsala.

Machado A, Lina JM, Tremblay J, Lassonde M, Nguyen DK, Lesage F, Grova C. Detection of hemodynamic responses to epileptic activity using simultaneous Electro-EncephaloGraphy (EEG)/Near Infra Red Spectroscopy (NIRS) acquisitions. Neuroimage. 2011 May 1;56(1):114-25.

Malloy P, Mishra SK, Adler SH. Neuropsychological deficits in myotonic muscular dystrophy. J NeurolNeurosurgPsychiatry. 1990 Nov;53(11):1011-3.

Meola G, Sansone V, Perani D, Colleluori A, Cappa S, Cotelli M, et al. Reduced cerebral blood flow and impaired visual– spatial function in proximal myotonic myopathy. Neurology 1999;53:1042–1050.

Meola G, Sansone V, Perani D, Scarone S, Cappa S, Dragoni C, et al. Executive dysfunction and avoidant personality trait in myotonic dystrophy type 1 (DM-1) and in proximal myotonic myopathy (PROMM/DM-2). NeuromusculDisord 2003;13:813– 821.

Meola G, Sansone V. Cerebral involvement in myotonic dystrophies. Muscle Nerve*. 2007 Sep;36(3):294-306. Review.*

Miaux Y., Chiras J., Eymard B., et al. Cranial MRI findings in myotonic dystrophy. Neuroradiology 1997;39:166-170.

Modoni A, Silvestri G, Pomponi MG, Mangiola F, Tonali PA, Marra C. Characterization of the pattern of cognitive impairment in myotonic dystrophy type 1. Arch Neurol 2004;61: 1943–1947.

Negoro H, Sawada M, Iida J, Ota T, Tanaka S, Kishimoto T. Prefrontal dysfunction in attention-deficit/hyperactivity disorder as measured by near-infrared spectroscopy. Child Psychiatry Hum Dev*. 2010 Apr;41(2):193-203.*

Nguyen DK, Tremblay J, Pouliot P, Vannasing P, Florea O, Carmant L, Lepore F, Sawan M, Lesage F, Lassonde M. Non-invasive continuous EEG-fNIRS recording of temporal lobe seizures. Epilepsy Res. 2011 Nov 17.

Norio R, Koskiniemi M. (1979) Progressive myoclonus epilepsy: genetic and nosological aspects with special reference to 107 Finnish patients. Clin Genet 15:382–398.

Obrig, H., Wenzel, R., Kohl, M., Horst, S., Wobst, P., Steinbrink, J., Thomas, F., Villringer, A., 2000. Near-infrared spectroscopy: does it function in functional activation studies of the adult brain? Int. J. Psychophysiol. 35, 125–142.

Ogg RJ, Zou P, Allen DN, Hutchins SB, Dutkiewicz RM, Mulhern RK. Neural correlates of a clinical continuous performance test. MagnReson Imaging. 2008 May;26(4):504-12.

Ota M, Sato N, Ohya Y, Aoki Y, Mizukami K, Mori T, Asada T. Relationship between diffusion tensor imaging and brain morphology in patients with myotonic dystrophy. NeurosciLett. 2006 Oct 30;407(3):234-9.

Perini GI, Menegazzo E, Ermani M, Zara M, Gemma A, Ferruzza E, Cognitive impairment and (CTG)n expansion in myotonic dystrophy patients.

Pu S., T. Yamada, K. Yokoyama, H. Matsumura, H. Kobayashi, N. Sasaki, H. Mitani, A. Adachi, K. Kaneko, and K. Nakagome, "A multi-channel near-infrared spectroscopy study of prefrontal cortex activation during working memory task in major depressive disorder," Neurosci Res. Jan 14, (2011).

Quaresima V., P. Giosuè, R. Roncone, M. Casacchia, and M. Ferrari, "Prefrontal cortex dysfunction during cognitive tests evidenced by functional near-infrared spectroscopy," Psychiatry Res. Mar 31;171(3):252-7, (2009).

Roche-Labarbe N, Zaaimi B, Berquin P, Nehlig A, Grebe R, Wallois F.NIRS-measured oxy- and deoxyhemoglobin changes associated with EEG spike-and-wave discharges in children. Epilepsia. 2008 Nov;49(11):1871-80.

Romeo V, Pegoraro E, Ferrati C, Squarzanti F, Sorarù G, Palmieri A, Zucchetta P, Antunovic L, Bonifazi E, Novelli G, Trevisan CP, Ermani M, Manara R, Angelini C. Brain involvement in myotonic dystrophies: neuroimaging and neuropsychological comparative study in DM1 and DM2. J Neurol. 2010 Aug;257(8):1246-55.

Romeo V, Pegoraro E, Squarzanti F, Sorarù G, Ferrati C, Ermani M, Zucchetta P, Chierichetti F, Angelini C. Retrospective study on PET-SPECT imaging in a large cohort of myotonic dystrophy type 1 patients.Neurol Sci. 2010 Dec;31(6):757-63.

Rosvold, H. E., Mirsky, A. F., Sarason, I., Bransome Jr., E. D., & Beck, L. H. (1956). A continuous performance test of brain damage. Journal of Consulting and Clinical Psychology, 20, 343–350.

Sansone V.,Gandossini S., Cotelli M., Calabria M., Zanetti O., Meola G. Cognitive impairment in adult myotonic dystrophies: a longitudinal study. NeurolSci (2007) 28:9–15

Schecklmann M., M. Romanos, F. Bretscher, MM. Plichta, A. Warnke, and AJ. Fallgatter, "Prefrontal oxygenation during working memory in ADHD," J Psychiatr Res. Jul;44(10):621-8, (2010).

Sokol DK, Markand ON, Daly EC, Luerssen TG, Malkoff MD. Near infraredspectroscopy (NIRS) distinguishes seizure types. Seizure. 2000 Jul;9(5):323-7.

Spranger M, Spranger S, Tischendorf M, Meinck HM, Cremer M. The role of large triplet repeat length in the developmental of mental retardation. Arch Neurol 1997;54:251–254.

Steinhoff BJ, Herrendorf G, Kurth C. Ictal near infrared spectroscopy in temporal lobe epilepsy: a pilot study. Seizure. 1996 Jun;5(2):97-101.

Sturm, W., A. de Simone, B. J. Krause, K. Specht, V. Hesselmann, I. Radermacher, H. Herzog, L. Tellmann, H. W. Müller-Gärtner, and K. Willmes. Functional anatomy of intrinsic alertness: evidence for a fronto-parietal thalamic-brainstem network in the right hemisphere. Neuropsychologia 37(7):797–805, 1999.

Tanabe Y, Iai M, Tamai K, Fujimoto N, Sugita K. Neuroradiological findings in children with congenital myotonic dystrophy. ActaPaediatr 1992;81:613– 617.

Toichi M., Findling R.L., Kubota Y., Calabrese J.R., Wiznitzer M., McNamara N.K., and Yamamoto K., "Hemodynamic differences in the activation of the prefrontal cortex: attention vs. higher cognitive processing," Neuropsychologia2004;**42**(5), 698-706.

Unverricht H. (1891) Die Myoclonie. Franz Deuticke, Leipzig.

Wallois F, Patil A, Héberlé C, Grebe R. EEG-NIRS in epilepsy in children andneonates. NeurophysiolClin. 2010 Nov-Dec;40(5-6):281-92.

Wallois F, Patil A, Kongolo G, Goudjil S, Grebe R. Haemodynamic changes during seizure-like activity in a neonate: a simultaneous AC EEG-SPIR andhigh-resolution DC EEG recording. NeurophysiolClin. 2009 Oct-Nov;39(4-5):217-27.

Watanabe E, Maki A, Kawaguchi F, Yamashita Y, Koizumi H, Mayanagi Y. Noninvasive cerebral blood volume measurement during seizures using multichannel near infrared spectroscopic topography. J Biomed Opt. 2000 Jul;5(3):287-90.

Watanabe E, Maki A, Kawaguchi F, Yamashita Y, Koizumi H, Mayanagi Y. Noninvasive cerebral blood volume measurement during seizures using multichannel near infrared spectroscopic topography. J Biomed Opt. 2000 Jul;5(3):287-90.

Watanabe E, Nagahori Y, Mayanagi Y. Focus diagnosis of epilepsy usingnear-infrared spectroscopy. Epilepsia. 2002;43 Suppl 9:50-5.

Weber YG, Roebling R, Kassubek J, Hoffmann S, Rosenbohm A, Wolf M, Steinbach P, Jurkat-Rott K, Walter H, Reske SN, Lehmann-Horn F, Mottaghy FM, Lerche H. Comparative analysis of brain structure, metabolism, and cognition in myotonic dystrophy 1 and 2. Neurology. 2010 Apr 6;74(14):1108-17.

Westerlaken JH, Van der Zee CE, Peters W, Wieringa B. The DMWD protein from the myotonic dystrophy (DM1) gene region is developmentally regulated and is present most prominently in synapse-dense brain areas. Brain Res 2003; 971:116–127.

Whiting EJ, Waring JD, Tamai K, Somerville MJ, Hincke M, Staines WA, et al. Characterization of myotonic dystrophy kinase (DMK) protein in human and rodent muscle and central nervous tissue. Hum Mol Genet 1995;4:1063–1072.

Ye JC, Tak S, Jang KE, Jung J, Jang J. NIRS-SPM: statistical parametric mapping for near-infrared spectroscopy. Neuroimage*. 2009 Jan 15;44(2):428-47.*

Discussion

While NIRS and DOI hold great promise as tools for cognition and the neurosciences, there are limitations to their application, as well as technological advances that will enhance their application. Estimation of the oxy- and deoxyhemoglobin concentrations is sensitive to random measurement error and systematic errors arising from incorrect model parameters. Of significant concern is cross-talk in the estimate of the oxy- and deoxyhemoglobin concentrations. These errors can be partially reduced by judicial choice of measurement wavelengths (Sato et al., 2004; Strangman et al., 2003; Uludag et al., 2002; Yamashita et al., 2001).

The diffuse nature of photon migration through the tissue limits the penetration depth and thus the sensitivity to brain activation occurring subcortically. The sensitivity to brain activation is further compromised by contamination from several systemic physiological signals, which can have a larger percent signal variation than that of the brain activation and in some cases may even phase-lock with the stimulation (Franceschini et al., 2003; Obrig et al., 2000; Toronov et al., 2000).

DOI can potentially achieve spatial resolution of 1 cm in the axes parallel to the scalp in the adult human brain close to the skull, while resolution degrades rapidly with increasing depth in the brain.

However, current measurement strategies primarily utilize nonoverlapping geometric arrangements of sources and detectors, and thus spatial resolution is rarely better than the typical source-detector separation of 3 cm (Boas et al.,

>> KeyPoints

>time resolved fNIRS can easily differentiate between truly cortical and systemic changes, by separating intra- and extra-cerebral contributions to NIRS signal

>Increasing the number of NIRS channels is not priceless. In many cases, a greater amount of data have to be discarded, due to movement artifacts and to the uncomfortable setup.

> The distance between optodes and receivers needs to be accurately calibrated. Two details have to be verified: depth penetration and channel positioning, which is usually located half way between source and detector.

> The hair is a confound. The darker is the hair, the worse can be the acquired signal

>Tests and cognitive stimulations must be properly designed. The slowness of the hemodynamic response needs to be taken into account.

> Multimodal recording with fMRI and TMS can help in locating properly the NIRS activation, at least in research. Brain atlases are of crucial importance, when choosing the registration tools.

> Last: theory, studies and simulations can still lack in estimating some subjective peculiarities. Physiological differences between subjects can still play a major role, remaining beyond our modeling possibilities. Pathology could conceal even bigger surprises. This is the part of my PhD. work I will probably never be able to discuss!

2004). Spatial resolution in the depth axis is significantly worse in adult humans, due to the small source-detector separations that can be used (up to 5 cm). Depth resolution could be improved if transmission measurements were made. However, while this is possible in newborn babies (Hintz et al., 1999), it is generally not possible in adult humans.

The limited depth resolution of DOI causes significant partial volume error and, in the case of cw-NIRS, prevents absolute amplitude accuracy in the estimates of the hemoglobin concentration response to brain activation. As a result, quantitative comparison of response amplitudes from different brain regions within a subject and from the same brain region between subjects is compromised. Prior spatial information is required to overcome the partial volume problem. This information can be provided by fMRI if the brain activations measured by fMRI and DOI are correlated in space and time.

Time resolved NIRS represents an improvement with respect of this issue. Indeed, by injecting pulses of light through the scalp, is provides photons countings directly related to the previously injected pulse of light. By analyzing the distribution in time of the received photon countings, it is possible to trace back the number of photons which travelled through the tissues at various depths. In doing so, the quantitative measurement of received light at specific depths is made feasible.

7.1 Methodological issues

7.1.1 Intra- and extra-cerebral contributions

Transcutaneous NIRS is reflective of a heterogeneous tissue field containing arteries, veins, and capillary networks and also other non-vascular tissue. For NIRS of cerebral tissue, photons must penetrate several tissue layers including scalp, skull, and dura, which can contain various concentrations of blood and tissue-derived chromophores. As a result, the main limitation of fNIRS technique resides in the fact that signals contain contributions from both the brain and the overlying tissues (Liebert et al., 2004). Specifically, fNIRS signal can be highly sensitive to extra-cerebral blood volume changes. Besides, differences in the dynamics of HbO and HHb variations have been often reported in fNIRS studies, and have been generally interpreted as a potential indicator of differences in physiological mechanisms of neurovascular coupling across cortical areas (Huppert et al., 2006). Surveys have also shown that this fact may indeed depend partly on hemodynamic changes unrelated to the cortical increase in blood flow. Then, the most reliable hypothesis is that this difference may be caused by systemic changes (Boas et al., 2004).

In contrast to other neuroimaging methods and to the continuous wave fNIRS, time resolved fNIRS can easily differentiate between truly cortical and systemic changes. Time-resolved measurements are based on a temporal approach: on average, photons detected after long times of flight probe deeper tissue layers than early photons (Del Bianco et al., 2002; Liebert et al., 2004; Selb, 2005; Steinbrink, 2001). In doing so, a statistical separation of surface and cortical contributions is made feasible. In the present PhD. work, extra-cerebral activation was isolated and separately treated in order to obtain neater information from the cortex.

7.1.2 Increasing number of channels

The advantages of increasing the number of channels are clear. However this is confounded by the inevitable increase in weight and size of the headgear. This may explain the higher proportion of excluded optical data due to excessive movement artifacts in those fNIRS studies using a high number of channels. For example Watanabe et al.

(2008) used up to 84 channels to measure multiple cortical regions but excluded data from almost 70% of the participants. Similarly, Nakano et al. (2009) used a 48-channel system and excluded data from 56% of the participants.

This is not to say that other studies where a lower number of channels were used have always reported a lower proportion of excluded data, but rather that an increase in the number of channels is one factor that impacts the quality of the optical signal unless this is carefully considered within the headgear design.

7.1.3 The cortical area of interest

The cortical area of interest can affect the probe and headgear design in terms of the depth of the underlying cortex from the surface of the skin, the distribution and arrangement of the channels over the area of interest and the accommodation of the curvature of the skull.

Theoretically, if the source to detector distance is increased, the detected light is more likely to provide information about a hemodynamic response occurring in deeper tissue (Fukui et al., 2003). However, this assumption is limited by the intensity of the source light and the diffuse nature of optical scattering in tissue. To reach the cortex, the separation between source and detector should be, at minimum, double that of the distance between the skin surface and the surface of the cortex, but often this is not enough. To ensure that the measurement is taken from within the cortex, when studying adult brain responses, the channel separations are usually between 30 and 50 mm (Okada et al., 1997). Indeed, both computer simulation and experimental tissue models of transcranial NIR light transmission have demonstrated an elliptical photon distribution centred around the transmitter whose mean depth is proportional to the separation of the optodes by a factor of ~1/3 (Germon et al., 1999). Increasing transmitter/receptor distance increases depth of penetration and minimizes the effect of extracerebral tissue (Germon et al., 1999), but power must be limited to prevent direct thermal tissue damage. Since signal intensity is inversely proportional to the square of the pathlength, 5cm separation appears to be the functional maximal optode spacing (Ohmae et al., 2006). This provides a mean depth of NIR light penetration ~1.7 cm giving increased weighting to cerebral vs. extracerebral tissue (Ohmae et al., 2006). As there is still significant attenuation from extracerebral tissue even with optimized transmitter/receiver separation, tr-NIRS still remains the favourable technique.

An increase in the separation between source and detector will also lead to a decrease in the number of channels over a given area and will in turn affect the design of the headgear. The intensity of the light can effect measurements as the stronger the intensity, the more light will reach the detectors, and the better the signal to noise ratio will be in the optical signal. As the intensity of the sources can vary across NIRS systems, a separation that is ideal for one system may not be for another.

The anatomical structure of the head varies within and between Individuals. Thus the optimal separation may vary across areas of the cortex and between individuals. In addition to using a single separation, one method to overcome the issue of choosing the ideal separation is to use a probe design that incorporates several source-detector separation distances. This multi-separation source-detector approach allows for several depths of the cortex to be measured simultaneously, leading to depth discrimination of cortical activation, and allowing the selection of the optimal distance for the subject.

In cw-NIRS technique, this multi-separation source-detector approach is also applied for the separation of intra-cerebral and extra-cerebral contributions to NIRS signal. Indeed, the extractions of contributions based on the photons time-of-flight is not feasible in this case.

Finally, the curvature of the skull will have a dramatic effect on the design of the probe and headgear. As mentioned earlier, a major challenge is to ensure that the probe sits flat and securely against the head. Therefore, areas of the head that are more curved or have more individual variability, such as the forehead, are more difficult to accommodate. Despite these challenges, designs are now in use for occipital, frontal, temporal and parietal regional investigation. "Total brain" helmets and caps for NIRS measurement are also available with some cw-NIRS commercial devices, and can be home made.

Very recently, integrated caps and helmets allowing the simultaneous detection of NIRS and EEG signals have been produced, for devices endowment, by Honda (Japan), NIRx (Germany) and some other cw-NIRS suppliers (Fig.7.1).

Fig.7.1 "total brain" integrated EEG/NIRS helmet. Honda Asimo. The helmet, when connected to the NIRS and EEG devices, provides simultaneous measurement of EEG and NIRS signals from the whole brain.

7.1.4 The hair

Although the design of the probes and headgear for fNIRS studies has improved significantly, there remains one issue that continues to frustrate researchers: the challenge of dealing with participants' hair. Firstly, hair reduces the grip of the headgear and probes on the head, lowering friction and increasing the effects of the movement of the subject. Secondly, the layering, differing orientation and colour of the hair lying between the probe and subject's head will cause attenuation of the light and can lead to unreliable measurements. If the hair is particularly dark the optical data may simply be unusable. A great deal of time is usually spent moving hair away from the area directly under the optodes. Nevertheless, this is largely impractical.

7.1.5 Study design

First and foremost, the design of the study must take into consideration the temporal characteristics of the hemodynamic response. The majority of NIRS work has been

conducted using a block design for stimulus presentation. The common method is to present the experimental condition for a period of 3–30 s followed by a control condition typically of longer duration to allow the hemodynamic response initiated during the experimental condition to return to a baseline level. This control condition is usually either of minimal stimulation (e.g. silence) or designed to cause stimulation to a lesser extent than the experimental condition. Consequently the hemodynamic response to the experimental condition is measured in relation to the control condition.

An important consideration when designing a fNIRS study is the effect of physiological oscillations in the optical signal. One approach to reduce such physiological and anticipatory effects in a block design is to jitter experimental stimulus onset by varying the duration of the control trials so that they do not follow a predictable pattern.

These stimuli should be asynchronously presented with differing control trial durations to maintain unpredictable intervals of presentation.

Moreover, there are two considerations to be taken into account that affect the required number of trials for a given experimental condition. Firstly, one must establish the number of trial repetitions required for a robust response. Under ideal experimental conditions a single trial would be sufficient to yield a significant response (see Colier et al., 1999). However inadequate signal to noise and the presence of motion artifacts typically require the repetition of several trials. NIRS studies do not require, however, as many repetitions as ERP.Secondly, the repetition of several trials can result in adaptation effects where neural responses to repeated stimuli can diminish over time (Krekelberg et al., 2006). If the signal to noise ratio is adequate, fewer trials could yield more reliable data.

7.1.6 Registration

One of the main difficulties of NIRS data interpretation is localizing the origin of the hemodynamic response. NIRS measurements are made from the surface of the scalp making it difficult to establish the exact spatial origin within the brain, of the hemodynamic response. In NIRS and EEG studies it is standard practice to use the 10/20 system (Jasper, 1958) to localize regions of interest using external landmarks, but this method does not inform the internal organization of the brain. Hence, NIRS can benefit greatly from the accurate structural cerebral information provided by brain imaging techniques such as MRI, or from the functional information provided by transcranial magnetic stimulation (TMS). Multimodal data acquisition could contribute crucial information for improving data registration, at least in research. Besides, the choice of brain atlases becomes very important whenever NIRS recording is not combined with MRI assessment.

7.1.7 Cerebral arterial/venous blood partitioning

Cerebral NIRS devices measure mean tissue oxygen saturation and, as such, reflect hemoglobin saturation in venous, capillary, and arterial blood comprising the sampling volume. For cerebral cortex, average tissue hemoglobin is distributed in a proportion of ~70% venous and 30% arterial (McCormick et al., 1991), based on correlations between position emission tomography (PET) and NIRS (Ohmae et al., 2006). However, clinical studies have demonstrated that there can be considerable biological variation in individual cerebral arterial/venous (A/V) ratios between patients, further underscoring that the use of a fixed ratio can produce significant divergence from actual in vivo tissue oxygen saturation, thus confounding even 'absolute' measures of cerebral oxygenation, for example, fd-NIRS or tr-NIRS (Watzman et al., 2000). Every human being bears peculiarity, which goes beyond our modeling possibility!

7.2 Conclusion

Near-infrared spectroscopy is able to measure hemodynamic, metabolic neuronal responses to brain activation with inexpensive and portable instrumentation. These capabilities are making NIRS, in its present technological state, an important tool in cognition and the neurosciences. The extension of NIRS to diffuse optical imaging and the introduction of time resolved NIRS technique will improve the sensitivity, resolution, and accuracy of the optical estimates of the hemodynamic response to brain activation, as well as the metabolic and neuronal response. Through examples and studies, we identified many issues and illustrated some potential solutions that should be further addressed and explored with much research over the next several years.

Bibliography

Boas D.A., Dale AM, Franceschini MA. Diffuse optical imaging of brain activation: approaches to optimizing image sensitivity, resolution, and accuracy. Neuroimage. 23 Suppl 1:S275-88, 2004.

Colier, W.N., Quaresima, V., Oeseburg, B., Ferrari, M., 1999. Human motor-cortex oxygenation changes induced by cyclic coupled movements of hand and foot. Exp. Brain. Res. 129, 457–461.

Del Bianco S., Martelli F, Zaccanti G. Penetration depth of light re-emitted by a diffusive medium: theoretical and experimental investigation. Phys. Med. Biol. 47, 4131-4144, 2002.

Franceschini, M.A., Fantini, S., Thompson, J.H., Culver, J.P., Boas, D.A., 2003. Hemodynamic evoked response of the sensorimotor cortex measured noninvasively with near-infrared optical imaging. Psychophysiology 40, 548–560.

Fukui, Y., Ajichi, Y., Okada, E., 2003. Monte Carlo prediction of near-infrared light propagation in realistic adult and neonatal head models. Appl. Opt. 42, 2881–2887.

Germon TJ, Evans PD, Barnett NJ, Wall P, Manara AR, Nelson RJ. Cerebral near infrared spectroscopy: emitter-detector separation must be increased. Br J Anaesth 1999; 82: 831–7

Hintz, S.R., Benaron, D.A., Siegel, A.M., Zourabian, A., Stevenson, S.K., Bas, D.A., 2001. Bedside functional imaging of the premature infant brain during passive motor activation. J. Perinat. Med. 29, 335–343.

Huppert T.J., Hoge RD, Diamond SG, Franceschini MA, Boas DA. A temporal comparison of BOLD, ASL, and NIRS hemodynamic responses to motor stimuli in adult humans. NeuroImage 29,368–382, 2006.

Jasper H.H., "The ten twenty electrode system of the International Federation. Electroencephal. Clin. Neurophys., vol. 10, pp. 371–375, 1958.

Krekelberg, B., Boynton, G.M., Wezel, R.J.A., 2006. Adaptation: from single cells to BOLD signals. Trends Neurosci. 29, 250–256.

Liebert A., Wabnitz H, Steinbrink J, Obrig H, Möller M, Macdonald R, Villringer A, Rinneberg H. Time-resolved multidistance near-infrared spectroscopy of the adult head: intracerebral and extracerebral absorption changes from moments of distribution of times of flight of photons. Appl Opt. May 20;43(15):3037-47, 2004.

McCormick PW, Stewart M, Goetting MG, Balakrishnan G. Regional cerebrovascular oxygen saturation measured by optical spectroscopy in humans. Stroke 1991; 22: 596–602

McCormick PW, Stewart M, Goetting MG, Dujovny M, Lewis G, Ausman JI. Noninvasive cerebral optical spectroscopy for monitoring cerebral oxygen delivery and hemodynamics. Crit Care Med 1991; 19: 89–97

Nakano, T., Watanabe, H., Homae, F., Taga, G., 2009. Prefrontal cortical involvement in young infants' analysis of novelty. Cereb. Cortex 19, 455–463.

Obrig, H., Neufang, M., Wenzel, R., Kohl, M., Steinbrink, J., Einhaupl, K., Villringer, A., 2000. Spontaneous low frequency oscillations of cerebral hemodynamics and metabolism in human adults. NeuroImage 12, 623–639.

Ohmae E, Ouchi Y, Oda M, et al. Cerebral hemodynamics evaluation by near-infrared time-resolved spectroscopy: correlation with simultaneous positron emission tomography measurements. Neuroimage 2006; 29: 697–705

Okada, E., Firbank, M., Schweiger, M., Arridge, S.R., Cope, M., Delpy, D.T., 1997. Theoretical and experimental investigation of near-infrared light propagation in a model of the adult head. Appl. Opt. 36, 21–31.

Sato, H., Kiguchi, M., Kawaguchi, F., Maki, A., 2004. Practicality of wavelength selection to improve signal-to-noise ratio in near-infrared spectroscopy. NeuroImage 21, 1554– 1562.

Selb J. Improved sensitivity to cerebral hemodynamics during brain activation with a time-gated optical system: analytical model and experimental validation. Journal of Biomedical Optics, Vol. 10, No. 1, 11013, 2005.

Steinbrink J., Wabnitz H, Obrig H, Villringer A, and Rinneberg H. Determining changes in NIR absorption using a layered model of the human head. Phys. Med. Biol. 46, 879-896, 2001.

Strangman, G., Franceschini, M.A., Boas, D.A., 2003. Factors affecting the accuracy of near-infrared spectroscopy concentration calculations for focal changes in oxygenation parameters. NeuroImage 18, 865–879.

Toronov, V., Webb, A., Choi, J.H., Wolf, M., Michalos, A., Gratton, E., Hueber, D., 2001. Investigation of human brain hemodynamics by simultaneous near-infrared spectroscopy and functional magnetic resonance imaging. Med. Phys. 28, 521– 527.

Uludag, K., Kohl, M., Steinbrink, J., Obrig, H., Villringer, A., 2002. Cross talk in the Lambert-Beer calculation for near-infrared wavelengthsestimated by Monte Carlo simulations. J. Biomed. Opt. 7,51– 59.

Watanabe, H., Homae, F., Nakano, T., Taga, G., 2008. Functional activation in diverse regions of the developing brain of human infants. NeuroImage 43, 346–357.

Watzman HM, Kurth CD, Montenegro LM, Rome J, Steven JM, Nicolson SC. Arterial and venous contributions to near-infrared cerebral oximetry. Anesthesiology 2000; 93: 947–53

Yamashita, Y., Maki, A., Koizumi, H., 2001.Wavelength dependence of the precision of noninvasive optical measurement of oxy-, deoxy-, and total-hemoglobin concentration. Med. Phys. 28, 1108– 1114.